E M B R I T T L E M E N T O F S T E E L

B Y N I T R I D I N G

A thesis submitted for the degree of

Doctor of Philosophy

of the University of Newcastle upon Tyne

by

Brigitte Billon

Crystallography Laboratory

Department of Metallurgy and Engineering Materials

University of Newcastle upon Tyne

October 1983

PREFACE

This thesis describes original work which has not been submitted for a degree at any other University.

The investigations were carried out in the Crystallography Laboratory, Department of Metallurgy and Engineering Materials of the University of Newcastle upon Tyne, during the period October 1979 to March 1982 under the supervision of Professor K.H. Jack and Dr. A. Hendry.

The nitriding behaviour of an austenitic stainless steel together with its structure and mechanical properties are described as part of a wider investigation at Newcastle of the effect of nitriding heat treatments on the behaviour of iron and steels.

ACKNOWLEDGEMENTS

I wish to thank Professor K.H. Jack and Dr. A. Hendry for advice, discussion, encouragement and general supervision of the work.

I also wish to thank:

the United Kingdom Atomic Energy Authority (U.K.A.E.A.) for the award of a maintenance grant;

Dr. P.D. Parsons (Project Liaison Officer) of Springfields Laboratories, U.K.A.E.A. for advice and discussion;

members of the electron optical unit of Springfields Laboratories for their help with ion beam thinning;

members of the electron optical group, Department of Metallurgy and Engineering Materials, for their assistance with scanning electron microscopes;

many colleagues, past and present, in the Crystallography Laboratory for their friendship and stimulating discussion;

the technical staff of the Crystallography Laboratory for their assistance;

Professor J. Foct of Universite de Lille and Professor R. Ouziaux of E.N.S.A.M., Lille, for providing the opportunity to complete my thesis in France;

Mrs. A. Rule for typing the script.

ABSTRACT

Nitriding of AISI 316 stainless steel leads to the formation of a multilayered case and the distribution of the phases through the nitrided layer depends on the reaction temperature and cooling rate. Optical microscopy, electron microscopy and X-ray techniques are used to identify the phases formed.

Nitriding kinetics are studied between 550° and 800°C and the results are explained in terms of the phase distribution. Internal nitriding theory is valid at 800°C but at temperatures lower than 650°C abnormally high nitriding rates are observed due to the formation of a thick "white layer" of massive γ'-Fe_4N with CrN.

Three-point bend tests of sheets of nitrided AISI 316 are described and it is shown that the extent of brittle behaviour depends on the nitriding temperature, the thickness, hardness and composition of the nitrided layer and also on the metallurgical state of the core. Bending of hollow nitrided tubes of the same steel in four-point bend leads to deformation of the material at the level of the anvils of the jig while the mechanical properties of filled nitrided tubes depend on the nature of the filling material.

CONTENTS

LINE DRAWINGS NEGATIVE NUMBER INDEX

Figure	Negative Number
II.1	D 39838
II.2	D 39710
II.3	D 39713
II.4	D 39898
II.5	D 39711
II.6	D 39716
II.7	D 39719
II.8	D 39771
II.9	C 50716*
II.10	C 13375**
II.11	D 39437
II.12	D 39709
II.13	D 39702
II.14	D 39721
II.15	D 39436
III.1	D 25076
III.2	C 67456***
III.3	D 24897
III.4	D 28513
III.5	C 90729****
V.1	D 39839
V.14	D 39896
V.15	D 39718
V.16	D 39707
V.22	D 39841
VII.1	D 39703
VII.2	D 39708
VII.3	D 39842
VII.4	D 39717
VII.5	D 40118
VII.7	D 39706
VII.8	D 39705
VIII.1	D 39899
VIII.2	D 40890
VIII.3	D 40889
VIII.5	D 39897
VIII.7	D 40888
VIII.9	D 39895

* without "Fig. I.2 The iron-nitrogen diagram Jack, K.H. 1951"

** without "22"

*** without "Gas-flow system for NH_3-H_2 and N_2-H_2 equilibrations"

**** without "Preparation of ceramic thin foils for examination by transmission electron microscopy"

"ion beam thinning apparatus"

Chapter I

INTRODUCTION

On nitriding AISI 316 stainless steel a hard case is formed at the surface and work carried out in the Springfields Laboratories of the United Kingdom Atomic Energy Authority has shown that nitriding is a suitable process for the deliberate embrittlement of AISI 316. The steel is used as a fuel-canning alloy in nuclear reactors and some means for its embrittlement is a necessary part of the spent-fuel recovery process.

Investigations on nitriding binary iron alloys (Fe-Ti, Atasoy & Kirkwood, 1973; Fe-Cr, Mortimer et al., 1972; Fe-Ti and Fe-Mo, Jack et al., 1973; Fe-Ti and Fe-Cr, Lightfoot & Jack, 1973, and other studies carried out at Newcastle) have shown that the rate of nitriding is a function of the strength of the interaction between the alloying element and nitrogen, the concentration of alloying elements, the reaction temperature and the potential of nitrogen in the gas mixture.

Nitriding of stainless steel leads to the formation of a multilayer case the composition of which depends on the nitrogen potential. Previous investigations have shown

that the rate of nitriding obeys internal nitriding theory (Kindlimann & Ansell, 1970; Evans, 1972; Lebrun et al., 1972; Smith & Evans, 1973; Unthank, 1974). However, little work is published on the nitriding of AISI 316 stainless steel and attempts to fit internal nitriding theory at low temperatures have not been successful (Cordwell et al., 1974; Wilson, 1978). The maximum case depth in the temperature range studied (500°-800°C) is obtained at 600°C (Cordwell et al., 1974), and the kinetics of nitriding are independent of the composition of the gas mixture at low nitrogen potentials (Tyfield & Mackway, 1975). The changes in mechanical properties of nitrided AISI 316 with nitriding temperature (Stanley, 1969; Wilson & Wilson, 1981) may be due to changes in the phase distribution. It is worthwhile, therefore, to try to explain the abnormal nitriding behaviour of AISI 316 and its mechanical properties, particularly in relation to embrittlement, in terms of the phase distribution in the nitrided case.

Experimental methods used in the present investigation include controlled metal-gas equilibration, X-ray diffraction, electron microscopy and mechanical testing, together with standard metallographic techniques.

Chapter II

PREVIOUS WORK

II.1 Stainless steels

(a) Introduction

The corrosion resistance of chromium steels was first appreciated more than seventy years ago and these steels were called "stainless steel". This name was also given to austenitic Fe-Cr-Ni compositions which were developed in Germany at about the same time. The metallurgical development of stainless steels is reviewed in a series of historically significant papers edited by Pickering (1979) some of which are referred to below. At the present time there are many different stainless steels the main types of which can be summarised as:

(i) Martensitic steels containing 12-17wt% chromium, 0-4wt% nickel, 0.1-1.0wt% carbon with possible additions of molybdenum, vanadium, niobium, aluminium or copper. These steels are usually quenched and tempered to produce useful combinations of strength, ductility and toughness and may also be precipitation-hardened;

(ii) Ferritic steels containing 15-30wt% chromium, low carbon, no nickel and often some molybdenum, niobium or

titanium. They are resistant to aqueous corrosion, high temperature oxidation and are reasonably formable;

(iii) Austenitic steels which contain 18-25wt% chromium with 8-20wt% nickel and low carbon. Less highly alloyed austenitic steels are metastable and can transform to martensite by quenching from high temperature ($>1000^{\circ}C$). Austenitic steels may also contain additions of molybdenum, niobium or titanium. Austenite is soft with a very low elastic limit but is very tough and has a characteristically high work-hardening rate.

(b) The effect of alloying elements on austenite stability

The effect of nickel on the structure of iron is to lower the $\gamma \rightarrow \alpha$ transformation temperature. The γ - austenite phase (see Figure II.1) can be stabilised in the presence of nickel to temperatures as low as $400^{\circ}C$ and under certain cooling conditions it is possible to obtain austenite at room temperature. The iron-nickel equilibrium diagram also shows the formation of an intermetallic phase ($FeNi_3$) at low temperature.

The iron-chromium system has been widely studied because of the industrial importance of such alloys (Pickering, 1979). Because chromium is a ferritic stabiliser the austenite phase is present only in a very narrow loop, and for a chromium content higher than 13wt% no γ is formed;

Fe wt% Ni

20 40 60 80

1500

1000

500

0

temperature /°C

γ

α+γ

α

$FeNi_3$

20 40 60 80

Fe at% Ni

see Figure II.2. With chromium contents greater than 17wt% at temperatures below 800°C Fe-Cr alloys show considerable embrittlement. Between 550° and 800°C σ -phase precipitation is responsible and below 550°C the phenomenon known as "475°C embrittlement" occurs. Sigma-phase has a composition of FeCr but can dissolve an additional 5wt%Cr or Fe and forms congruently from ferrite at 815°C although the kinetics of formation are sluggish and are accelerated by cold working. The effect of σ on mechanical properties depends on its distribution. Small isolated colonies have relatively little effect but continuous networks can lead to dramatic embrittlement (Lena, 1954). The effect of σ -phase in reducing toughness is considered to be a problem only below 600° or 650°C and sigma is not normally encountered in the processing of commercial ferritic stainless steels. The rate of formation of σ -phase in austenitic steels is very slow; it forms directly from austenite although it is usually poorer in nickel than the original composition of the steel. Aging Fe-Cr alloys for long times between 450° and 550°C dramatically reduces toughness and this embrittlement has been explained by a miscibility gap in the α solid solution and the formation of a chromium rich precipitate, α′ . There is some evidence that mechanical properties are affected before α′ precipitation which suggests the existence of a Guinier-Preston zone stage. Studies of the influence of nitrogen on "475°C embrittlement" showed that clustering of

Figure II.2

The iron-chromium equilibrium diagram

(Elliott, 1965)

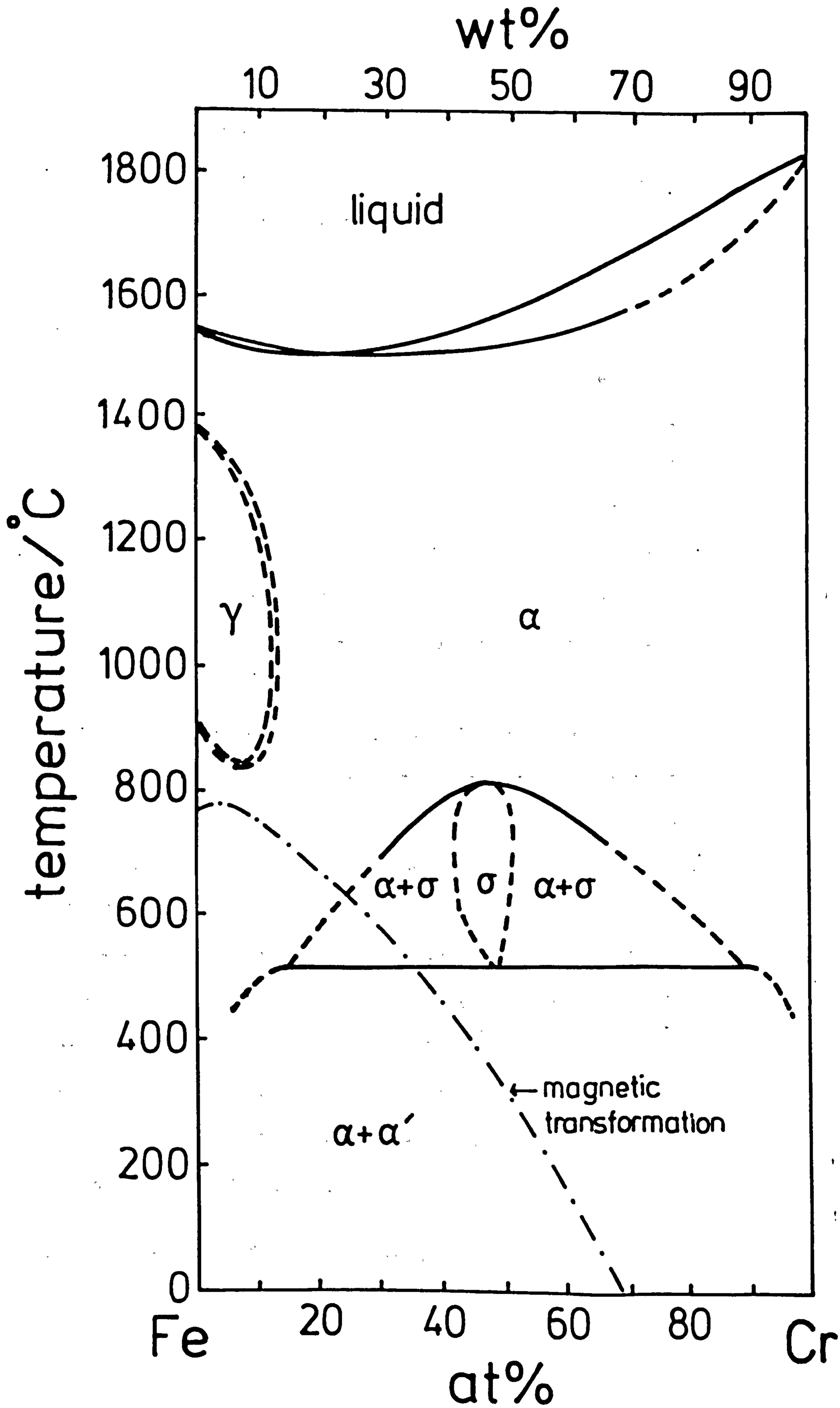
wt%
10
30
50
70
90
1800
1600
1400
1200
1000
800
600
400
200
0
temperature/°C
liquid
γ
α
α+σ
σ
α+σ
α+α'
magnetic
transformation
Fe
20
40
60
80
Cr
at%

chromium and nitrogen is the cause of embrittlement and suggested that the clusters are spherical within the spinodal while outside disc-shaped precipitates are formed by a nucleation and growth process (Hendry et al., 1979).

To overcome the embrittlement of ferritic stainless steel and in order to find a greater resistance to aqueous corrosion, the iron-chromium-nickel system has been extensively studied. Figure II.3 shows the stability of the γ -austenite phase at high temperature (900°-1300°C) in the ternary Fe-Cr-Ni diagram. Rees et al. (1949) studied the constitution of iron-chromium-nickel alloys after annealing between 650° and 800°C for periods up to 200 days. At 800°C, for example, an alloy containing 7wt%Cr and 10wt%Ni is fully austenitic but at 650°C it is a mixture of ferrite and austenite. There are also areas in the ternary system with compositions typical of austenitic stainless steels where σ -phase is detected but only with α -ferrite or with γ -austenite. Lena (1954) reviewed the formation of sigma-phase in iron-chromium and iron-chromium-nickel alloys and compared the influence of temperature, composition and different alloying elements on the precipitation of σ before concluding that sigma precipitates more rapidly in ferrite than in austenite. Shao & Machlein (1979) found that addition of molybdenum promotes sigma formation.

Keating (1956) showed that at 18wt% chromium a

Figure II.3

The iron-chromium-nickel system

(a) at 900° to 1300°C (Bain & Aborn, 1948)

(b) at 1100°C (Pugh & Nisbet, 1950)

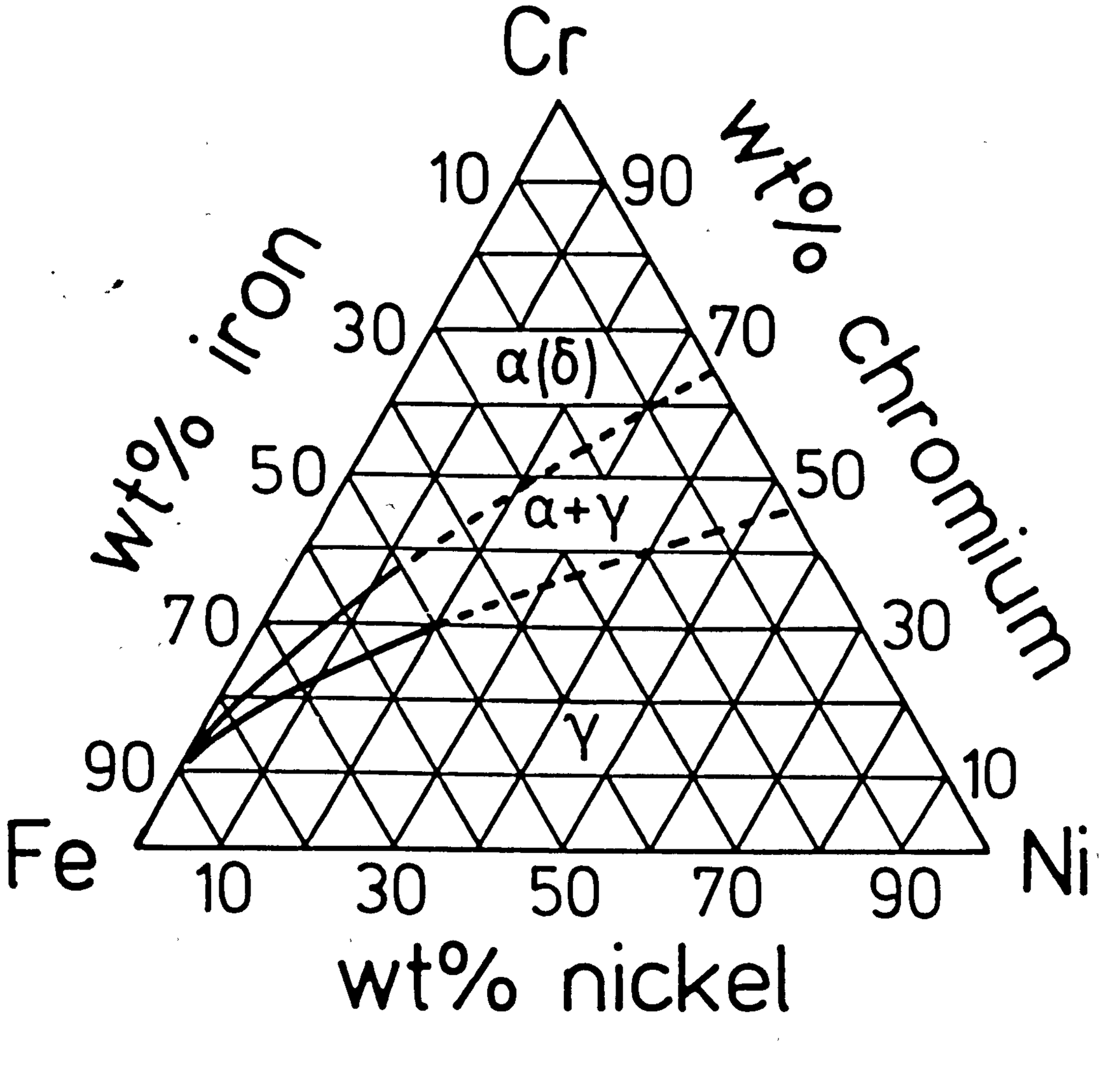
Cr
10
90
wt%
chromium
30
70
α(δ)
wt% iron
50
50
α+γ
70
30
γ
90
10
Fe
Ni
10
30
50
70
90
wt% nickel

(a)

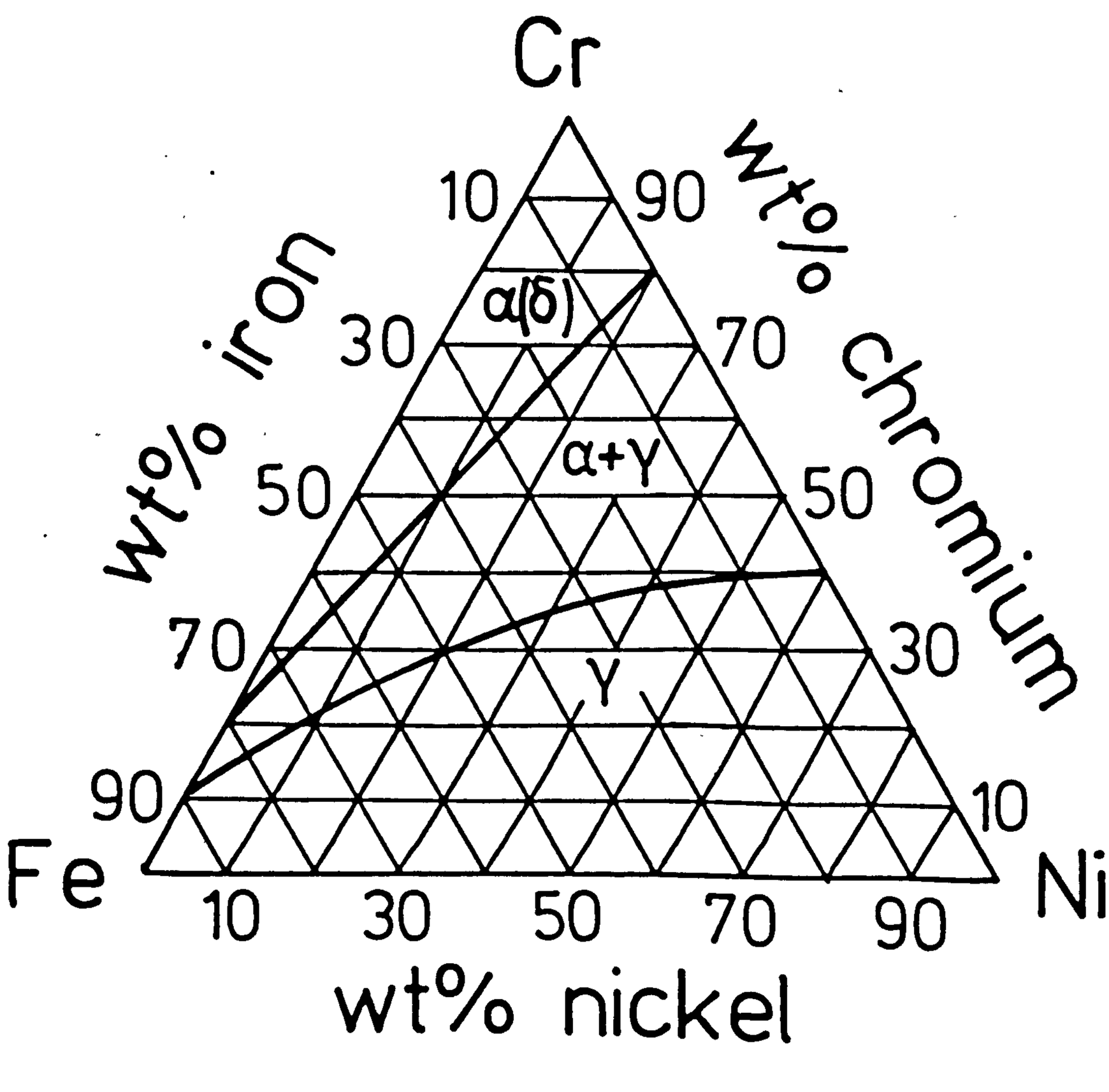
Cr
10
90
wt%
chromium
30
70
α(δ)
wt% iron
50
50
α+γ
70
30
γ
90
10
Fe
Ni
10
30
50
70
90
wt% nickel

(b)

minimum nickel content (8wt%) is required under normal cooling conditions to promote a fully austenitic structure which is stable at room temperature; see Figure II.4. The structure of conventional austenitic stainless steels can change under certain cooling conditions; for example by slow-cooling precipitation may occur and change the ratio of chromium to nickel in some areas and thus lead to the transformation $\gamma \longrightarrow \alpha$; see Figure II.4. By quenching to room temperature from temperatures at which the structure is fully austenitic, ferrite or martensite can be formed as well as unstable austenite which may transform to ferrite by cold-working (Bain & Aborn, 1948; Speich, 1973).

Recent development of austenitic steels started from the familiar 18-8 chromium-nickel steel, originally with some additions of carbon, which was traditionally the most economical fully austenitic material. Higher nickel contents are used to avoid the formation of α -ferrite which can produce edge cracking during hot-working. The effect of nickel on hot workability is maximised by lowering the carbon and nitrogen contents (Ludwigson & Brickner, 1969) and the effect of nickel in relation to nitrogen concentration was confirmed by Janson (1971). However the trend is now to lower carbon contents and the compositions of Standard American Iron and Steel Institute grades of austenitic stainless steels are given in Table II.1. To improve particular properties, alloying elements are added

Figure II.4

Effect of nickel and chromium on the constitution of 0.1wt%C steels

(Keating, 1956)

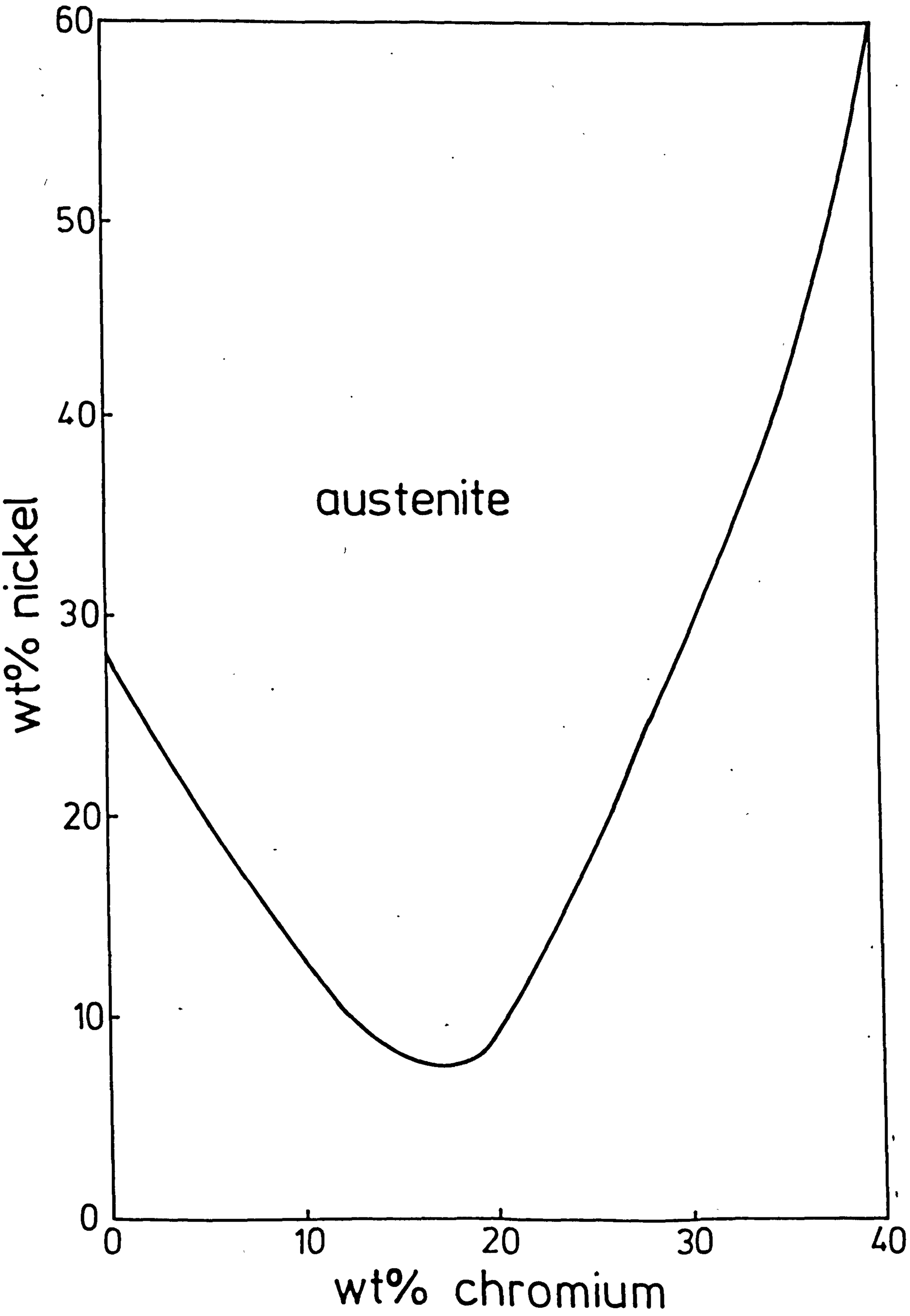
austenite
wt% nickel
wt% chromium
60
50
40
30
20
10
0
0
10
20
30
40

Table II.1

Typical compositions of some American Iron and Steel Institute (AISI) grades of austenitic stainless steels

steel AISI type	element wt%								
	C max	Mn max	P max	S max	Si max	Cr	Ni	Mo	Other
201	0.15	5.50-7.50	0.060	0.030	1.00	16.00-18.00	3.50-5.50		N 0.25
202	0.15	7.50-10.0	0.060	0.030	1.00	17.00-19.00	4.00-6.00		N 0.25
205	0.12-0.25	14.00-15.0	0.060	0.030	1.00	16.50-18.00	1.00-1.75		N 0.32-0.40
301	0.15	2.00	0.045	0.030	1.00	16.00-18.00	6.00-8.00		
302	0.15	2.00	0.045	0.030	1.00	17.00-19.00	8.00-10.00		
304	0.08	2.00	0.045	0.030	1.00	18.00-20.00	8.00-10.50		
L304	0.03	2.00	0.045	0.030	1.00	17.00-19.00	8.00-10.00		Cu 3.00-4.0
N304	0.08	2.00	0.045	0.030	1.00	18.00-20.00	8.00-10.50		N 0.10-0.16
316	0.08	2.00	0.045	0.030	1.00	16.00-18.00	10.0-14.0	2.00-3.00	
L316	0.03	2.00	0.045	0.030	1.00	16.00-18.00	10.0-14.0	2.00-3.00	
N316	0.08	2.00	0.045	0.030	1.00	16.00-18.00	10.0-14.0	2.00-3.00	N 0.10-0.16
L317	0.03	2.00	0.045	0.030	1.00	18.00-20.00	11.0-15.0	3.00-4.00	

and these may influence the range of austenite stability. For example, chromium, molybdenum, silicon, titanium, and niobium are considered as α -ferrite stabilisers whereas nickel, manganese, carbon and nitrogen increase the γ - austenite range. Usually austenitic stainless steels contain up to 0.08 or 0.15wt% carbon and Figure II.5 shows that in AISI steels (listed in Table II.1) $M_{23}C_6$ is the only carbide to be precipitated. Higher carbon contents are necessary to precipitate M_7C_3. $M_{23}C_6$ is essentially chromium carbide with other elements in partial substitution e.g. $(Cr,Fe)_{23}C_6$ and $(Cr,Fe,Mo)_{23}C_6$. Precipitation of $M_{23}C_6$ occurs at 500°-$950^{\circ}C$ the kinetics of which depend on the chemical composition of the steel. $M_{23}C_6$ precipitation causes chromium depletion (Joshi & Stein, 1972; Pande et al., 1977) so that transformation can occur on cooling. Chromium depletion is also the cause of a decrease in corrosion resistance. Thus, one way to reduce intergranular corrosion is to stabilize the steel with titanium or niobium since these elements have a greater affinity for carbon than chromium. The formation of $M_{23}C_6$ is therefore suppressed by the formation of NbC or TiC. Niobium is found to be a better stabiliser than titanium since after long aging times $M_{23}C_6$ tends to replace TiC (Thorwaldsson & Dunlop. 1979).

Nitrogen is a strong austenite stabiliser and if a small concentration of nitrogen is added less nickel is

Figure II.5

Effect of nickel and carbon on

Fe-18wt%Cr alloys

(Tuma et al., 1976)

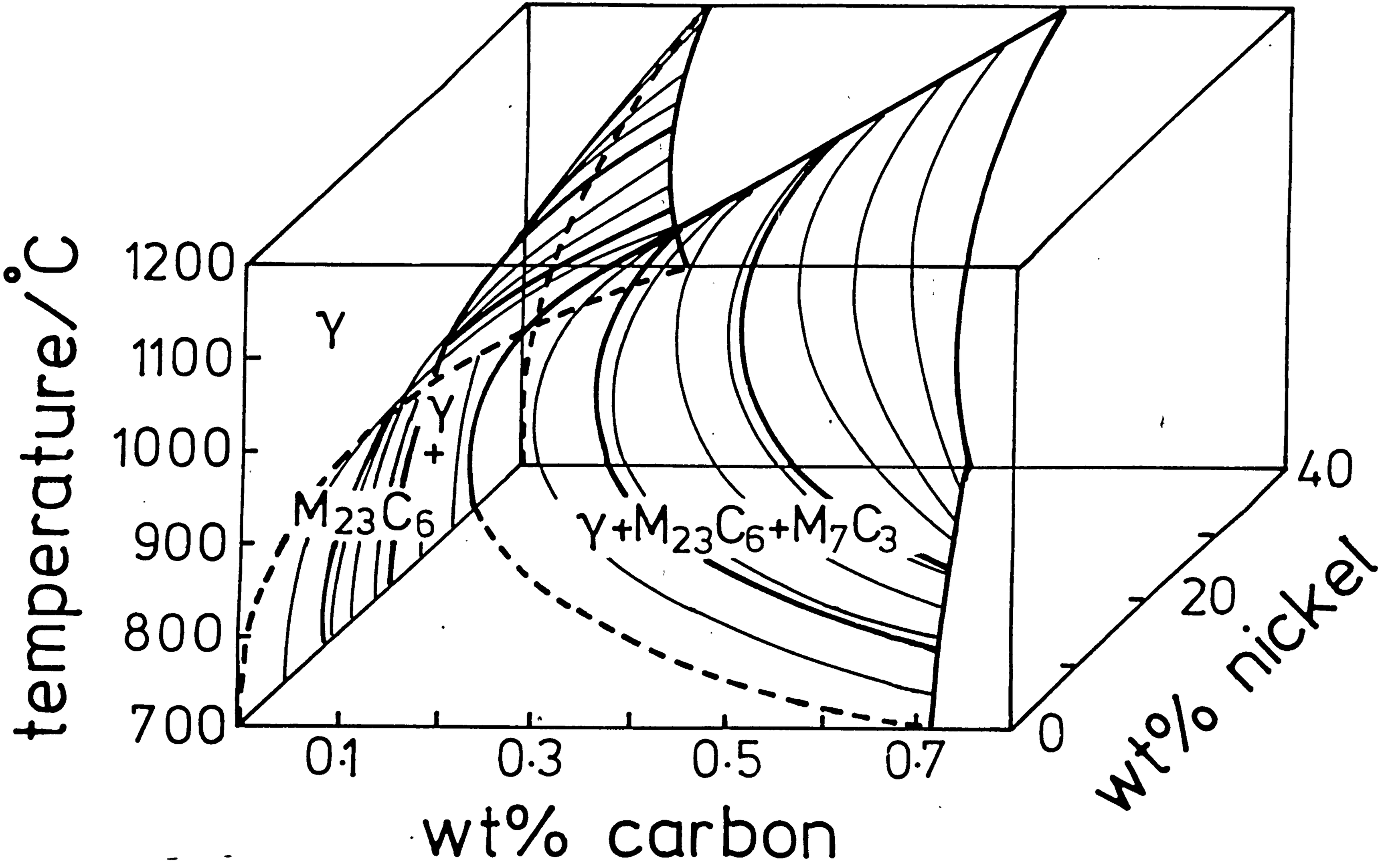
temperature/°C
1200
1100
1000
900
800
700
γ
γ+M23C6
γ+M23C6+M7C3
0·1
0·3
0·5
0·7
wt% carbon
0
20
40
wt% nickel

required to stabilise the γ-austenite. Tisinai et al. (1956) found it possible to obtain an austenitic structure in nickel-free steels containing 21-33wt% Cr at above 1200°C by adding suitable amounts of carbon and nitrogen; austenite could be retained at room temperature by rapid quenching but on slow cooling these alloys decomposed into ferrite, carbides and nitrides.

Imai et al. (1967b) studied the quaternary system Fe-18wt% Cr-C-N at 700°-1300°C for a range of carbon and nitrogen contents up to 0.5wt% and found that the carbon concentration influences the precipitation of chromium nitrides while nitrogen has a similar effect on the precipitation to chromium carbide. Thier et al. (1969) found that addition of nitrogen delays the precipitation of $M_{23}C_6$ as shown schematically by Figure II.6.

(c) AISI 316

AISI 316 is an austenitic steel containing chromium, nickel, molybdenum and manganese; see Table II.1. The designation "316" is sometimes preceded or followed by a letter (Table II.1) which indicates the carbon or nitrogen content of the alloy: "L" is used for low carbon content (0.03wt% maximum); "M" means that the steel contains between 0.03-0.06wt% C (medium carbon content); and "N" is used for steels containing between 0.10-0.16wt% nitrogen.

Figure II.6

Effect of nitrogen on $M_{23}C_6$ precipitation

(Thier et al., 1969)

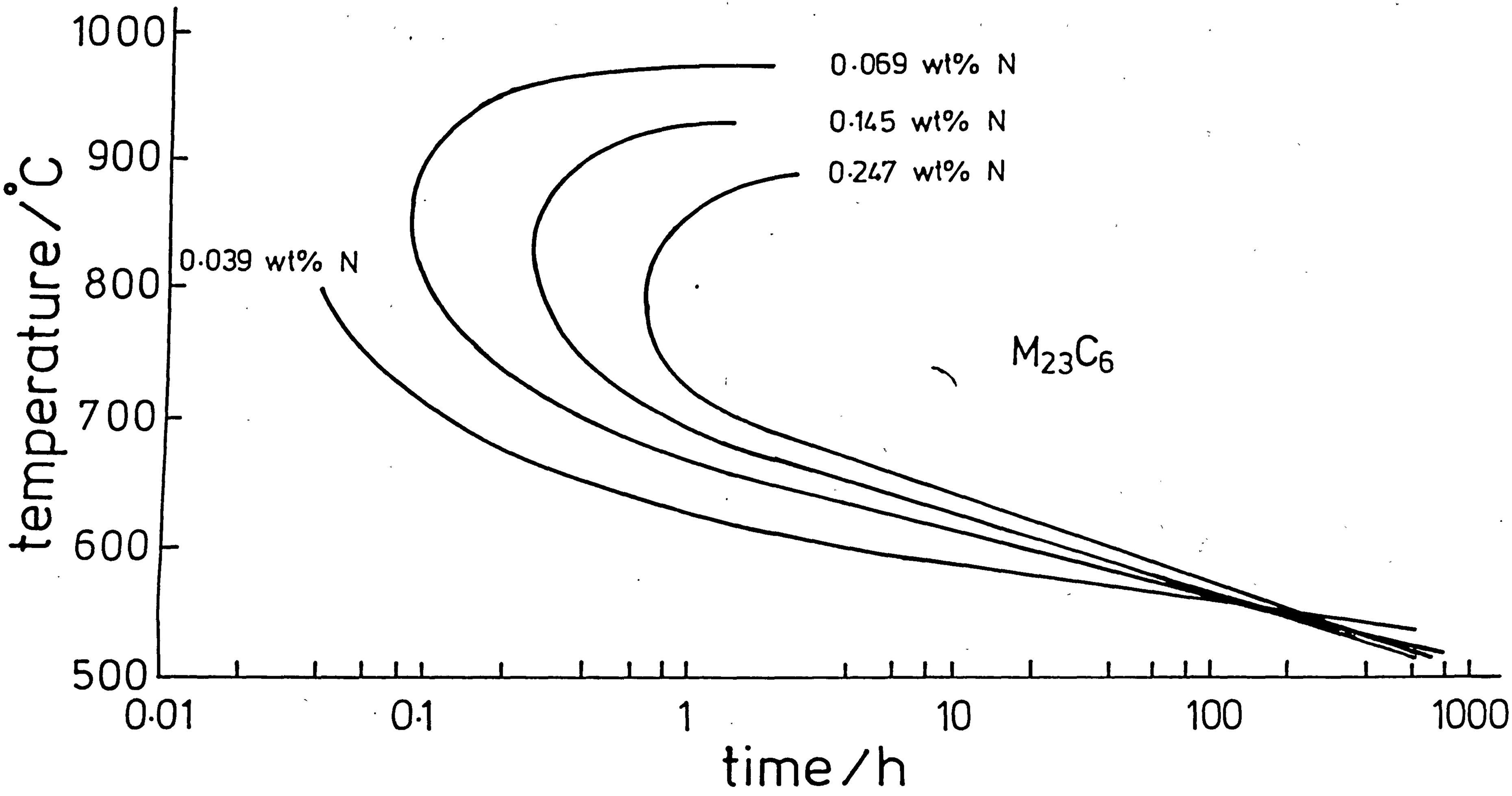
1000
900
800
700
600
500
temperature/°C
0·039 wt% N
0·069 wt% N
0·145 wt% N
0·247 wt% N
$M_{23}C_6$
0·01
0·1
1
10
100
1000
time/h

The maximum carbon content allowed in AISI 316 is 0.08wt%. AISI 316 is similar in composition to AISI 304 with addition of molybdenum (2.5wt%) and Defranoux (1974) showed that the presence of molybdenum accelerates the rate of passive film formation during aqueous corrosion. AISI 316 was originally developed for marine use because of its high corrosion resistance. It is now one of the steels used in nuclear power generation, especially as fuel pins in fast-breeder reactors. Among the many problems that may arise during service, swelling of the steel during irradiation occurs and leads to changes in the matrix composition (Bates, 1977; Brager & Garner, 1978) which result in the formation of complex intermetallic phases. Addition of Ti or Nb and Si (Johnston et al., 1976; Lee et al., 1979; Nagasaki et al., 1979), or cold working (Johnston et al., 1976), reduce swelling by the formation of finely dispersed coherent NbC or TiC precipitates and dislocations which act as sinks for vacancies. Low temperatures enhance radiation swelling, which reaches a maximum on cooling from 500°C (Foster & Boltax, 1980).

The fuel pins are usually 20% cold-worked and with this small degree of deformation formation of twins and recrystallisation phenomena are not significant. Partial recrystallisation of cold-worked material occurs over the range of temperature 580°-800°C (Yang & Spruiell, 1982), and gain growth below 950°C is negligible (Balbi & Silva, 1978).

Aging and creep of AISI 316 at 600°-800°C have been extensively studied. During aging carbides ($M_{23}C_6$, M_6C) and intermetallic phases (σ , χ , η) are observed. The kinetics of precipitation of $M_{23}C_6$ in AISI 316 as a function of carbon content and annealing temperature (grain-size) are shown in Figure II.7. The carbon content has no influence at temperatures lower than 700°C but higher annealing temperatures, which lead to a higher quenched-in vacancy concentration, enhance carbide precipitation. The time-temperature-precipitation diagrams for AISI L316 annealed and 20% cold-worked are shown in Figure II.8 and, as expected, cold working which introduces a high density of dislocations accelerates precipitation (Weiss & Stickler, 1972; Morris & Harries, 1978). However, the rate of precipitation of $M_{23}C_6$ is only affected for times less than one hour. Precipitation of carbides and the formation of intermetallic phases after aging for long times have been studied by optical and electron microscopy by several workers (Yamane & Veda, 1963; Blenkinsop & Nutting, 1967; Mimino et al., 1969; Weiss & Stickler, 1972; Spruiell et al., 1973; White & Le May, 1974; Lai & Meshkat, 1978; Stoter, 1981). Unfortunately the results reported by different authors are not always consistent and comparable but there is general agreement that carbides precipitate before the intermetallic phases.

Nitrogen is also added to AISI 316 to improve mechanical

Figure II.7

Kinetics of precipitation of $M_{23}C_6$ in AISI 316 steel (Weiss & Stickler, 1972)

(a) effect of annealing temperature

(b) comparison of types 316 (0.066wt%C and L316 (0.023wt%C)

(a)

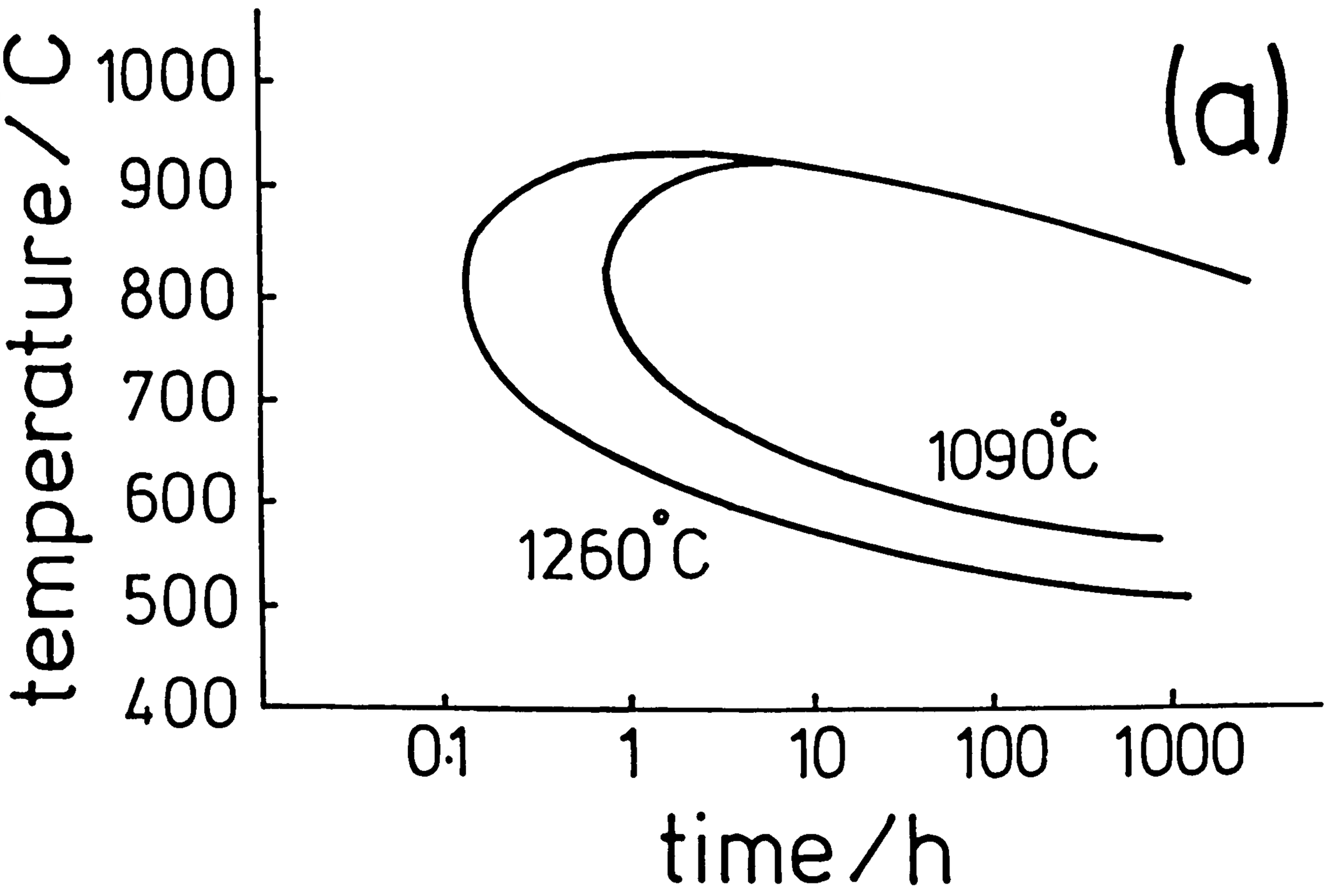
temperature/°C
1000
900
800
700
600
500
400
1090°C
1260°C
0·1
1
10
100
1000
time/h

(b)

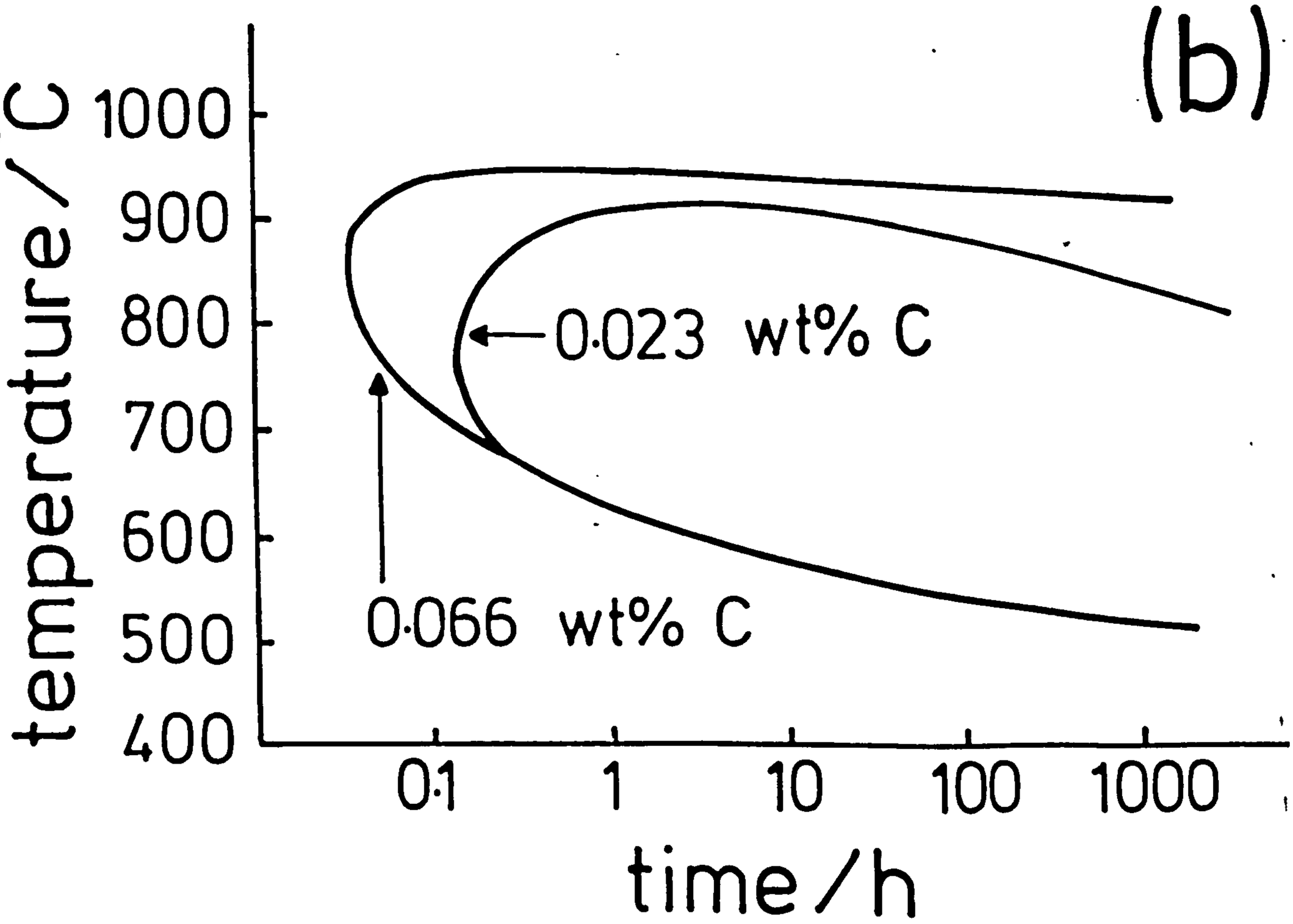
temperature/°C
1000
900
800
700
600
500
400
0·023 wt% C
0·066 wt% C
0·1
1
10
100
1000
time/h

Figure II.8

Time-temperature-precipitation diagrams
for AISI L316

(a) annealed (Weiss & Stickler, 1972)

(b) 20% cold-worked (Spitznagel & Stickler, 1974)

annealing temperature — — 1090°C
— 1260°C

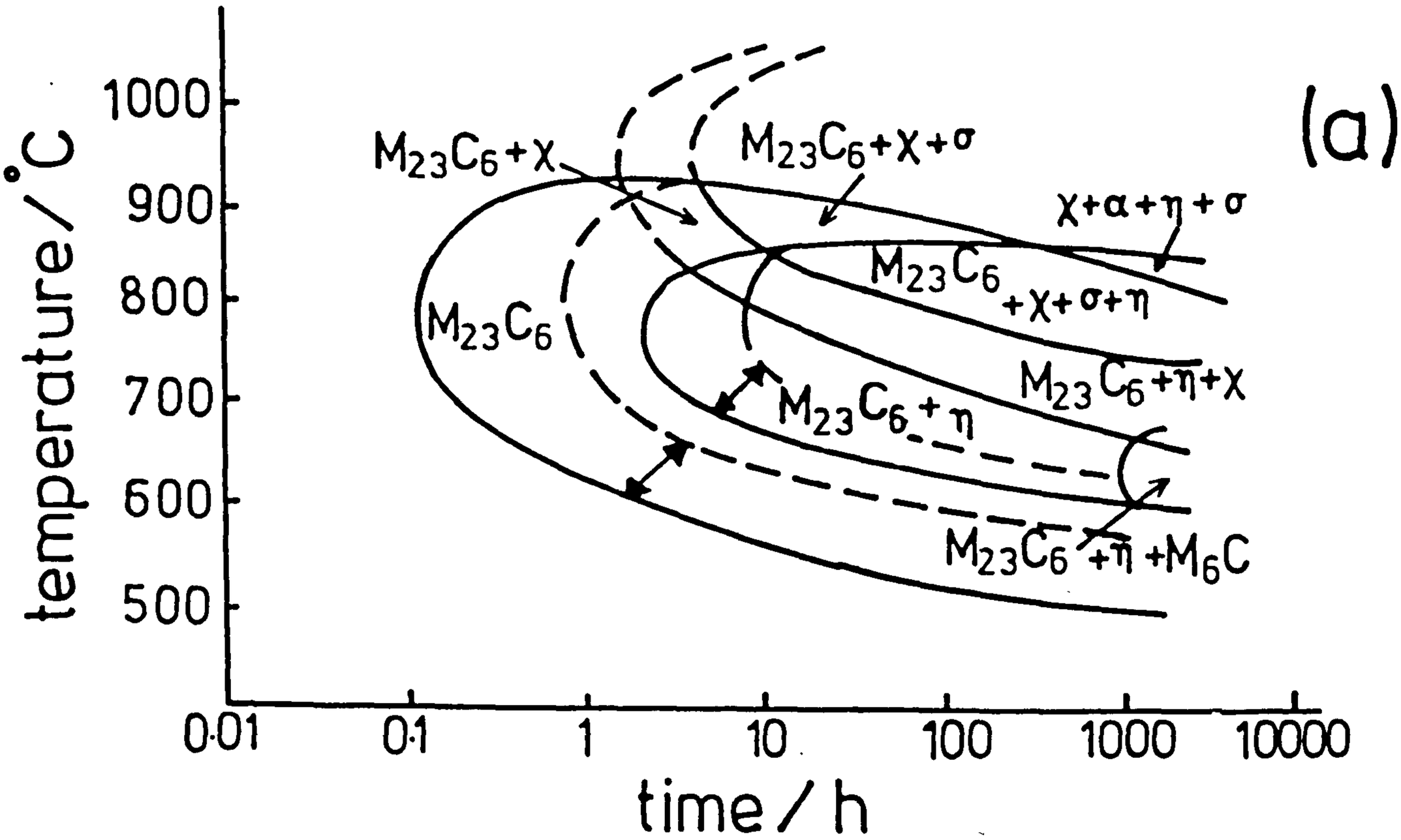

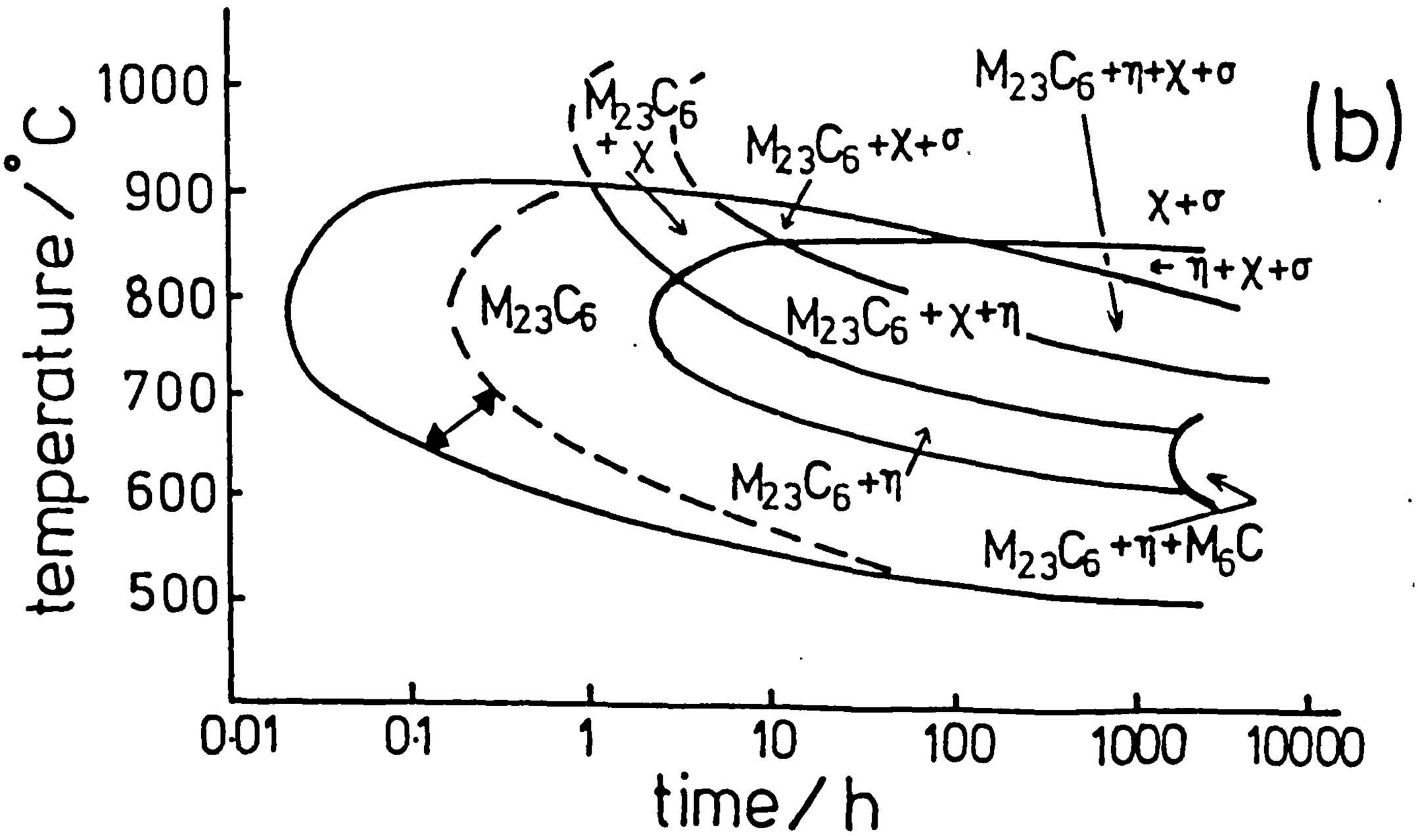

properties. However, the strengthening effects obtained by addition of nitrogen can not be explained by solution hardening mechanisms alone (Norström, 1977). The contribution of nitrogen to yield stress can be divided into two parts: (i) a temperature-dependent contribution over the range 10^{o}-600^{o}C (true solution hardening) independent of grain-size, and (ii) an athermal contribution with an increase of the grain-size coefficient in the Hall-Petch equation as the nitrogen concentration increases. Thus, a combination of nitrogen addition and grain-size refinement gives very high strengths to AISI 316 in the annealed state.

II.2 Nitriding of iron and iron alloys

(a) The iron-nitrogen system

The iron-nitrogen system is shown in Figure II.9 with unit-cell dimensions and composition limits of the different iron-nitrogen phases in Table II.2. The α' and α'' phases are not represented on the diagram; α'-nitrogen martensite is obtained by quenching nitrogen-austenite and α''-$Fe_{16}N_2$ is formed by tempering nitrogen-martensite or aging super-saturated nitrogen-ferrite at low temperature.

γ'-Fe_4N has a face-centred cubic arrangement of iron atoms as in austenite and the nitrogen occupies one set of octahedral interstices in an ordered manner as shown in

Figure II.9

The iron-nitrogen diagram

(Jack, 1951a)

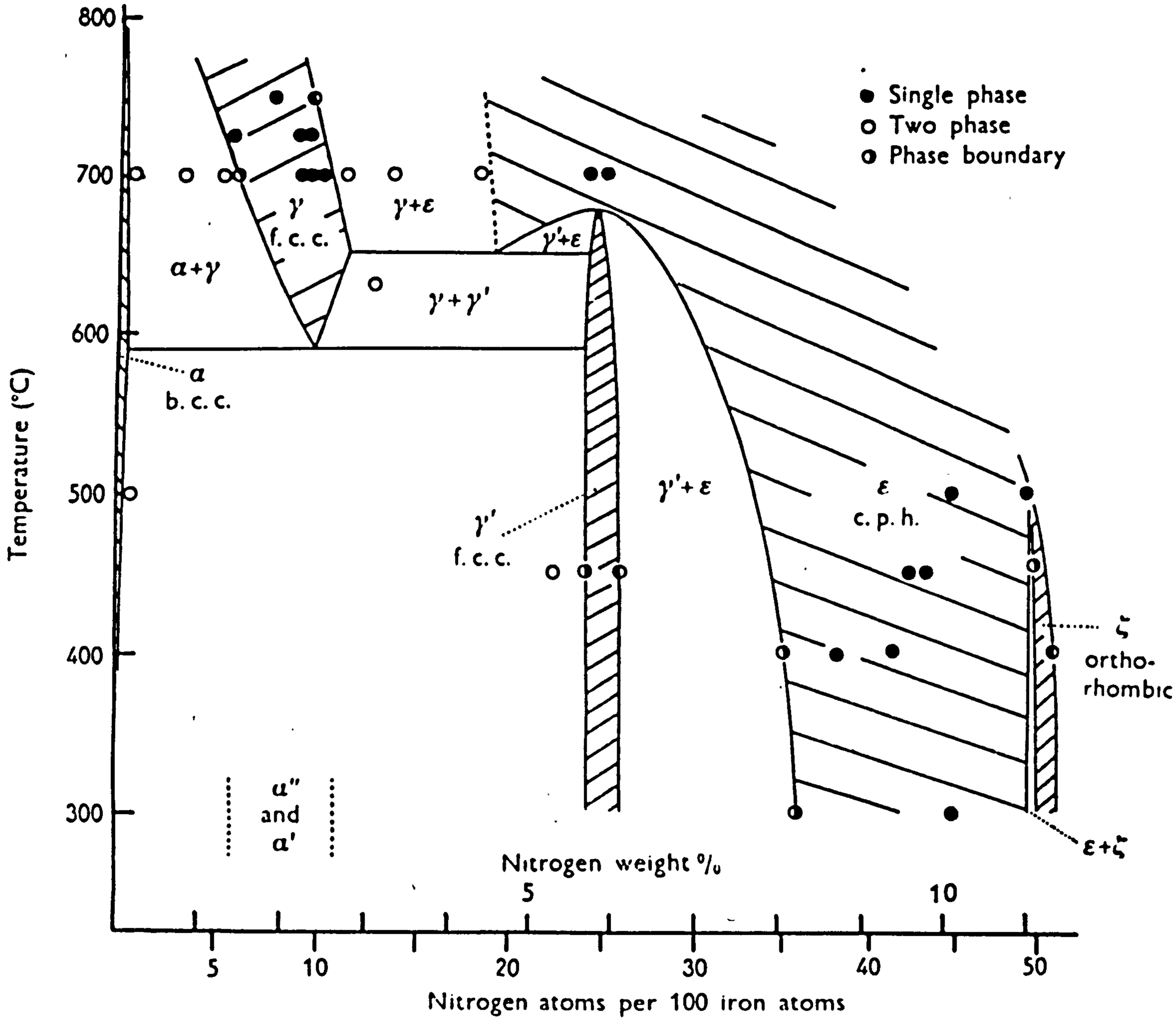
Single phase
Two phase
Phase boundary
Temperature (°C)
800
700
600
500
400
300
γ
f. c. c.
γ+ε
γ'+ε
α+γ
γ+γ'
α
b. c. c.
γ'
f. c. c.
γ'+ε
ε
c. p. h.
ζ
ortho-
rhombic
ε+ζ
α"
and
α'
Nitrogen weight %
5
10
5
10
20
30
40
50
Nitrogen atoms per 100 iron atoms

Figure II.10. The basic structure of γ'-Fe_4N is therefore face-centred cubic but the nitrogen atoms have a primitive cubic arrangement which give superlattice reflexions on X-ray diffraction patterns (Jack, 1948).

ε-Fe_2N_{1-x} has a wide range of composition and a close-packed hexagonal arrangement of iron atoms; Jack (1952) reported a superstructure with $a' = \sqrt{3}\,a$, $c' = c$. Figure II.11 shows that $\underline{a}$ increases with nitrogen content more quickly than $\underline{c}$ so the $\underline{c}/\underline{a}$ ratio decreases.

(b) The iron-chromium-nitrogen system

The chromium-nitrogen diagram (Figure II.12) shows the existence of two chromium nitrides: CrN and Cr_2N. CrN has a face-centred cubic structure of lattice parameter 4.150 Å (Mortimer, 1971), while Cr_2N (Mortimer, 1971) has a close-packed arrangement of metal atoms with:

$$\underline{a} = 4.790\ \text{Å}, \quad \underline{c} = 4.469\ \text{Å}, \quad \underline{c}/\underline{a} = 0.933.$$

Nucleation of Cr_2N in α-ferrite (Bywater & Dyson, 1975) is heterogeneous with small needles in areas of high dislocation density and large single needles or globular precipitates in ferrite grain-boundaries (Lagneborg, 1967). The $\langle 311 \rangle_\alpha$ growth direction corresponds to a minimum of mismatch and elastic strain energy; Lagneborg (1967) reported a $(0001)_{Cr_2N} // (011)_\alpha$ and $(10\bar{1}1)_{Cr_2N} // (101)_\alpha$

Table II.2

Unit-cell dimensions and composition limites of iron-nitrogen phases

phase symbol	crystal structure	composition limits	unit-cell dimensions Å	wt% N	references
α -ferrite	b.c.c.	0-0.1wt% N, $Fe-FeN_{0.004}$	a = 2.8663 a = 2.8690	0 0.1	Ferguson (1981)
γ -austenite	f.c.c.	0-2.8wt% N, $Fe-FeN_{0.12}$	a = 3.615 a = 3.654 a = 3.571 a = 3.645	1.5 2.8 0 2.4	Paranjpe et al. (1950) Jack (1951a)
γ′ -Fe_4N	cubic	5.29-5.7wt% N, $FeN_{0.23}-FeN_{0.24}$ 5.75-6.10wt% N, $FeN_{0.24}-FeN_{0.26}$	a = 3.791 a = 3.801 a = 3.787 a = 3.795	5.29 5.71 5.75 6.10	Paranjpe et al. (1950) Jack (1951a)
ε -Fe_2N_{1-x}	c.p. hexagonal (dimensions for pseudo-cell)	5.70-11.0wt% N, $FeN_{0.24}-FeN_{0.49}$	a = 2.660; c = 4.344 a = 2.764; c = 4.420 a = 2.657; c = 4.380 a = 2.770; c = 4.432	5.70 11.0 7.30 11.0	Jack (1952) Paranjpe et al. (1950)
ζ -Fe_2N	orthorhombic (dimensions for pseudo-cell)	11.1-11.3wt% N, $FeN_{0.50}-FeN_{0.51}$	a = 2.762; b = 4.830; c = 4.416	11.3	Jack (1948)
α′ -martensite	b.c. tetragonal	as γ-austenite	a = 2.851; c = 3.071	2.30	Jack (1951a)
α″ -$Fe_{16}N_2$	tetragonal	3.1wt% N, $FeN_{0.13}$	a = 5.72; c = 6.29	3.1	Jack (1951b)

Figure II.10

Crystal structure of γ -nitrogen austenite and γ'-Fe_4N (Jack, 1949)

γ

nitrogen
austenite

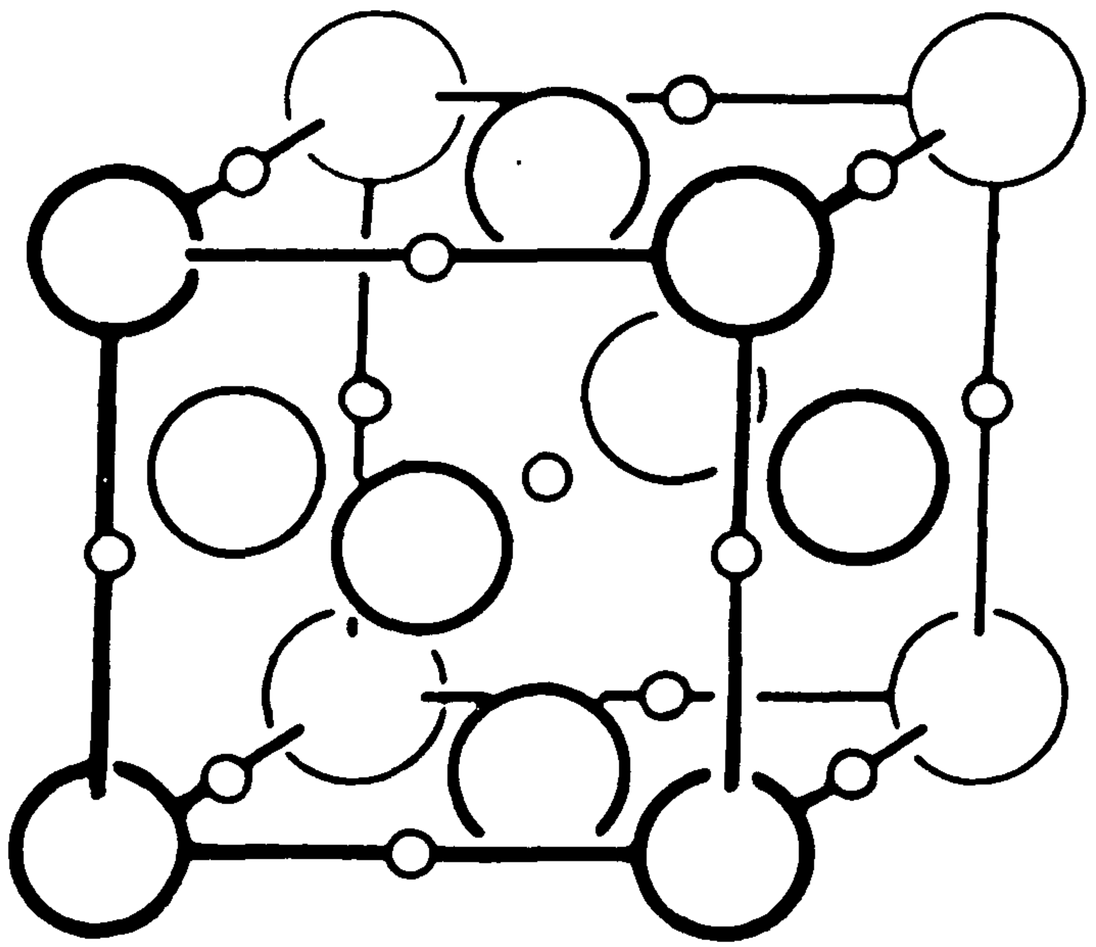

γ′

Fe_4N

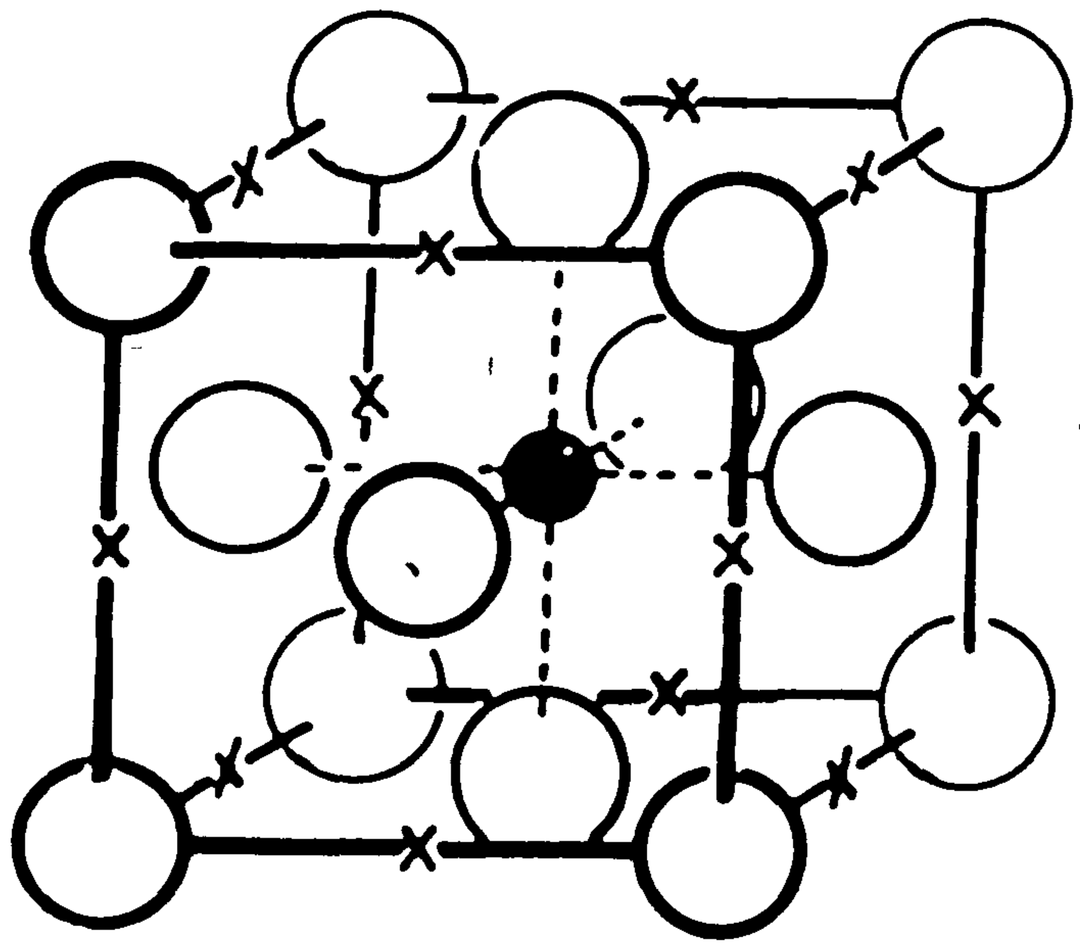

○ Fe atoms

× unoccupied interstices

o octahedral interstices
1 in 10 randomly filled

● N atom

Figure II.11

Variation of unit-cell dimensions

of ε -Fe_2N_{1-x} with nitrogen content

(Jack, 1952)

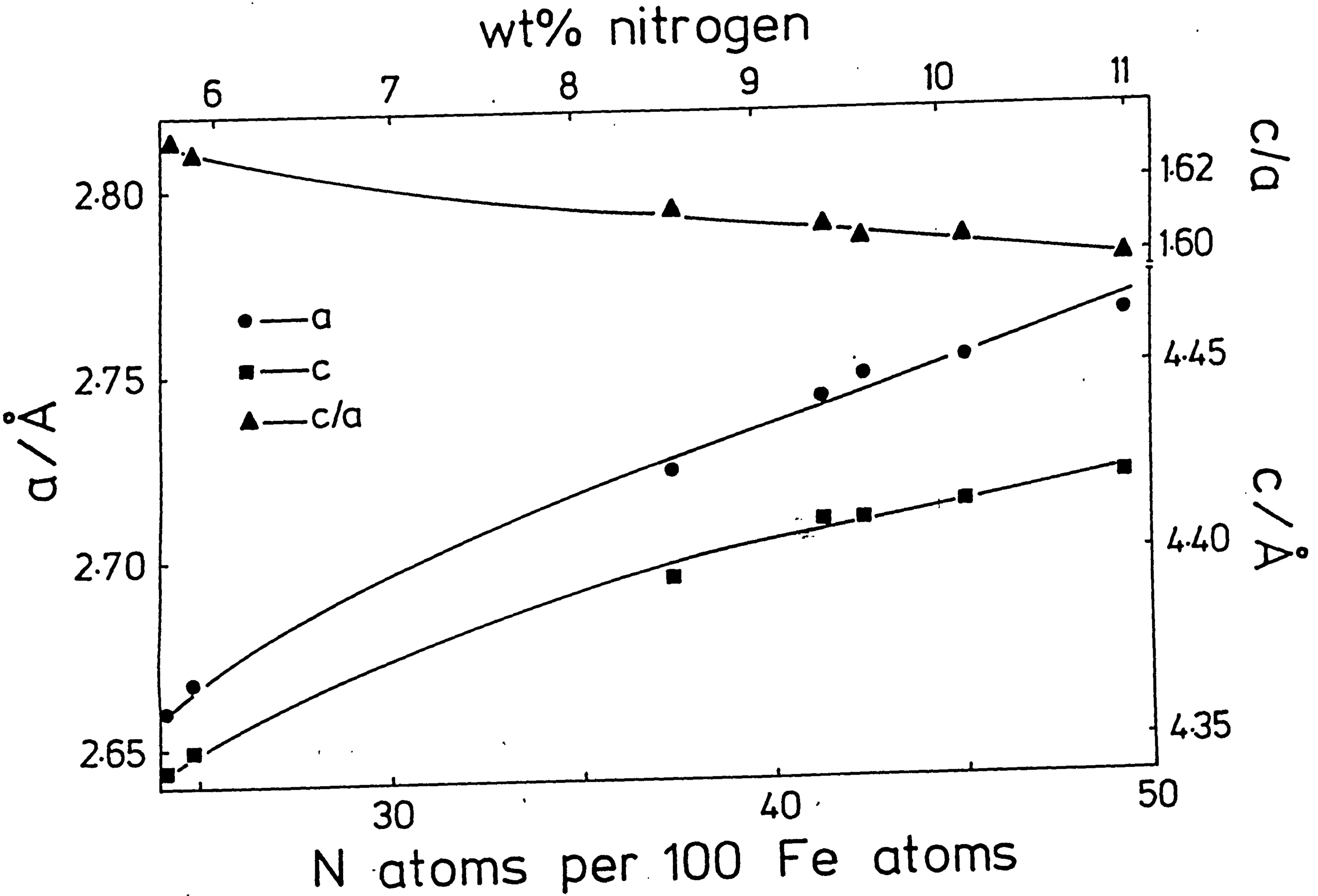
wt% nitrogen
6
7
8
9
10
11
2·80
2·75
2·70
2·65
a/A°
●—a
■—c
▲—c/a
1·62
1·60
4·45
4·40
4·35
c/A°
c/a
30
40
50
N atoms per 100 Fe atoms

Figure II.12

The chromium-nitrogen diagram

(Adcock, 1926)

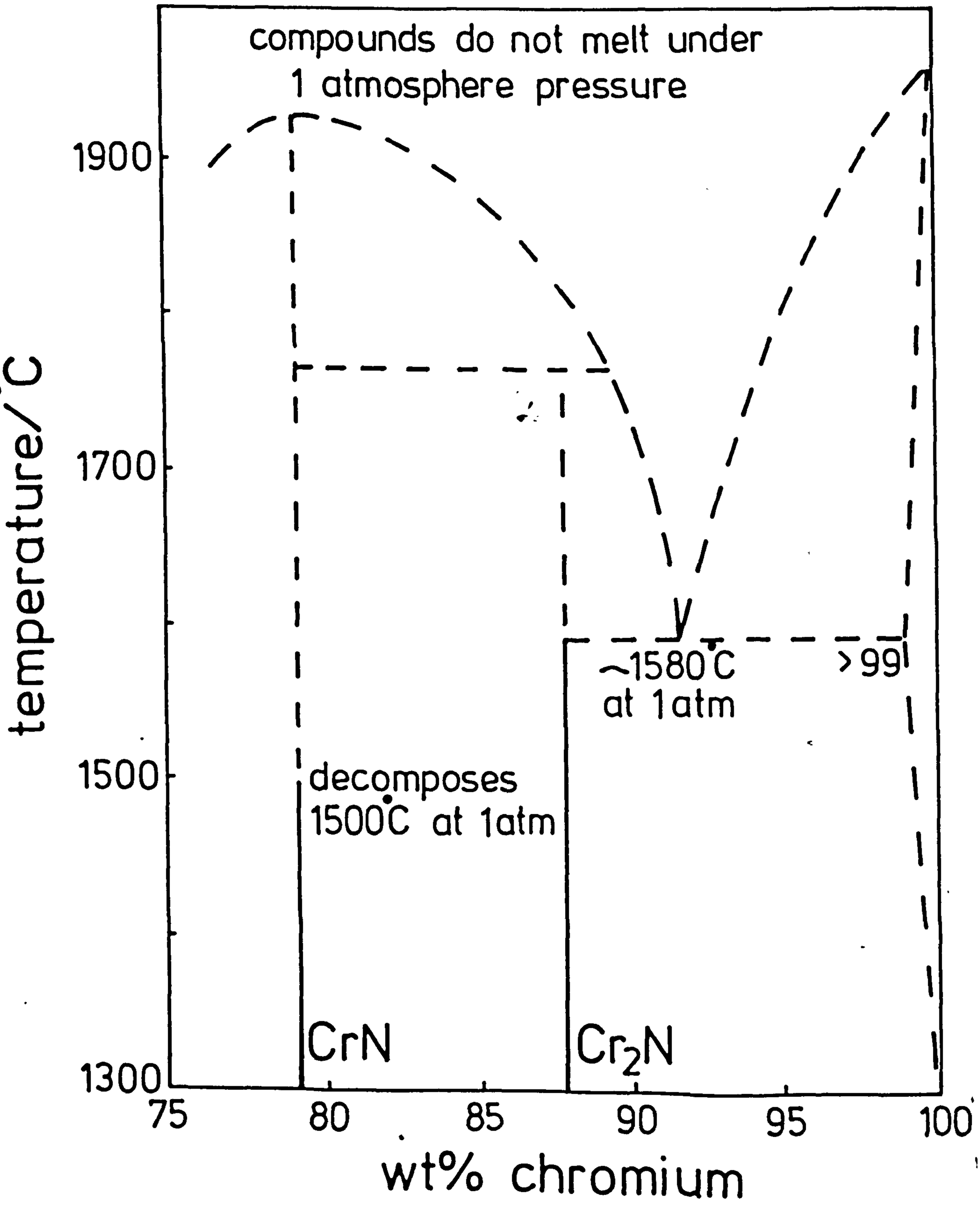
compounds do not melt under
1 atmosphere pressure
1900
1700
1500
1300
temperature/°C
decomposes
1500°C at 1atm
y
~1580°C
at 1atm
>99
CrN
Cr2N
75
80
85
90
95
100
wt% chromium

orientation relationship similar to that for the precipitation of ε -iron carbide in martensite (Jack, 1951c).

Nitrogen has a profound effect on the γ loop in Fe-Cr alloys (Turkdogan & Ignatowicz, 1958), and Masumoto & Imai (1969) claimed that the effect of nitrogen in stabilising γ -austenite is about twenty-five times that of nickel. The ternary diagram Fe-Cr-N has been studied by Imai et al. (1967a) between 700°-1300°C in the range 0-40wt% Cr and up to 1wt% N and the different nitrides precipitated, depending on the nitrogen content and temperature, were γ'-Fe_4N, CrN and Cr_2N. No γ'-Fe_4N and CrN were detected at 800°C or higher; Figure II.13 shows the Fe-Cr-N phase diagrams after Imai et al. at 700° and 800°C. In the same system, Turkdogan & Ignatowicz (1958) showed that chromium increases the solubility of nitrogen and that CrN is present at 600°C.

(c) The iron-chromium-nickel-nitrogen system

In the Fe-18wt% Cr-Ni-N system at 500°-1300°C for 0-20wt% nickel and up to 0.4wt% nitrogen Masumoto & Imai (1969) found that the only nitride precipitate was Cr_2N and that the solubility of nitrogen in γ -austenite decreases with increasing nickel content. The effect of both nickel and chromium and the solubility of nitrogen in γ decreases with increasing temperature (Figure II.14) indicating an

Figure II.13

The iron-chromium-nitrogen system at 700° and 800°C

(Imai et al., 1967a)

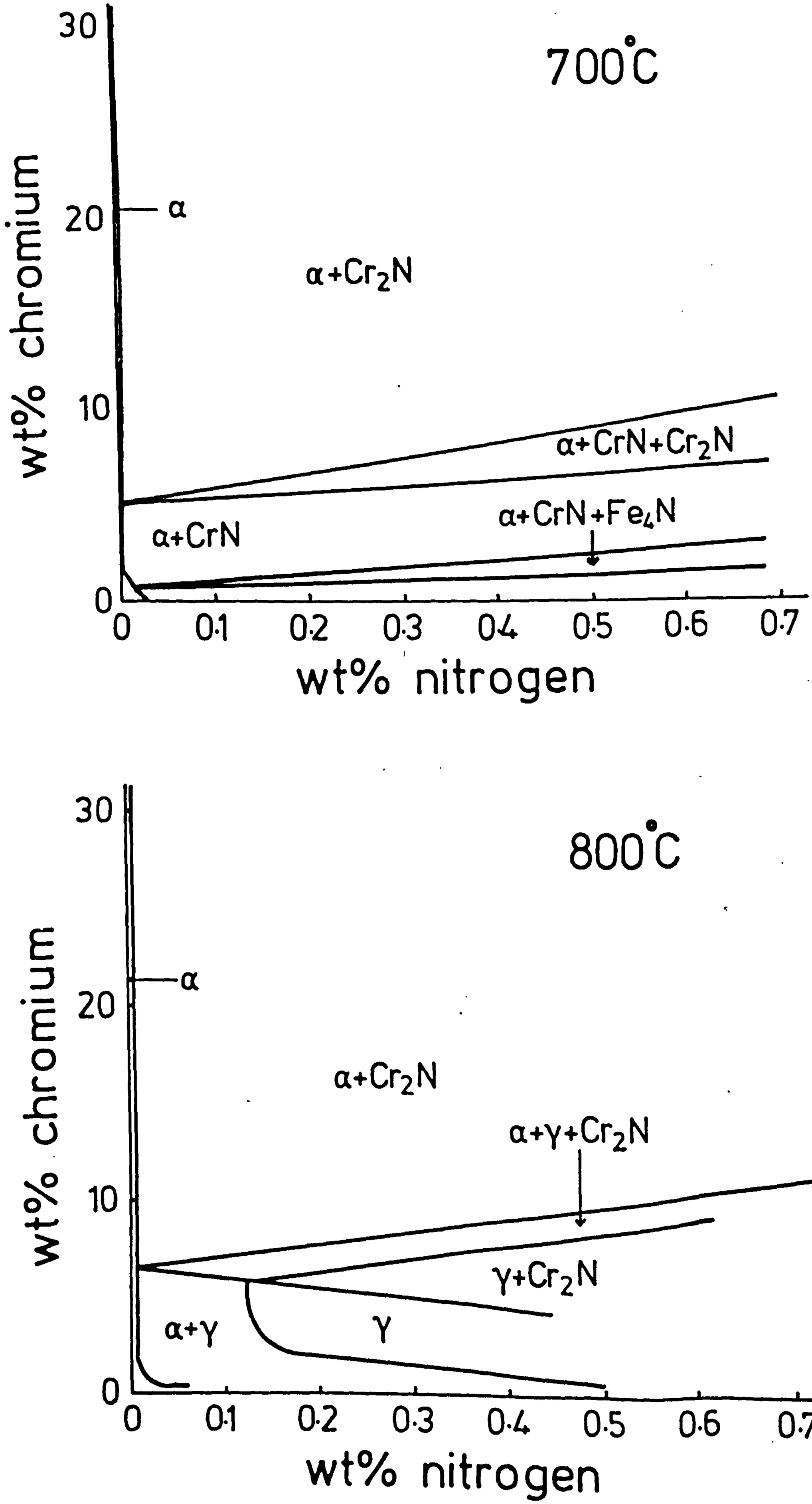
700°C
30
20
10
0
chromium
wt% c
α
α+Cr2N
α+CrN+Cr2N
α+CrN+Fe4N
α+CrN
0
0·1
0·2
0·3
0·4
0·5
0·6
0·7
wt% nitrogen
800°C
30
20
10
0
wt% chr
α
α+Cr2N
α+γ+Cr2N
γ+Cr2N
α+γ
γ
0
0·1
0·2
0·3
0·4
0·5
0·6
0·7
wt% nitrogen

Figure II.14

Effect of chromium concentration on the solubility of nitrogen at 1 atm in pure iron and stainless steel

● —— Fe (Corney & Turkdogan, 1955)

■ —— Fe -Cr (Turkdogan & Ignatowicz, 1958)

▲ —— 18-8 stainless steel (Turkdogan & Ignatowicz, 1959)

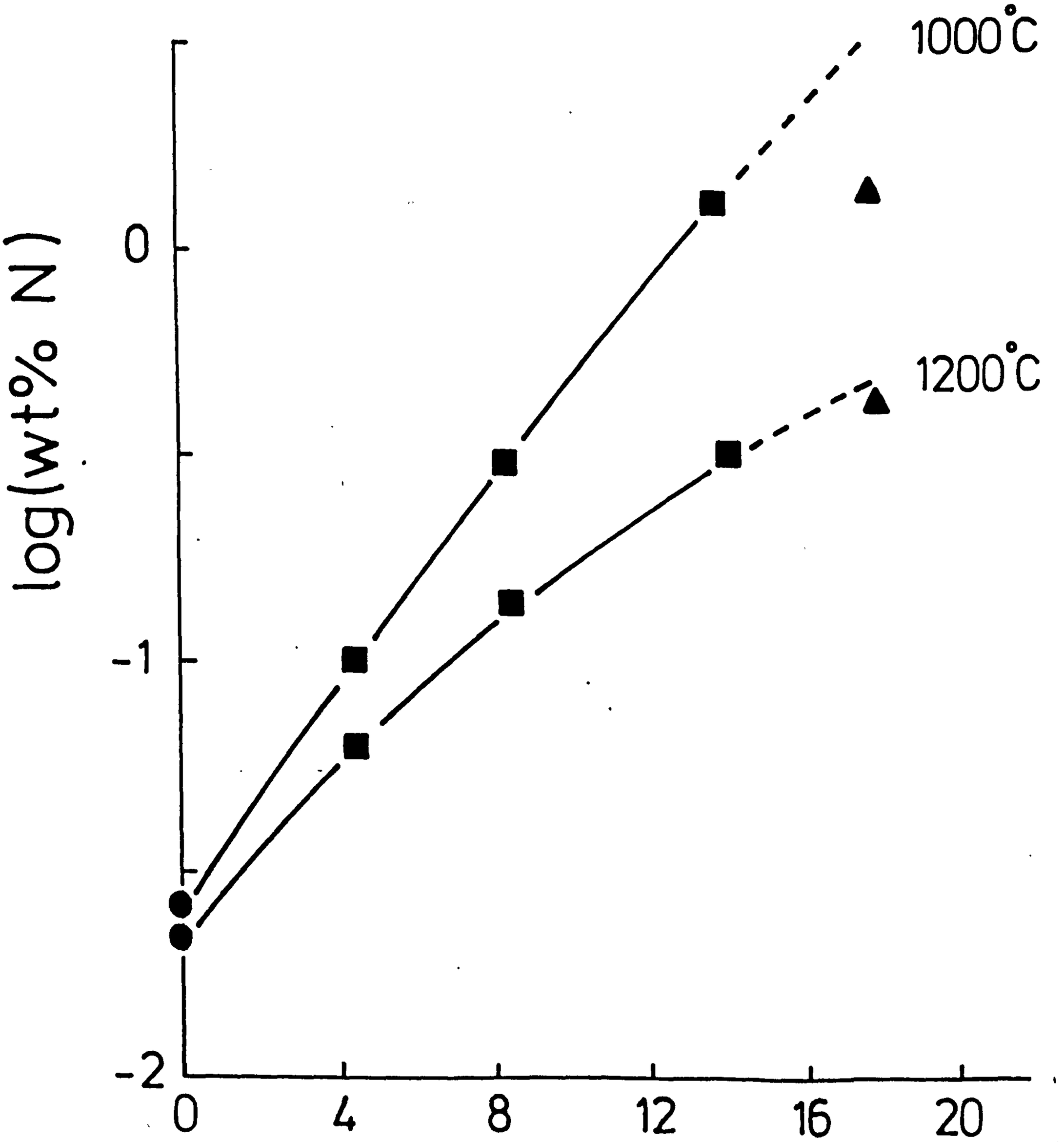

increase in the heat of solution of nitrogen in stainless steels with increasing temperature.

(d) Precipitation in nitrided iron-chromium and iron-chromium-nickel alloys

Only three nitrides have been reported when nitriding iron-nickel alloys: γ'-$(Fe,Ni)_4N$ (Arnott & Wold, 1960; Atkinson & Bodsworth, 1970; Handley, 1974); Ni_3N (Arnott & Wold, 1960) and ε-Fe_2N_{1-x} (Atkinson & Bodsworth, 1970; Handley, 1974).

γ'-$(Fe,Ni)_4N$ has the face-centred cubic Fe_4N structure with a high solubility of nickel (0-80wt%) and its lattice parameter decreases with nickel content (Arnott & Wold, 1960). Wiener & Berger (1955) proposed an ordered structure for Fe_3NiN in which nickel atoms replace the iron atoms at the corner of the unit-cell. Further investigation by Arnott & Wold (1960) on $(Fe,Ni)_4N$ showed by comparing the intensities of the superlattice reflections (100) and (110) of this phase that the first nickel atom is at the corner of the unit-cell while other nickels substitute randomly for iron atoms.

By nitriding Fe-Cr or Fe-Cr-Ni alloys at high nitrogen potentials a multilayer subscale of nitride precipitates is obtained which can be divided into a compound layer or "white layer" formed by ε-Fe_2N_{1-x} and

γ'-Fe_4N and a diffusion layer of CrN or Cr_2N in the matrix (Lebrun et al., 1972; Lightfoot & Jack, 1975; Mittemeijer et al., 1981). When nitriding in ammonia: hydrogen mixtures the amount of nitrogen introduced can be controlled by the nitrogen potential (see Chapter III.4). Lehrer (1930) showed that the formation of iron nitrides depends on the nitrogen potential and on the temperature. Therefore as reported by Lightfoot & Jack (1975) the formation of the "white layer" is controlled by the NH_3:H_2 ratio. Considering the formation of the nitrided layer of an iron-chromium alloy at high nitrogen potential with the presence of a compound layer the following equilibria going from the surface towards the centre should be expected:

$$\text{gas} \rightleftharpoons \varepsilon\text{-}Fe_2N_{1-x} \quad \text{(high nitrogen)} \qquad \ldots\ \text{II.1}$$

$$\varepsilon\text{-}Fe_2N_{1-x}\,\text{(low nitrogen)} \rightleftharpoons \gamma'\text{-}Fe_4N\ \text{(high nitrogen)} \qquad \ldots\ \text{II.2}$$

$$\gamma'\text{-}Fe_4N\ \text{(low nitrogen)} \rightleftharpoons CrN \text{ or } Cr_2N \qquad \ldots\ \text{II.3}$$

$$CrN \text{ or } Cr_2N \rightleftharpoons \alpha\text{ - ferrite (high nitrogen)} \qquad \ldots\ \text{II.4}$$

The gradient in nitrogen concentration results in the growth of the nitrided layer. The formation of the different iron-nitrides has an influence on nitriding kinetics. A high nitriding rate is obtained when the nitrogen solubility is in equilibrium with $\varepsilon\text{-}Fe_2N_{1-x}$ and then the nitriding rate

decreases and is governed by the nitrogen concentration in equilibrium with γ'-Fe_4N (Jack & Stoney, 1972). With chromium steels no discontinuity in nitriding rate was observed even when γ'-Fe_4N precipitates, but a high supersaturation was found to be necessary to form γ' in these alloys and this supersaturation is maintained when Fe_4N is present (Lightfoot & Jack, 1975). These authors also reported that when nitriding chromium alloys containing carbon, the carbon diffuses ahead of the nitriding front towards the centre of the sample and the case depth decreases as the carbon content increases.

Nitriding iron-chromium alloys is widely used in industry (either by gas nitriding or iron nitriding) and especially in the car industry e.g. in case hardening gears. Nitriding is also applied in petrochemical plants and in aerospace applications where austenitic stainless steels are used. The nitriding behaviour of austenitic stainless steel has been widely investigated, especially those steels stabilized with titanium (Kindlimann & Ansell, 1970; Evans, 1972; Smith & Evans, 1973; Unthank et al., 1974). Nitriding rates are determined by internal nitriding theory (see Chapter VII) and a multilayer case is formed.

The nitriding behaviour of AISI 316 in ammonia:hydrogen mixtures at 500°-800°C has been studied at the C.E.G.B. and U.K.A.E.A. laboratories. Nitriding in pure ammonia at low temperatures ($<600^{\circ}C$) does not given an even nitrided layer

(Cordwell et al., 1974; Wilson, 1978) but nitriding AISI 316 was reported to be controlled by diffusion of nitrogen in austenite. A two-layer case is found between 450° and 700°C composed of a thin ($<5\ \mu m$) surface layer of mixed nitrides ε -Fe_2N_{1-x} and γ' -Fe_3NiN and an inner case of CrN. Wilson (1978) reported the presence of α - ferrite in the inner nitrided layer at 550° and 600°C and also that at these temperatures the case is heavily cracked while Cordwell et al. (1974) found a thinner case at 700°C than at 600°C.

Nitriding in ammonia:hydrogen gives an even nitrided layer only for temperatures $\geqslant 750°C$, and at 800°C nitriding does not seem to be affected by nitrogen potential. Only a slight difference in the case depth is observed between $P_{NH_3} / P_{H_2}^{3/2} = 0.073$ and $P_{NH_3} / P_{H_2}^{3/2} = 0.013$ (Tyfield & Mackway, 1975) although nitriding in NH_3:H_2 mixtures is reported to obey a parabolic law. It should be noted however that these workers maintained the ammonia flow rate constant and changed the hydrogen flow rate which meant that an increase in the ammonia partial pressure was achieved by decreasing the total flow rate of gas through the furnace. Thus, because ammonia dissociation increases as the flow rate decreases (see Table III.2), the real nitrogen potential was probably nearly constant in all experiments. No iron nitrides were observed under these experimental conditions.

A more complete study has been carried out by Lebrun

et al. (1972) on ion nitriding 18-10 stainless steel in pure ammonia at 500°-800°C. A difference in phase distribution between 600° and 650°C was observed which corresponds to a difference in nitriding kinetics. Nitriding at 600°C and lower temperatures gives a high nitriding rate which is related to the presence of ferrite in the nitrided layer next to the core, and the authors concluded that nitriding is therefore controlled by diffusion of nitrogen in ferrite; nitriding at higher temperatures is controlled by nitrogen diffusion in austenite. The phase distribution in the nitrided layer at temperatures $\leqslant 600^{\circ}C$ is: a subscale ($< 5\ \mu m$) of Fe_2N_{1-x}, Fe_4N and γ ; a layer ($\sim 5\ \mu m$) of $\gamma + CrN$; a diffusion layer of $CrN + \gamma + \alpha$; an inner subscale ($\sim 4\ \mu m$) of $\gamma + \alpha$; and finally a thin layer formed by twinned austenite. At higher temperatures the nitrided layer is formed by a subscale of $\gamma' - Fe_4N$; an inner layer which contains $CrN + Cr_2N + \gamma$; and then a layer containing $CrN + Cr_2N + \gamma + \alpha$. The interface between the nitrided layer and the core is formed by a thin subscale of dislocations and twins in the austenite. The formation of α -ferrite at 600°C and lower temperatures is reported to be different to that at 800°C. In the first case the formation of α is caused by the presence of dislocations due to stresses at the nitrided layer-core interface, while in the second case it is associated with precipitation of Cr_2N which destabilizes γ by chromium depletion; see Figure II.4.

II.3 Microstress and properties of nitrided steels

(a) Sources of stress in a nitrided case

Stresses in a nitrided case are comparable to those observed in oxidised or carburized layers. The stresses are the consequences of the following phenomena that occur during nitriding:

(i) On nitriding there is a change in volume. For example, by formation of γ'-Fe_4N from γ-austenite of high nitrogen content there is an increase of 12% in specific volume, the white layer is therefore in compression compared with the inner subscale.

(ii) The nitrogen concentration is not constant through the nitrided layer. Compositional changes can occur and a nitrogen concentration profile can lead to a stress profile due to changes in lattice parameter (Mittemeijer, 1981).

(iii) On cooling from nitriding temperature a stress is generated due to the difference in thermal expansion coefficients of the nitrides and the steel matrix (Mittemeijer, 1981). Rapid cooling can also be the source of residual stresses due to the difference in cooling rate between the centre and the surface of the specimen (Ebert, 1978).

Stresses in oxidised Fe-Cr alloys have been detected by oxidising a thin strip of specimen on one side only while

the other side was protected by a layer of platinium; the sample was heavily bent after oxidation (Howes & Richardson, 1969). A similar phenomenon has been observed in the present study by nitriding one side a thin sheet of AISI 316 (the other side was copper plated), or by decreasing the flux of nitrogen on one side (by nitriding a specimen which has been previously oxidised on one side). A very small difference in case depth between the two sides leads to bending of the specimen.

Thus, when nitriding Fe-Cr alloys with formation of a "white layer" a complex distribution of stresses is expected through the nitrided layer, with a tensile residual stress on the surface of the diffusion layer. Residual stresses influence the mechanical properties of the material (Ebert, 1978) but the effects are difficult to quantify because of the influence of other parameters such as case depth and case hardness which are also related to the residual stresses. In carburized case-hardened steels residual compressive stresses are known to improve bend and fatigue resistance.

(b) Properties of nitrided steels

Nitrogen is deliberately added to certain stainless steels and mainly to stabilized grades for which precipitation-hardening is used to improve creep strength by introducing a

dispersed phase such as NbN or TiN to act as a sink for dislocations.

The formation of a hard nitrided or carburized surface case gives to the steel brittle properties despite the fact that the core is still ductile. The mechanical properties of such materials depend on the thickness of the case, the phase distribution, and the microhardness of the layer. Case-hardened steel can be studied as a composite material with a complex distribution of stresses during testing. Figure II.15 is a schematic illustration of the interaction generated between case and core during the simple loading of such a composite. In (a) both case and core are in the elastic region and so only axial and uniform stresses are detected while (b) shows that if the case is still in the elastic region with the core in the plastic-elastic zone then transverse stresses are generated in radial and circumferential directions. These stresses depend on the case depth and hardness (Ebert, 1978).

Only very little work on the mechanical properties of nitrided case hardened austenitic steels has been reported. Stanley (1969) studied the mechanical properties of nitrided AISI 304, 316, 321 and 347 but was unable to relate these to the proportion of nitrided area although an increase in yield stress and a decrease in ductibility were observed. The load-extension curves showed a drop in load after the yield point for nitriding temperatures $\geqslant 540^{o}C$ and a similar

Figure II.15

Schematic illustration of the interaction between case and core on simple loading of a composite material

(Ebert, 1978)

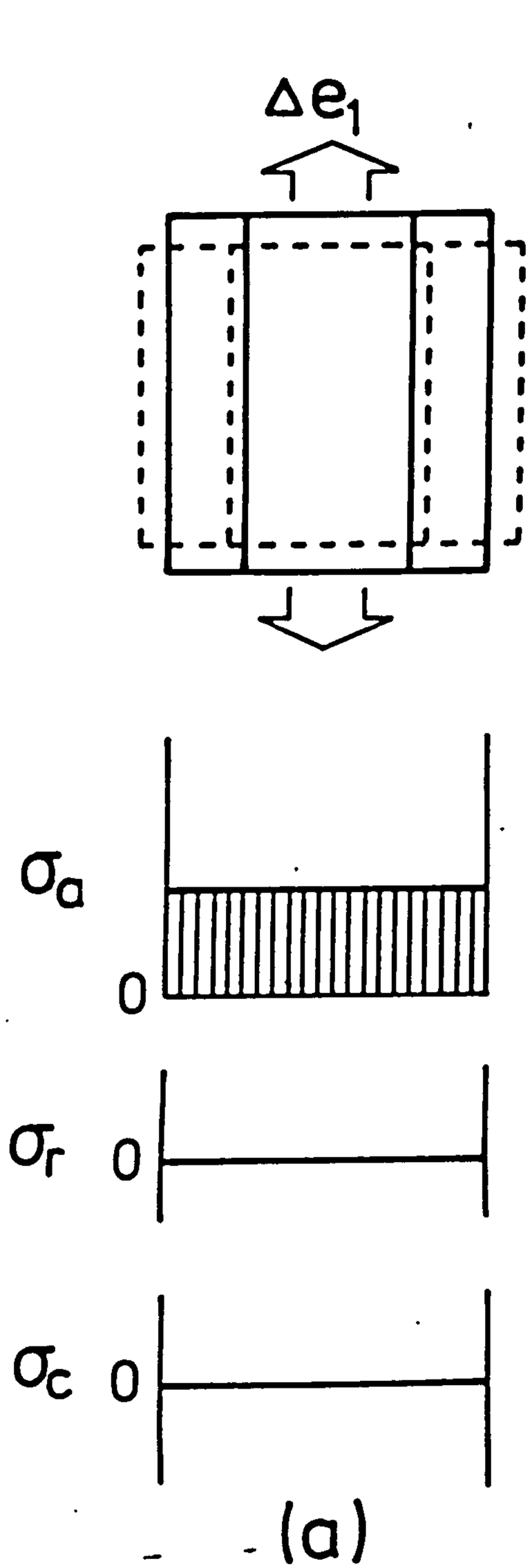
Δe1
σa
0
σr
0
σc
0
(a)

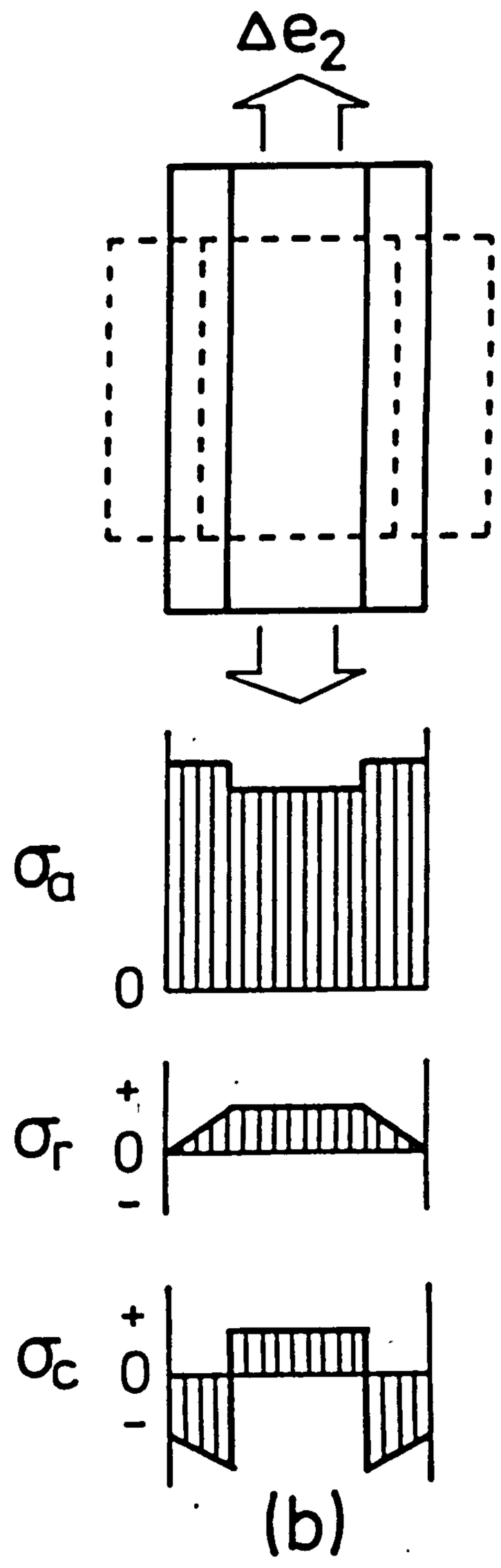
Δe2
σa
0
σr
+
0
-
σc
+
0
-
(b)

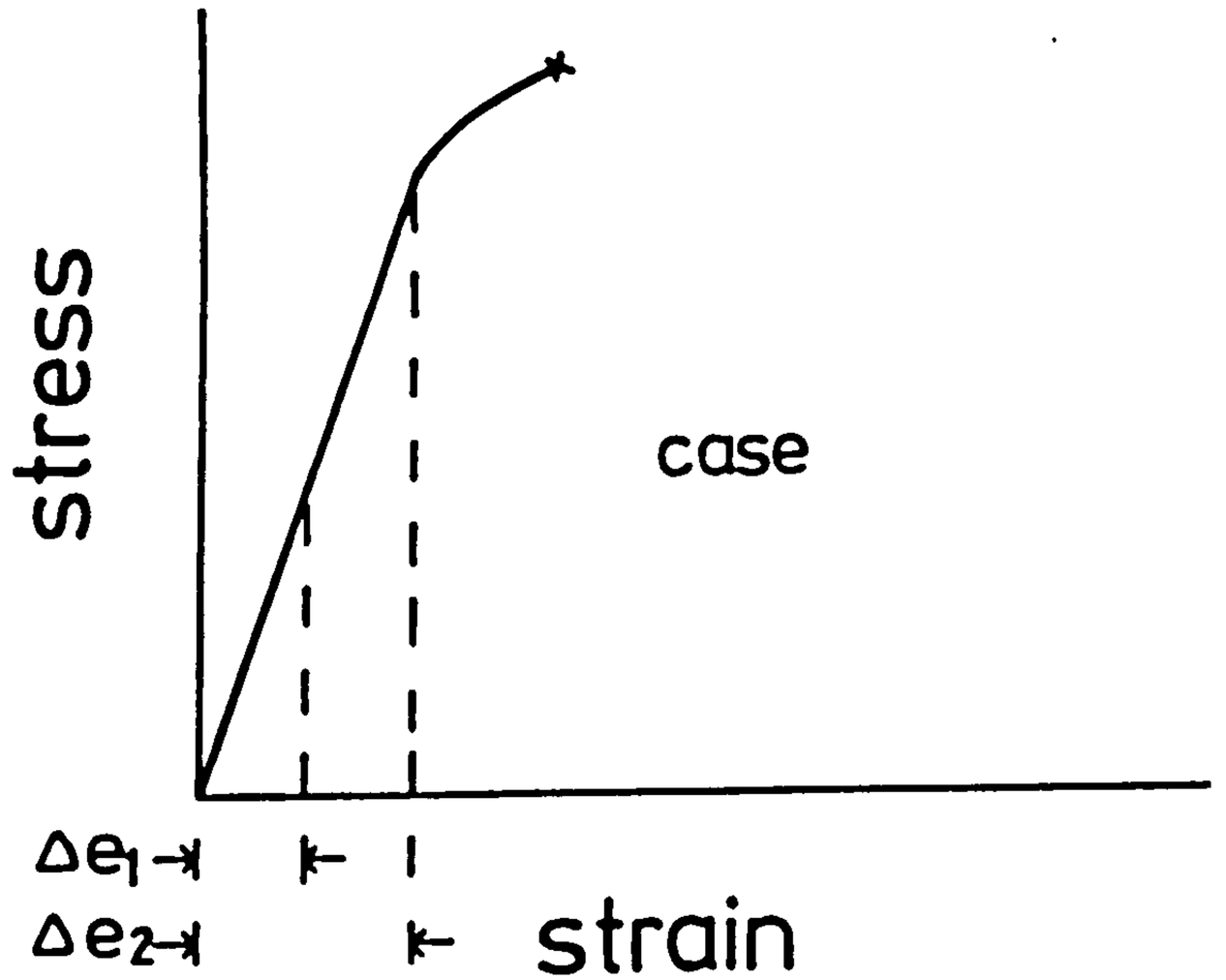
stress
case
Δe1
Δe2
strain

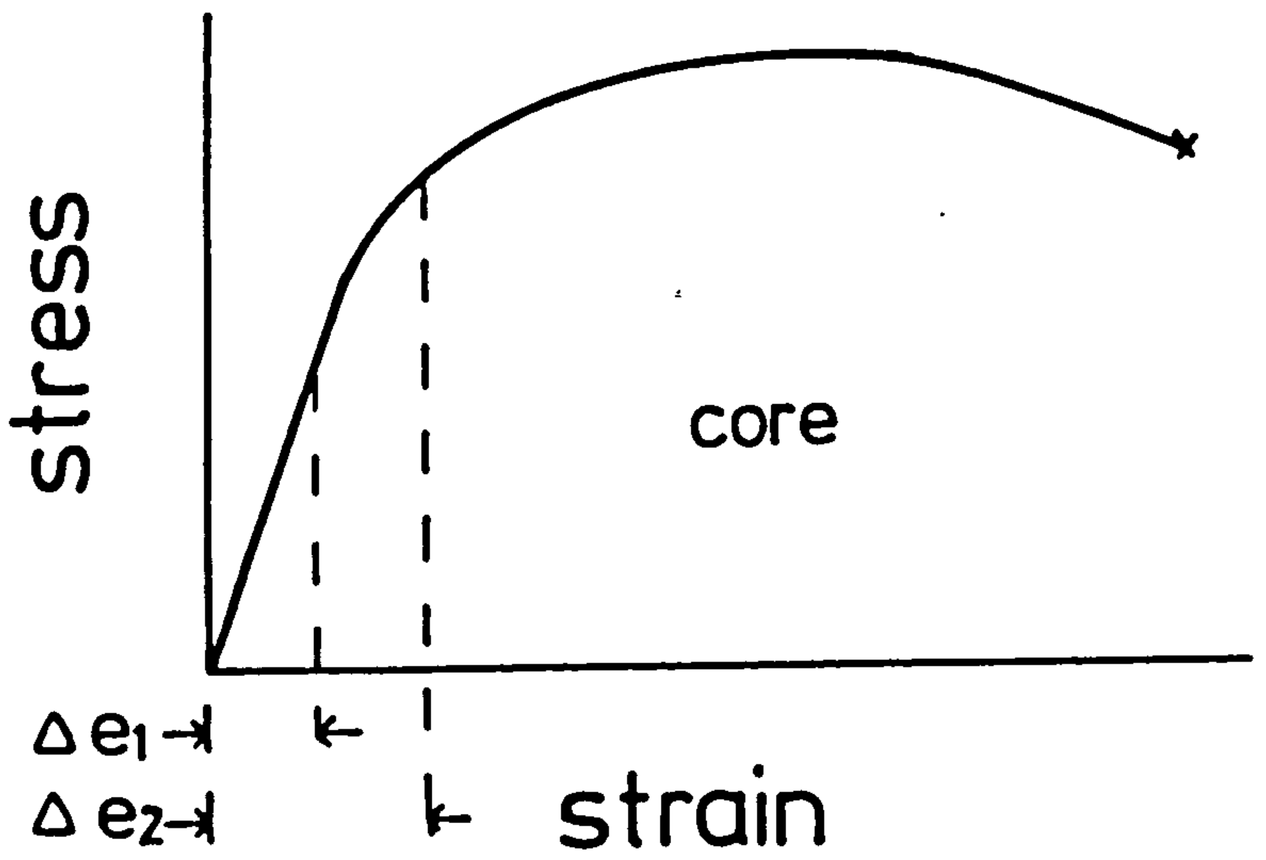
stress
core
Δe1
Δe2
strain

phenomenon was reported by Cordwell et al. (1974) for nitrided AISI 316 and was related to the occurrence of cracks in the nitrided case. A maximum in yield stress with exposure temperature was obtained by these authors at 600°C despite the fact that the nitrided layer is nearly the same thickness as when nitrided at 700°C although the micro-hardness is lower.

Four-point bend tests on 20% cold-worked AISI M 316 nitrided tubes (Wilson & Wilson, 1981) show that a minimum case depth is necessary for total fracture of the tubes and this minimum decreases with increasing nitriding temperature between 600° and 750°C. Failure of a case-hardened steel by bend testing depends on crack propagation through the ductile core. The maximum reduction in toughness for carburized steels tested by notched three-point bending is realised when the tip of a surface crack penetrates into the core, and the velocity of the crack tip through the hard case does not influence the toughness (Barnby et al., 1975). Therefore the toughness is high as long as part of the carburized case exists below the crack tip.

Chapter III

EXPERIMENTAL METHODS

III.1 Preparation of alloys

All steels used in the present investigation were classified as AISI 316 and were provided by the U.K.A.E.A. Springfields Laboratories. Chemical analysis, thickness and form of the steels are given in Table III.1.

The steel was nitrided in the as-received condition except that (i) wire used for X-ray analysis was drawn to 0.8mm and then annealed in a sealed vitreous silica capsule at 1050°C for 1h and (ii) thick specimens (2.7mm) were cold-rolled to 1mm foil with total deformation of 63%.

III.2 Nitriding procedure

Nitriding experiments were carried out in either a vertical (Figure III.1) or horizontal tube furnace. On the vertical furnace a high vacuum tap is attached for quenching. In both cases the furnace has an alumina reaction tube 20mm diameter heated by a Kanthal resistance winding which gives a uniform hot zone 50mm in length. The reaction temperature was maintained constant ($\pm$ 3°C) by an Ether controller

Table III.1

Composition of steels used in the present investigation (wt%)

Cast no.	C	Si	S	P	Mn	Ni	Cr	Mo	N_2	form
S 6077	0.07	0.49	0.13	0.20	1.56	12.86	17.40	2.7		sheet annealed 0.38mm thick
F 7545	0.02	0.24	0.027	0.16	1.76	12.06	17.78	2.43		sheet annealed 1mm thick
F 7545	"	"	"	"	"	"	"	"		sheet annealed 2.7mm thick
F 7545	"	"	"	"	"	"	"	"		sheet 20% cold-worked 1mm thick
SV 6958	0.06	0.44	0.009	0.016	1.62	13.32	17.04	2.36	0.021	tube 20% cold-worked outside diameter 5.82mm inside diameter 5.05mm
VA 7384	0.03	0.39	0.004	0.009	1.78	13.53	17.03	2.26	0.016	wire 1.6mm diameter

composition in Fe:balance

Suppliers:
S 6077 : Knight Strip Metals Ltd.
F 7545 : Arthur Lee & Sons Ltd.
SV 6958 : Accles & Pollock Ltd.
VA 7384 : Firth Vickers Stainless Steels Ltd.

Figure III.1

The vertical NH_3:H_2 equilibration apparatus

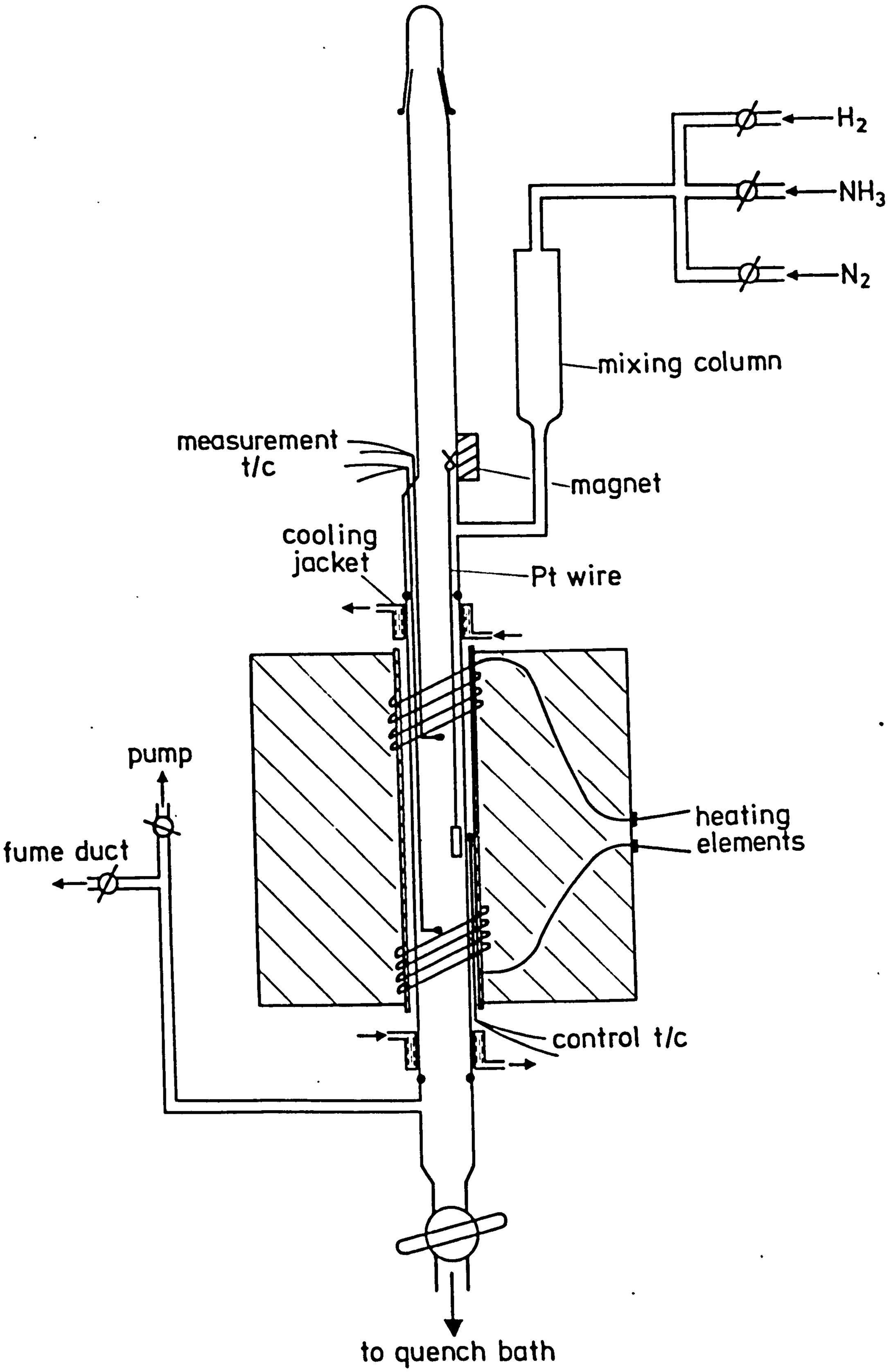
H_2
NH_3
N_2
mixing column
measurement t/c
magnet
cooling jacket
Pt wire
pump
fume duct
heating elements
control t/c
to quench bath

connected to a Pt/Pt-13Rh thermocouple placed between the reaction and winding tubes. The specimen temperature was measured by a separate Pt/Pt-13Rh thermocouple protected by an alumina sheath positioned alongside the specimen.

Commercial gases were used (N_2, NH_3, H_2, Ar), purified by standard methods (Schwerdtfeger & Turkdogan, 1970) as shown in Figure III.2. The activated copper was pre-reduced in hydrogen at 220°C and then used at 140°C during the experiments. The glas flow-rate was regulated by a capillary flowmeter (Figure III.3), calibrated by a bubble displacement method (Darken & Gurry, 1945) and the gas pressure was maintained slightly higher than atmospheric by 10-20mm of oil in an exit bubbler.

Specimens for nitriding were electropolished (electropolishing solution No. 1 of Table III.3) or cleaned with "chemiclene" and weighed prior to nitriding. In the vertical furnace samples were suspended in the cold upper zone of the furnace by a platinium wire attached to a piece of iron, held in position by a magnet, and in the horizontal furnace specimens were placed in a silica boat attached to an alumina rod which was moved by a magnet.

The sealed system was evacuated and filled with nitrogen and then the correct ammonia:hydrogen mixture passed for about 1h before moving the specimens into the hot zone of the furnace. After nitriding the specimens were either cooled

Figure III.2

Gas purification system for NH_3:H_2 equilibration

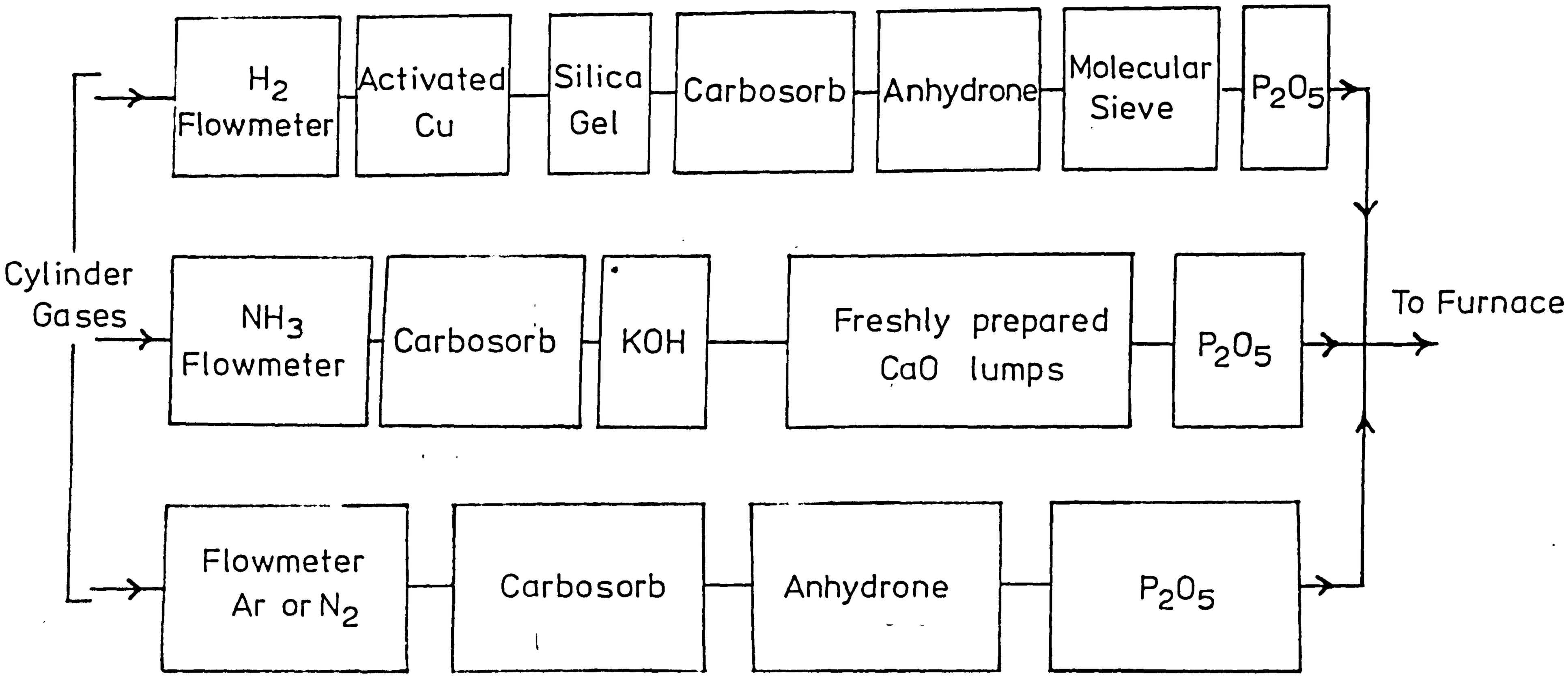
H_2 Flowmeter
Activated Cu
Silica Gel
Carbosorb
Anhydrone
Molecular Sieve
P_2O_5
Cylinder Gases
NH_3 Flowmeter
Carbosorb
KOH
Freshly prepared CaO lumps
P_2O_5
To Furnace
Flowmeter Ar or N_2
Carbosorb
Anhydrone
P_2O_5

Figure III.3

A capillary flowmeter (schematic)

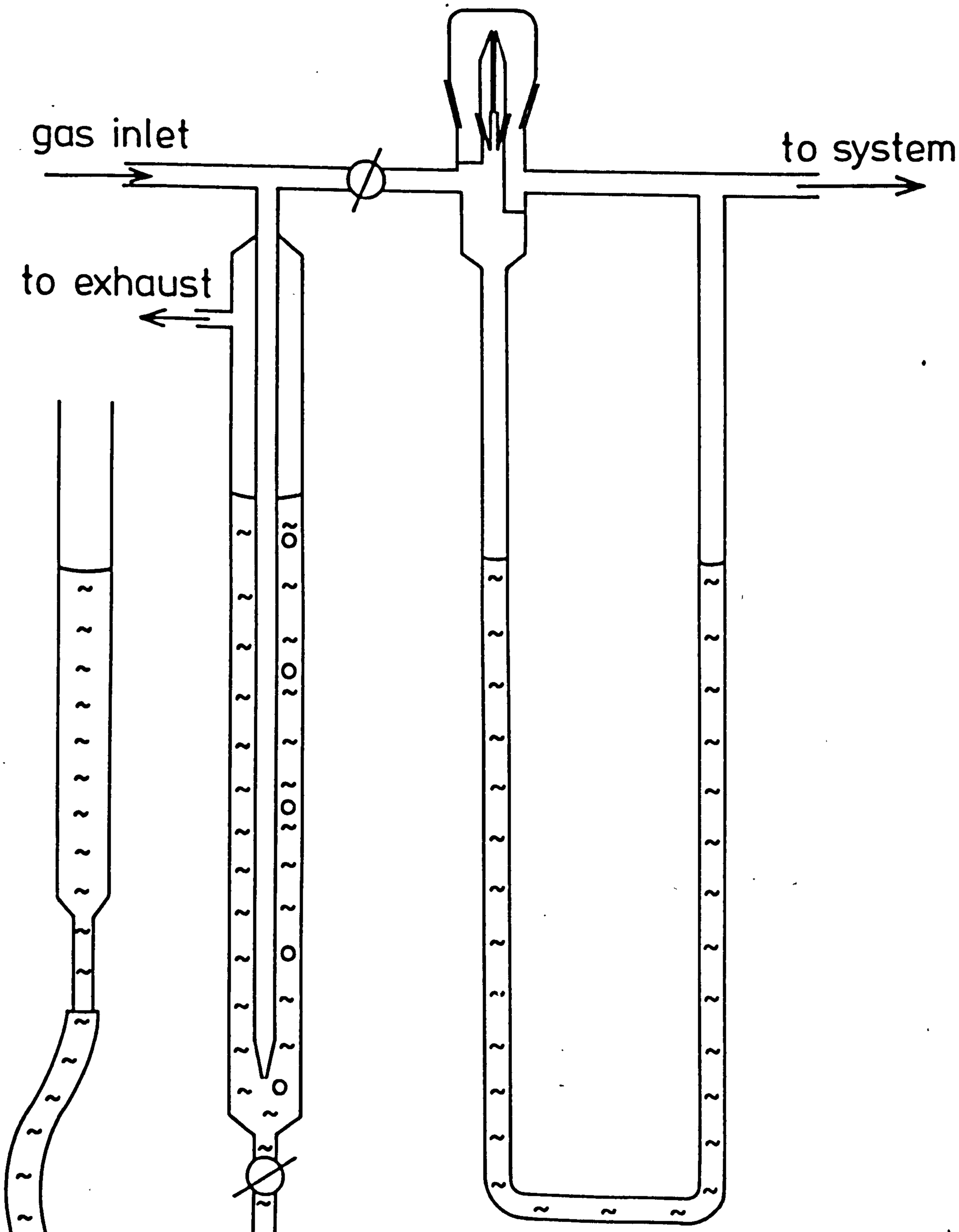
gas inlet
to system
to exhaust

slowly by withdrawing from the hot zone or quenched in a degassed ice-brine bath. Specimens were reweighed after nitriding.

III.3 Dissociation of ammonia

The dissociation of ammonia is an important parameter because the rate of nitriding, the surface nitrogen concentration, the formation of precipitates and the sequence of phases in case and core all depend on the nitrogen potential, $p_{NH_3} / p_{H_2}^{3/2}$. This potential is controlled by the dissociation of ammonia

$$NH_3 \rightleftharpoons 1/2\ N_2 + 3/2\ H_2 \quad \ldots\ \text{III.1}$$

Therefore dissociation of ammonia as a function of flow-rate and temperature was studied. The method used the solubility of ammonia in water in a volumetric measurement of the amount of insoluble gas $(N_2 + H_2)$ in a sample of exit gas taken from the bottom of the furnace in a one litre burette. The lower tap of the burette was then opened under water and as ammonia dissolved a partial vacuum was created and water was drawn into the burette. The percentage of dissociated ammonia was measured with an error of $\pm$ 1% by the difference in weight of the burette full of water and the burette with

water drawn in during the experiment. From equation III.1 the dissociated ammonia can be calculated

$$\% NH_3 \text{ dissociated} = \frac{(Wf-We)/2}{(Wf-Wo) - (Wf-We)/2} \times 100 \quad \ldots\ldots \text{III.2}$$

Wo: weight of burette (kg)

Wf: weight of burette + weight of 1 litre of water (kg)

We : weight of burette + weight of water absorbed during the experiment (kg)

The degree of dissociation of ammonia depends on the reaction temperature, the linear flow-rate of gas and the surface area of specimens in the furnace (see Table III.2). At 600°C the degree of dissociation is negligible even in the presence of specimens but at 800°C it increases rapidly with decreasing flow-rate and with increasing surface area of specimens in the furnace.

ε-iron nitride has a wide range of composition (Figure II.9) and a constant nitrogen content can be obtained either by nitriding at high temperature with a given ammonia potential or by nitriding at a lower temperature with a higher ammonia potential; see Figures II.9 and III.4. The nitrogen content of the ε-phase is obviously affected by the thermal dissociation of ammonia.

A constant linear flow-rate of 0.6 cm s^{-1} was used in all experiments.

Table III.2

Dissociation of ammonia

temperature °C	flow-rate cm s^{-1}	specimens	dissociation %
550	0.6	1 sheet	1
600	0.6	none	0
	0.03	none	1
	0.006	none	9
	0.6	1 sheet	5
	0.6	2 sheets	8
650	0.6	1 sheet	10
700	0.6	none	2
	0.15	none	4
	0.03	none	5
	0.6	1 sheet	20
	0.6	2 sheets	23
750	0.6	1 sheet	32
800	0.6	none	9
	0.15	none	28
	0.03	none	39
	0.006	none	75
	0.6	1 sheet	61
	0.6	2 sheets	72

dimension of sheet: 15x10x1mm

Figure III.4

Equilibrium between NH_3:H_2 gas mixtures (1atm) and solid phases of the iron-nitrogen system (Lehrer, 1930)

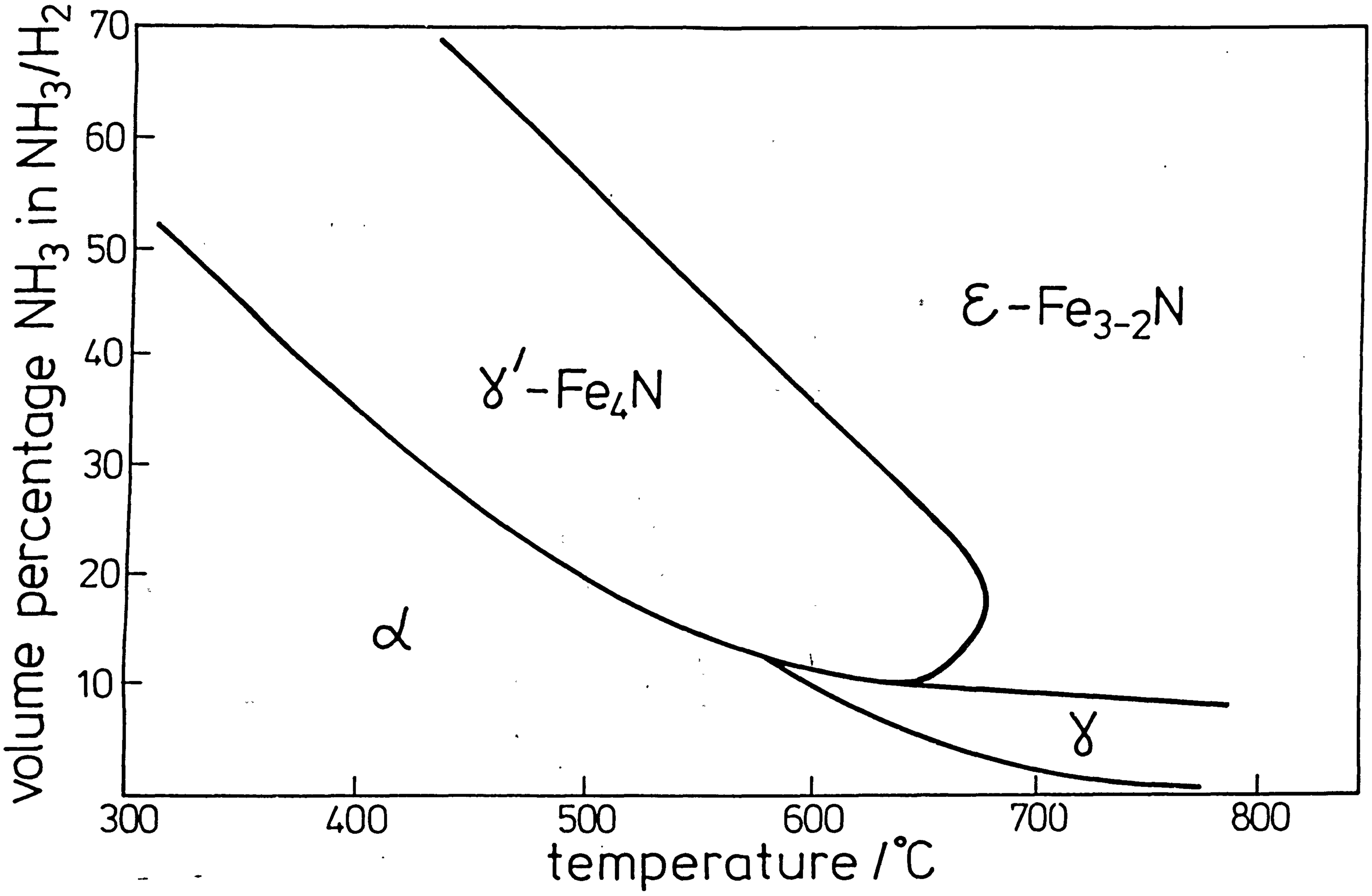
volume percentage NH_3 in NH_3/H_2
70
60
50
40
30
20
10
300
400
500
600
700
800
temperature /°C
ε-$Fe_{3-2}N$
γ'-Fe_4N
α
γ

III.4 Nitriding in ammonia:hydrogen gas mixtures

The reactions that occur when ammonia is in contact with iron alloys at temperatures of about 600°C, include:

$$NH_3(g) \rightleftharpoons 1/2\ N_2(g) + 3/2\ H_2(g) \quad \ldots\ \text{III.3}$$

$$NH_3(g) \rightleftharpoons \underline{N} + 3/2\ H_2(g) \quad \ldots\ \text{III.4}$$

$$NH_3(g) \rightleftharpoons 1/2\ N_2(g) + 3\underline{H} \quad \ldots\ \text{III.5}$$

where $\underline{N}$ and $\underline{H}$ indicate that nitrogen and hydrogen are in solid solution.

Reaction III.5 takes place to a negligible extent (Darken & Gurry, 1953) and a flow-rate of 0.6 cm s^{-1} is chosen to avoid reaction III.3 which is the thermal dissociation of ammonia (see Table III.2). Thus it is reasonable to assume that only reaction III.4 takes place during nitriding.

The equilibrium constant for the nitriding reaction is:

$$K\ (T) = a_{\underline{N}} \cdot P_{H_2}^{3/2} / P_{NH_3} \quad \ldots\ \text{III.6a}$$

where $a_{\underline{N}}$ is the activity of nitrogen in the nitride phase and P_{H_2}, P_{NH_3} are the partial pressures of hydrogen and ammonia respectively. The nitrogen activity is therefore:

$$a_{\underline{N}} = K\ (T) \cdot p_{NH_3} / p_{H_2}^{3/2} \quad \ldots\ \text{III.6b}$$

and so is proportional to the nitrogen potential of the gas, $p_{NH_3} / p_{H_2}^{3/2}$.

Previous work (Turkdogan & Ignatowicz, 1959) has shown that Henry's law is valid for the solubility of nitrogen in 18-8 stainless steel

$$a_{\underline{N}} = k_H \cdot (\text{wt\% N}) \quad \ldots\ \text{III.7}$$

where k_H is the Henry's law constant.

Thus:

$$\text{wt\% N} = k \cdot p_{NH_3} / p_{H_2}^{3/2} \quad \ldots\ \text{III.8}$$

where $k = K\ (T) / k_H$

The amount of nitrogen introduced into a steel can therefore be controlled by the $NH_3{:}H_2$ ratio in a mixture of gases.

For the iron-nitrogen system the phases in equilibrium with various ammonia:hydrogen gas mixtures at any temperature have been determined by Lehrer (1930) and are shown in Figure III.4

III.5 Metallographic examination

Nitrided sheets were mounted vertically either in cold mounting resin (for extremely brittle samples) or by hot mounting in bakelite at 140°C under a pressure of 17 MPa. The samples were then polished on two grades of silicon carbide papers followed by three grades of diamond paste (8, 3, 1 μm). Specimens were etched to show different parts of the structure using a number of different solutions summarised in Table III.3. The nitrided case depth was measured on a Reichert projection microscope after etching in 2% nital and Vickers microhardness measurements were carried out on the same equipment using a constant load of 50g.

Grain-sizes of as-received and heat-treated material were measured after etching electrolytically in 10% oxalic acid and by using the mean linear intercept (m.l.i.) which is sometimes referred to as the Heyn intercept. The mean linear intercept is measured by counting the number of grains or grain-boundaries which intercept a line of length L. The m.l.i. is given by:

$$\text{m.l.i.} = \bar{d} = \frac{L}{N} = \frac{I}{N_L}$$

where N is the number of grains or grain-boundaries and N_L the number of grains or grain-boundaries per unit length. There is also a relationship between $\bar{d}$ and the A.S.T.M.

Table III.3

Compositions of electropolishing solutions and etching reagents

Solution	Composition	Conditions	Uses
electropolishing No. 1	68v% acetic acid 16v% perchloric acid 16v% 2-butoxy-ethanol	18-20v at 0°C	
electropolishing No. 2	50g CrO_3 400ml orthophosphoric acid	12-15v at 35-40°C	
2% nital	2ml nitric acid 98ml ethanol	10-40 seconds	structure of nitrided layer carbides not etched
10 picral:1 nital	10ml picric acid 1ml nitric acid 110ml ethanol	5-20 seconds	structure of nitrided layer
sulfate-chloride	1.25g copper sulfate 2.5g cupric chloride 2ml hydrochloric acid 10g magnesium chloride 100ml distilled water Dilute to 1l with ethanol	20-60 second	structure of nitrided layer

(contd.)

Table III.3 (contd.)

Solution	Composition	Conditions	Uses
Kalling's reagent	5g cupric chloride 100ml hydrochloric acid 100ml ethanol 100ml distilled water	10-20 seconds	structure of nitrided layer
Marble's reagent	10g copper sulfate 50ml hydrochloric acid 50ml distilled water	10-50 seconds	total case depth of nitrided layer, reveals extent of carbide precipitation
aqua regia/glycerol	1 part nitric acid 1 part hydrochloric acid 1 part glycerol	3-10 seconds at 40°C	chromium carbide
Oberhoffer's reagent	1g cupric chloride 30g ferric chloride 0.5g stannous chloride 50ml hydrochloric acid 500ml distilled water 500ml ethanol	2-5 seconds 20-30 seconds	for compound zone for carbide-enriched layer
10% oxalic acid (electrolytic etch)	10g oxalic acid 100ml distilled water	15-45 seconds 3-6v	carbide precipitation and grain boundaries in stainless steel

grain-size numbers compiled by Pickering (1976). An average of seven lines per specimen were drawn to measure the grain-size and the results are given in Table III.4. Heat-treatment at 600° and 800°C up to 100h does not change the grain-size, but 2.5h at 1250°C gives very large grains. The as-received steel containing 0.02wt% C showed numerous twin boundaries and the shape of the grains was not regular.

III.6 Preparation of specimens for electron microscopy

A chemical-mechanical method for the preparation of transmission electron microscopy (TEM) thin foils of nitrided layers was developed. The depth at which the microstructure was to be studied was decided and a corresponding amount of the nitrided layer removed by surface grinding using 1mm thick samples to minimise bending and distortion. The specimen was turned over and ground from the reverse side until a total thickness of 300 μm remained. The surface to be studied was then lacquered and thinning started by electropolishing the reverse side in electropolishing solution No. 1; see Table III.3. With this solution the exposed surface remains bright when polishing the austenitic core but when the γ +CrN layer is exposed the specimen surface becomes dull. When all the austenite layer was removed (the surface was then completely dull), electro-polishing was continued using electropolishing solution No. 2

Table III.4

Grain-size of annealed, as-received and heat-treated samples

carbon content wt%	heat-treatment conditions	$\bar{d}$ mm	A.S.T.M. number
0.02	as-received	0.024	7-8
0.02	600°C-24h	0.025	7-8
0.02	600°C-100h	0.025	7-8
0.02	800°C-24h	0.025	7-8
0.02	800°C-100h	0.026	7-8
0.02	1250°C-2.5h	0.25	0-1
0.07	as-received	0.009	10
0.07	600°C-24h	0.010	9-10
0.07	600°C-48h	0.010	9-10
0.07	600°C-100h	0.010	9-10
0.07	800°C-24h	0.0115	9-10
0.07	800°C-48h	0.0115	9-10
0.07	800°C-100h	0.0115	9-10
0.07	1250°C-2.5h	0.250	0-1

of Table III.3 and when perforation occurred the lacquer was removed from the obverse side and polishing continued from both sides to complete perforation by the normal window technique.

A second method of preparing thin foils consists of mechanical grinding followed by ion-beam thinning. A 3mm diameter disc was cut from a 0.38mm thick nitrided specimen by an ultrasonic drill and on one side the nitrided layer was removed by grinding to the depth at which the microstructure was to be studied. The specimen was turned over and ground on the reverse side until the disc was 120μm thick and the specimen was then placed in the ion-beam thinner shown schematically by Figure III.5. Only one ion gun was directed on the reverse side at a potential of 8 kV under a pressure of $5x10^{-3}$ Pa of Ar which gave a current of 90-100μA. The angular inclination of the specimen to the ion-beam was approximately 30^{o}. Under these conditions a thinning rate of 3 μm per hour was achieved. After perforation both guns were used at a thinning angle of $5-10^{o}$ in order to provide a smooth surface with the maximum of thinned area.

The advantages of ion-beam thinning over chemical methods of polishing for the present samples are that larger thinned areas are produced and, as Morris (1979) has shown, handling of brittle specimens is facilitated.

Figure III.5

Ion-beam thinning apparatus

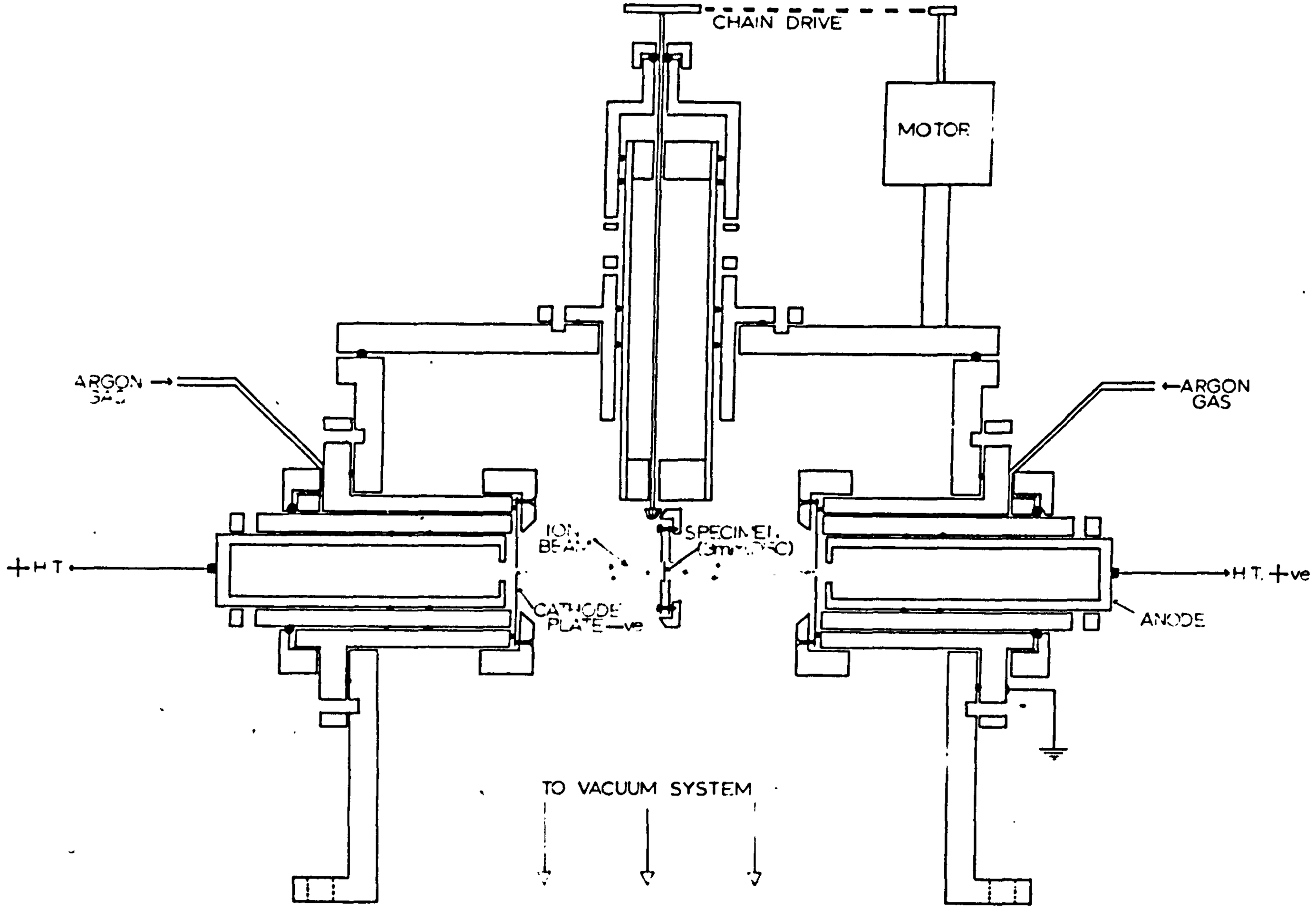
CHAIN DRIVE
MOTOR
ARGON GAS
ARGON GAS
+H T
ION BEAM
SPECIMEN
CATHODE PLATE —ve
H.T. +ve
ANODE
TO VACUUM SYSTEM

TEM specimens were prepared from carbon replicas. Samples were mounted in bakelite, polished and etched in 1% nital and then coated with plastic. The dried plastic film was stripped from the specimen, shadowed with Au-Pd alloy and then carbon coated before dissolving the plastic in acetone and depositing the carbon replica on a copper support grid.

TEM was carried out using either Philips EM 300 or Jeol 100U electron microscopes both equipped with goniometer stages.

Scanning electron microscopy (SEM) studies of fracture surfaces of tensile or bend-test specimens were made on uncoated specimens in either a Jeol T20 or a Cambridge stereoscan S600 equipped with EDAX facilities.

III.7 X-ray methods

The identification of phases in wire samples was carried out by taking X-ray powder photographs with a Unicam 90mm diameter camera using LiF single-crystal reflected monochromatic CrK_{α} radiation in order to minimise background intensity. The films were compared with standard films of iron nitrides and chromium nitrides. The iron nitrides were prepared in a horizontal furnace from pure iron powder (sponge iron, Johnson Mattley Ltd.) nitrided at temperatures

and $NH_3:H_2$ ratios according to Lehrer's data (1930); see Figure III.4. CrN was obtained by nitriding chromium powder in $95NH_3:5H_2$ at 900°C while Cr_2N was obtained together with CrN by pressure nitriding with molecular nitrogen at 35atm and 1000°C for 75 hours; see Roberts, 1970.

The lattice parameters of the different phases were calculated from the line positions on the X-ray films measured with a glass scale (Hilger & Watts Ltd.).

The identification of the phases distributed through the nitrided layer was carried out by progressively grinding a flat specimen and recording an X-ray reflexion scan using a Philips diffractometer with graphite-crystal monochromated Cu K_α radiation after successive removal of each 5 μm.

Thermal expansion coefficients of γ'-Fe_4N (prepared as mentioned above) was determined from powder photographs taken every 50°C in the range 20°-550°C. A high temperature camera contained in a vacuum system to minimise atmospheric absorption of the diffracted beams was used with Fe-filtered Co K_α radiation and lattice parameters were calculated by Nelson-Riley (1945) extrapolation.

III.8 Mechanical testing

Mechanical testing was carried out on an Instron 1115

with automatic chart control and stepped zero suppression facilities.

For tensile tests flat specimens of 20mm gauge length and cross section of either 0.38x5mm or 1x5mm were used and for which the strain rates were $1.7x10^{-4}s^{-1}$ and $4.2x10^{-4}s^{-1}$ respectively.

Three-point and four-point bend tests were made on flat sheets (1mm or 0.38mm thick) and on tubes using two different bending speeds, $3.3x10^{-3}$mm s^{-1} and $3.3x10^{-2}$mm s^{-1}. For the three-point bend the span of the bend jig was 19mm while for four-point bending the inside and outside spans were respectively 10mm and 20mm.

Chapter IV

SCOPE OF THE PRESENT INVESTIGATION

The present study was proposed by the U.K.A.E.A. in order to understand and expand on previous empirical work carried out at Springfields Laboratories which had shown that nitrogen was a promising method for the embrittlement of nuclear fuel cans in order to aid spent-fuel recovery. A combination of optical microscopy, electron microscopy and X-ray diffraction has been used to determine the phase distribution in the nitrided layer in order to explain the nitriding kinetics and the mechanical properties of nitrided AISI 316.

In Chapter V the effect of temperature, cold-working and nitrogen potential of the gas mixture on the phase distribution in the nitrided case is reported while in Chapter VI the microstructure and nature of the precipitation in the different subscales of the nitrided layer at 600^{o} and $800^{o}C$ are described. The formation of γ'-Fe_4N on samples nitrided at high temperature ($800^{o}C$)is explained.

In Chapter VII abnormally high nitriding rates at low temperature ($<650^{o}C$) are reported and are explained by the appearance of cracks due to formation of a thick "white layer" at reaction temperature; at higher temperatures

internal nitriding theory is valid. A complete study of the influence of carbon in solid solution or as a precipitate has been necessary to explain the difference in nitriding kinetics between AISI L316 and AISI 316.

The mechanical properties of nitrided AISI 316 are presented in Chapter VIII. No mathematical model is given but the difference in bending behaviour is explained in terms of microstructure.

In Chapter IX general observations on nitriding of stainless steels are described and the advantages and disadvantages of different surface phases for industrial use are discussed.

Finally, Chapter X presents the conclusions of the present study with suggestions for further investigation and development of the gaseous nitriding of stainless steels.

Chapter V

NITRIDING OF AISI 316

V.1 Introduction

The phases formed by nitriding at constant activity depend on the nitrogen potential of the gas mixture and on the temperature. Nitriding stainless steel is difficult (Turkdogan & Ignatowicz, 1959; Wilson, 1978) due to the formation of a passive film of oxide on the surface of the specimens. Ion-nitriding (or plasma-nitriding) is often used in industry for nitriding stainless steels such as AISI 304, as one advantage of glow discharge over other methods of nitriding is the depassivation of the surface.

Previous work carried out at Newcastle in nitriding AISI 316 in pure ammonia at 550° and 600°C (Wilson, 1978) showed that a hard and duplex nitrided case is formed, although the layer is often uneven and cracked. X-ray analysis showed the presence of ε-Fe_2N_{1-x}, γ'-Fe_4N, CrN, γ and α phases. Chromium nitrides are thermodynamically more stable than iron nitrides (see Table V.1 and Figure V.1) and so the formation of ε-Fe_2N_{1-x} and γ'-Fe_4N requires a higher nitrogen potential (Lehrer, 1930) than is required for chromium nitrides (Mortimer, 1971).

Chapter V

NITRIDING OF AISI 316

V.1 Introduction

The phases formed by nitriding at constant activity depend on the nitrogen potential of the gas mixture and on the temperature. Nitriding stainless steel is difficult (Turkdogan & Ignatowicz, 1959; Wilson, 1978) due to the formation of a passive film of oxide on the surface of the specimens. Ion-nitriding (or plasma-nitriding) is often used in industry for nitriding stainless steels such as AISI 304, as one advantage of glow discharge over other methods of nitriding is the depassivation of the surface.

Previous work carried out at Newcastle in nitriding AISI 316 in pure ammonia at 550° and 600°C (Wilson, 1978) showed that a hard and duplex nitrided case is formed, although the layer is often uneven and cracked. X-ray analysis showed the presence of ε-Fe_2N_{1-x}, γ'-Fe_4N, CrN, γ and α phases. Chromium nitrides are thermodynamically more stable than iron nitrides (see Table V.1 and Figure V.1) and so the formation of ε-Fe_2N_{1-x} and γ'-Fe_4N requires a higher nitrogen potential (Lehrer, 1930) than is required for chromium nitrides (Mortimer, 1971).

Table V.1

Thermodynamic data for the formation of metal nitrides (Kubaschewski & Alcock, 1979)

nitrides	ΔH^{o}_{298} kJ	S^{o}_{298} J/K
$4Fe + 1/2N_2 \rightleftharpoons Fe_4N$	-11.1	155.6
$Cr + 1/2N_2 \rightleftharpoons CrN$	- 123	328.4
$2Cr + 1/2N_2 \rightleftharpoons Cr_2N$	- 114	74.1
$3Ni + 1/2N_2 \rightleftharpoons Ni_3N$	+ 0.8	-
$2Mo + 1/2N_2 \rightleftharpoons Mo_2N$	- 69	87.9

Figure V.1

The standard free energy of formation

of some nitrides

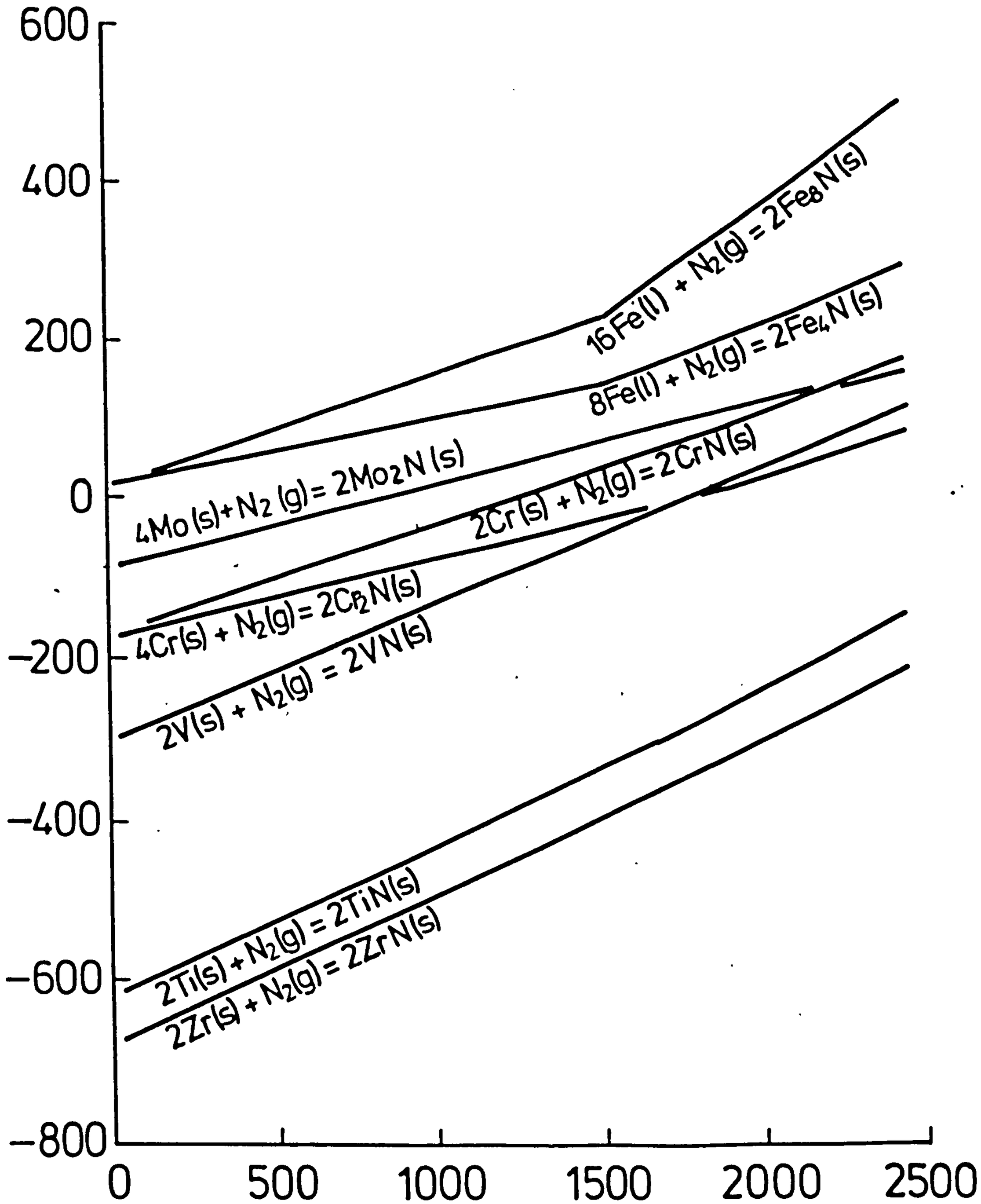

The reference states are pure phases which are stable at one atmosphere pressure and the designated temperature.

The phases formed on nitriding depend on the temperature and the nitrogen potential of the gas mixture and also on the gas flow-rate because of the dissociation of ammonia; see Table III.2A. Variation of the phase distribution through the nitrided layer is also expected due to the decrease in nitrogen potential from the surface to the core (Lightfoot & Jack, 1975).

During heat-treatment of cold-worked material recrystallisation occurs very slowly at 600°C and partial recrystallisation is observed at 800°C. Thus the microstructure of the case of cold-worked samples depends on the nitriding temperature and on the degree of cold-working.

Nitriding of (i) annealed, (ii) 20% cold-worked and (iii) 63% cold-worked specimens containing 0.02wt% C was carried out between 500° and 800°C in pure ammonia and also for annealed samples in ammonia:hydrogen mixtures. Several etching reagents were used to show the differences in microstructure of the nitrided layer; see Mridha & Jack, 1982a. Samples were quenched from the reaction temperature to retain the nitrided structure and the phase distribution was compared with that of air-cooled samples.

The nitriding of 20% and 63% cold-worked materials was compared with annealed and nitrided specimens, and the recrystallisation of cold-worked samples has been followed during heat-treatment for up to 100 hours at 600° and 800°C.

The surfaces of 20% and 63% cold-worked samples were examined by X-ray diffractometry before and after nitriding and are compared with annealed specimens.

V.2 Effect of temperature on nitriding in pure ammonia

The surface appearance of nitrided specimens changes with nitriding temperature and cooling-rate. Specimens nitrided at 600°C have a silvery surface with blisters if air-cooled while at 800°C a matte-grey appearance is observed which darkens when specimens have been quenched. Figure V.2 shows SEM micrographs of the surface of samples nitrided at 600° and 800° and air-cooled. The micro-structure of specimens nitrided at 800°C (d) is coarser than that nitrided at 600°C (b), while specimens nitrided for only 2 hours ((a) at 600°C and (c) at 800°C) show a smoother surface than those nitrided for 74 hours. This is explained by precipitation of ε-Fe_2N_{1-x} which is incomplete after 2 hours nitriding. ε-Fe_2N_{1-x} has been reported to grow outwards from the original iron surface while γ'-Fe_4N grows inwards. Thus, when the layer of γ'-Fe_4N is formed the rate of formation of ε decreases. The photo-micro-graphs of Figure V.2 show clearly that ε nucleates and grows on the steel surface and completely covers the surface after 2 hours. No difference on surface appearance is detected between 16h and 74h of nitriding.

Figure V.2

SEM micrographs of AISI L316 nitrided in pure ammonia

(a) at 600°C for 2h

(b) at 600°C for 74h

(c) at 800°C for 2h

(d) at 800°C for 74h

All samples air-cooled

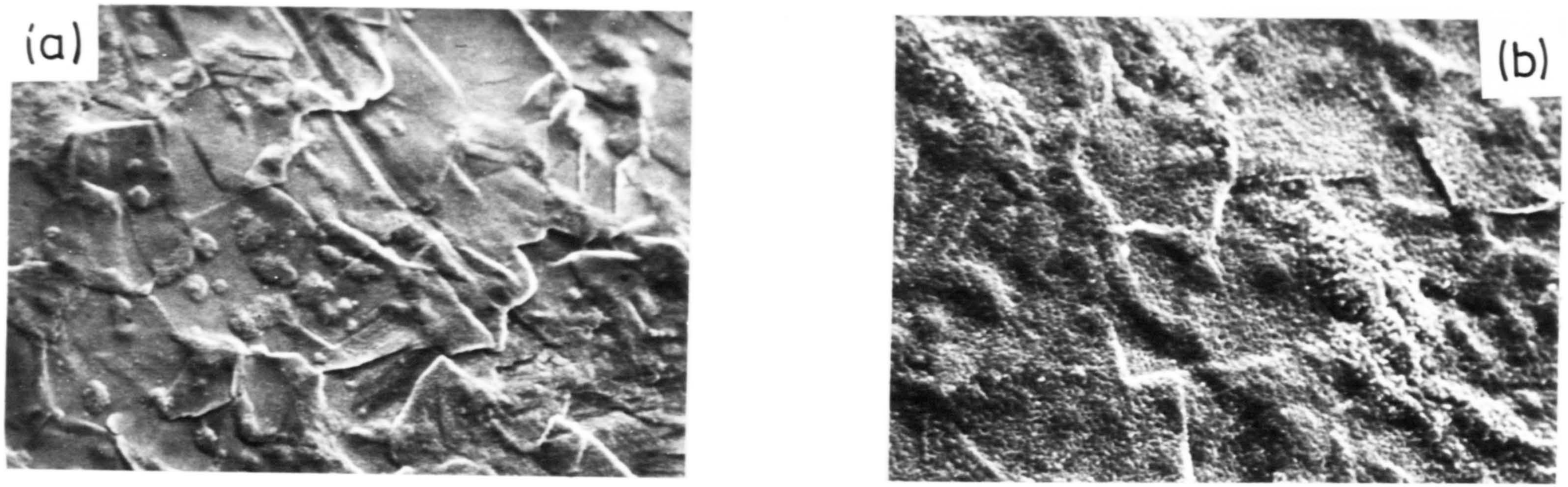
(a)
(b)
20μ
(c)
(d)

(a) Optical microscopy of the nitrided layer

Nitrided and air-cooled specimens sectioned perpendicular to the surface when etched in 2% nital or 10 picral:1 nital consist of a white surface layer and an etched subscale for all nitriding temperatures.

Nitriding at 500°C gives a thin nitrided layer which is uneven and not well defined. The case is very hard, brittle and breaks easily (Figure V.3) while samples nitrided at 550°C show a more even case composed of a "white layer" and a fine subscale (Figure V.3).

A three-layer case is formed at 600°C but only a two-layer case is observed on air-cooled specimens at 700° and 800°C (Figure V.4). The "white layer" of 20 μm is already formed at 600°C after 1 hour nitriding and does not grow with time (Figure V.5) and no difference is observed between the air-cooled sample of Figure V.6(a) and the quenched sample of Figure V.6(b). The "white layer" on samples quenched from 700°C is thinner than on samples air-cooled from 700°C (Figure V.7) and is absent on specimens quenched from 800°C; see Figure V.8(b).

Other etching solutions have been used (see Table III.3) to study the metallography of the nitrided layers and a difference in the attack of the "white layer", depending on the nitriding temperature, is observed when etched in sulfate-chloride solution (Figure V.9). The "white layer"

Figure V.3

Optical micrographs of AISI L316 nitrided in pure ammonia for 24h at 500° and 550°C; etched in 2% nital

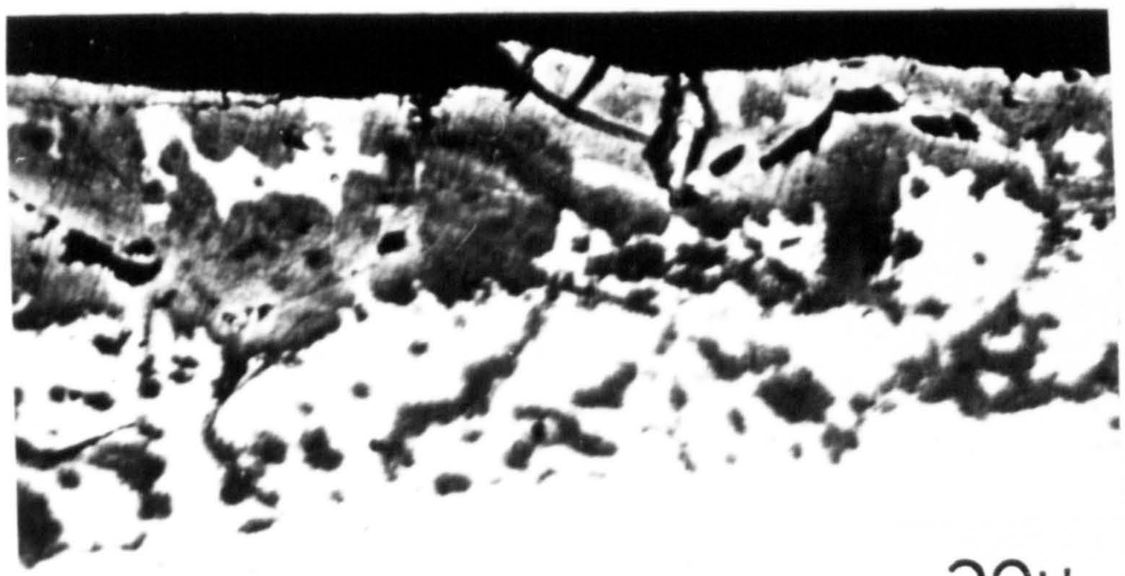

500°C

20μ

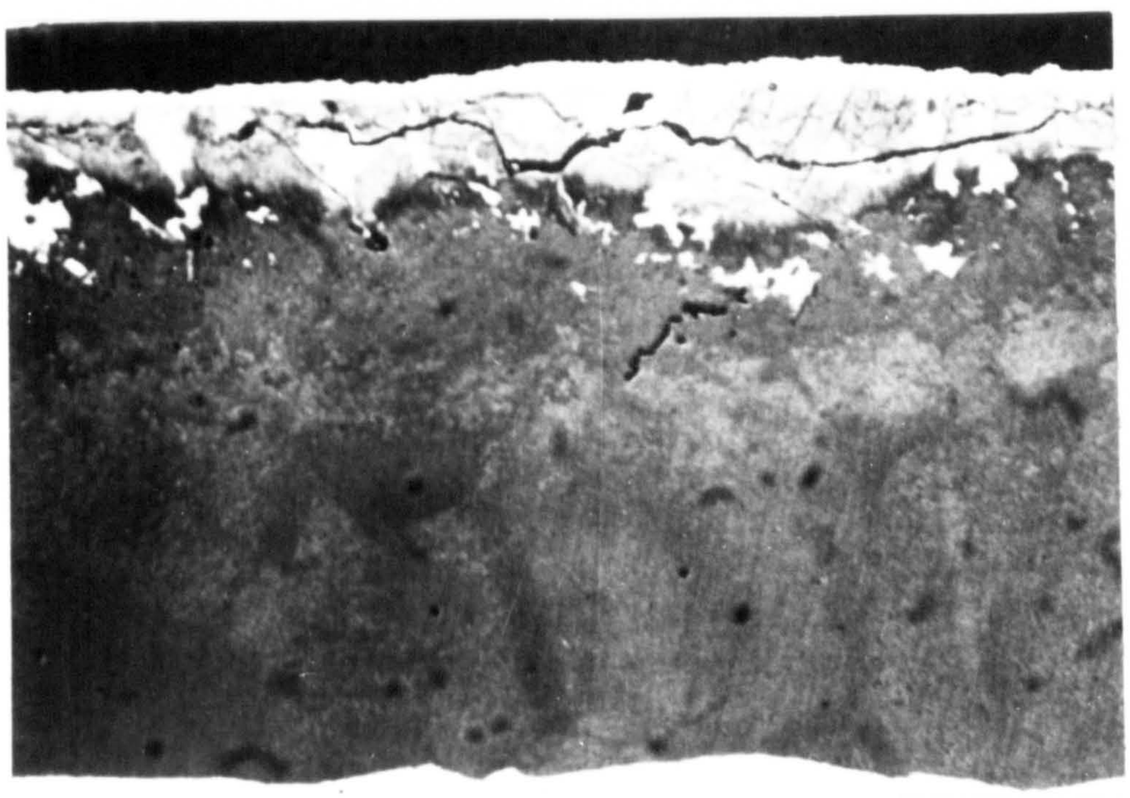

550°C

20μ

Figure V.4

Optical micrographs of AISI L316 nitrided in pure ammonia for 24h at 600°, 700° and 800°C; etched in 10 picral: 1 nital

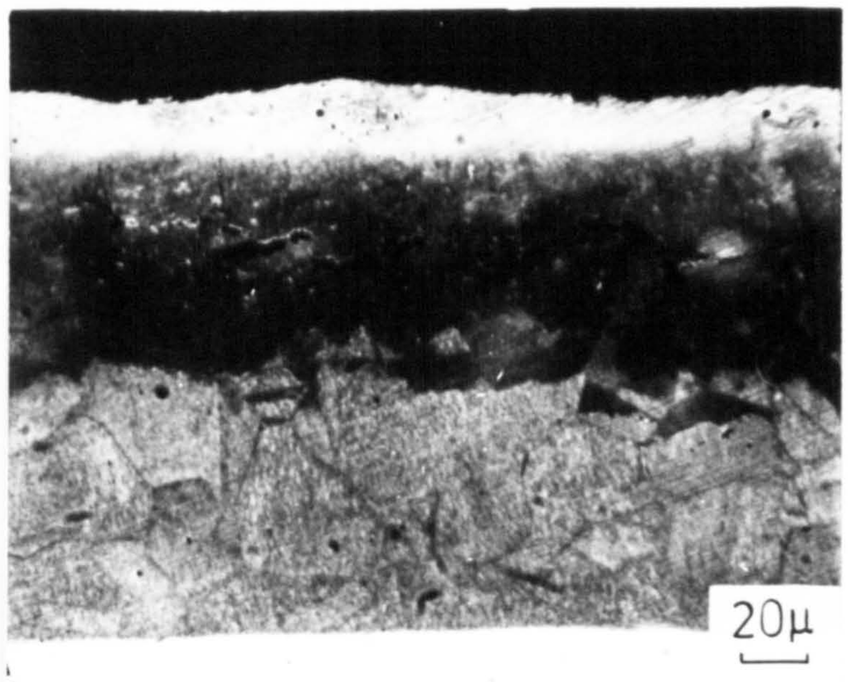

600°C

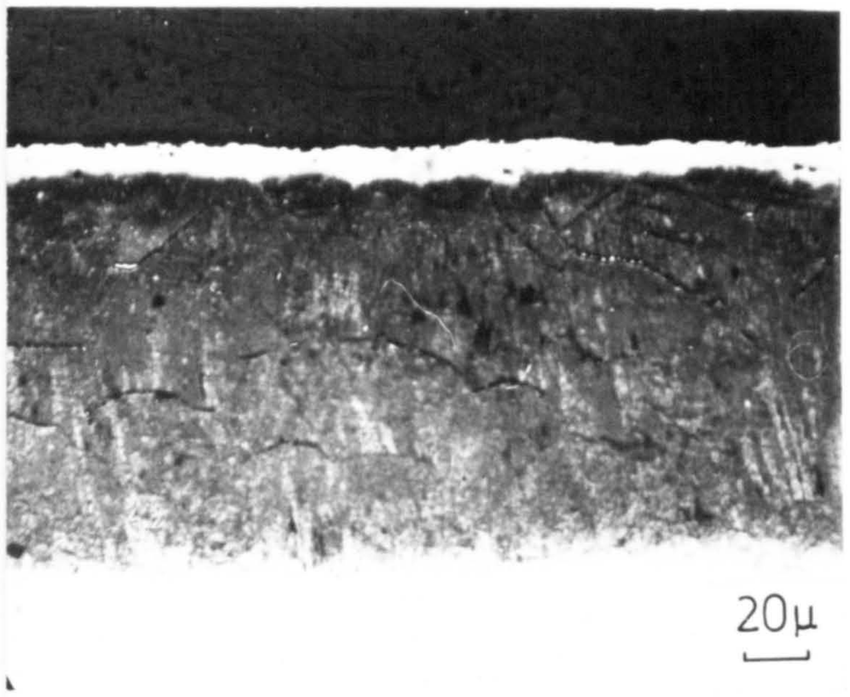

700°C

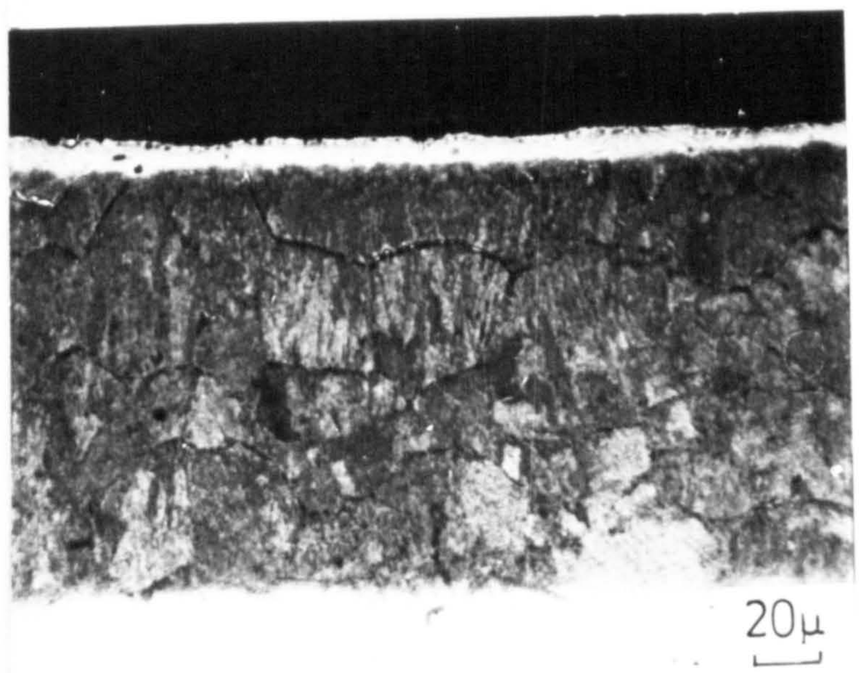

800°C

10 Picral : 1 Nital

Figure V.5

Optical micrographs of AISI L316 nitrided in pure ammonia at 600°C for 1h, 10h and 24h; etched in 2% nital

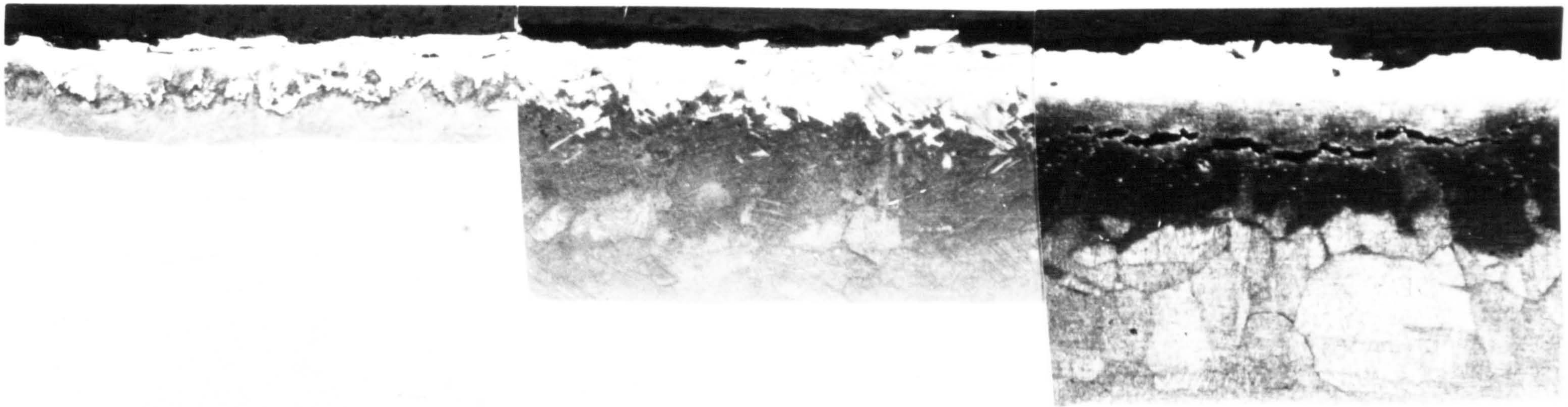

40μ

1h

10h

24h

Figure V.6

Optical micrographs of AISI L316 nitrided in pure ammonia for 24h at 600°C; etched in 2% nital

(a) air-cooled

(b) quenched

20μ

20μ

Figure V.6

Optical micrographs of AISI L316 nitrided in pure ammonia for 24h at 800°C; etched in 2% nital

(a) air-cooled

(b) quenched

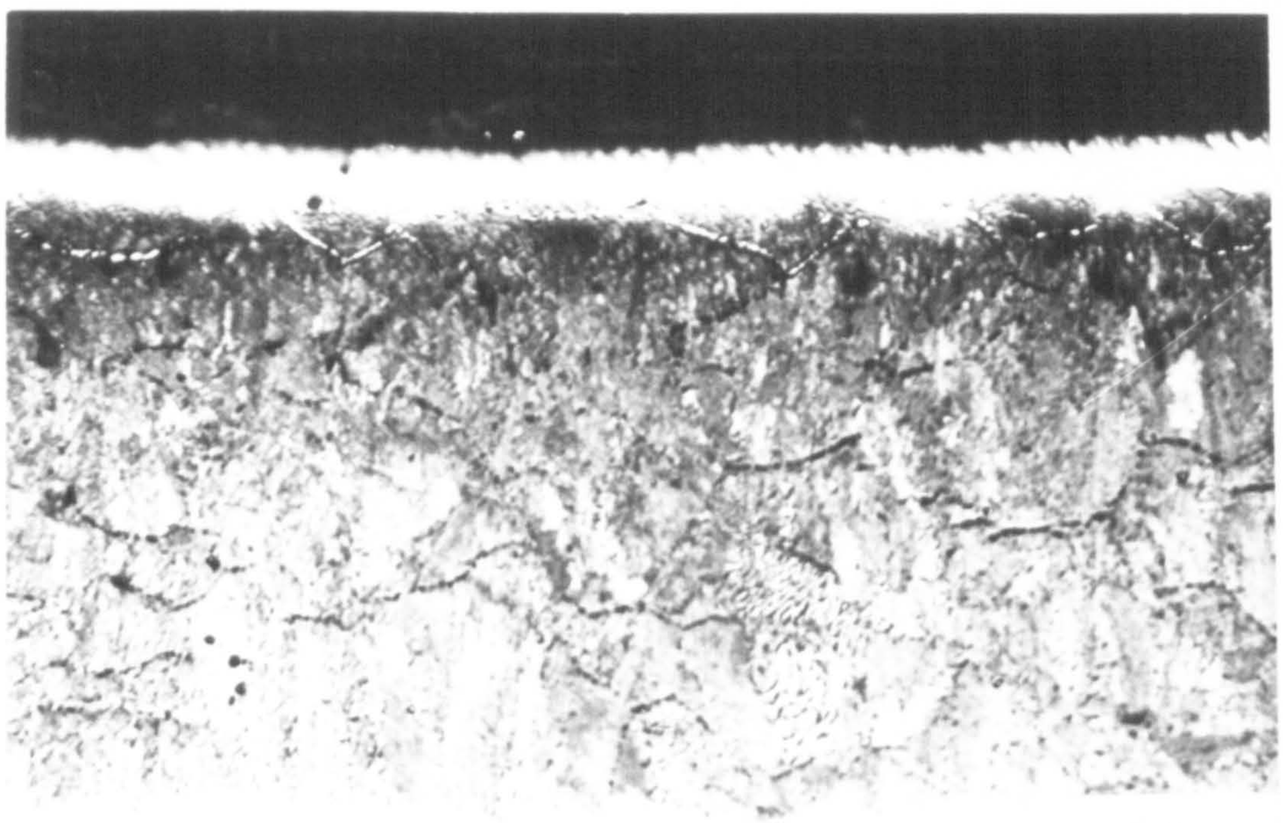

20μ

(a)

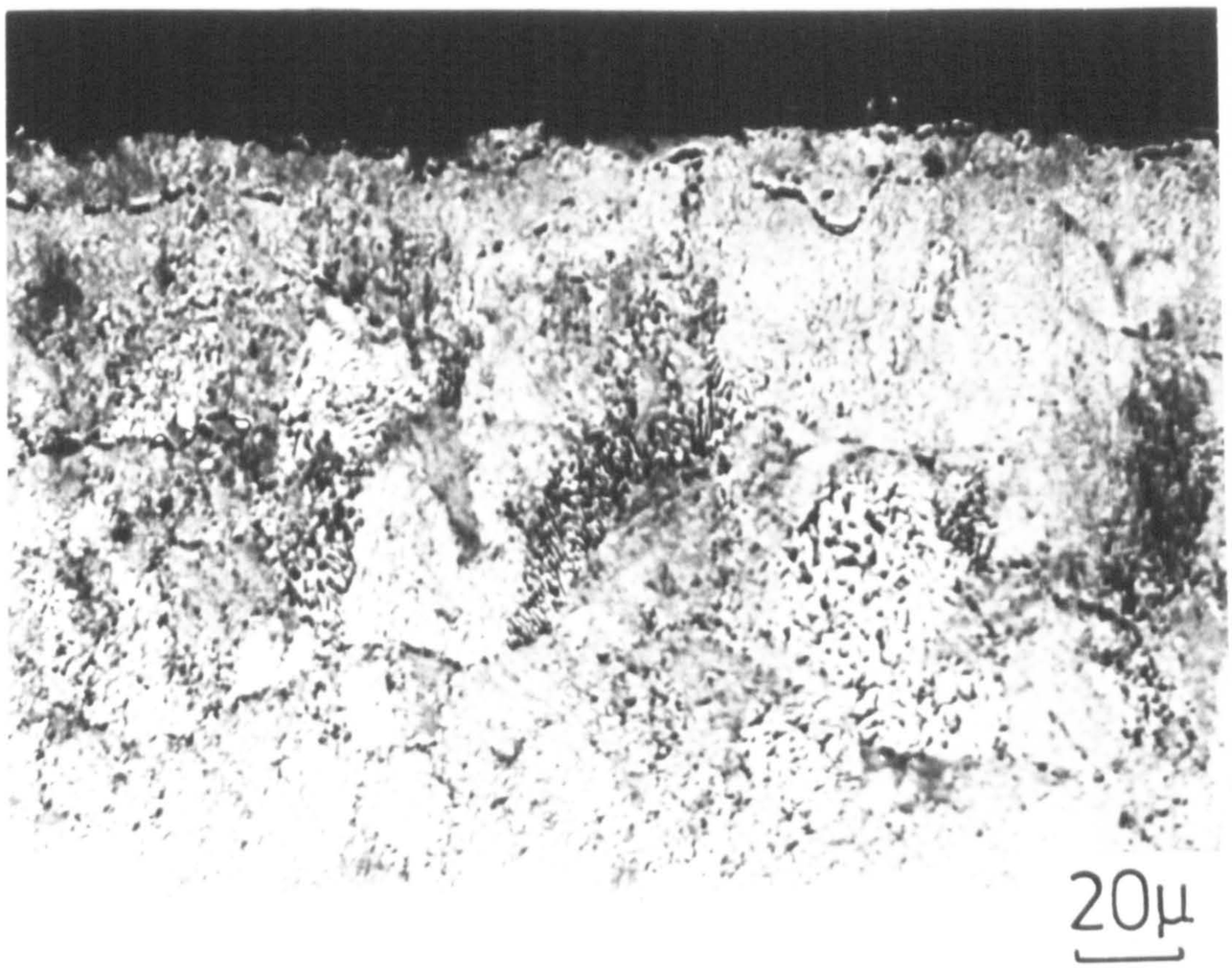

20μ

(b)

etches darker when γ'-Fe_4N is formed at nitriding temperature, for example at 600°C, than when it is formed by air-cooling from 800°C; see Figure V.9. This reagent also shows a difference in the inner subscale at 700°C and 800°C which may be explained by the presence of Cr_2N or by a lower nitrogen concentration than on the surface. Mridha & Jack (1982a) reported that picral and Oberhoffer's reagent were among the best etching solutions to distinguish γ'-Fe_4N from ε-Fe_2N_{1-x}. However, in the present study no differences in the attack of the compound layer were observed which may be explained by the difference in the chromium concentrations (3wt% for Mridha & Jack compared with 17wt%) or by the presence of nickel in AISI316.

Marble's reagent was found to be the best etchant to show the carbide precipitation that occurs ahead of the nitrided layer (Lightfoot & Jack, 1975; Mridha & Jack, 1982b) and Figure V.10 shows specimens etched in this way containing 0.02wt% and 0.07wt% C and nitrided at 600° and 800°C.

Specimens containing 0.07wt% C, nitrided at 800°C for 48h are almost through nitrided and the grain-boundaries in the core are visible without etching. The core, which remains unetched in 2% nital, is heavily etched by Marble's reagent (Figure V.10) due to the high density of carbides which are formed by diffusion of carbon ahead of the nitrided layer.

Specimens nitrided at 600°C (0.02wt% C) show a thin

Figure V.9

Optical micrographs of AISI L316 nitrided in pure ammonia for 24h at 600°, 700° and 800°C; etched in sulfate-chloride solution

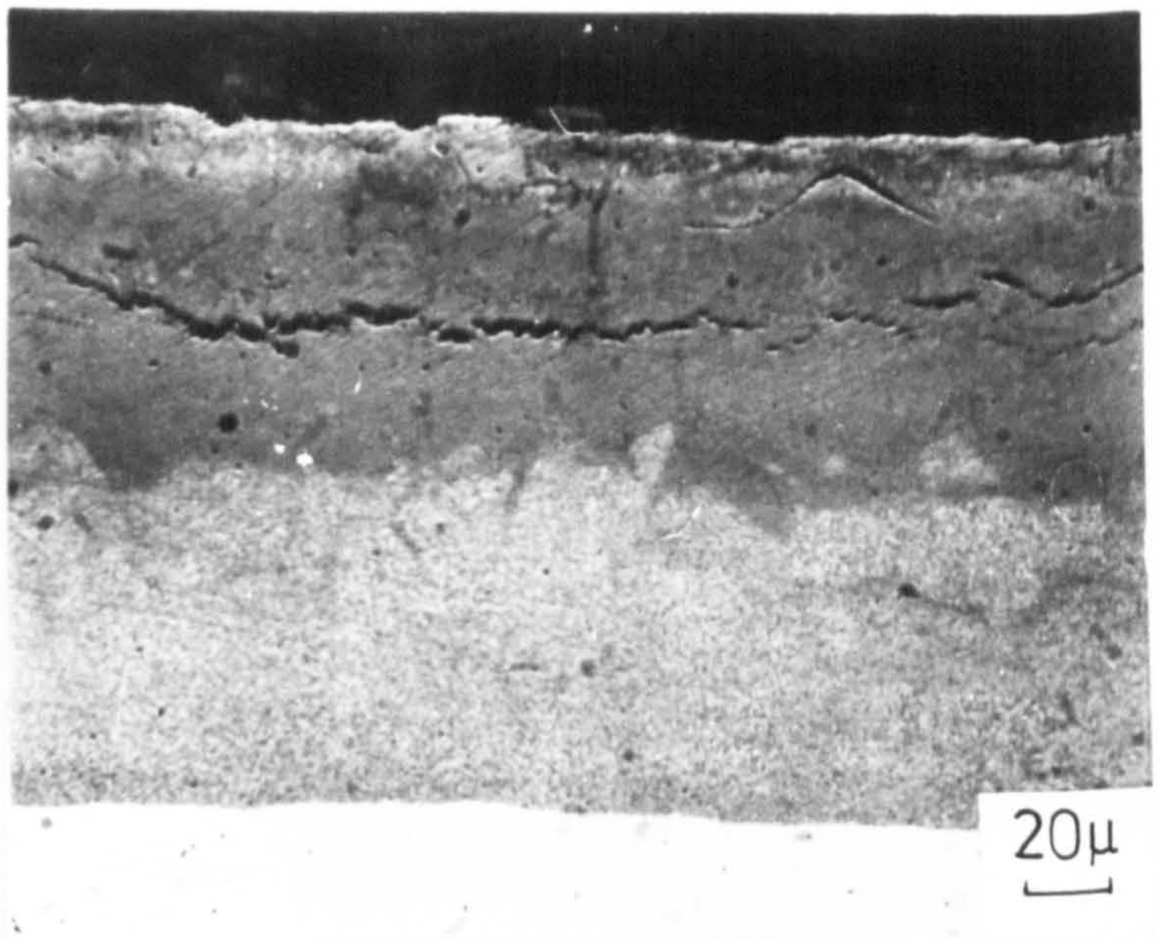

600°C

20μ

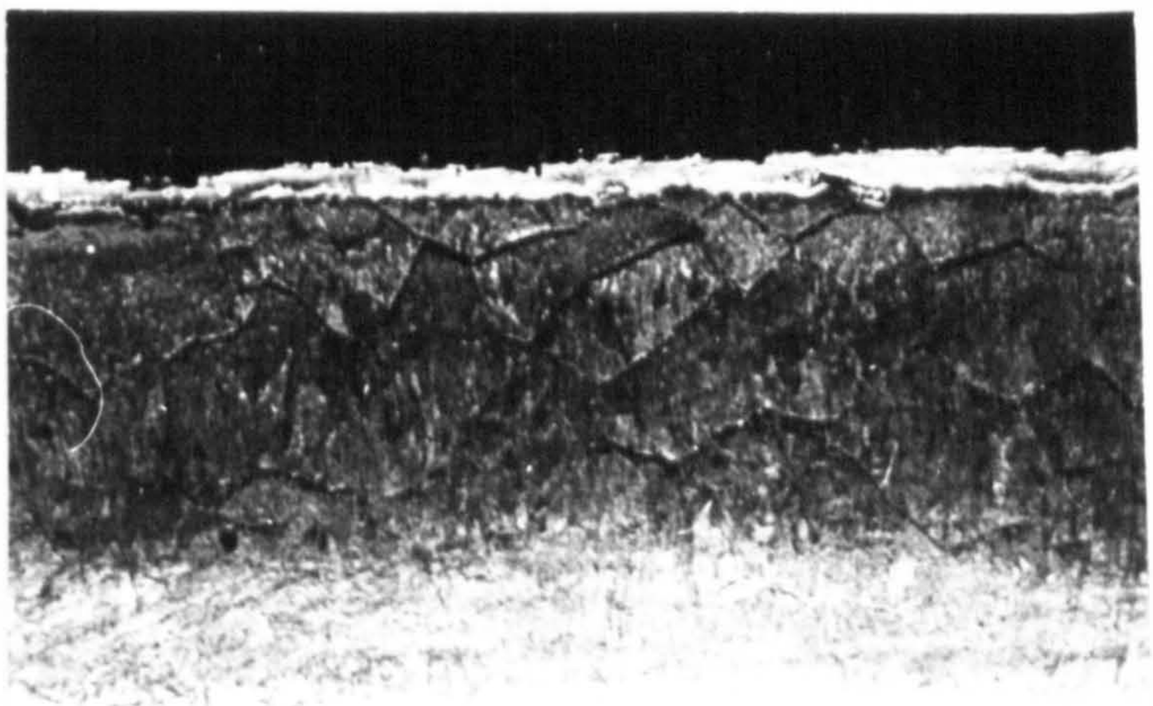

700°C

20μ

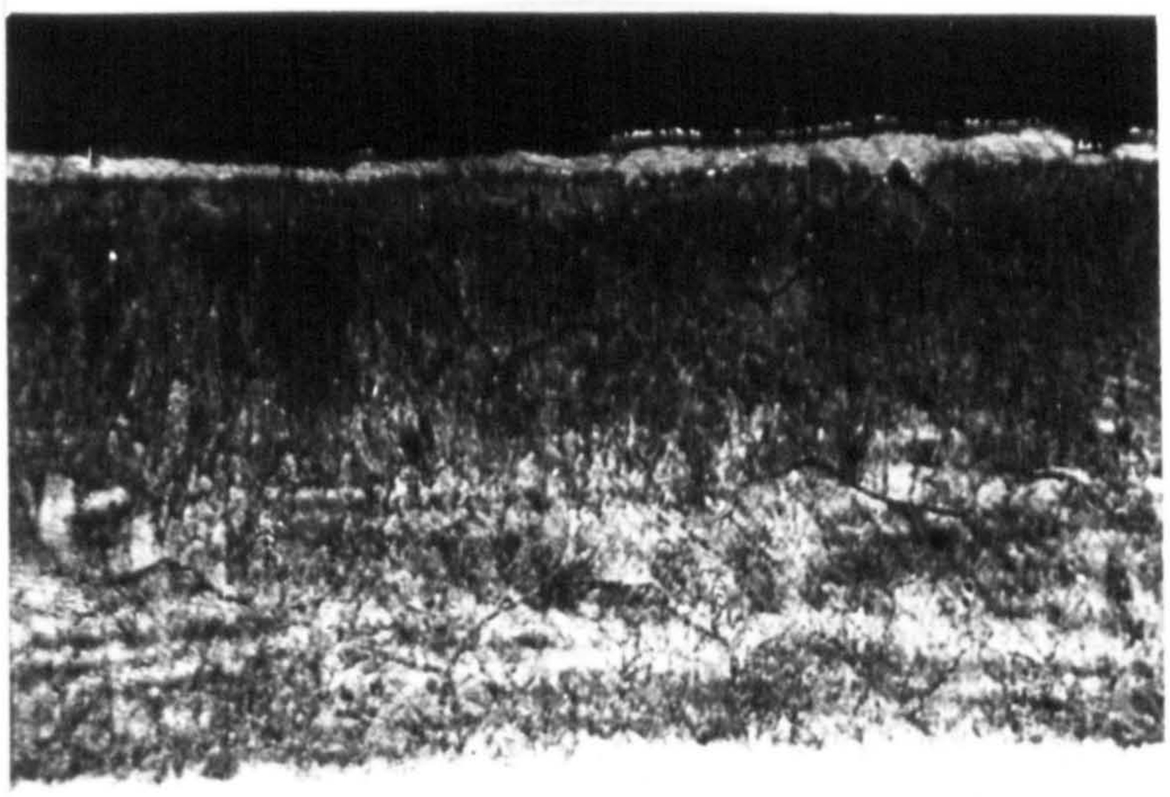

800°C

20μ

$CuSO_4 : CuCl_2$

Figure V.10

Optical micrographs of AISI L316 (0.02wt% C)

(i) nitrided at 600°C in pure ammonia for 24h

(ii) nitrided at 800°C in pure ammonia for 100h

and (iii) AISI 316 (0.07wt% C) nitrided at 800°C in pure ammonia for 48h

all etched in Marble's reagent

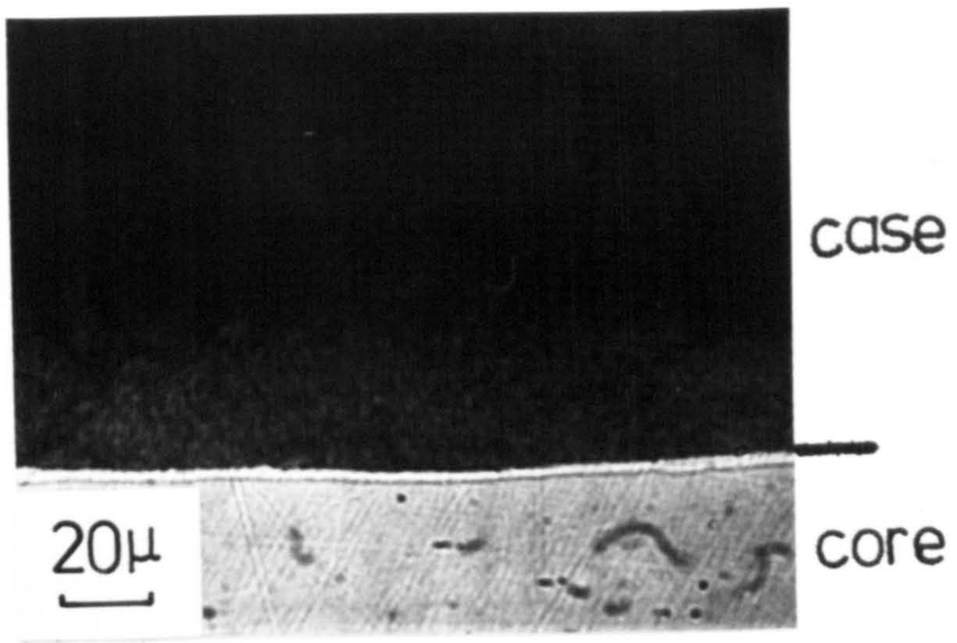

0.02 wt% C
600°C-24h

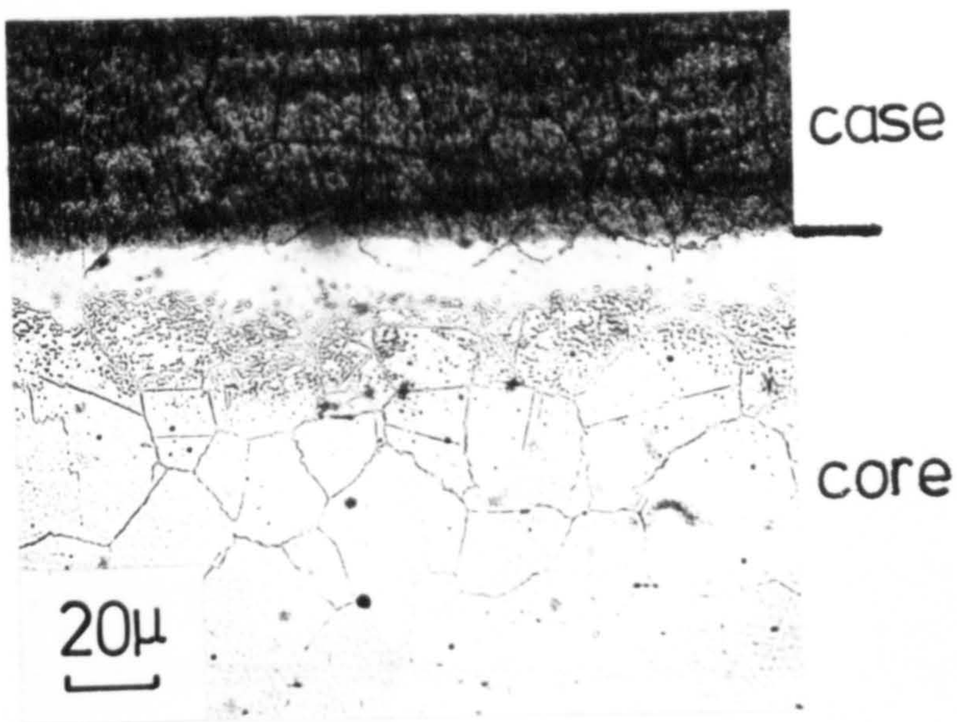

0.02 wt% C
800°C-100h

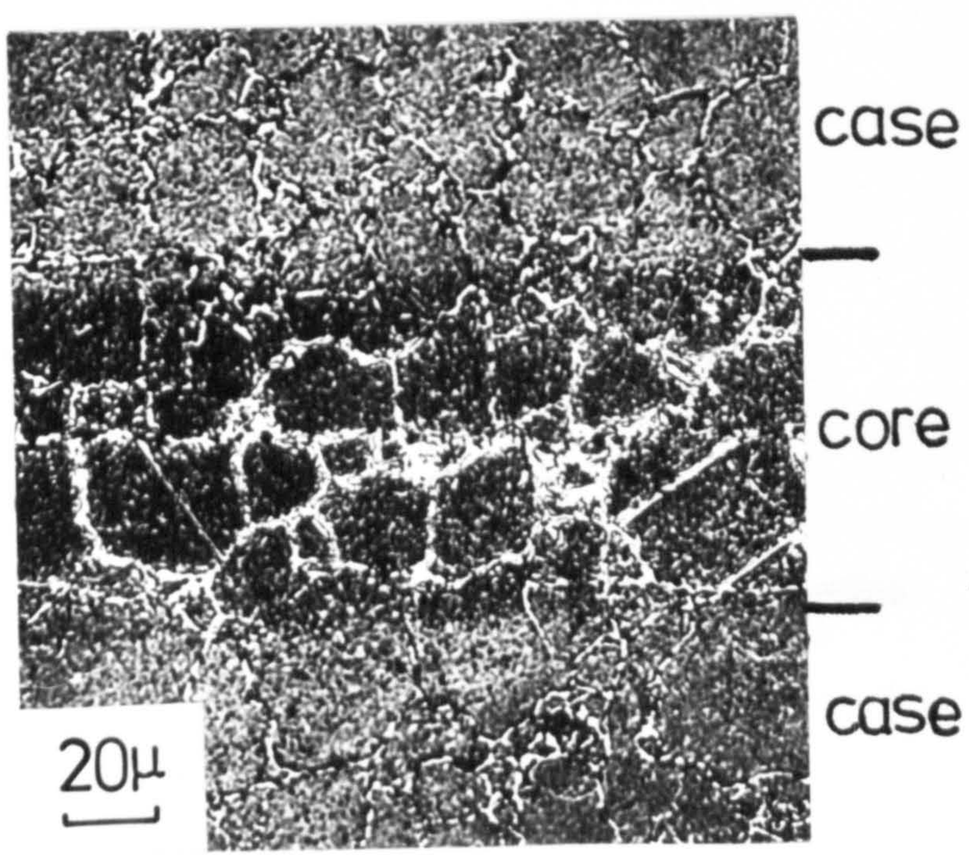

0.07 wt% C
800°C-48h

interface between the nitrided layer and the core (also reported by Tyfield & Mackway, 1975), while specimens nitrided at 800°C show a thicker interface and also fine carbide precipitation in the core just below this layer; see Figure V.10.

(b) X-ray identification

The distribution of phases in the surface layers depends on the nitriding temperature as well as on the cooling-rate. X-ray diffraction patterns of the surface of wire nitrided at 600°, 700° and 800°C and either air-cooled or quenched are shown in Figure V.11. The very weak reflexions that are not indexed are from oxide formed during quenching. The measured lattice parameters of the different phases are given in Table V.2. No Cr_2N is detected on the surface of nitrided specimens but its structure is close to that of ε-Fe_2N_{1-x} (Bywater & Dyson, 1975), and the lattice parameters of both phases change with nitrogen content.

The following important observations can be made regarding Figure V.11:

(i) the intensity of γ-austenite reflexions on air-cooled specimens increases with temperature (a, c, e);

(ii) the diffraction patterns of specimens nitrided at 600° and 700°C and quenched (b, d) show the same phases

Figure V.11

X-ray diffraction photographs of AISI L316 nitrided in pure ammonia for 24h at

600°C (a) air-cooled

(b) quenched

700°C (c) air-cooled

(d) quenched

and 800°C (e) air-cooled

(f) quenched

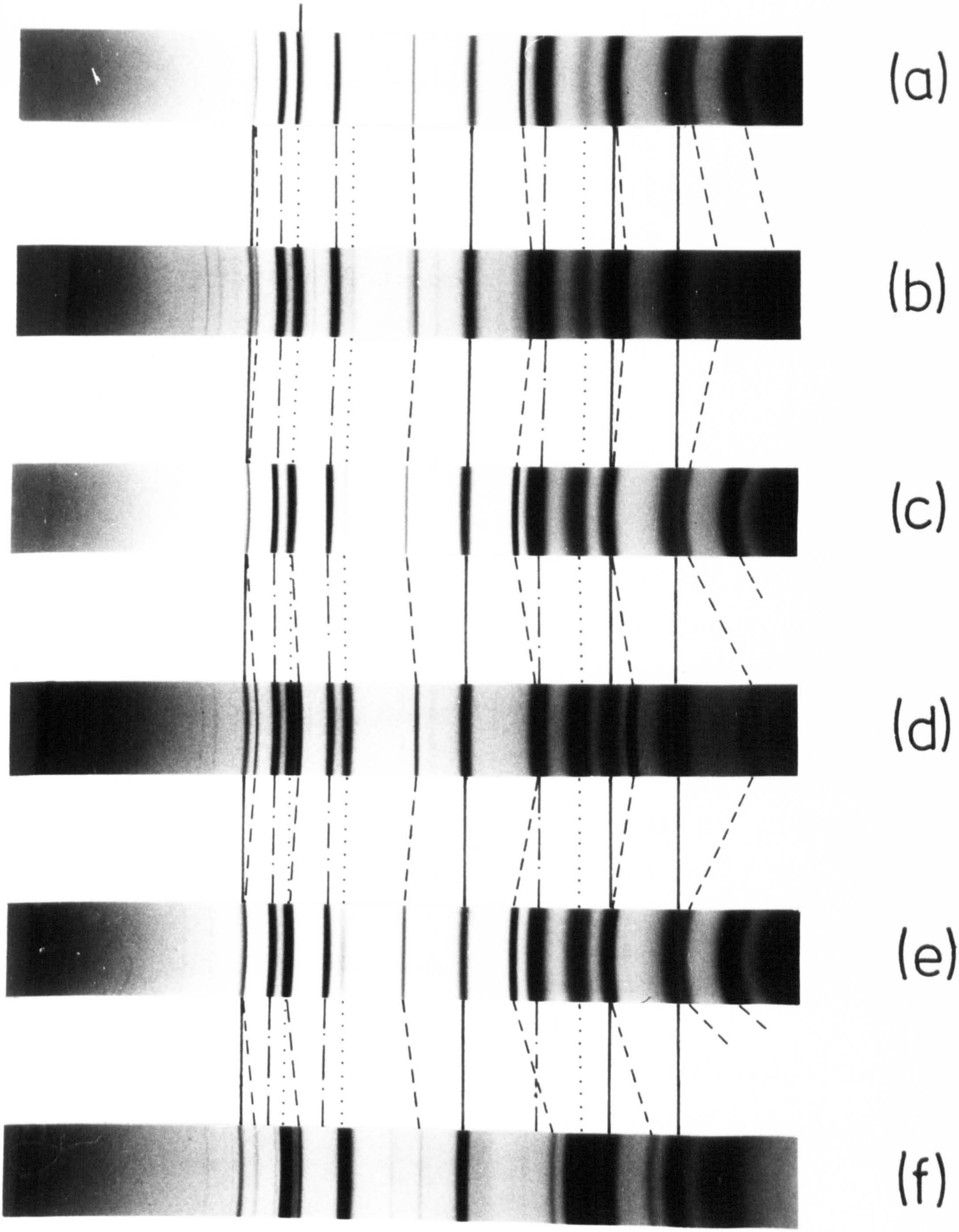

..... γ-Fe

-·-·- γ'-Fe_4N

—— CrN

- - - - ε-Fe_2N_{1-x}

as those air-cooled (a, c) but the lattice parameter of the ε-phase decreases with increasing cooling-rate and nitriding temperature (b, d, e). This is consistent with the iron-nitrogen phase diagram which shows that the solubility of nitrogen in ε decreases with increasing temperature. The approximate nitrogen contents of ε-Fe_2N_{1-x} formed by nitriding AISI L316 at 600°, 700° and 800°C in pure ammonia are given in Table V.2;

(iii) after nitriding at 800°C no γ'-Fe_4N reflexions are observed in X-ray photographs of quenched samples (f) and optical metallography shows the absence of a "white layer" when etched in 2% nital (Figure V.8(b)). However γ'-Fe_4N is not stable at temperature above 690°C (see Figure II.9), although some increase of this temperature should be expected due to the presence of nickel. Thus the precipitation of γ'-Fe_4N on samples nitrided at 800°C occurs during cooling while at 700°C some γ' is formed at nitriding temperature and the remainder by slow-cooling. Note that a difference in the thickness of the "white layer" is observed between slow-cooled and quenched specimens; see Figure V.7;

(iv) in samples quenched from 800°C a double reflexion of γ-austenite is observed which corresponds to austenite of two discrete compositions.

No ε-Fe_2N_{1-x} reflexions are observed in specimens nitrided at low flow-rates (0.15 and 0.03cm s^{-1}) at 700° and

Table 5.2

Lattice parameters of the phases observed by nitriding AISI 316 in pure ammonia

temperature	cooling-rate	ε -Fe_2N_{1-x}	γ' -Fe_4N	CrN	γ -austenite
600°C	air-cooled	a=2.748 Å; c=4.414 Å; c/a=1.606, 10wt% N	3.784 Å-3.785 Å	4.152 Å	-
	quenched	a=2.711 Å; c=4.388 Å; c/a=1.619, 8.5wt% N	3.784 Å	4.152 Å	-
700°C	air-cooled	a=2.748 Å; c=3.414 Å; c/a=1.606, 10wt% N	3.795 Å	4.150 Å	3.644 Å
	quenched	a=2.674 Å; c=4.350 Å; c/a=1.627, 6.2wt% N	3.784 Å	4.150 Å	3.635 Å
800°C	air-cooled	a=2.748 Å; c=4.413 Å; c/a=1.606 10wt% N	3.794 Å	4.150 Å	3.644 Å
	quenched	a=2.620 Å; c=4.307 Å; c/a=1.644 estimated 5.3wt% N	-	4.150 Å (broad)	3.639 Å-3.593 Å

800°C and only γ'-Fe_4N, CrN and γ reflexions are present. At these flow-rates dissociation of ammonia is significant (see Table III.2) and therefore the actual nitrogen potential is not sufficiently high to form ε-Fe_2N_{1-x} (see Figure III.4). The presence of γ'-Fe_4N in samples nitrided at 800°C is due to slow cooling as described above.

The phase distribution through the nitrided layer was studied for specimens nitrided at 600°, 700° and 800°C for 24 and 100 hours and then air-cooled. After 24 hours at 600°C and 800°C (Table V.3) ε-Fe_2N_{1-x} is present only on the surface of the specimens and in the thicknesses of less than 5 μm. The difference between specimens nitrided at 600° and at 800°C is in the variation of intensity of the γ'-Fe_4N pattern with distance from the surface. In specimens nitrided at 600°C, γ' reflexions are observed up to a depth of 50 μm although optical microscopy shows a "white layer" of only $\sim$ 20 μm (Figure V.4). Thus the "dark-etched" layer of specimens nitrided at 600°C must also contain γ'. At 800°C, the "white layer" of 10-15 μm (Figure V.4) is in agreement with the X-ray depth profile (Table V.3). The presence of α-ferrite is observed at approximately 80 μm depth for both specimens but whereas at 600°C the reflexions are always weak, at 800°C they are relatively strong. Next to the interface the austenite reflexions become broad corresponding to a range of nitrogen concentration; see Figure V.12 for 600°C and Figure V.13

Table V.3

Phase distribution in the nitrided layer of specimens nitrided in pure ammonia for 24 hours and air-cooled

temperature °C	distance from surface µm	phases Fe_2N_{1-x}	Fe_4N	CrN	γ	α	Cr_2N
600	0	S	VS	S			
	5		VS	S			
	10		VS	S	VW		
	20		VS	S	W		
	25		S	S	M		
	30		M	S	M		
	35		W	S	S		
	50			S	VS		
	70			S	VS		
	110			S	VS	VVW	
	120			S	S diffuse	W	
	140			M	low VS high W	W	
	150				low VS high W		
800	0	S	S	S	W		
	10		M	S	M		
	15		VW	S	M		
	30			S	S		
	40			S	VS		
	80			S	VS	M	VVW
	90			S	low VS high VW	M	VW
	120			S	low VS high VW	M	VW
	125			S	broad	M	VW
	135			S	broad	M	W
	138			M	broad	M	W
	140				broad	VW	W

VS: very strong
S : strong
M : medium
W : weak
VW : very weak
VVW: very very weak

Figure V.12

AISI L316 nitrided at 600°C in pure ammonia for 24h. X-ray diffraction photographs at depth of

(a) 130 μm

(b) 145 μm

and (c) 150 μm

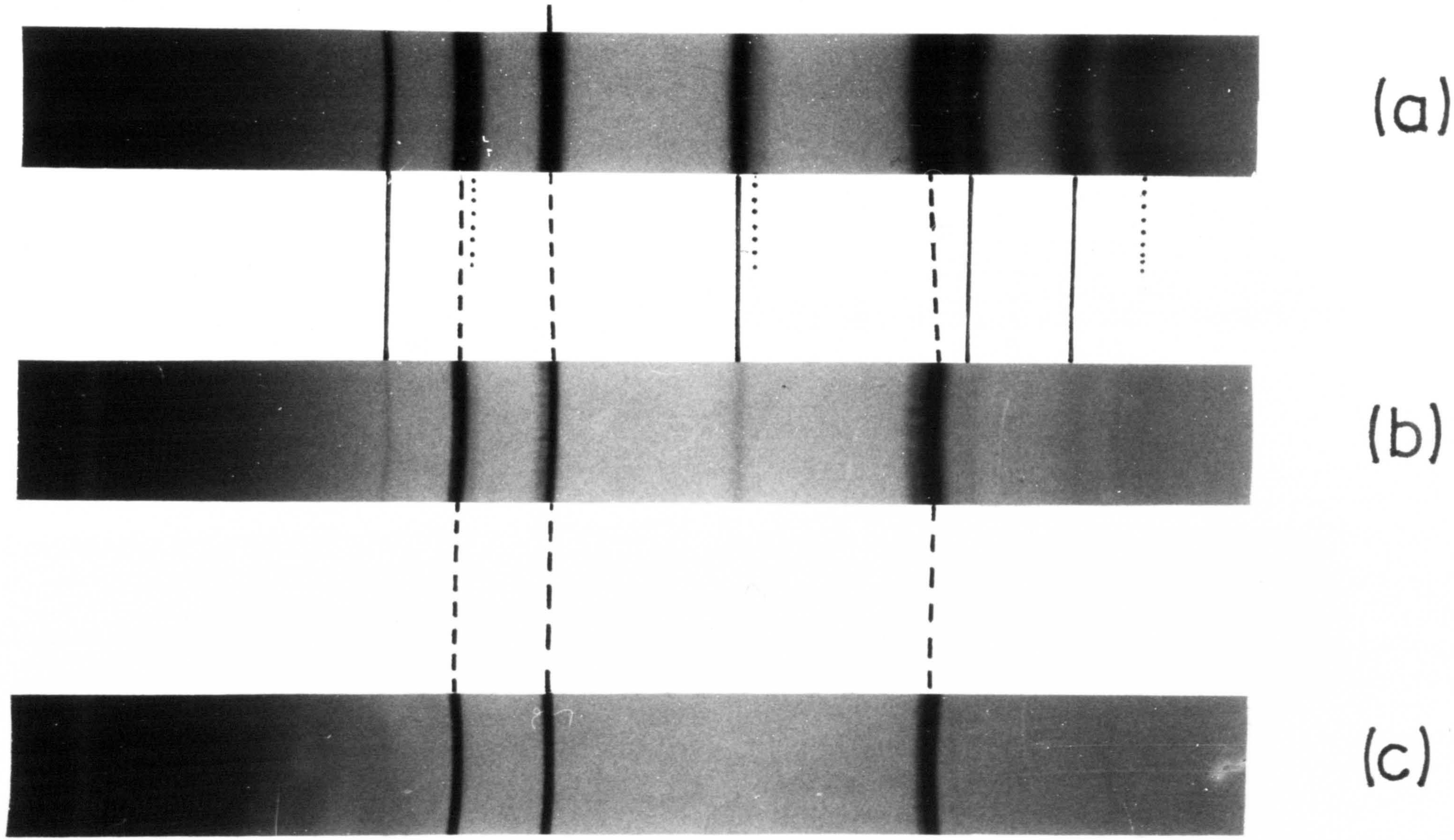
(a)
(b)
(c)
..... α-Fe
----- γ-Fe
—— CrN

Figure V.13

AISI L316 nitrided at 800°C in pure ammonia for 24h. X-ray diffraction photographs at depths of

(a) 125 μm

and (b) 145 μm

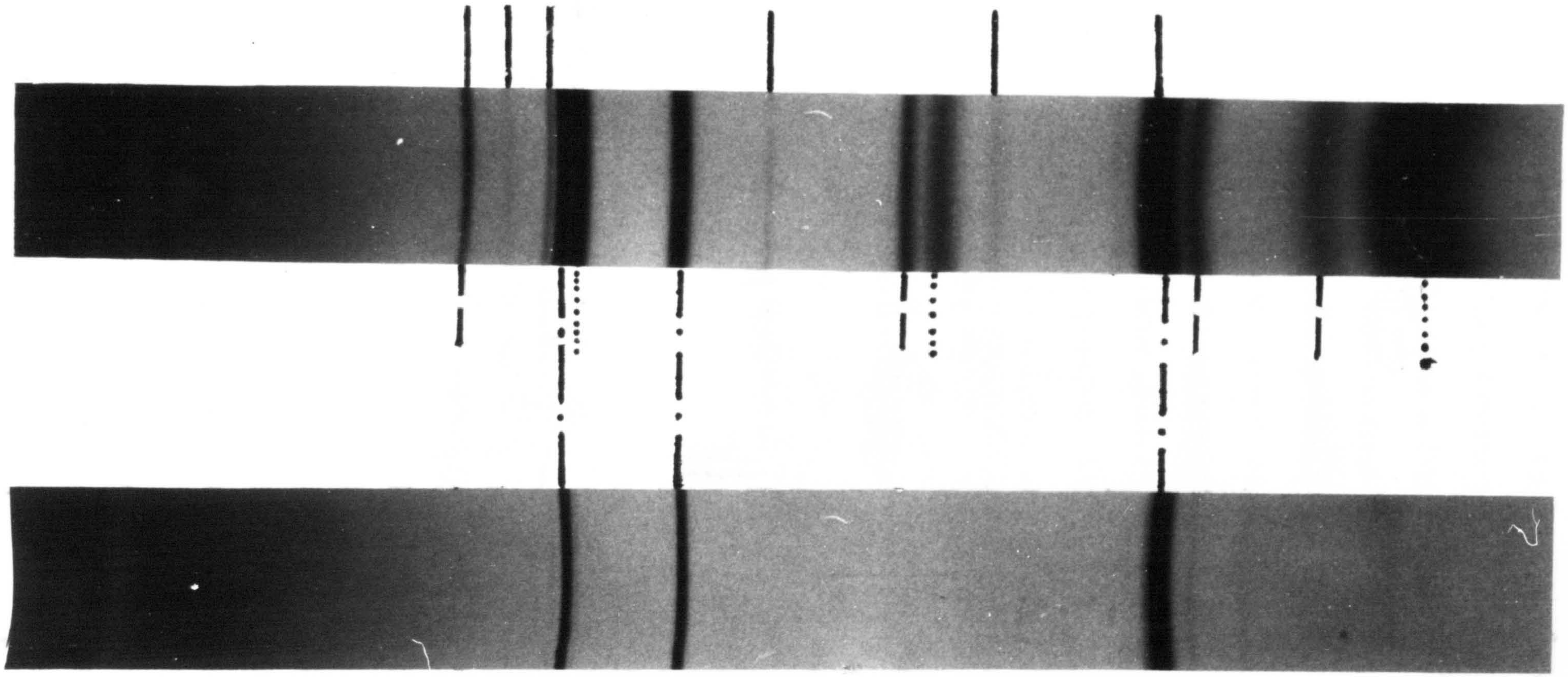

(a)

(b)

—·— γ-Fe

····· α-Fe

- - - - CrN

—— Cr_2N

for 800°C. At 800°C weak reflexions of Cr_2N are present from 90 μm depth up to the interface between case and core. As CrN is precipitated, the chromium concentration in the austenite decreases and ferrite is formed (see Figure II.4). Cr_2N then precipitates in a ferritic matrix because at this depth the nitrogen concentration is lower than at the surface. With increasing nitriding time at 800°C the thickness of the layer containing α-ferrite increases and so the formation of α must occur at the nitriding temperature. Quenched specimens show the same phase distribution in the inner subscale as those air-cooled, but AISI 316 samples heat-treated in an inert atmosphere and quenched from 800°C do not contain ferrite.

Specimens nitrided at 550°C show the same phase distribution as those at 600°C, while for samples nitrided at 700°C the phase distribution is similar to that at 800°C except that Cr_2N and α-ferrite are extremely weak.

From optical observations and X-ray diffraction measurements conclusions can be drawn concerning the distribution and composition of phases in the nitrided layer. For samples nitrided at 600°C, the nitrided surface is made up of: (i) a compound layer ("white layer") which consists of a very thin layer of ε-Fe_2N_{1-x} and a layer containing γ'-Fe_4N+CrN; (ii) a "dark-etched" layer of γ'-Fe_4N +CrN+γ; and (iii) an inner subscale of γ+CrN which grows with nitriding time. Some α-ferrite is also present

next to the core. At 800°C there is a thin layer of ε and the "white layer", which is formed by slow-cooling consists of γ'+CrN+γ . The inner subscale at 800°C can be divided in two parts: (i) a layer of γ +CrN; and (ii) a layer of CrN+Cr_2N+ γ + α which grows with nitriding time. At both temperatures the austenite shows a sharp gradient of nitrogen concentration next to the interface between case and core. The nitrided layer formed at 700°C consists of ε with a "white layer" of γ'-Fe_4N+ CrN and an inner subscale identical to that formed at 800°C but with less Cr_2N and α -ferrite.

The difference in etching behaviour of the compound layer observed in Figures V.4 and V.9 is due to precipitation of γ'-Fe_4N. At 600°C the "white layer" is followed by an inner "dark-etched" layer (Figure V.4) which, as X-ray diffraction shows, contains γ'-Fe_4N (Table V.3). The different response to sulphate-chloride etching (Figure V.9) with nitriding temperature arises because γ' is precipitated at the nitriding temperature at 600°C but not at 700° and 800°C, whereas it precipitates on cooling from 700° and 800°C. The lighter layer observed in the inner subscale at the highest temperatures corresponds to the presence of Cr_2N and α -ferrite together with CrN+γ . However, the nitrided layer is complex as shown by the nitrogen profiles of air-cooled samples nitrided for 24 hours; see Figure V.14. High surface nitrogen concentration corresponding to the

Figure V.14

Schematic nitrogen profile of AISI L316 nitrided at 600°, 700° and 800°C in pure ammonia for 24h and air-cooled

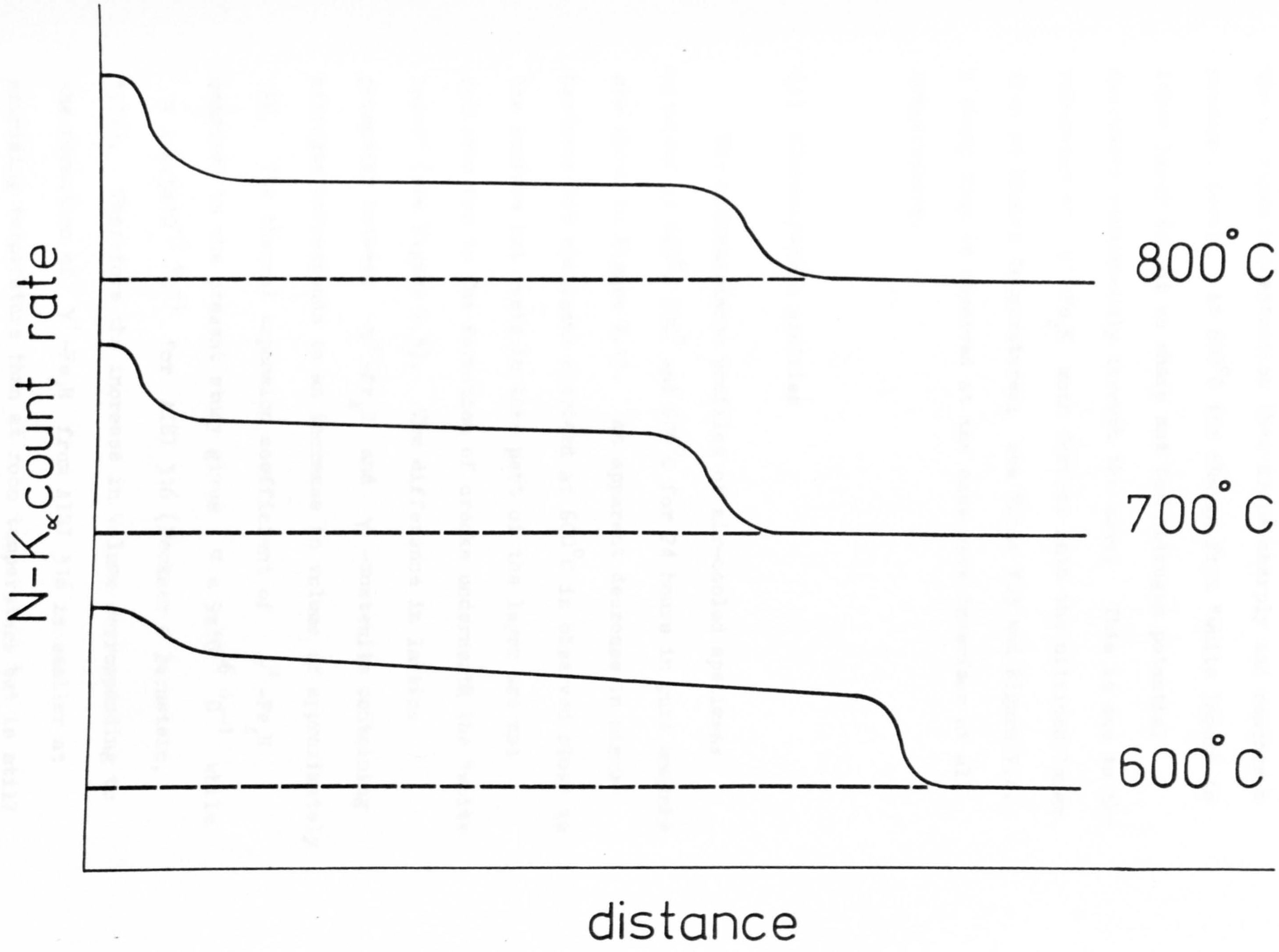
N-K$_\alpha$ count rate
800°C
700°C
600°C
distance

formation of ε and γ' is obtained at 700° and 800°C but the nitrogen concentration then drops sharply and reaches a constant level. At 600°C the change from "white layer" to inner layer is not so sharp and the nitrogen potential decreases continuously through the case. This is due to the formation of γ'-Fe_4N much further into the nitrided layer than at higher temperatures; see Table V.3 and Figure V.4. A sharp drop is observed at the case-core interface at all temperatures.

(c) Microhardness profiles

The microhardness profiles of air-cooled specimens nitrided at 600°, 700° and 800°C for 24 hours in pure ammonia are shown in Figure V.15. An apparent decrease in microhardness for specimens nitrided at 600°C is observed close to the surface but tests in this part of the layer are not reliable due to the formation of cracks underneath the "white layer" (see Figure V.5). The difference in lattice parameter between γ'-Fe_4N and γ-austenite containing nitrogen corresponds to an increase in volume of approximately 12%. The thermal expansion coefficient of γ'-Fe_4N measured in the present study gives $\alpha = 9\times10^{-6}\ ^{o}C^{-1}$ while $\alpha = 6.5\times10^{-5}\ ^{o}C^{-1}$ for AISI 316 (Peckner & Bernstein, 1977). Therefore the increase in volume corresponding to the formation of γ'-Fe_4N from AISI 316 is smaller at nitriding temperature than at room temperature but is still

Figure V.15

Microhardness profiles of AISI L316 nitrided at 600°, 700° and 800°C in pure ammonia for 24h and air-cooled

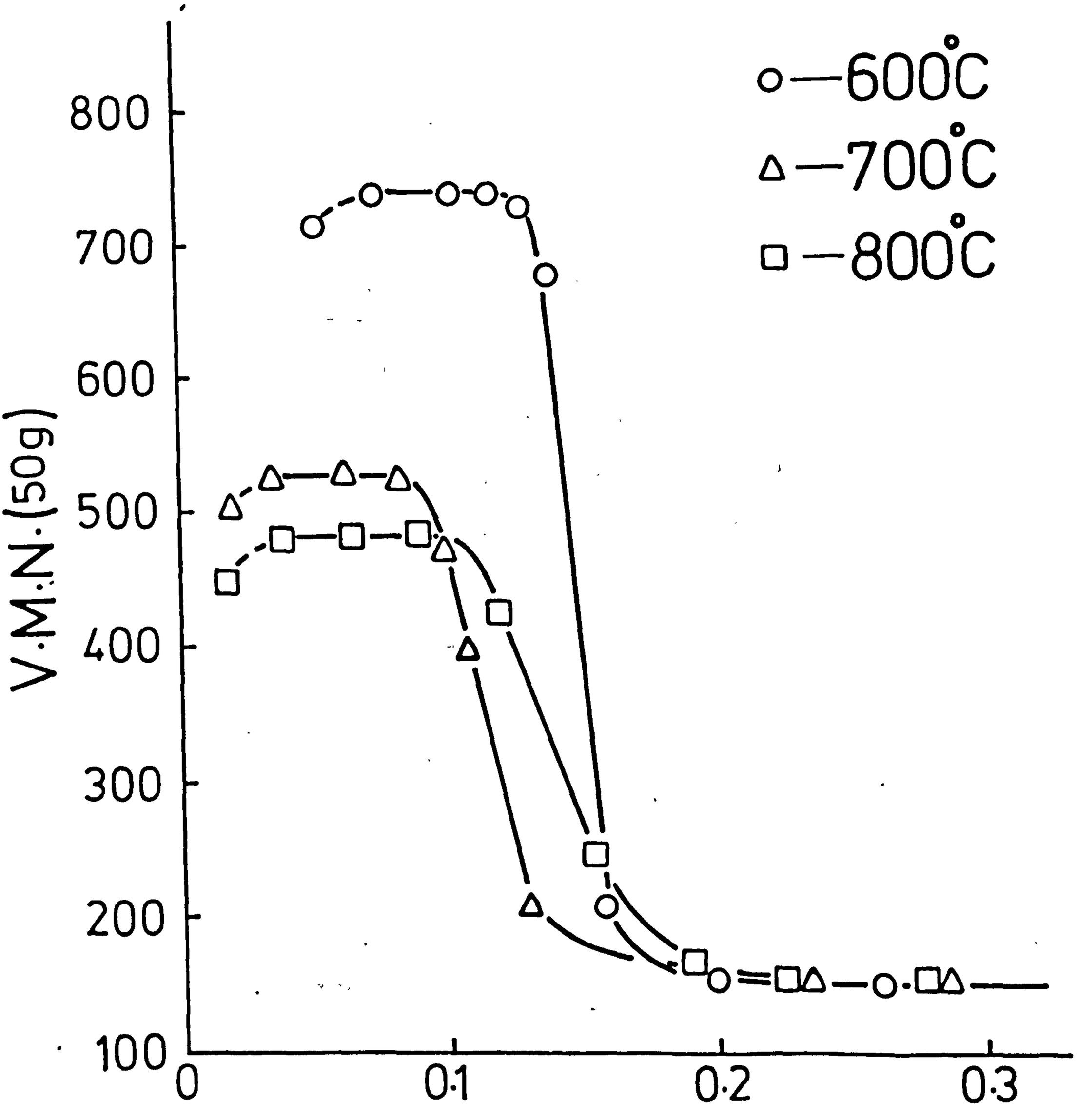
800
700
600
500
400
300
200
100
V.M.N.(50g)
0
0·1
0·2
0·3
distance from surface/mm
○—600°C
△—700°C
□—800°C

significant. The "white layer" is thus in compression at all temperatures. When this compound layer thickens the stresses relax at the outer surface but the inner surface is constrained to give a bending force which causes the outer surface to lift outwards and produce lateral cracks. The "white layer" is reported to be the hardest and most brittle part of the nitrided layer and its spalling is such a problem that its formation is avoided in industrial practice; see Bell et al., 1975; Brokman et al., 1979.

The present results show however that hardening of the diffusion layer of samples nitrided at 600°C is also extremely high but decreases with nitriding temperature (see Figure V.16). The high hardness obtained at 550°C and 600°C drops sharply between 600° and 650°C to become almost constant above 750°C. A similar profile is reported by Lebrun et al. (1972). In Figure V.16 the microhardness of the inner subscale of specimens nitrided at 500°C is not shown because this layer is not well-defined (see Figure V.3) but a VMN (50g) of 845 has been measured. The decrease in microhardness with increasing nitriding temperature can be explained by coarsening of the structure of the inner subscale as shown by the optical micrographs of V.6-V.8 and more clearly by the TEM micrographs of Figure V.17 and the carbon replication of the inner subscale; see Figures V.18 (b), (c) and (d). Figure V.18(a) represents the structure of the "dark-etched" layer (Figure V.4) of samples nitrided

Figure V.16

Variation of microhardness of the inner subscale of nitrided AISI 316 with nitriding temperature

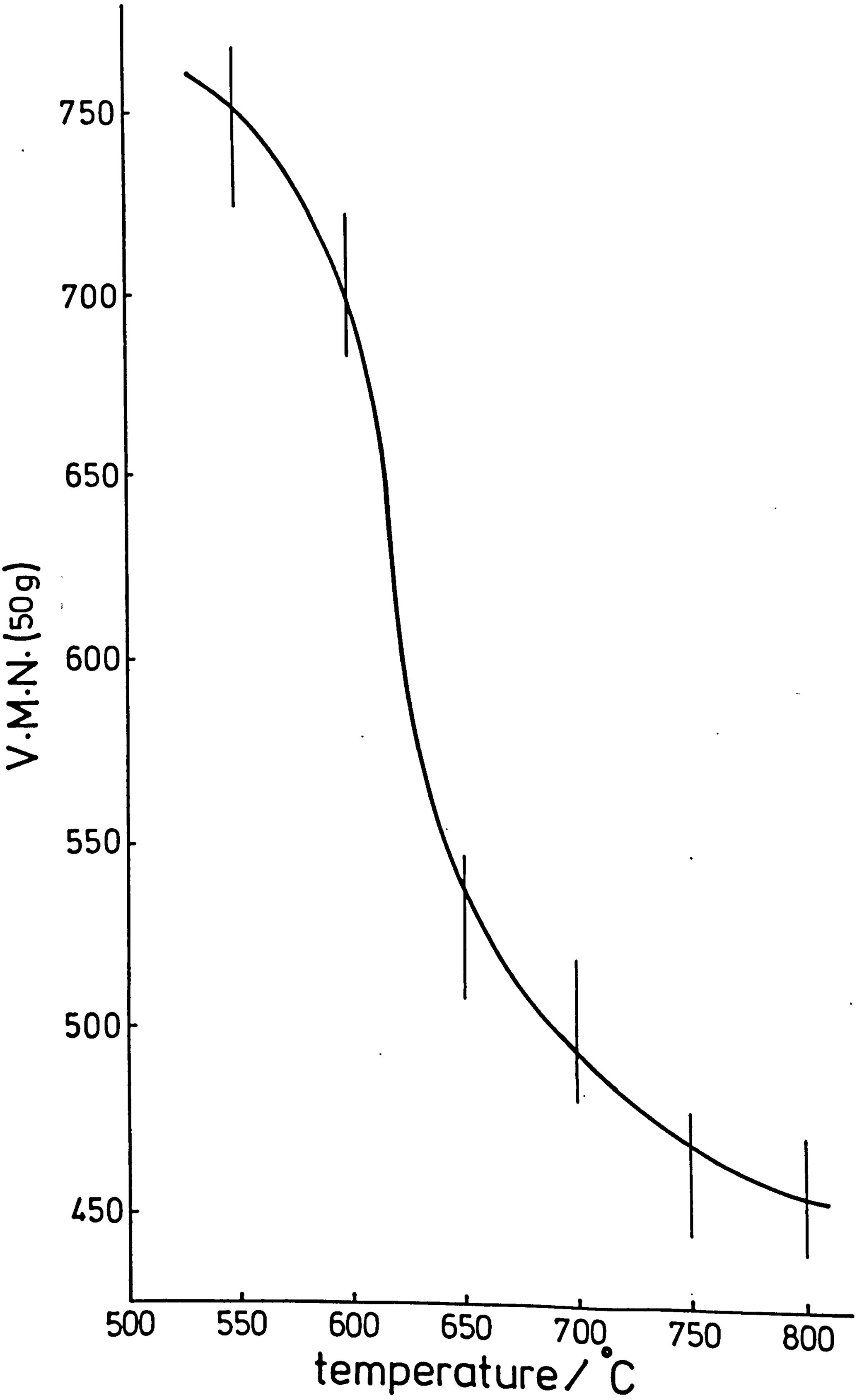
750
700
650
600
550
500
450
V.M.·N.·(50g)
500
550
600
650
700
750
800
temperature / °C

Figure V.17

TEM micrographs of the (γ + CrN) layer in specimens of AISI L316 nitrided in pure ammonia for 24h at 600° and 700°C

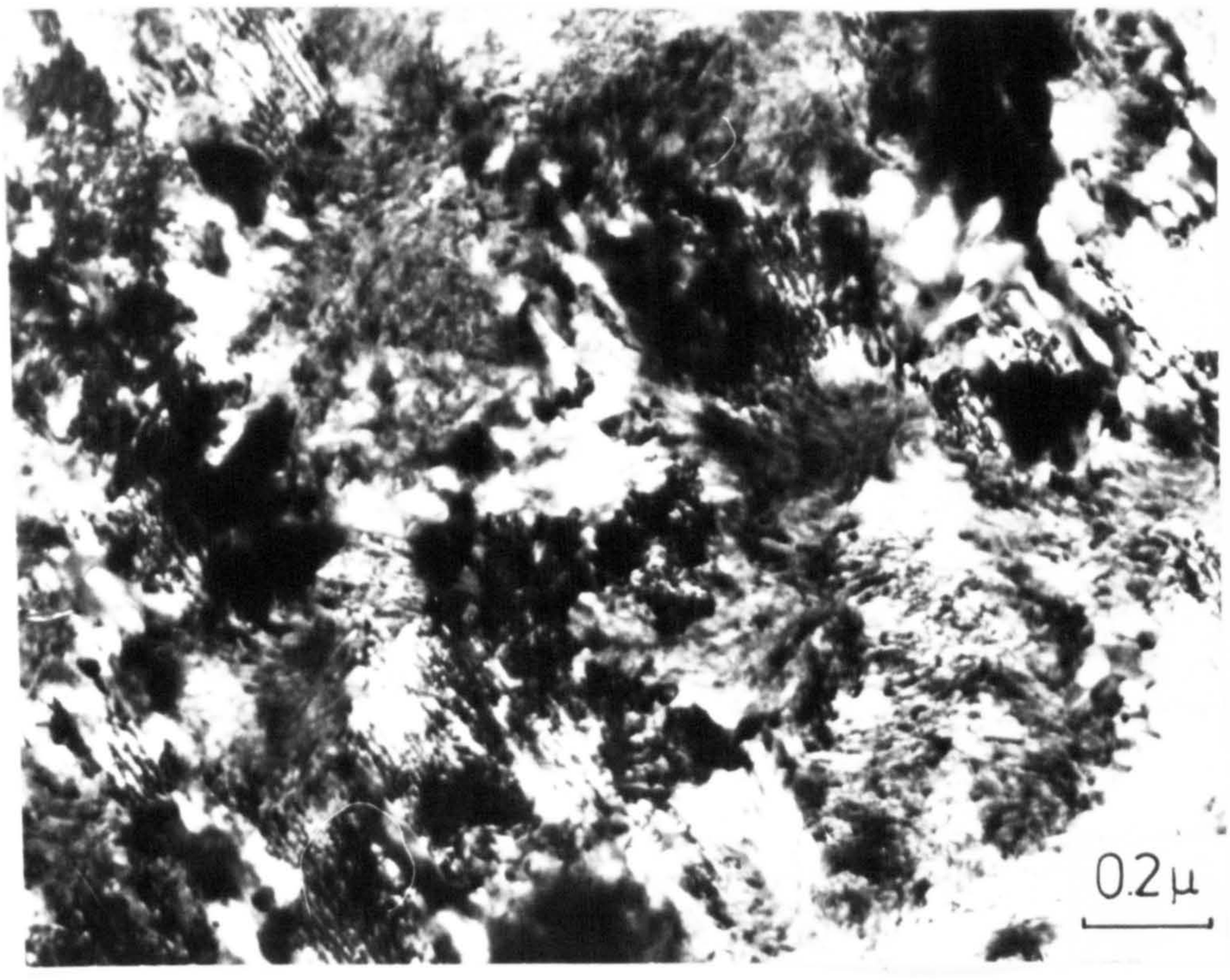

600°C

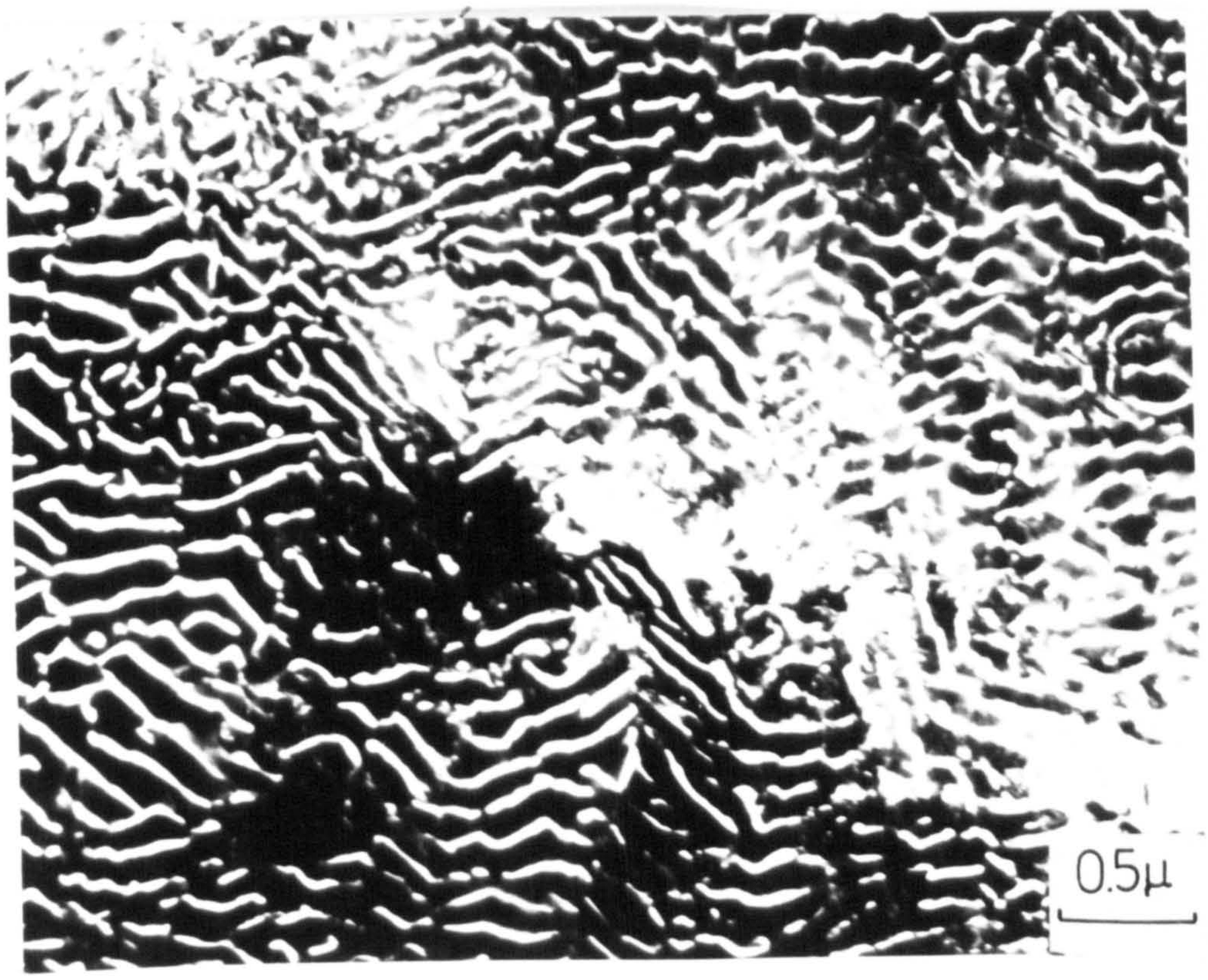

700°C

Figure V.18

TEM micrographs of carbon replicas of AISI L316 nitrided in pure ammonia for 24h:

(a) 600°C "dark-etched" layer

(b) 600°C inner layer

(c) 700°C inner layer

(d) 800°C inner layer

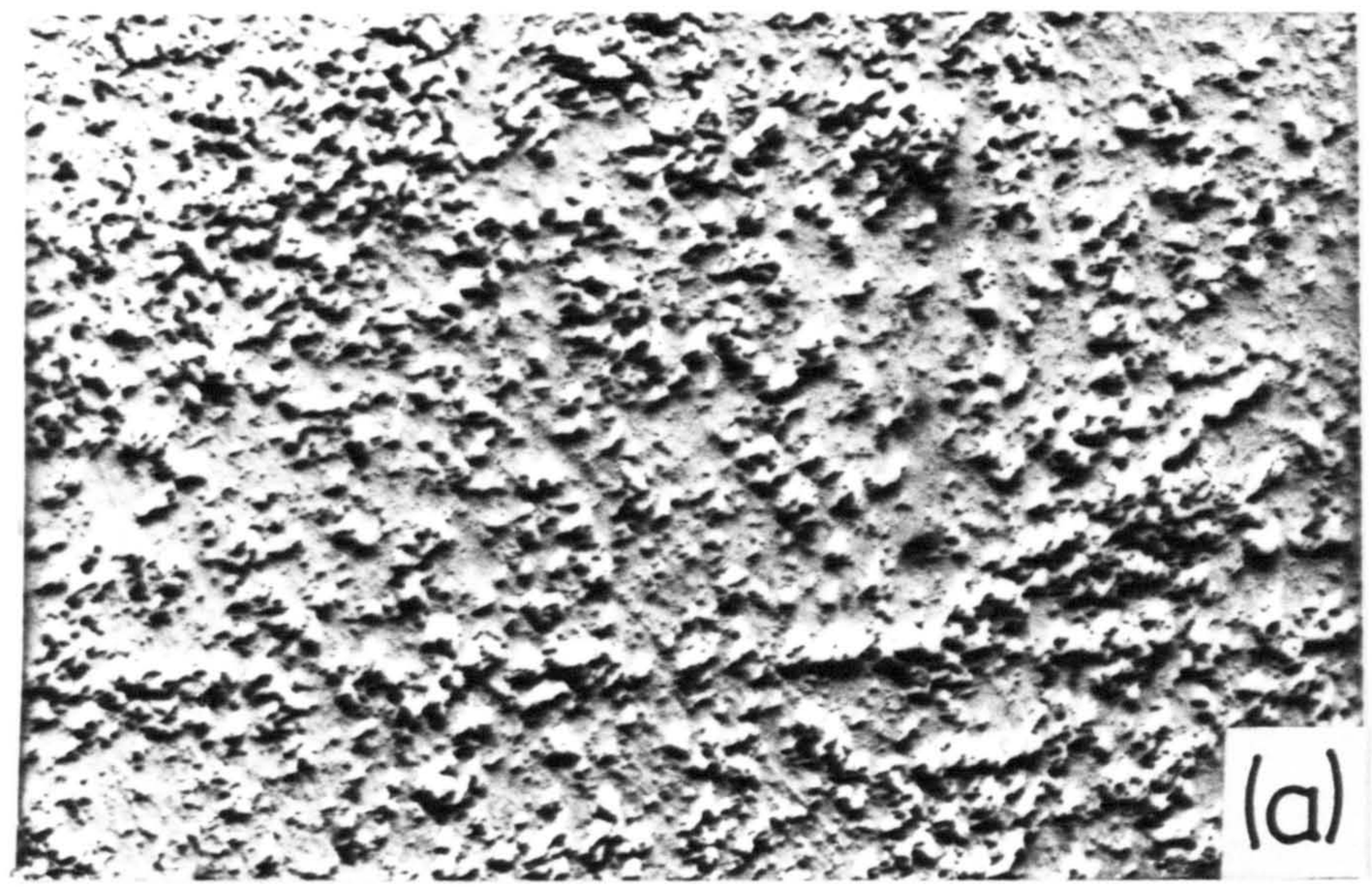

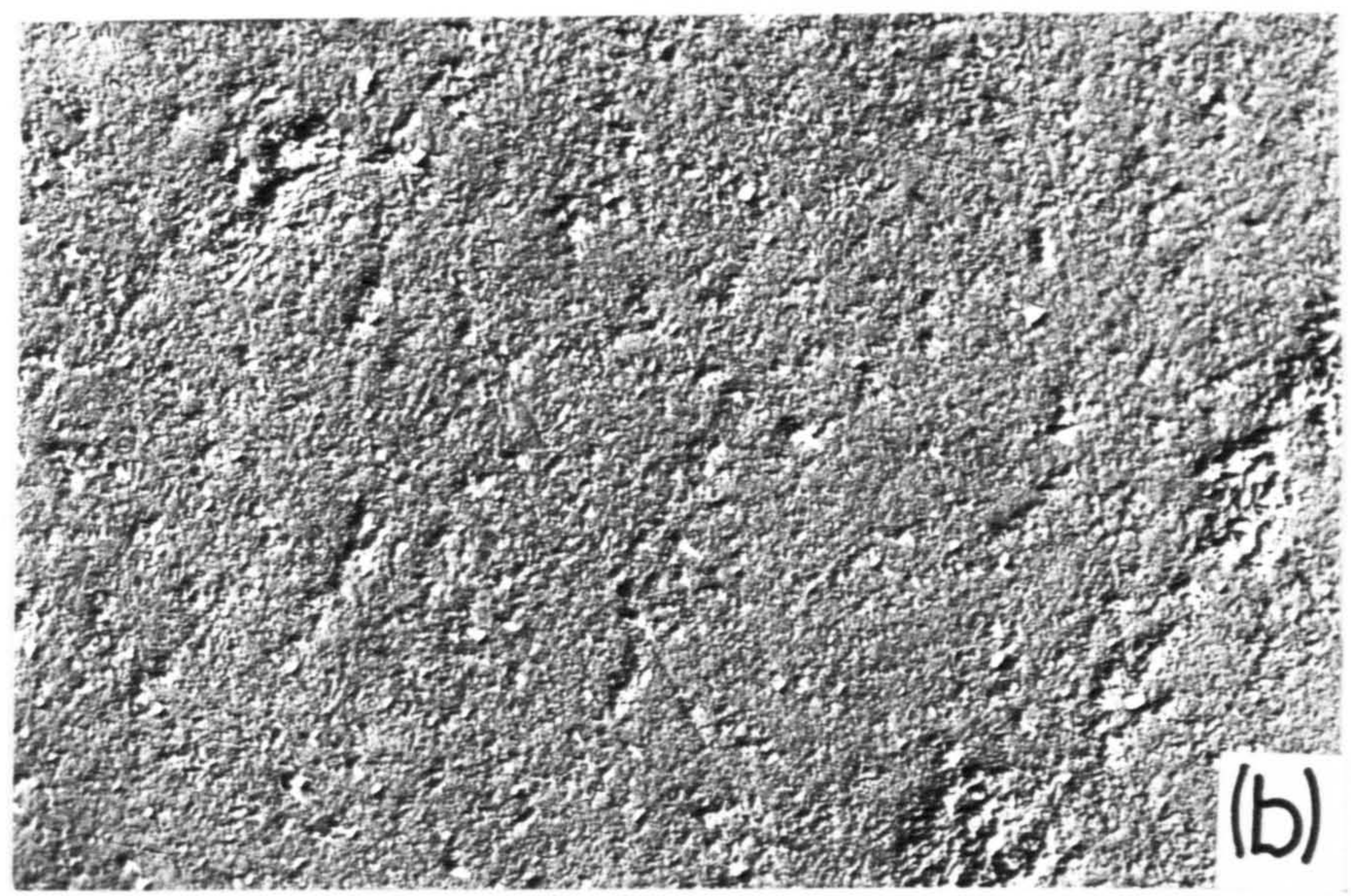

2μ

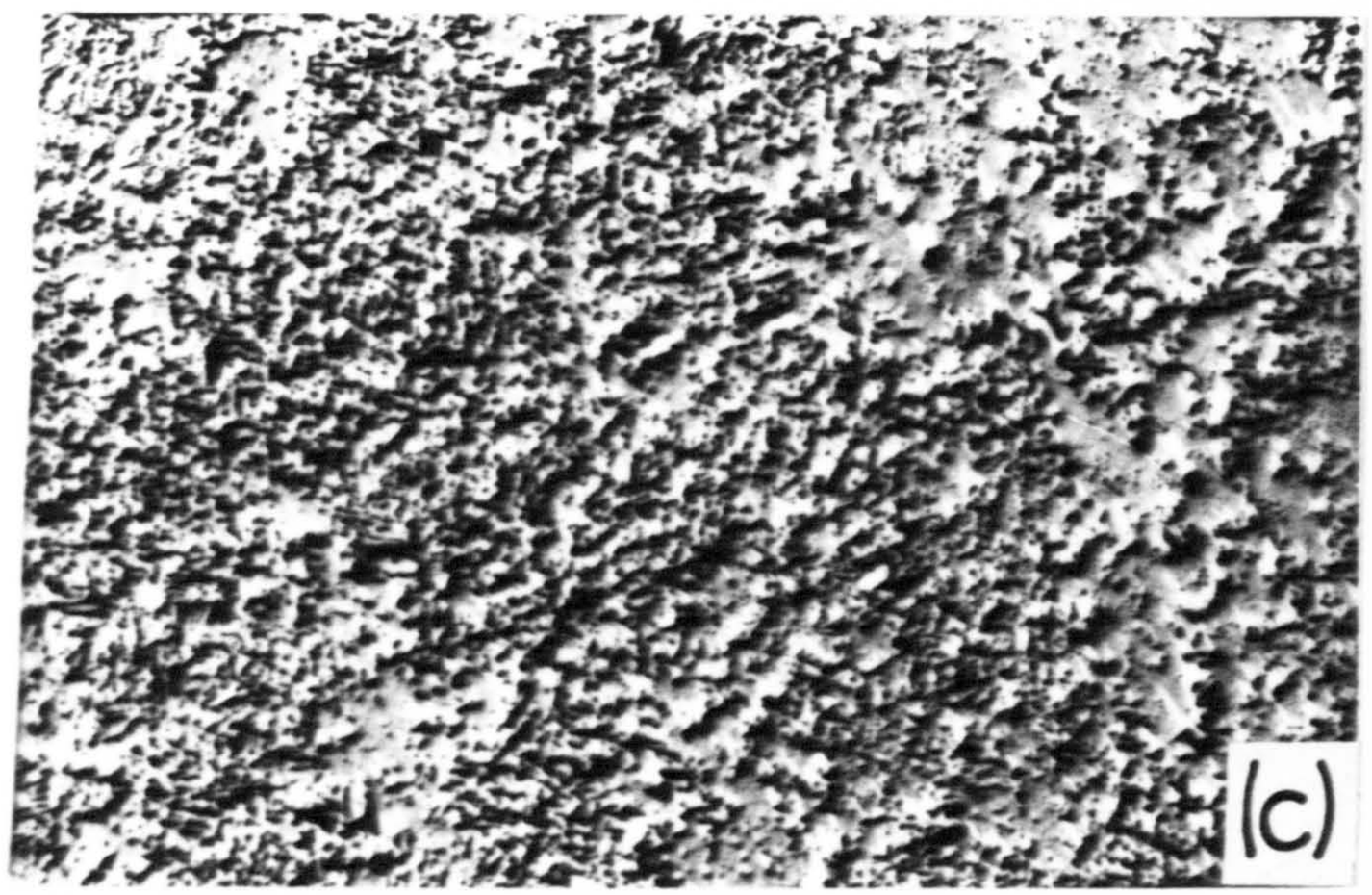

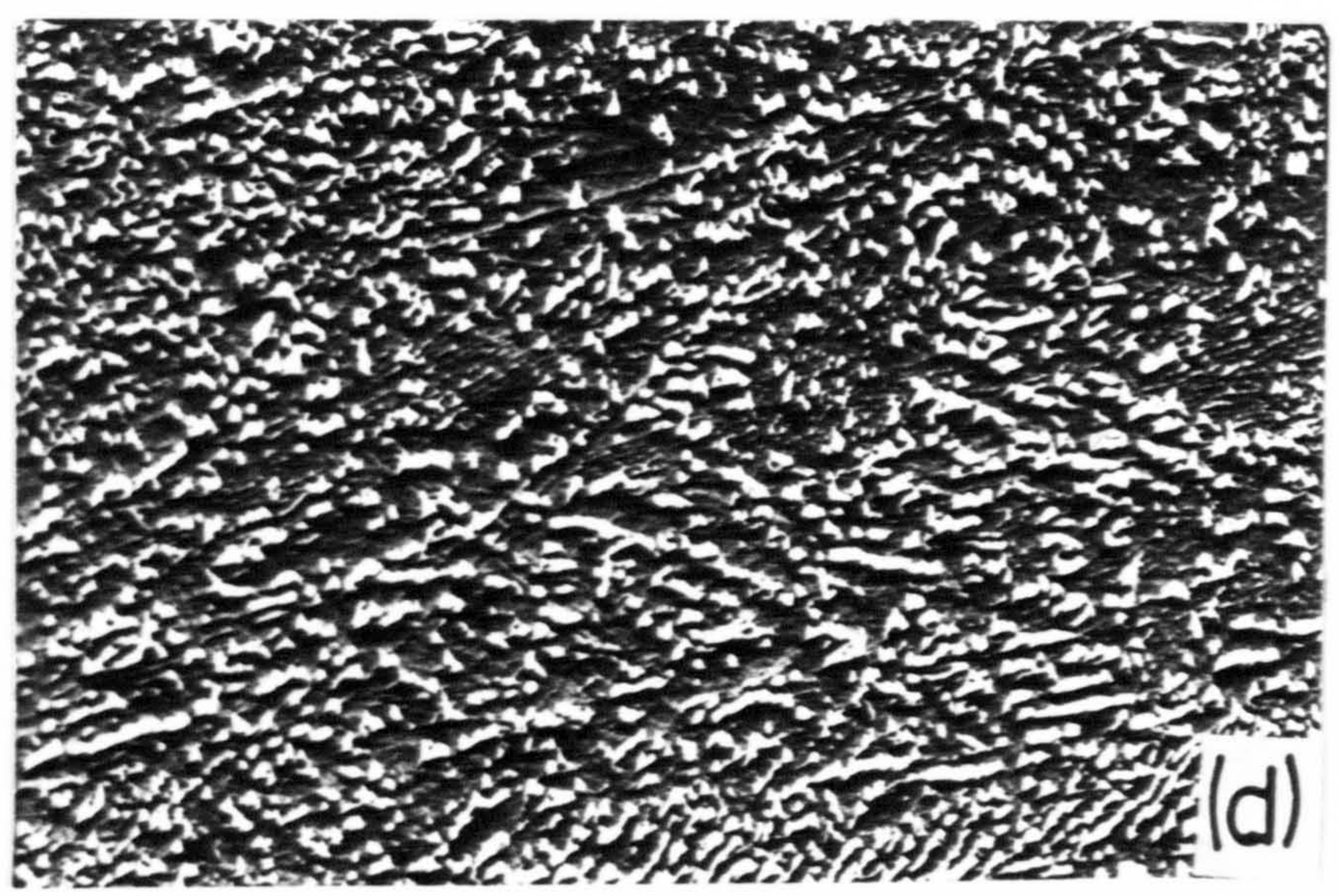

at 600°C. Overaging and coarsening of the structure of the diffusion layers is expected to occur during prolonged nitriding but only a slight decrease in hardness is observed with increasing nitriding time; the decrease is within the error bars of Figure V.16.

V.3 Effect of cold-work on the structure of the nitrided layers

(a) Recrystallisation of AISI L316 at 600° and 800°C

At 600°C, recrystallisation of 20% and 63% cold-worked AISI 316 is very slow and even after 100h heat-treatment the microhardness is still high (Table V.4). Figures V.19(b) and (e) show the microstructures of 20% and 63% cold-worked materials respectively after heat-treatment at 600°C for 24h while in (a) and (d) the microstructures of as-received material with respectively 20% and 63% cold-work are shown. At 800°C, partial recrystallisation occurs in the first 2h, and the microhardness decreases from 246 to 226 VMN (50g) for 20% cold-work and from 397 to 227 VMN (50g) for 63% cold-work. Between 2 and 72.5h the hardness decreases only slightly and reaches 210 VMN (50g); see Table V.4. For fully annealed samples the hardness is around 150 VMN (50g). At the temperatures investigated, grain-growth is negligible and Figures V.18(c) and (f) show respectively the micro-

Table V.4

The microhardness of cold-worked and heat-treated samples of AISI L316 and of the surface layer of nitrided specimens

temperature °C	time h	specimens	VMN (50g) after heat-treatment without nitriding	maximum VMN (50g) of nitrided case
600	0	20% cold-worked	246	
	2	"	246	933
	6	"	246	873
	16	"	237	762
	24	"	241	746
	48	"	233	724
	72	"	231	683
	100	"	222	680
	0	63% cold-worked	397	
	2	"	397	933
	6	"	397	845
	16	"	392	769
	24	"	392	769
	48	"	390	735
	72	"	376	693
	100	"	366	683
800	0	20% cold-worked	246	
	2	"	226	521
	6	"	224	506
	24	"	222	461
	48	"	215	450
	72.5	"	208	420
	0	63% cold-worked	397	
	2	"	227	593
	6	"	226	578
	24	"	224	563
	48	"	220	548
	72.5	"	211	508

Figure V.19

Optical micrographs of AISI L316 etched in 10% oxalic acid:

(a) 20% cold-worked as received

(b) 20% cold-worked and heat-treated at 600°C for 24h

(c) 20% cold-worked and heat-treated at 800°C for 24h

(d) 63% cold-worked

(e) 63% cold-worked and heat-treated at 600°C for 24h

and (f) 63% cold-worked and heat-treated at 800°C for 24h

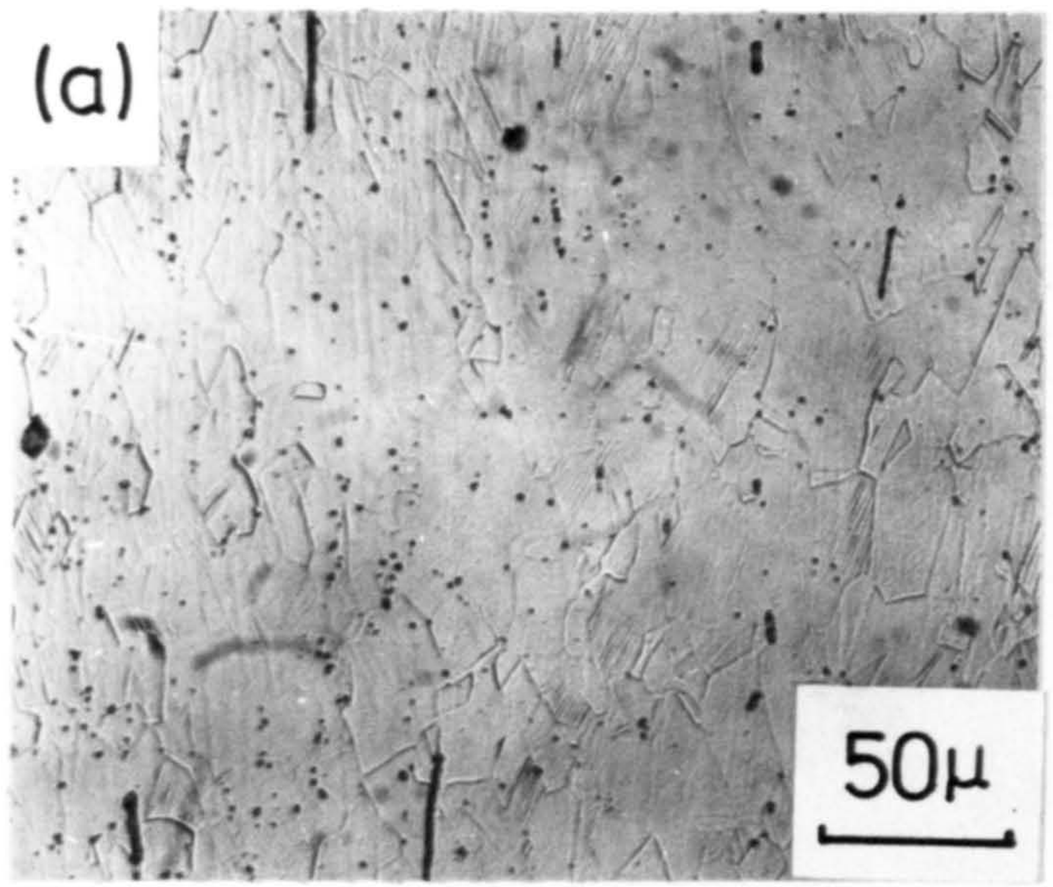
(a)
50μ

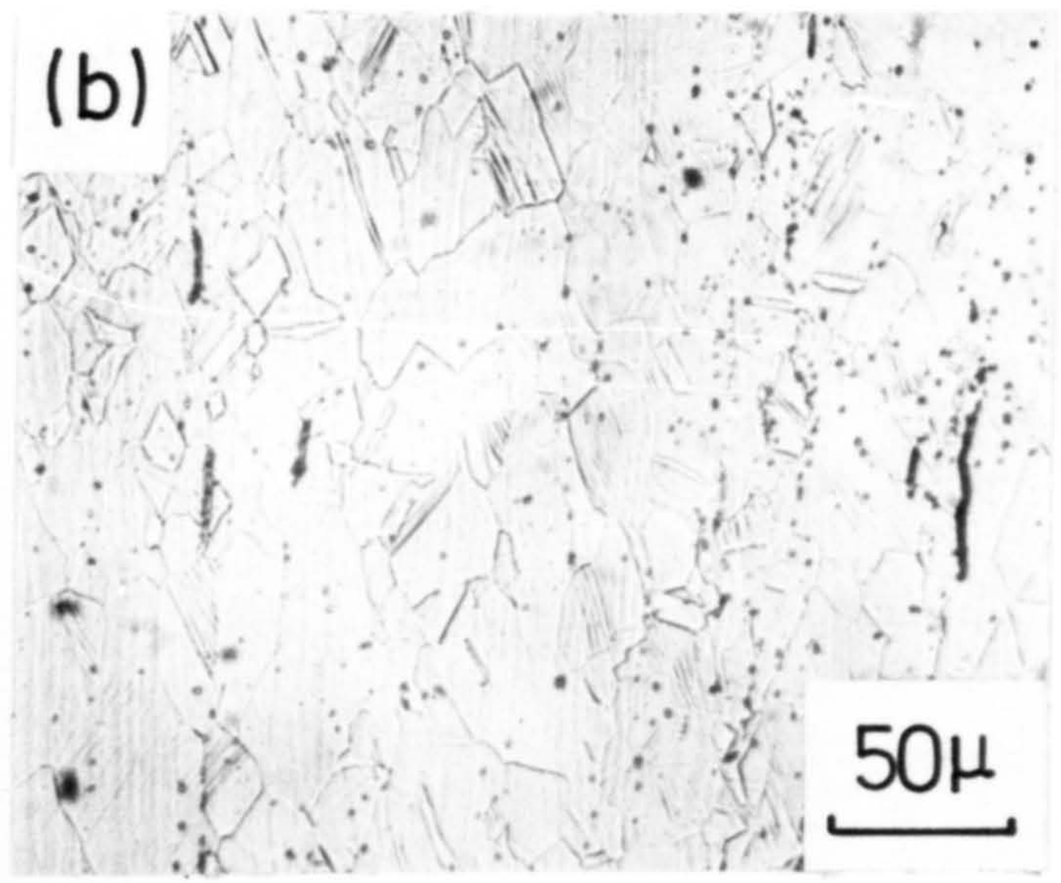
(b)
50μ

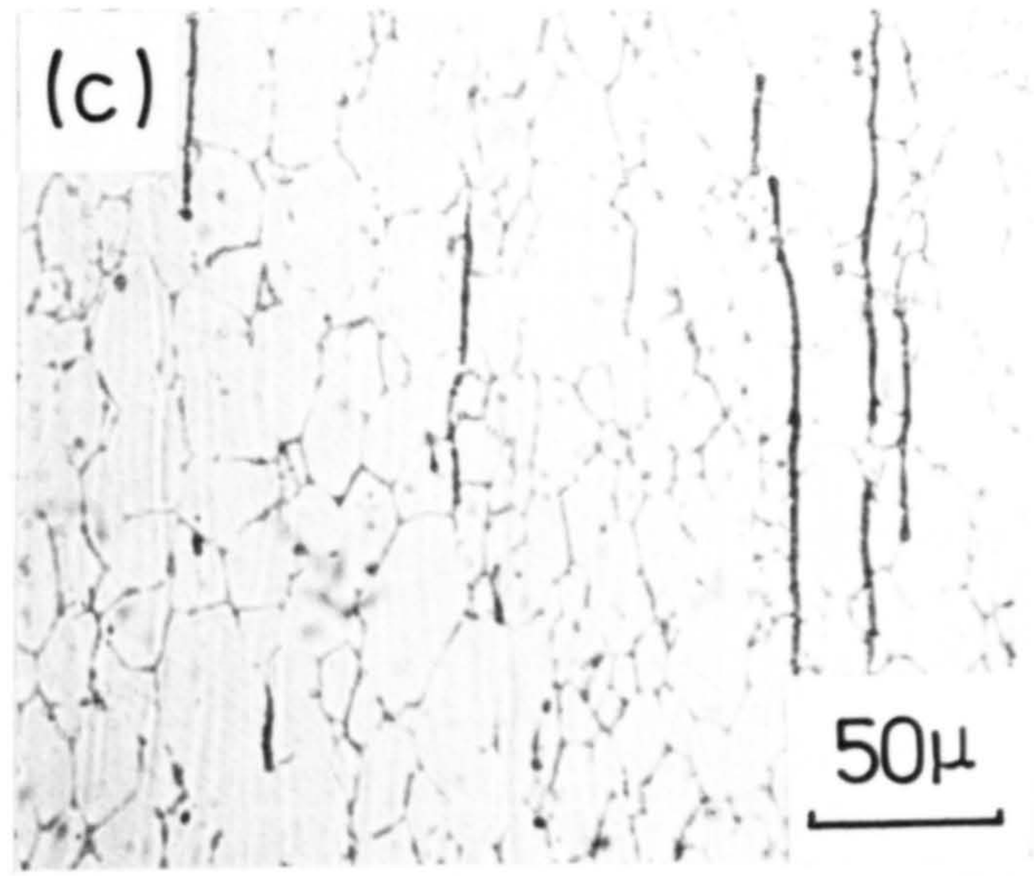
(c)
50μ

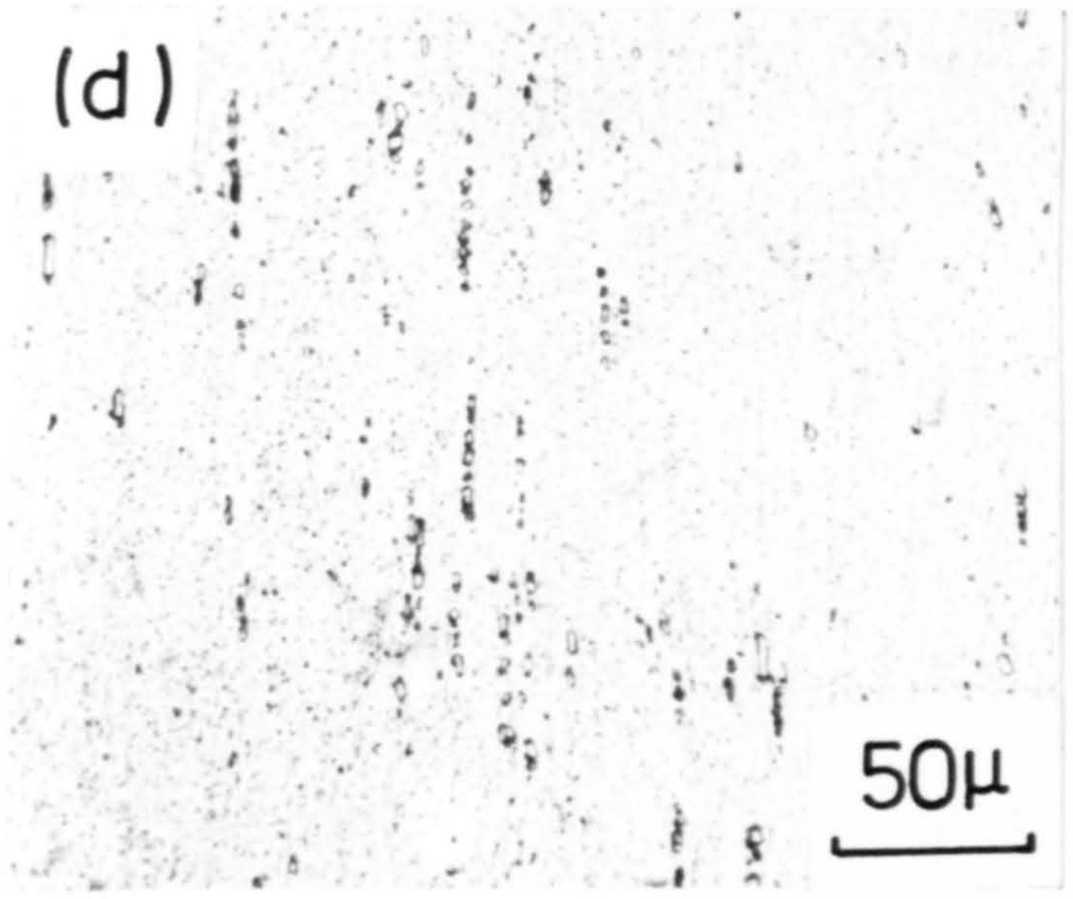
(d)
50μ

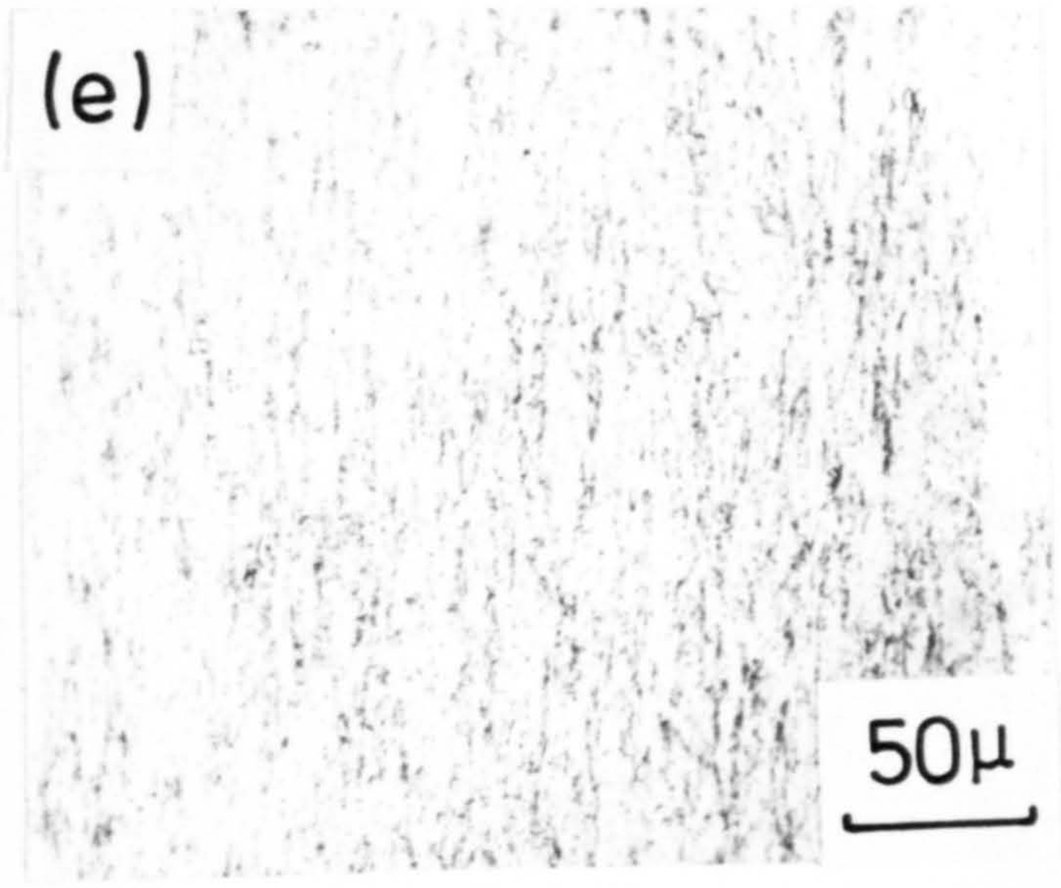
(e)
50μ

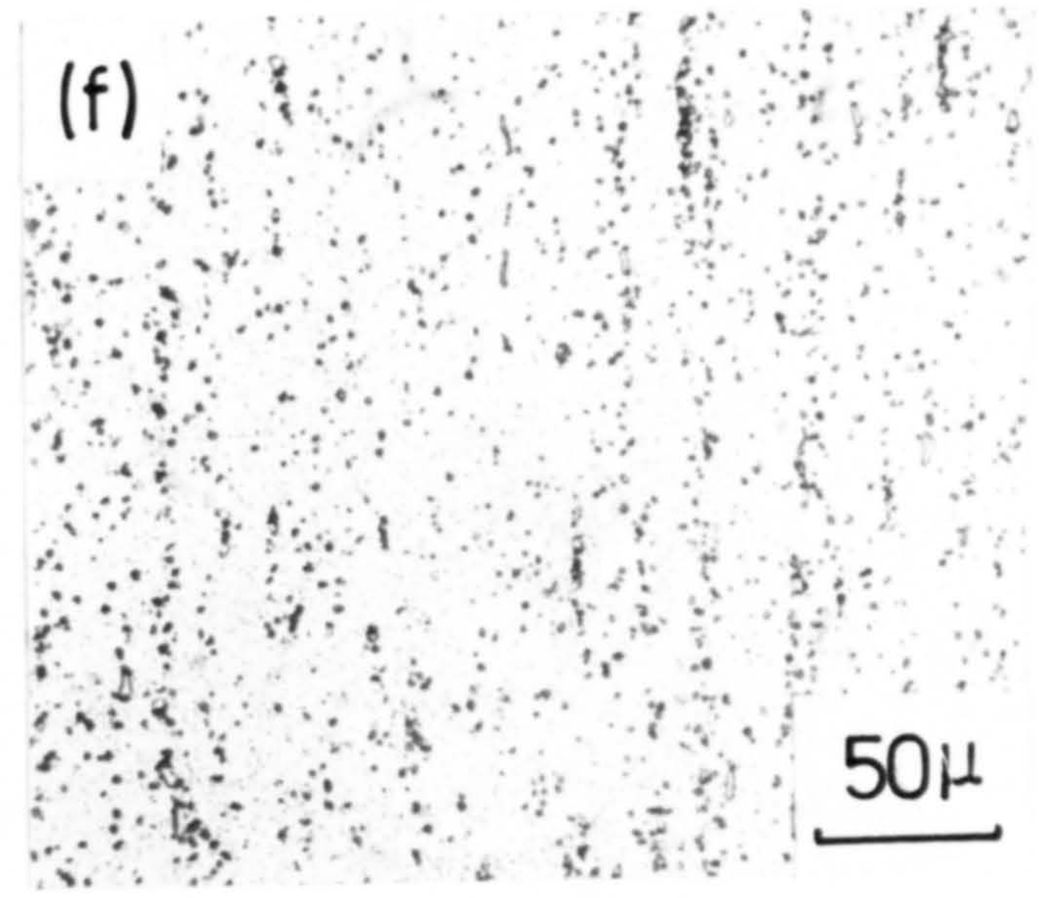
(f)
50μ

structures of 20% and 63% cold-worked samples heat-treated at 800°C for 24 hours. At both temperatures after prolonged heat-treatment the microstructure of 20% cold-worked specimens is close to that of as-received materials but a significant difference is observed with 63% cold-worked specimens. The relatively high microhardness of the core of samples heat-treated at 800°C for 72.5h compared with solution-treated alloys is due to carbide precipitation (Figure V.19(c) and (f)) which is accelerated by cold-working (Figure II.8).

(b) Optical microstructure of the nitrided layer

When etched in 2% nital, cold-worked specimens nitrided at 600°C show a white layer which does not grow with nitriding time. The microstructures of the cases of 20% and 63% cold-worked samples nitrided at 600°C are shown in Figure V.20. The 20% cold-worked sample (a) has the same appearance as the nitrided layer of fully annealed samples (some white precipitates are also seen in the grain boundaries of the "dark-etched"part) while the rolling texture is clearly retained in the nitrided layer of the 63% cold-worked specimen (b). Specimens nitrided at 800°C and quenched do not show a "white layer" (Figure V.21). When nitriding highly deformed specimens at 800°C recrystallisation has not taken place during the first stages of nitriding and therefore the surface of the nitrided layer still retains the cold-worked structure. Then, when recrystallisation occurs,

Figure V.20

Optical micrographs of AISI L316 nitrided in pure ammonia at 600°C for 24h and quenched; etched in 2% nital

(a) 20% cold-worked

(b) 63% cold-worked

(a)

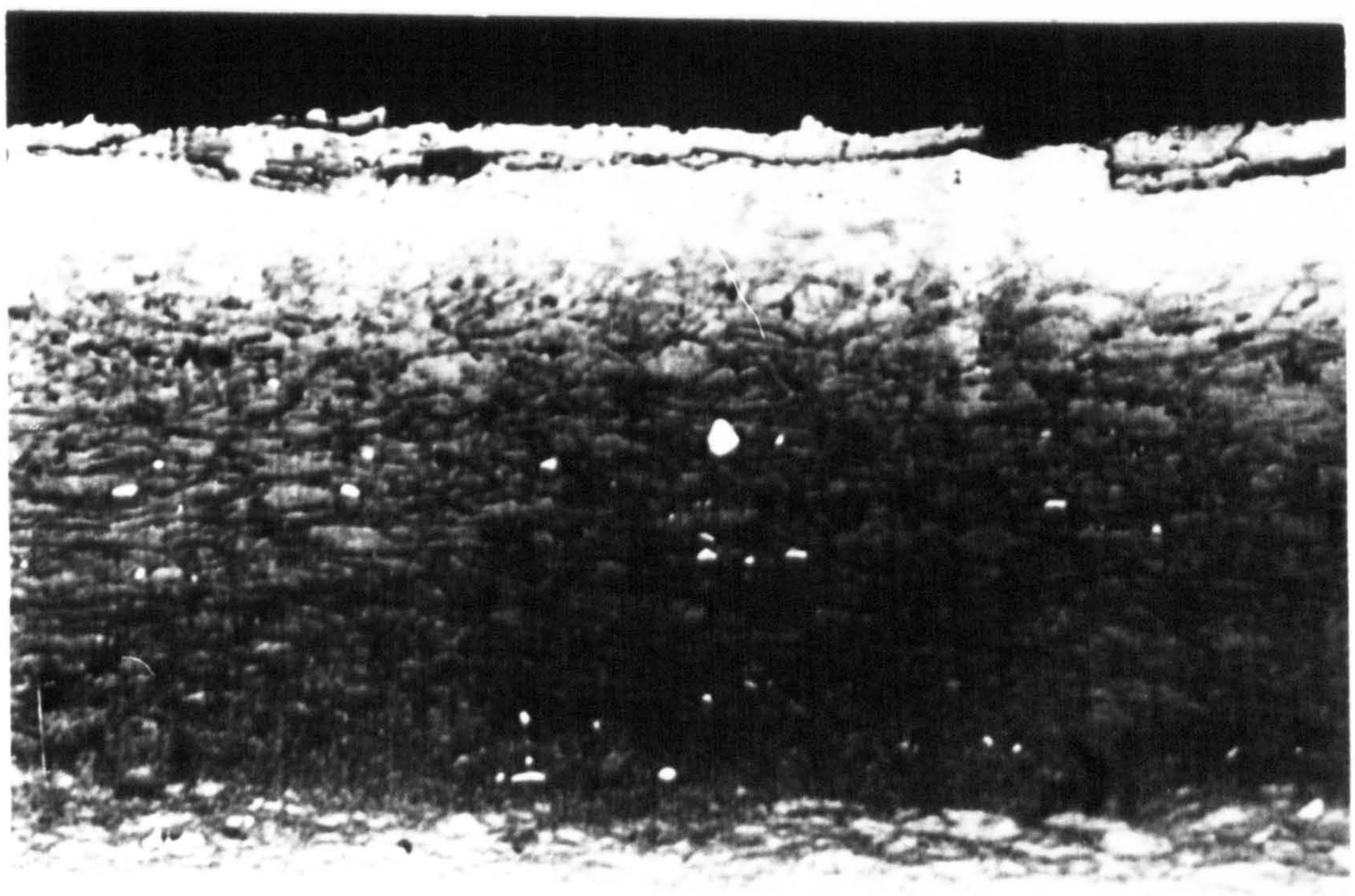

(b)

Figure V.21

Optical micrographs of AISI L316 nitrided in pure ammonia at 800°C for 24h and quenched; etched in 2% nital

(a) 20% cold-worked

(b) 63% cold-worked

(a)

20μ

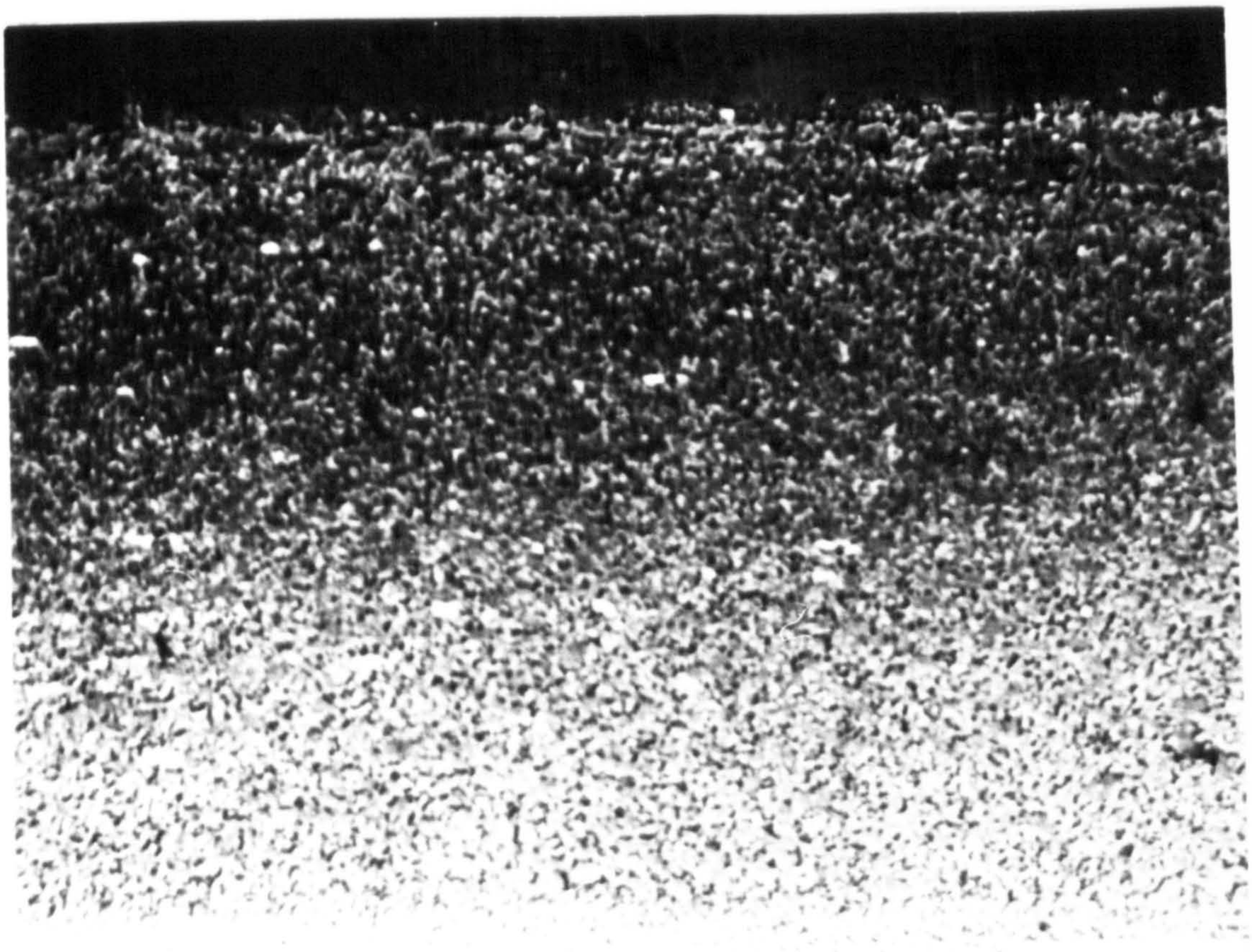

(b)

20μ

grain growth is limited by the precipitation of nitrides. This sequence explains the difference in the microstructures of 20% cold-worked (a) and 63% cold-worked (b) nitrided layers shown in Figure V.21. Vickers microhardness numbers of the nitrided subscales of cold-worked specimens are given in Table V.4 for different degrees of reduction, nitriding temperatures and times. The relatively high value of 508 VMN (50g) for the nitrided case at 800°C after 72.5h nitriding in the 63% cold-worked materials clearly shows that some of the cold-worked structure is retained.

(c) X-ray identification

Specimens with 20% cold-work show little evidence of texture and the strongest reflexion on X-ray diffractometer traces is $\{200\}$, as is the case for as-received material. 63% cold-worked samples show a pronounced $\{111\}$ texture, that is a $\{111\}$ surface orientation while the $\{220\}$ reflexion is weak.

After nitriding cold-worked samples and quenching from 600°C, ε -Fe_2N_{1-x}, γ'-Fe_4N and CrN are identified in the surface layer, while for specimens nitrided at 800°C and quenched only γ -austenite and CrN are detected. However when samples nitrided at 800°C are examined on a 90mm Unicam powder camera very weak reflexions of ε -Fe_2N_{1-x} or Cr_2N are detected and 63% cold-worked samples show faint reflexions

of b.c.c. α -ferrite. Slightly deeper in the nitrided layer Cr_2N precipitates are also present.

The intensities of γ'-Fe_4N reflexions have a strong orientation dependance and for annealed and 20% cold-worked samples the $\{200\}$ and $\{220\}$ have equal intensity but for 63% cold-worked samples the $\{111\}$ reflexion is the strongest as would be expected from the preferred orientation of the rolled sheet. When nitriding at 600°C the intensities of ε -Fe_2N_{1-x} and γ'-Fe_4N reflexions increase with nitriding time although no difference in the thickness of the "white layer" is detected by optical microscopy.

X-ray analysis through the nitrided layer of a specimen 63% cold-worked and nitrided at 600°C shows the presence of three zones: (i) $\varepsilon + \gamma' + CrN$; (ii) $\gamma' + CrN + \gamma$; and (iii) $CrN + \gamma + \alpha$. The layer containing α -ferrite is thicker than in annealed specimens. The nitrided layer of specimen 63% cold-worked and nitrided at 800°C is uniform but the intensities of α and Cr_2N reflexions increase slightly through the nitrided layer. Cold-working enhances the formation of α -ferrite during nitriding but does not affect the precipitation of iron nitride.

V.4 Effect of nitrogen potential on phase distribution

A difference in phase distribution in the nitrided layers is expected by varying the nitrogen potential of the gas mixture and so this was investigated at 600° and 800°C. The phases identified on the surface of quenched specimens are given in Table V.5 although lower nitriding temperatures often give an uneven case. At 600°C no γ'-Fe_4N or "white layer" were observed for an NH_3:H_2 ratio less than 40:60 as predicted by calculation (see section V.5), and at 800°C no γ'-Fe_4N is expected to form even in pure ammonia. When nitriding at 600°C at potentials lower than $50NH_3$:$50H_2$ the phase distribution is not always consistent with thermodynamic prediction and the results are not always reproducible. Formation of the "white layer", which is a consequence of the precipitation of ε-Fe_2N_{1-x} or γ'-Fe_4N is necessary to get a uniform layer as shown by the specimen exposed 15 min in pure ammonia prior to reducing the ammonia concentration in the gas mixture. By nitriding for 15 min at 600°C in pure ammonia a very thin white layer is formed (Table V.5) and this seems adequate to obtain a uniform nitrided layer.

V.5 Discussion

The differences observed in the surface microstructure

Table V.5

Phases identified after nitriding in ammonia: hydrogen mixtures for 24h and quenching

nitriding conditions		phases				thickness of "white layer"
temperature °C	$NH_3 : H_2$	ε-Fe_2N_{1-x}	Fe_4N	CrN		µm
600	80 : 20	X*	X	X	X	16
	70 : 30	X*	X	X	X	13
	60 : 40	X*	X	X	X	13
	60 : 40		X*	X	X	9
	55 : 45		X*	X	X	6
	40 : 60			X	X	
	25 : 75			X	X	
	10 : 90			X	X	
	15min-100:0+40:60**	X*	X	X	X	11
800	70 : 30			X	X	
	40 : 60			X	X	

* weak reflexion

** the specimen was exposed for 15 min in pure ammonia prior to nitriding in $40NH_3:60H_2$ for 24h.

of nitrided specimens are the consequence of differences in the phase distribution and reaction temperature.

The nitrogen potential and hence the $NH_3:H_2$ ratio required to precipitate iron nitrides in ferrous alloys at a given temperature (T) can be calculated from the following equations:

$$4Fe + \underline{N} \rightleftharpoons \gamma'\text{-}Fe_4N \qquad \ldots\ldots \text{V.1}$$

$$3Fe + \underline{N} \rightleftharpoons \varepsilon\text{-}Fe_3N \qquad \ldots\ldots \text{V.2}$$

with equilibrium constants respectively

$$K_1(T) = \frac{a_{Fe_4N}}{a_{\underline{N}} \cdot a_{Fe}^4} \qquad \ldots\ldots \text{V.3}$$

and $$K_2(T) = \frac{a_{Fe_3N}}{a_{\underline{N}} \cdot a_{Fe}^3} \qquad \ldots\ldots \text{V.4}$$

assuming that the activity of the iron nitrides are unity then from equation V.3 $a_{\underline{N}} \propto \frac{1}{N_{Fe}^4}$ and from equation V.4 $a_{\underline{N}} \propto \frac{1}{N_{Fe}^3}$, using the approximation $a_{Fe} = N_{Fe}$

where N_{Fe} is the atomic fraction of Fe in the alloy (in AISI 316 $N_{Fe} = 0.661$).

The formation of γ'-Fe_4N by nitriding in ammonia can be regarded as a combination of equations III.4 and V.1 and can be written:

$$4Fe + NH_3(g) \rightleftharpoons Fe_4N + 3/2\ H_2(g) \quad \ldots\ V.5$$

with an equilibrium constant

$$K(T) = \frac{a_{Fe_4N}}{a_{Fe}^4} \times \frac{p_{H_2}^{3/2}}{p_{NH_3}} \quad \ldots\ V.6$$

Data for the standard free energies $\Delta G_1^\circ(T)$ and $\Delta G_2^\circ(T)$ of reactions III.4 and V.1 respectively are available (Kubaschewski & Alcock, 1979):

$$\Delta G_1^\circ(T) = -10400 + 7.1T \log T - 3.79T \text{ (calories)} \quad \ldots\ V.7$$

$$\Delta G_2^\circ(T) = -200 + 11.62T \log T + 24.85T \text{ (calories)} \quad \ldots\ V.8$$

Thus, the free energy $\Delta G^\circ(T)$ for the reaction V.5 is

$$\Delta G^\circ(T) = \Delta G_2^\circ(T) - \Delta G_1^\circ(T) \quad \ldots\ V.9$$

$$= 10200 + 4.52T \log T - 28.64T \quad \ldots\ V.10$$

But $$\Delta G^\circ(T) = -RT \ln K(T) \quad \ldots\ V.11$$

and from equations V.6, V.10 and V.11,

$$RT \ln\left(\frac{a_{Fe_4N}}{a_{Fe}^{4}} \times \frac{p_{H_2}^{3/2}}{p_{NH_3}}\right) = -10200-4.52T \log T+28.64T \quad \ldots. \quad V.12$$

Putting $a_{Fe} = N_{Fe} = 0.661$ and $a_{Fe_4N} = 1.0$, then at 600°C a ratio $\frac{p_{NH_3}}{p_{H_2}^{3/2}} = 0.829$ is required to precipitate γ'-Fe_4N which corresponds to $39NH_3{:}61H_2$ when nitriding at amospheric pressure, and is in agreement with the experimental results presented in section V.4.

The minimum nitrogen potentials $p_{NH_3}/p_{H_2}^{3/2}$ required to precipitate ε-phase at 700° and 800°C from pure iron austenite are 0.110 and 0.091 respectively from Lehrer's diagram (Figure III.4). Thus the potentials required for AISI 316 are approximately $0.110/(0.661)^3 = 0.381$ at 700°C and $(0.091)/(0.661)^3 = 0.315$ at 800°C which correspond to $25NH_3{:}75H_2$ and $22NH_3{:}78H_2$ respectively. However, the degree of dissociation of ammonia at 800°C (Table III.2) is sufficiently high that the actual percentage of ammonia during the experiments at 800°C given in Table V.5 must be lower than the 22% calculated above since no ε is observed.

The nitrogen potential decreases through the nitrided layer and therefore the phase distribution varies, but a sharp difference is observed only at the interface between the case and the core.

At temperatures of 600°C and lower in pure ammonia a thick "white layer" is formed at nitriding temperature and corresponds with formation of massive γ'-Fe_4N and precipitation of CrN. In fact, γ'-Fe_4N formed at 600°C in the "white layer" has a lower lattice parameter (3.784 Å) than that in the "dark-etched" layer (3.789 Å) or that formed by slow-cooling from 800°C which suggests that on the surface at 600°C the phase formed is γ'-$(Fe,Ni)_4N$ as reported by Lebrun et al. (1972). The thickness of the "white layer" decreases with decrease in nitrogen potential in the gas mixture and is not formed below $40NH_3:60H_2$ (see Table V.5). The "white layer" does not grow with nitriding time which suggests that the nitrogen potential decreases very rapidly through the nitrided layer. Further details of precipitation of γ'-Fe_4N and the formation of the "white layer" are reported in Chapter VI where the formation of α-ferrite is also discussed.

During nitriding a carbon rich layer is formed at the case-core interface by diffusion of carbon ahead of the nitrided case. Evidence of carbon diffusion towards the centre in the present work is shown in Figure V.10 and also by the increase in microhardness ahead of the nitrided layer in thin sheet (0.38mm) of AISI 316 containing 0.07wt% C nitrided at 800°C (Figure V.22). Heat-treated samples do not show similar changes in microhardness. As nitrogen diffuses, carbide precipitates dissolve and by precipitation

Figure V.22

Microhardness profiles of AISI 316 (0.07wt% C) nitrided in pure ammonia at 800°C for the times shown

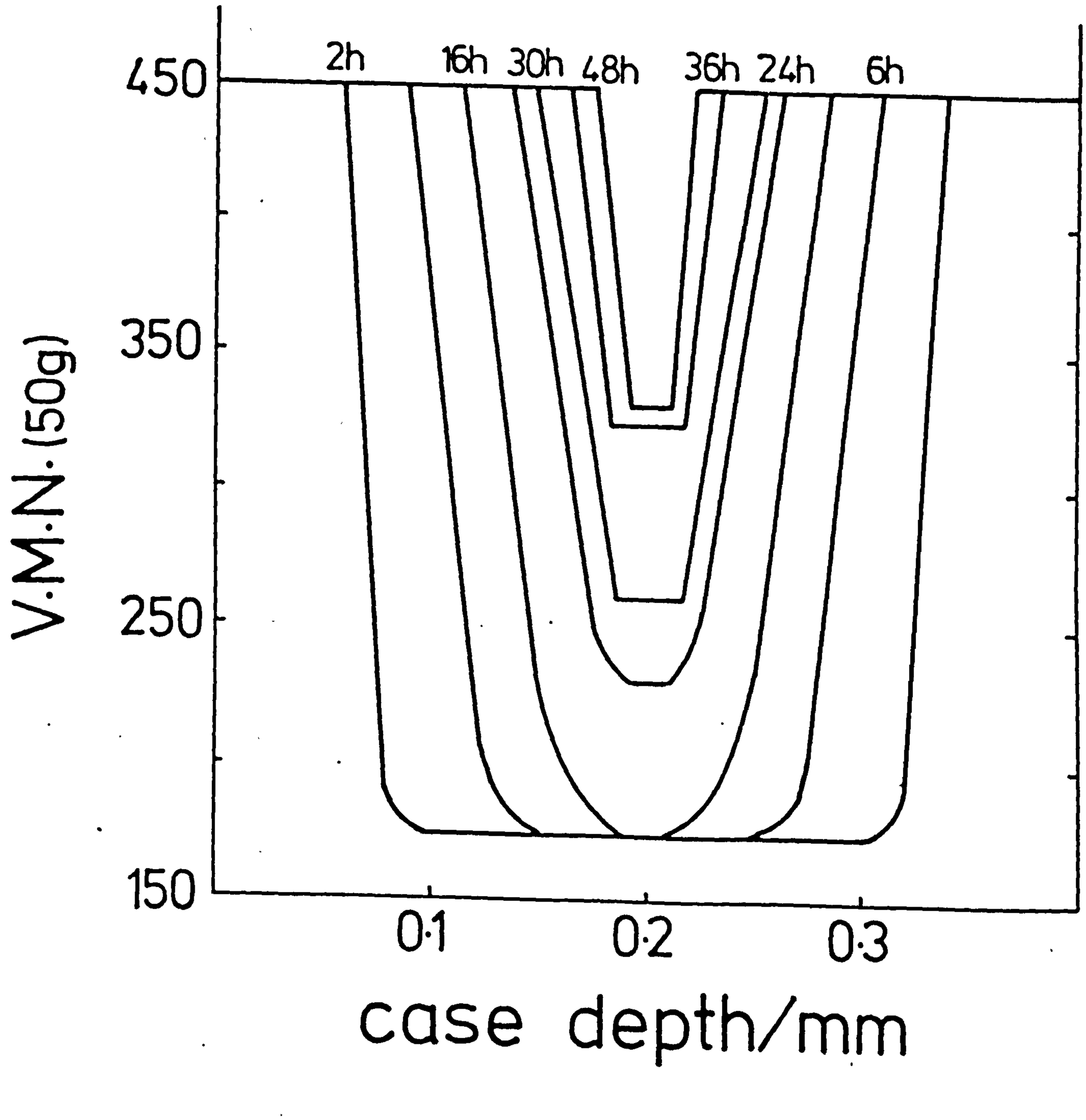
2h
16h
30h
48h
36h
24h
6h
450
350
250
150
V.M.N.(50g)
0·1
0·2
0·3
case depth/mm

of chromium nitrides the chromium activity decreases and therefore the carbon activity increases (Natesan & Kassner, 1973). Carbon diffuses from a high activity to a lower one, that is from the surface towards the centre. When specimens are almost through nitrided the core contains a high carbon concentration which explains its very high microhardness due to precipitation of chromium carbides.

V.6 Conclusions

(i) A combination of etching techniques and X-ray diffraction analysis have been used to determine the phase distribution in the nitrided layer.

(ii) The formation of the different phases depends on the reaction temperature and the nitrogen potential. At low temperatures the nitrided layer is not always uniform, especially when the nitrogen potential is low. The production of a surface layer of γ'-Fe_4N leads to the development of a uniform nitrided case.

(iii) Differences are observed between air-cooled and quenched specimens at temperatures higher than 700°C where the "white layer", related to the formation of γ'-Fe_4N, is formed during cooling.

(iv) Cold-working affects the phase distribution in

the nitrided layers by facilitating heterogeneous precipitation of CrN which is related to the formation of α -ferrite.

(v) Carbon is found to diffuse ahead of the nitrided layer.

Chapter VI

PRECIPITATION IN AISI 316 BY NITRIDING

VI.1 Precipitation at 600°C

Optical microscopy shows that the nitrided case formed at 600°C is composed of three different layers excluding the very thin layer of ε -Fe_2N_{1-x} at the surface. These separate layers have been examined by transmission electron microscopy (TEM).

TEM carried out on a thin foil of the surface of a nitrided specimen, that is of the compound layer, showed grains of single phase ε -Fe_2N_{1-x}. However Fe_2N_{1-x} and Cr_2N have similar crystal structures (Bywater & Dyson, 1975) and it is possible that some chromium is dissolved in the ε -phase. Imai et al. (1967b) also reported that Cr_2N can accommodate up to 0.05wt% of iron.

However, in the present investigation, the ε -Fe_2N_{1-x} layer is only 5 μm thick (Chapter V) and only a few grains were observed. The compound layer consists mainly of a distribution of fine particles of CrN in an $(Fe,Ni)_4N$ matrix. Figure VI.1 shows the structure of this layer in which no γ -austenite is present. Bright and dark field micrographs were taken in [110] zone orientation in which

Figure VI.1

TEM micrographs of the "white layer" in a specimen of AISI 316 nitrided at 600°C for 24h in pure ammonia

(a) bright field

(b) dark field, superlattice γ' reflexion

(c) dark field, CrN reflexion

and (d) dark field, γ' reflexion

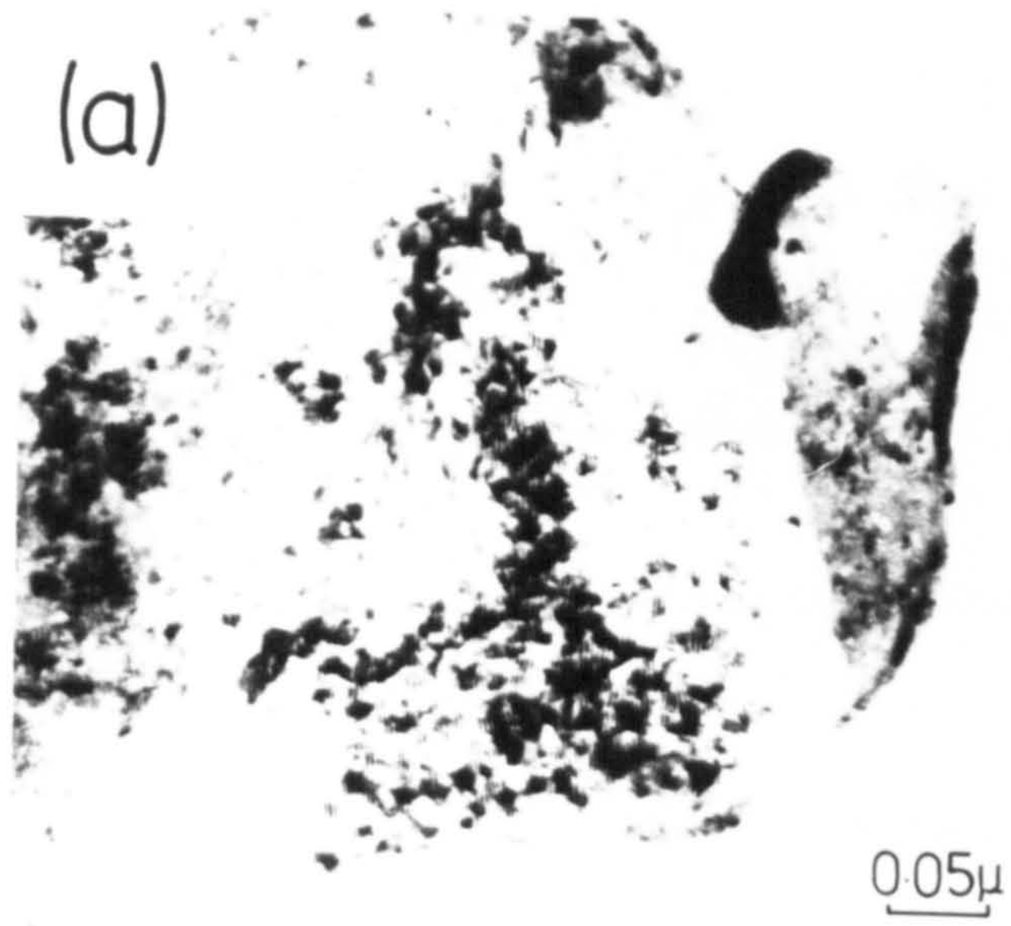
(a)
0.05μ

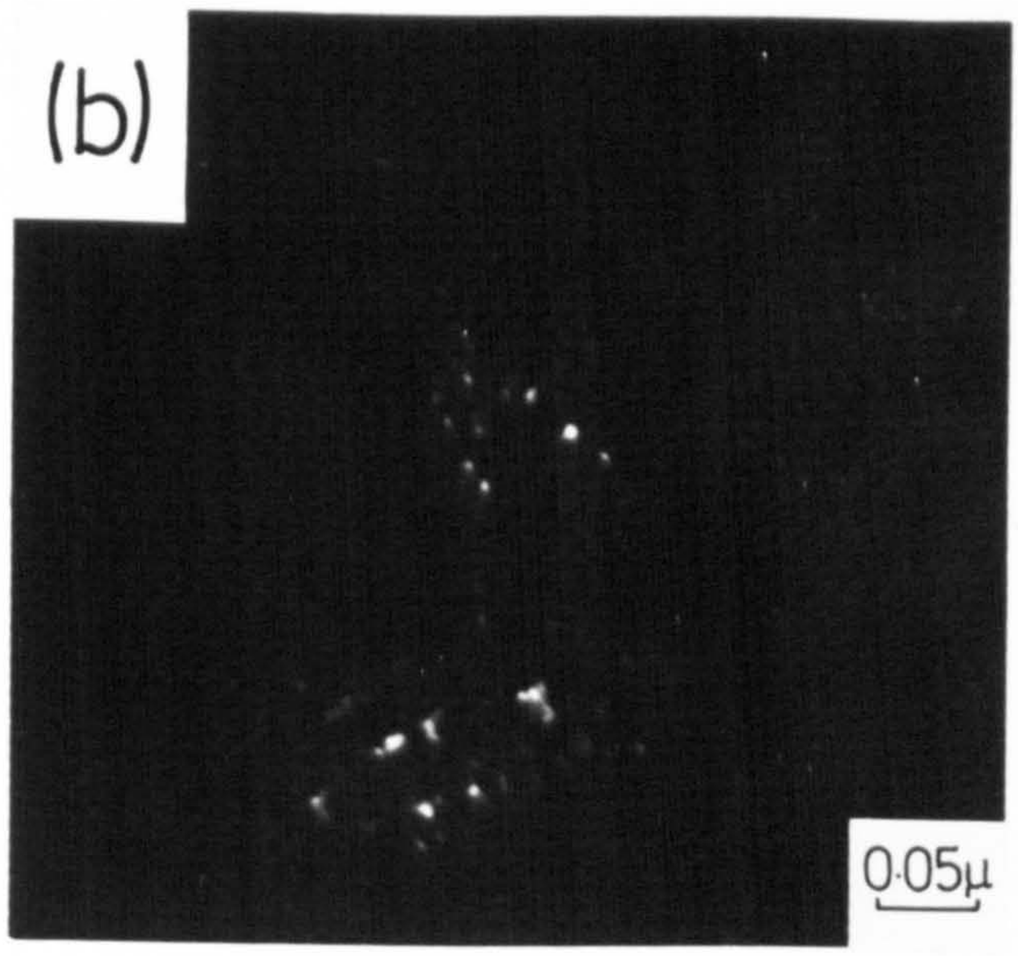
(b)
0.05μ

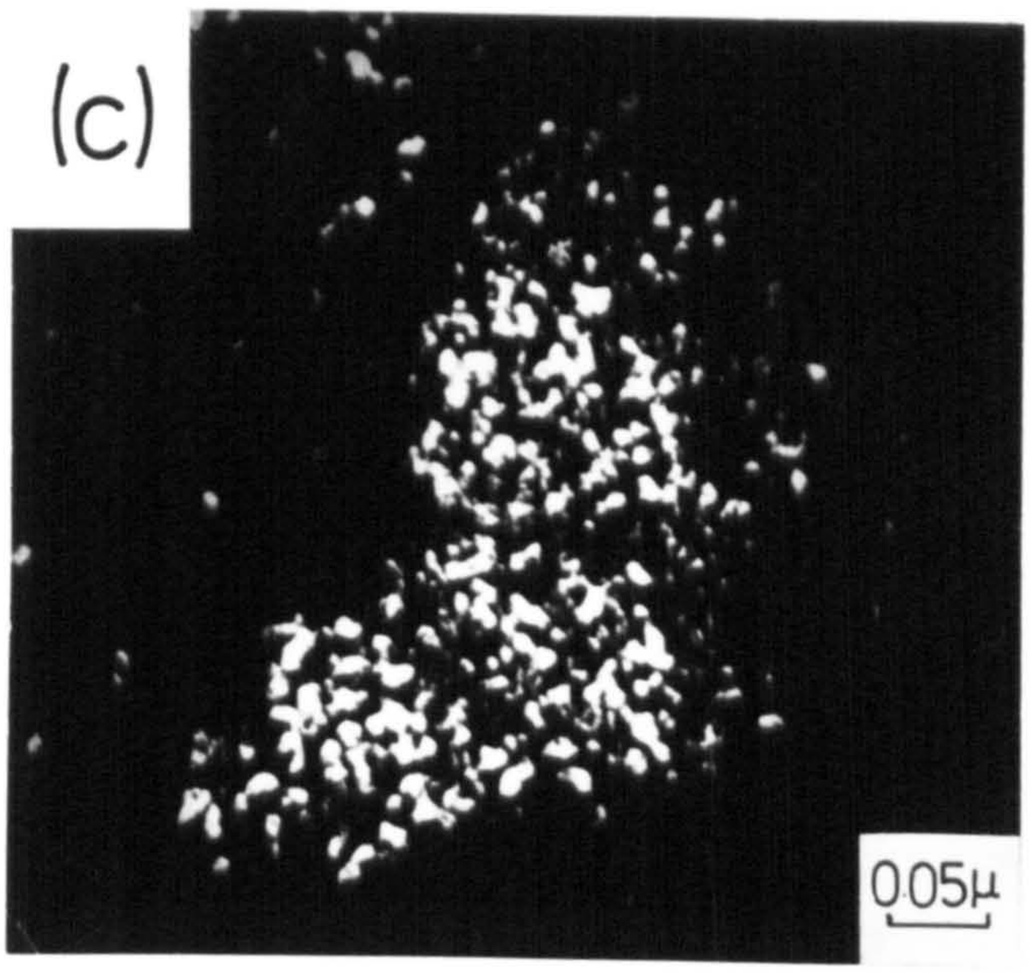
(c)
0.05μ

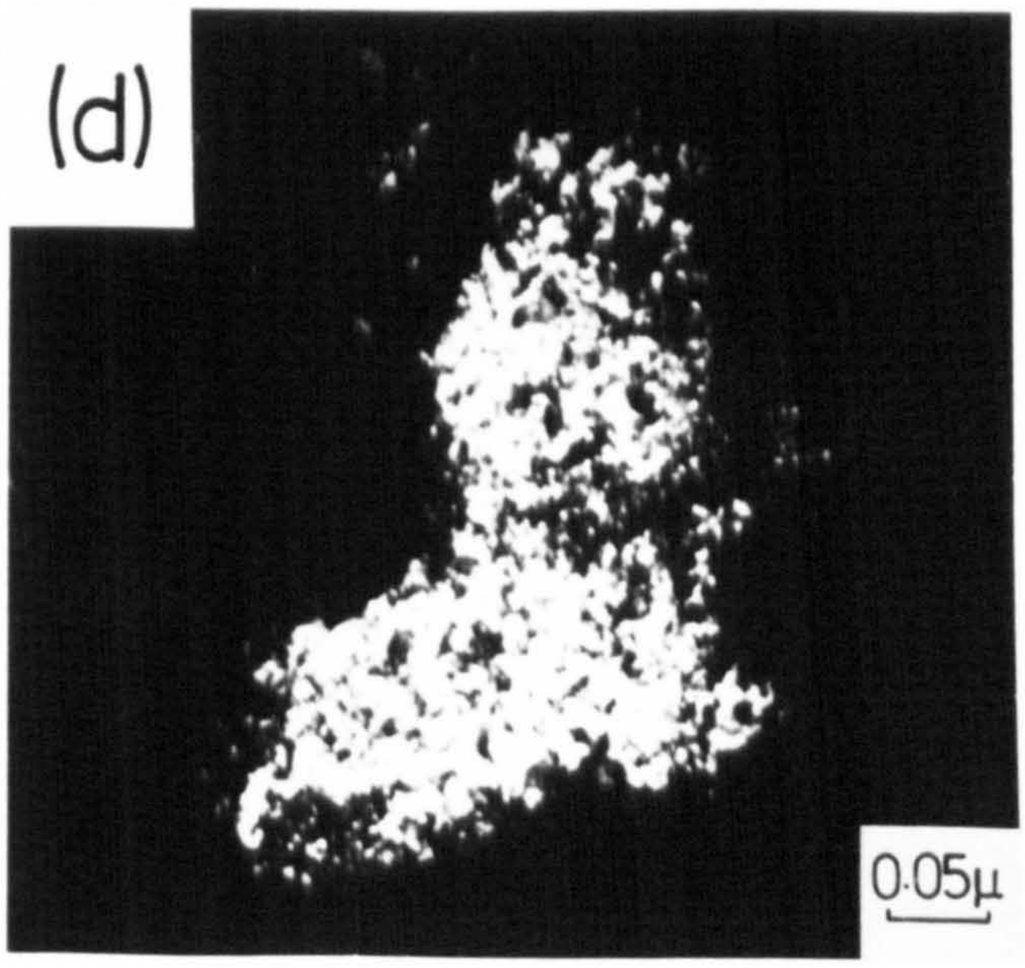
(d)
0.05μ

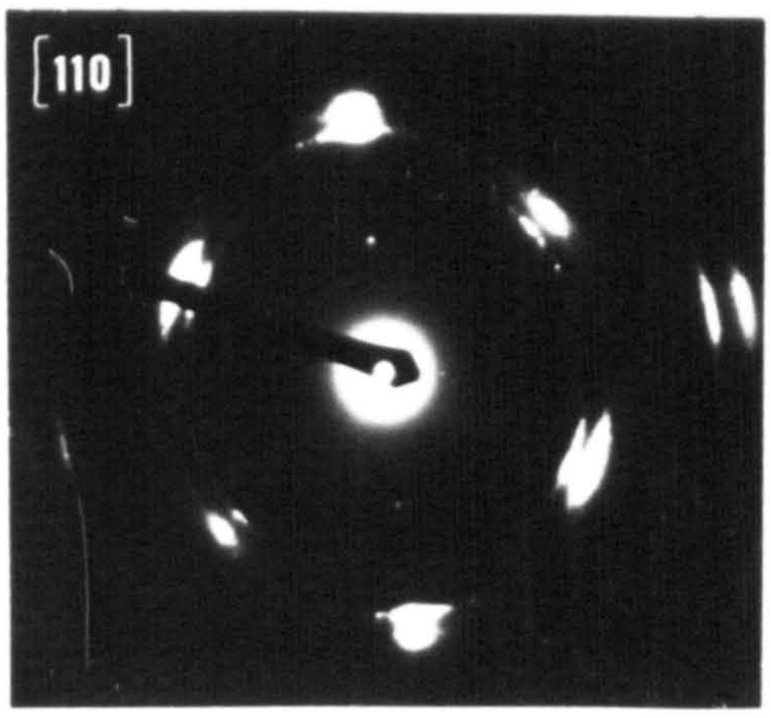
[110]

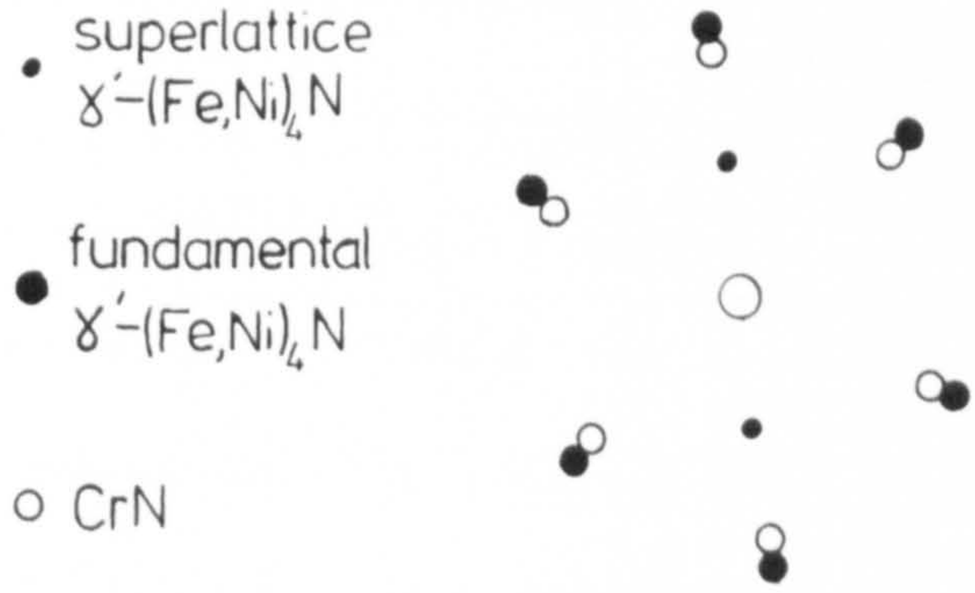
superlattice
γ′-(Fe,Ni)4N
fundamental
γ′-(Fe,Ni)4N
CrN

the (100) superlattice reflexion of γ' is visible (Figure VI.1). γ'-Fe_4N and CrN have the same crystal structures (i.e. a f.c.c. arrangement of metal atoms) and have a parallel orientation relationship.

The second nitrided layer is the "dark-etched" layer of Figure V.6 which corresponds to the precipitation of CrN and γ'-Fe_4N in an austenite matrix. The face-centred cubic phases present (CrN, γ' and γ) have similar unit-cell dimensions (a_{CrN} = 4.151 Å; $a_{\gamma'}$ = 3.789 Å; a_{γ} = 3.633 Å) and parallel orientation relationships. Thus, on electron diffraction patterns the reflexions from all three phases are adjacent to one another (see Figure VI.2(a)). The [110] zone is therefore identical to Figure VI.1 with additional austenite reflexions in a hexagonal array outside the γ' reflexions. Dark field images can be obtained from CrN reflexions using a very small objective aperture (10 μm) but it is impossible to obtain separate dark field images from the fundamental γ' reflexion and the adjacent γ austenite. The (100) superlattice reflexion of γ' was found to be too weak to give a dark field image. For electron diffraction the intensity of the $(200)_{\gamma'}$, reflexion is approximately 60 times stronger than (100), and in the "dark-etched" layer γ'-Fe_4N is present as a fine precipitate which means that the intensities of the reflexions are considerably weaker than those observed in the "white layer".

Figure VI.2

TEM micrographs of the "dark-etched" layer in a specimen of AISI 316 nitrided at 600°C for 24h in pure ammonia

(a) bright field, $[110]_{\gamma}$ orientation

(b) dark field, CrN reflexion

and (c) dark field, $\gamma + \gamma'$ reflexions

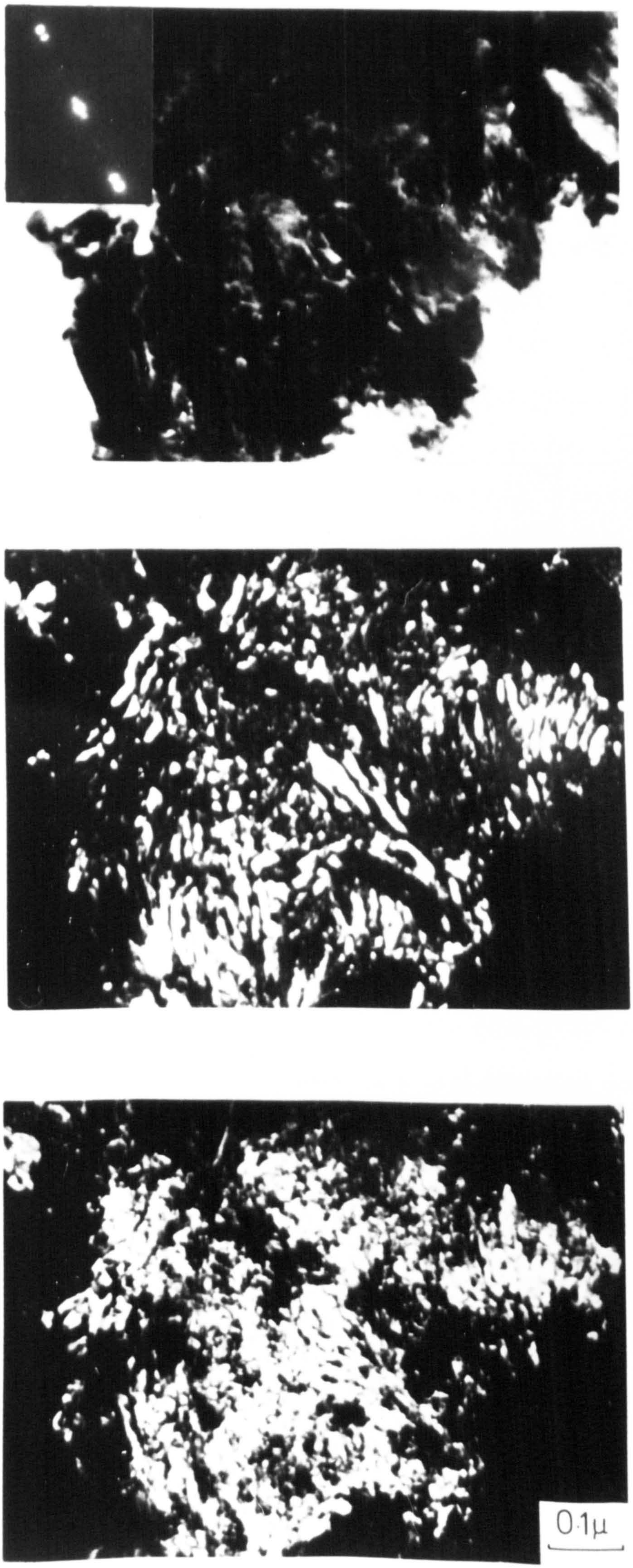
(a)
(b)
(c)
0·1μ

The third layer is the inner subscale which consists of CrN precipitates in an austenite matrix. Figure VI.3 shows the fine discontinuous lamellar structure observed in a [110] zone. Thin foils prepared at different depths of the layer showed the same type of structure. Close to the core-case interface some faint diffraction spots were identified as ferrite reflexions, but no particular orientation relationship was discernible because the α -Fe diffraction pattern consisted of diffuse rings. No dark field could be taken from these reflexions due to the number of phases present.

The interface between the case and the core observed by etching in Marble's reagent (Figure V.10) has been examined by TEM and shows the presence of large and small twins of austenite (depending on the area examined) and a high dislocation density; see Figure VI.4. X-ray diffraction photographs taken at 5 μm from the core (Figure V.12(b)) show reflexions of two austenites - weak reflexions giving a lattice parameter of 3.623 Å and strong reflexions with a = 3.584 Å. The former is a high-nitrogen austenite from the case and the latter corresponds to γ without nitrogen and undoubtedly comes from the core. A difference in lattice parameter in the two austenites leads to a high degree of deformation (twins, dislocations) and the intersection of slip bands or twins locally alters the ABCABC stacking sequence of the f.c.c. structure to ABCA/CAB of a

Figure VI.3

TEM micrographs of lamellar γ + CrN in a specimen of AISI 316 nitrided at 600°C for 24h in pure ammonia

(a) bright field, $[110]_{\gamma}$ orientation

(b) dark field, CrN reflexion

and (c) dark field, γ reflexion

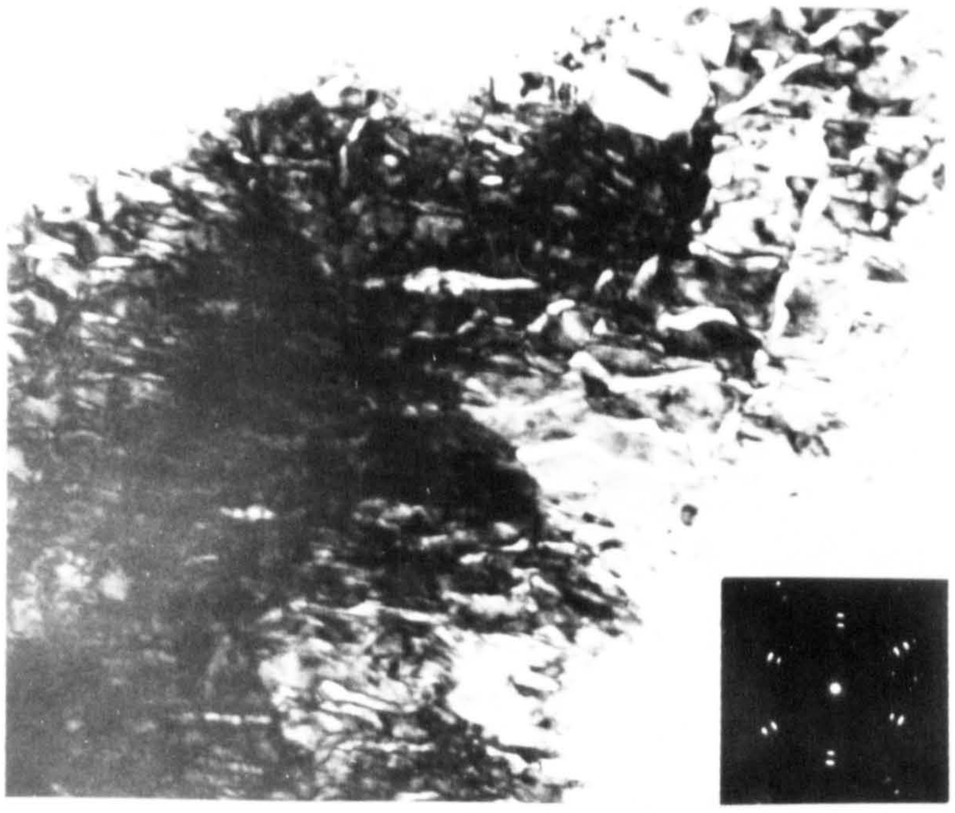

(a)

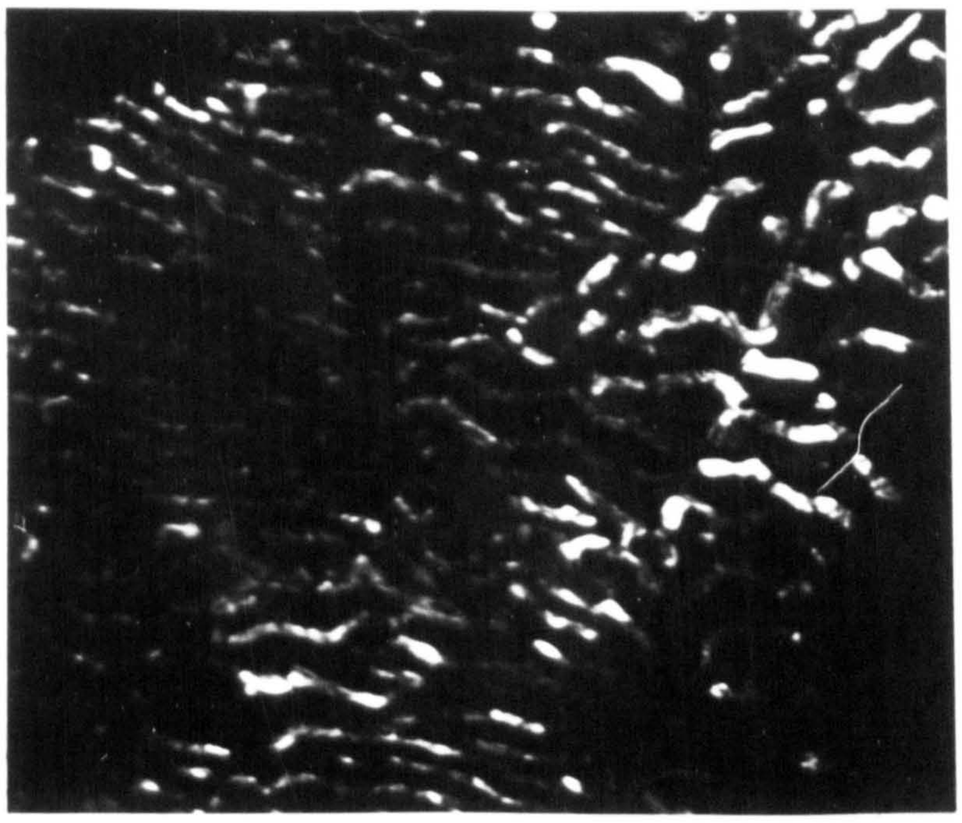

(b)

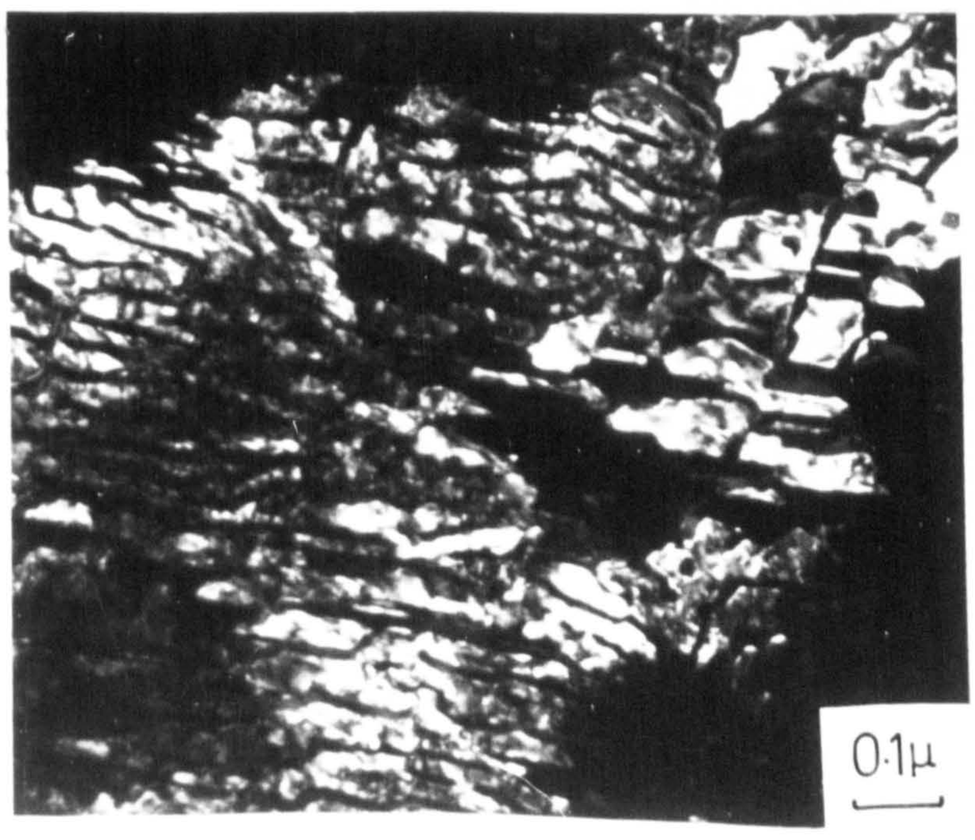

(c)

Figure VI.4

TEM micrographs of the case-core interface in a specimen of AISI 316 nitrided at 600°C for 24h in pure ammonia

(a) large twins of austenite

(b) fine twins of austenite

and (c) dislocations in the austenite matrix

(a)

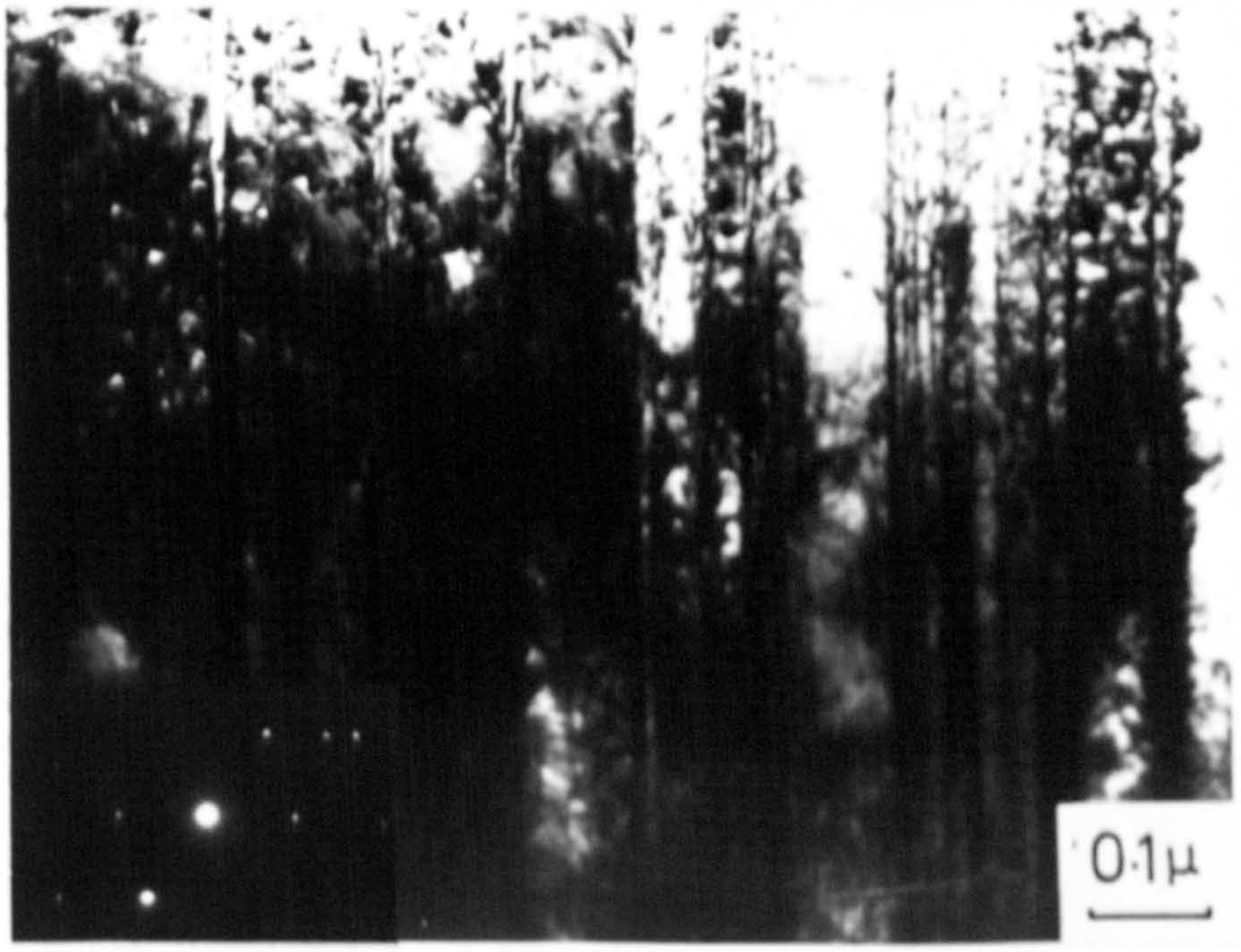

(b)

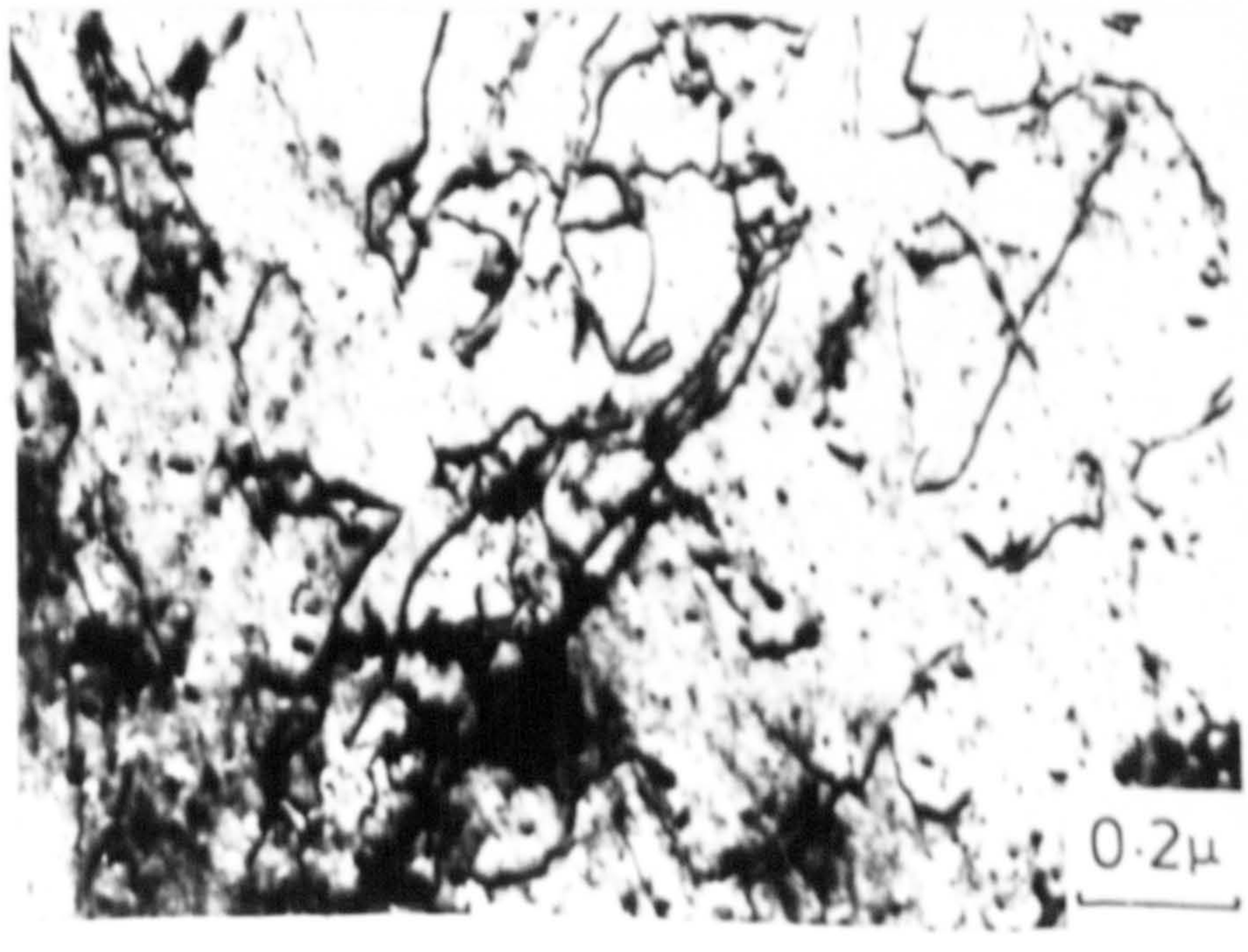

(c)

c.p.h. sequence. However c.p.h. ε-martensite is not stable and α' martensite with low tetragonality is formed (Breedis & Robertson, 1962; Dash & Otte, 1963; Olson & Cohen, 1975). By losing interstitial atoms, for example by precipitation, α-ferrite would then result. In the present study broad α-ferrite reflexions are present when the austenite reflexions are broad (a = 3.600-3.632 Å) and this mechanism may explain the formation of ferrite from what is an Fe-Ni-C-N austenite adjacent to the interface. Prolonged heat-treatment at 600°C in an inert atmosphere does not result in ferrite formation.

From the different phases formed through the nitrided layer and the electron probe microanalysis reported in Chapter V it is obvious that the nitrogen concentration decreases from the surface of the sample towards the core. An ε-$(Fe,Cr)_2N_{1-x}$ layer grows outward from the surface (Figure V.2) and is limited by the formation of the "white layer". High concentrations of nickel are expected below the ε-$(Fe,Cr)_2N_{1-x}$ layer and so a high-nickel γ'-$(Fe,Ni)_4N$ is precipitated as nitrogen diffuses inwards. The concentration of nickel in the γ' of the "white layer" is therefore higher than that in the "dark-etched" layer. Because nickel lowers the nitrogen solubility in iron and also because high nickel and low nitrogen contents both reduce the lattice parameter of γ'-Fe_4N (see section II.2), a smaller unit-cell of γ' is expected in the "white layer"

compared with that of the γ' in the "dark-etched" layer. In the "white layer" the lattice parameter of the γ'-phase is 3.784 Å while in the "dark-etched" layer it decreases from a high value (3.789) close to the "white layer" to 3.780 at greater depth. In this layer the lattice parameter of austenite is 3.633 Å which is smaller than required to precipitate γ'-Fe_4N in pure Fe-N alloys (Jack, 1951a). This is explained by the presence of nickel which decreases the lattice parameter and which also decreases the solubility of nitrogen in austenite.

Crack formation below the "white layer" reported in section V.2(c) is related only to massive γ'-$(Fe,Ni)_4N$; that is in the "white layer". In the dark etched layer optical microscopy shows that massive γ'-$(Fe,Ni)_4N$ precipitates only at grain-boundaries (see Figure V.6) and homogeneous precipitation within grains occurs where the nitrogen potential is sufficiently high.

It was found that the "white layer" on large-grained specimens was thinner than on those with small grains e.g. 9 μm for samples of A.S.T.M. number 0-1 compared to 20 μm for samples of A.S.T.M. numbers 7-8. Thus, the formation of the "white layer" is mainly dependent on diffusion of nitrogen in grain-boundaries.

A slight variation of the lattice parameter of CrN is observed.(4.152 Å in the "white layer"; 4.151 Å in the

"dark-etched" layer; and 4.150 Å in the inner subscale) that can be related to the presence or absence of γ -phase. Ettmayer et al. (1978) reported an appreciable solid solubility of MoN_{1-x} in nitrides such as CrN and VN and so it is reasonable to assume that when no γ -austenite is present (as in the white layer) the molybdenum atoms (2.4wt%) are accommodated by substitution in CrN.

VI.2 Precipitation at 800°C

TEM studies of the surface of quenched specimens confirm that no γ'-Fe_4N is present and the microstructure consists of ε -Fe_2N_{1-x}, CrN and austenite. Single grains of ε -$(Fe,Cr)_2N_{1-x}$ were found as well as a lamellar structure of ε +CrN+ γ or of CrN+γ . Optical micrographs show a two-subscale diffusion layer when specimens are etched in sulfate-chloride solution (see Figure V.9), the lighter one of which (the inner layer) has been related to the presence of α -ferrite and Cr_2N, and the outer one to CrN+ γ (Chapter V). Both of these subscales have been examined by TEM.

The outer layer, consisting of CrN+ γ , of a sample nitrided at 800°C is shown in Figure VI.5. The microstructure consists of coarse lamellar CrN in a γ -matrix and confirms the TEM replica observations (Figure V.18).

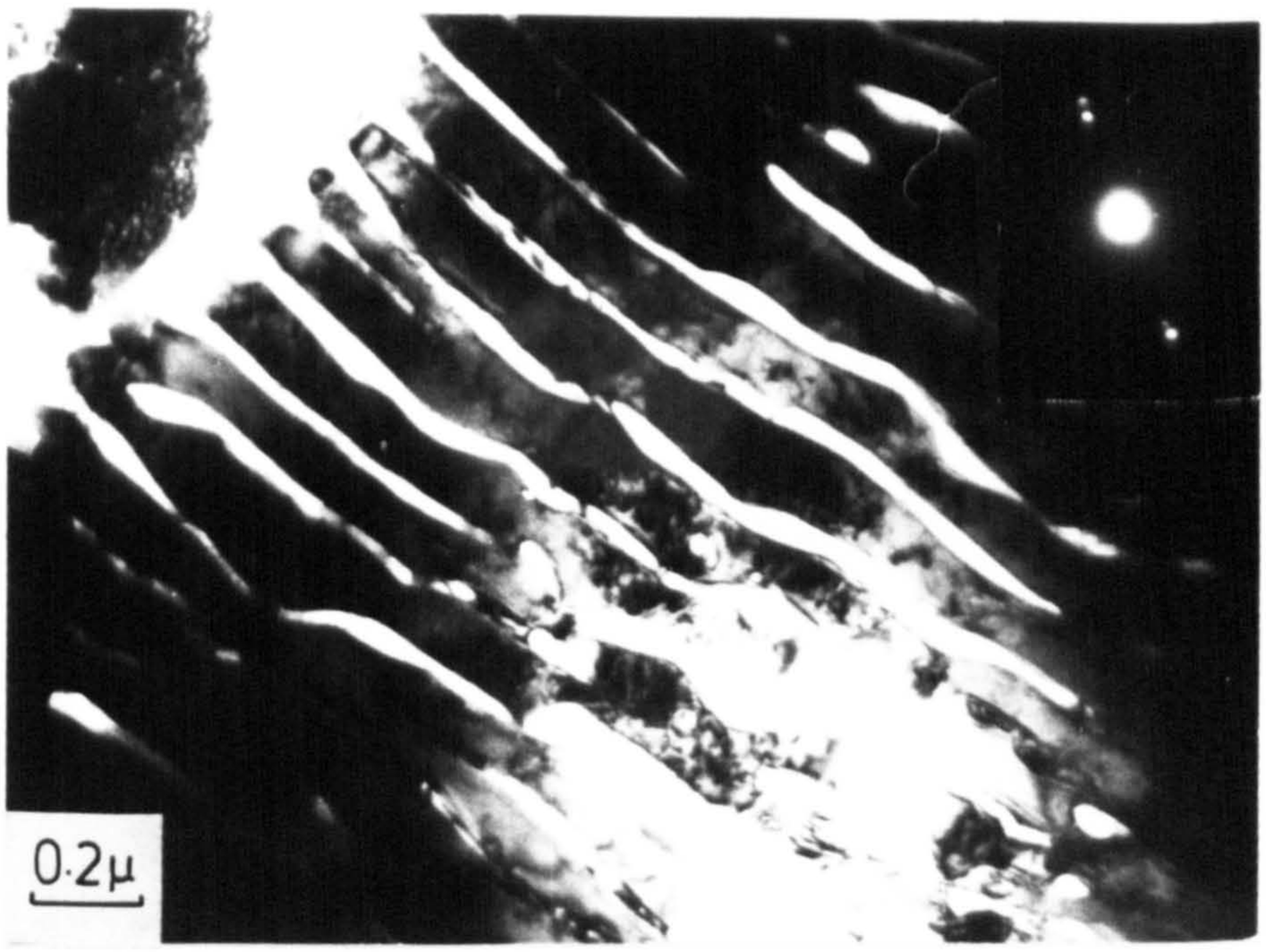

(a)

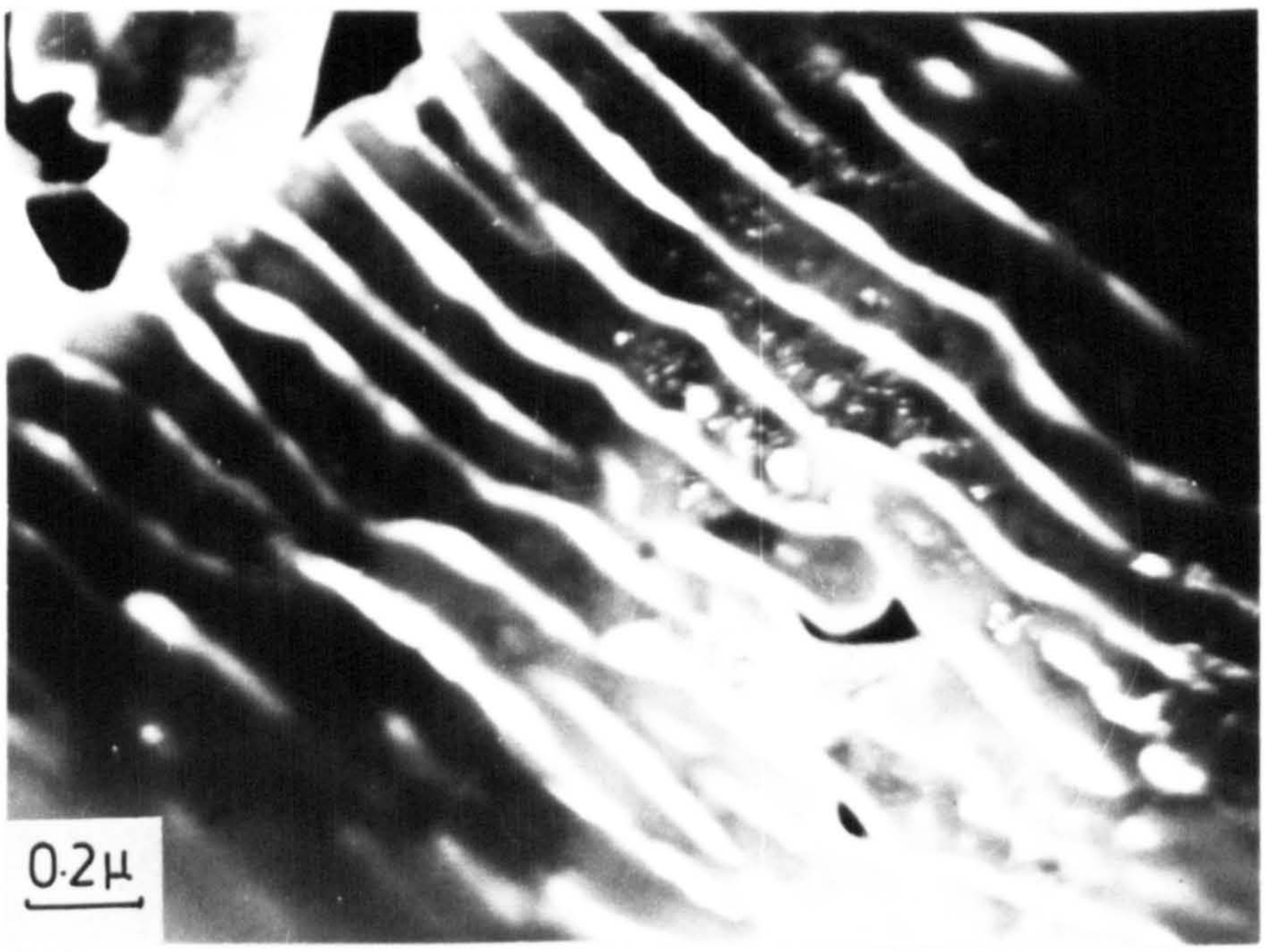

(b)

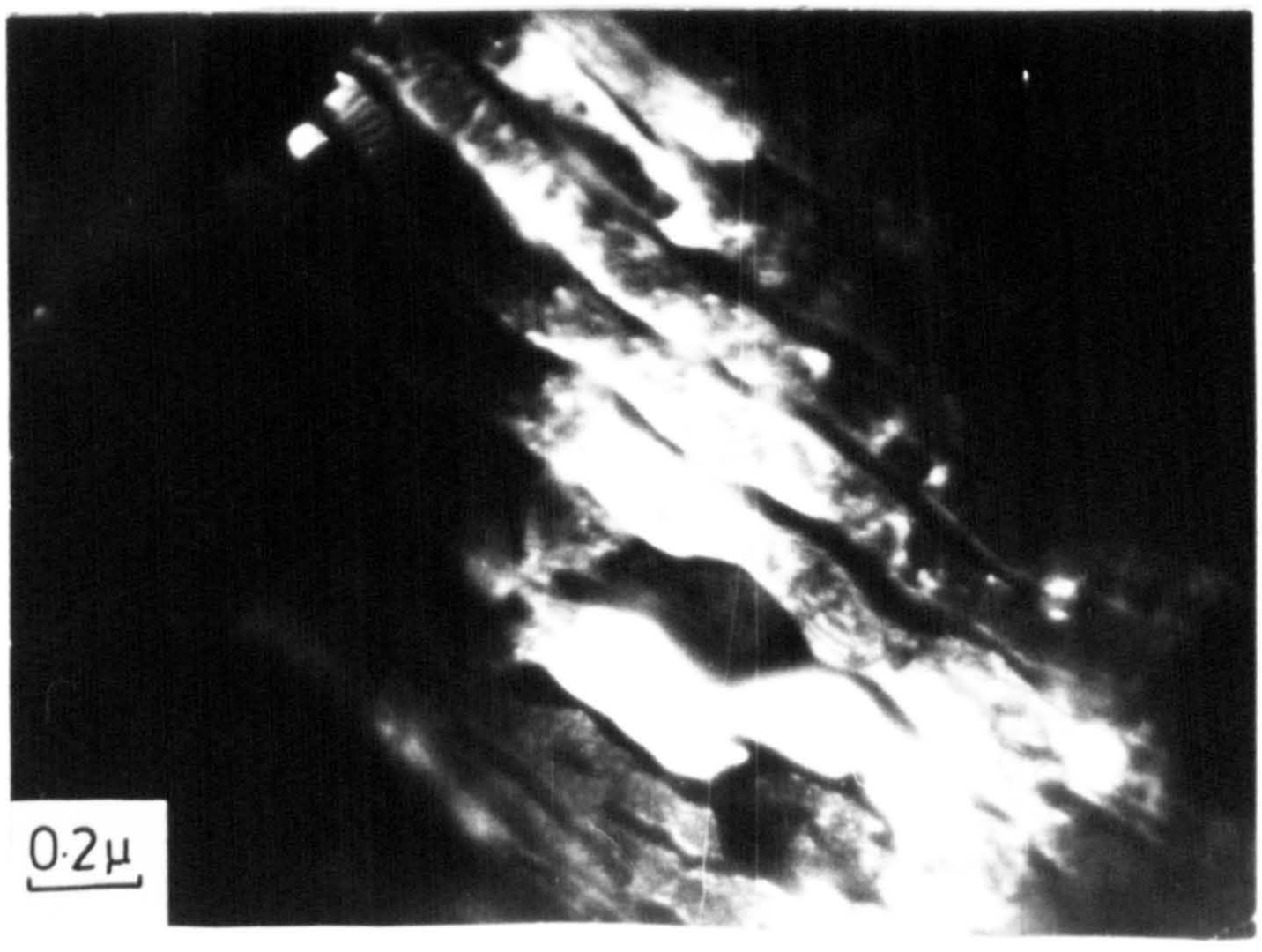

(c)

The lamellar structure formed by precipitation of CrN in an austenite matrix coarsens with nitriding temperature (Figures V.1 and VI.5). TEM of the inner subscale containing CrN, Cr_2N, γ and α shows that Cr_2N is always present in a ferrite matrix. A specimen at a depth of 125 μm (Table V.3) shows a few grains of lamellar CrN in austenite while the sample consisted mainly of c.p.h. Cr_2N in α - ferrite. The particles of Cr_2N are needle-shaped (Figure VI.6) in $[100]_\alpha$ orientation, with a similar diffraction pattern to that described by Bywater & Dyson (1975). The orientation relationship is:

$$(0001)_{Cr_2N} \;//\; (011)_\alpha \quad \text{and}$$

$$[11\bar{2}0]_{Cr_2N} \;//\; [11\bar{1}]_\alpha$$

Lebrun et al. (1972) suggested that ferrite is formed by chromium depletion after Cr_2N precipitation which would indicate a very low nitrogen potential at this depth of the nitrided layer. However in the present study Cr_2N was found to precipitate in a ferrite matrix which implies that Cr_2N is formed after the ferrite. As CrN precipitates from austenite, partial chromium depletion occurs and leads to the formation of ferrite (Figure II.4) from which Cr_2N is precipitated. The thickness of this layer increases with nitriding time.

Figure VI.6

TEM micrographs of the (α + Cr_2N) structure in a specimen of AISI 316 nitrided at 800°C for 24h in pure ammonia

(a) bright field, $[100]_\alpha$ orientation

and (b) dark field, Cr_2N reflexion

(a)

(b)

0·2 μ

Figure VI.7 shows austenite microtwins found in a CrN+ γ grain close to the case-core interface which again shows the high level of stress at the interface resulting from the expansion of the f.c.c. austenite lattice during nitriding.

VI.3 Formation of γ'-Fe_4N

According to the iron-nitrogen phase diagram (Figure II.9) γ'-Fe_4N is formed only below 690°C at potentials determined by the Lehrer diagram (Figure III.4). The structure is however stabilised by Ni and the formation of γ'-$(Fe,Ni)_4N$ has been discussed, but in order to explain the presence and distribution of this phase in specimens nitrided in pure ammonia and slow-cooled from 800°C (see Chapter V) a series of experiments was carried out involving different cooling atmospheres and cooling rates.

Annealed wire and sheet (1mm thick) of AISI L316 were used for X-ray identification and microstructure determination respectively. The phases present on the surface of the nitrided sheets were also characterized by X-ray diffractometry and no significant difference was observed between the two X-ray methods with the exception that films are more sensitive to weak reflexions. Nitrided specimens were etched in 2% nital to show whether or not a "white layer",

Figure VI.7

TEM micrographs of the nitrided layer close to the case-core interface in a specimen of AISI 316 nitrided at 800°C for 24h in pure ammonia

(a) bright field

and (b) dark field of austenite twins

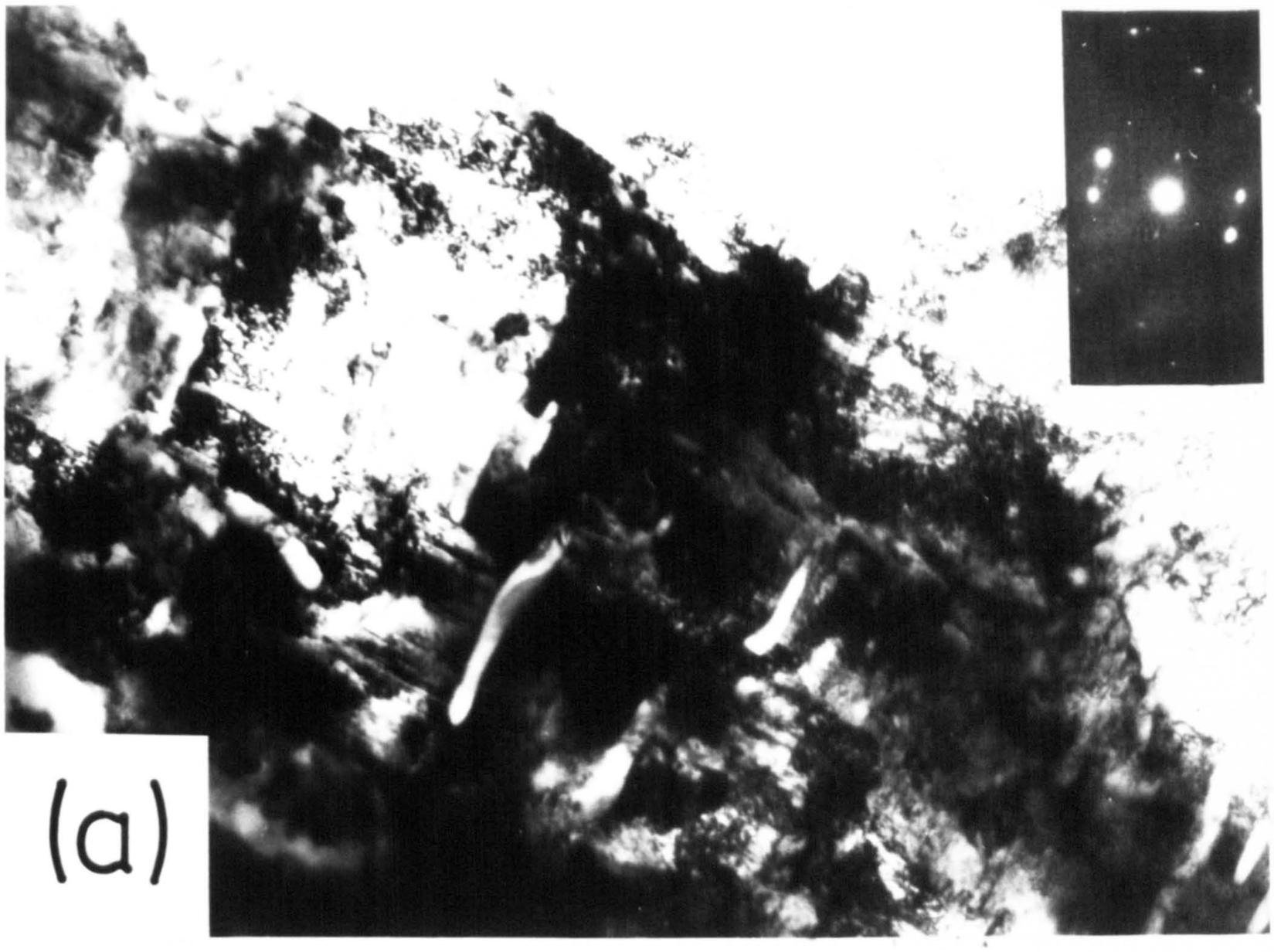
(a)

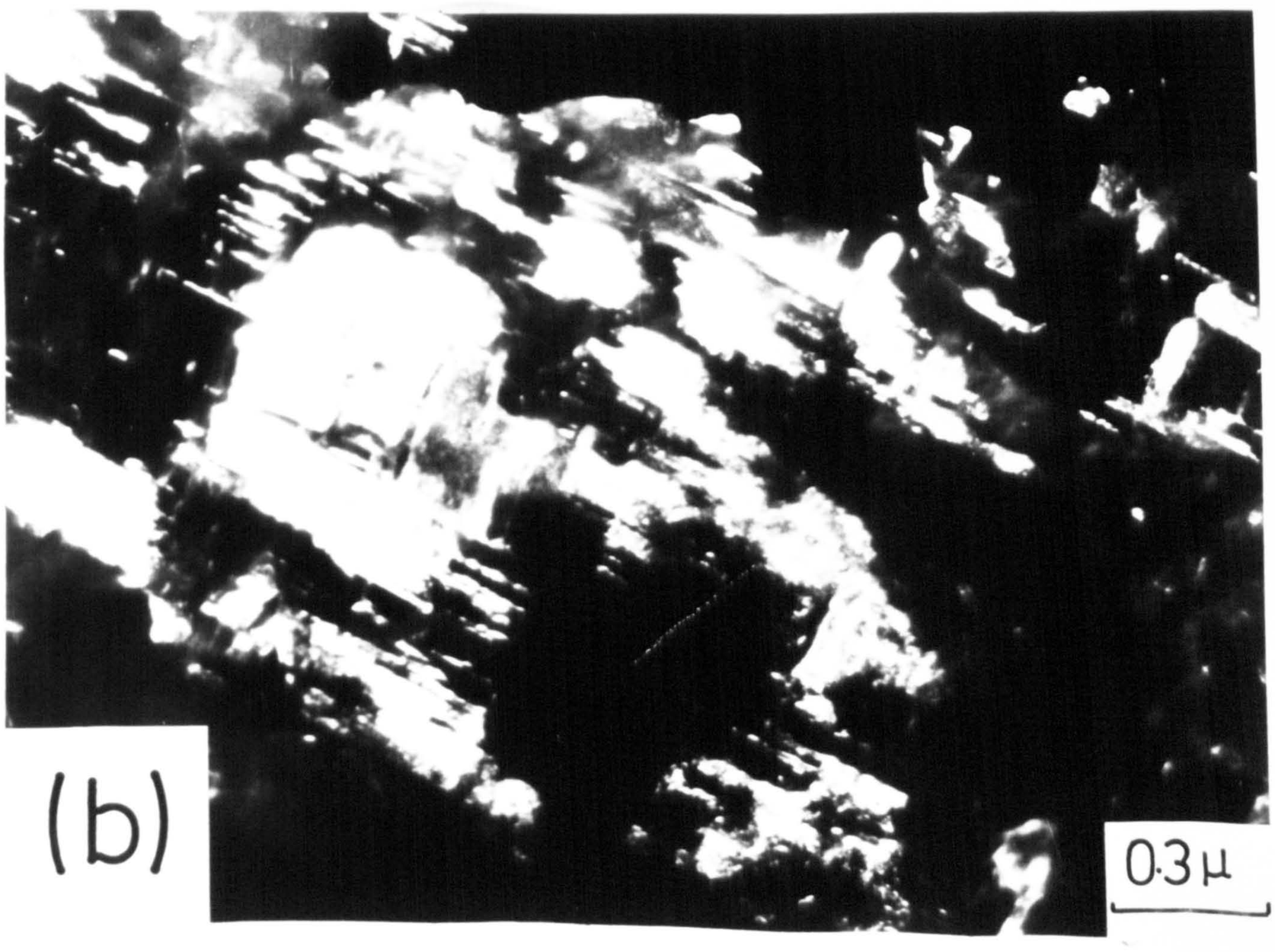
(b)
0·3 μ

which is related to the formation of massive γ'-Fe_4N, was formed. All specimens were nitrided at 800°C in pure ammonia for 24 hours before further treatment.

The results of X-ray and optical microscopy investigations are summarised in Table VI.1. After nitriding and cooling slowly from 800° to 500°C in argon (specimen i), only a few grains near the surface are etched differently from the subscale which contains CrN+γ (Figure VI.8(i)) and very weak reflexions of γ' are observed (Figure VI.9(i)) which suggests precipitation of fine γ'-Fe_4N in a γ matrix (see section VI.1). For a specimen (vi) quenched from 800°C no γ'-Fe_4N is detected by X-rays nor is any difference observed by etching in the nitrided layer; see Figure V.8(b). If the specimen (ii) is held at 550°C in argon for 24h a well defined "white layer" is observed (Figure VI.8) and the intensities of γ'-Fe_4N reflexions from specimens (i) and (ii) are similar (Figure VI.9). Specimen (iii) is the same as (i) but cooling was carried out in ammonia thus maintaining a high nitrogen concentration at the surface of the nitrided layer which is confirmed by the high lattice parameter of the ε-phase, strong γ' reflexions and a thick "white layer" (stronger γ' reflexions result in weaker γ reflexions due to X-ray absorption by the γ'-layer). The results are illustrated in Figures VI.8(iii) and VI.9(iii). If samples formed as in (iii) by cooling in NH_3 are held at 500°C, changes occur which depend on the

Table VI.1

White layer formation

(All specimens were nitrided for 24h in ammonia at 800°C and cooled as indicated)

specimen	cooling cycle	white layer thickness μm	phases ε	γ′	γ̀	CrN
(i)	Ar 800 ⟶ 500°C (2h) ⟶ Q	irregular - some grains not etched		vw	s	s
(ii)	Ar 800 ⟶ 500 (2h) ⟶ 500/Ar/24h	3 - 5		vw	s	s
(iii)	NH_3 800 ⟶ 500 (2h) ⟶ Q	13	m	s	m	s
(iv)	NH_3 800 ⟶ 500 (2h) ⟶ 500/Ar/24h	14	vw*	s	m	s
(v)	NH_3 800 ⟶ 500 (2h) ⟶ 500/NH_3/24h	20 - 41	s	s	vw	s
(vi)	800 ⟶ Q	-	vw*	-	s	s

vw = very weak
m = medium
s = strong

* low unit-cell dimensions

Figure VI.8

Optical micrographs of AISI L316 nitrided at 800°C in pure ammonia for 24h and cooled as indicated; etched in 2% nital

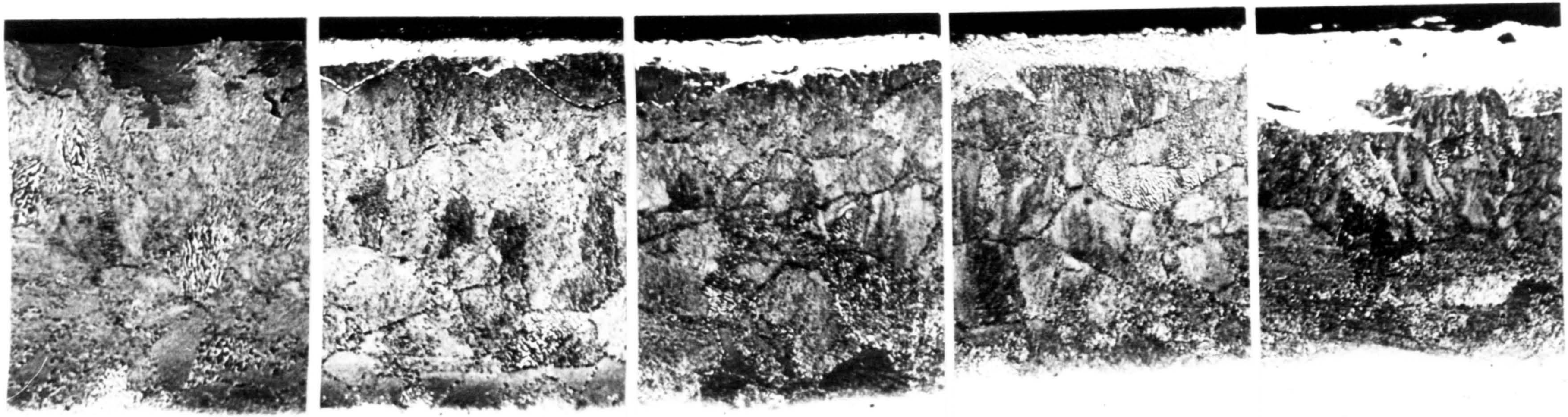

20μ

$800 \xrightarrow[2h]{Ar} 500$ + quenched (I)

$800 \xrightarrow[2h]{Ar} 500$ + 500/Ar/24h (II)

$800 \xrightarrow[2h]{NH_3} 500$ + quenched (III)

$800 \xrightarrow[2h]{NH_3} 500$ + 500/Ar/24h (IV)

$800 \xrightarrow[2h]{NH_3} 500$ + $500/NH_3/24h$ (V)

Figure VI.9

X-ray diffraction photographs of specimens

shown in Figure VI.8

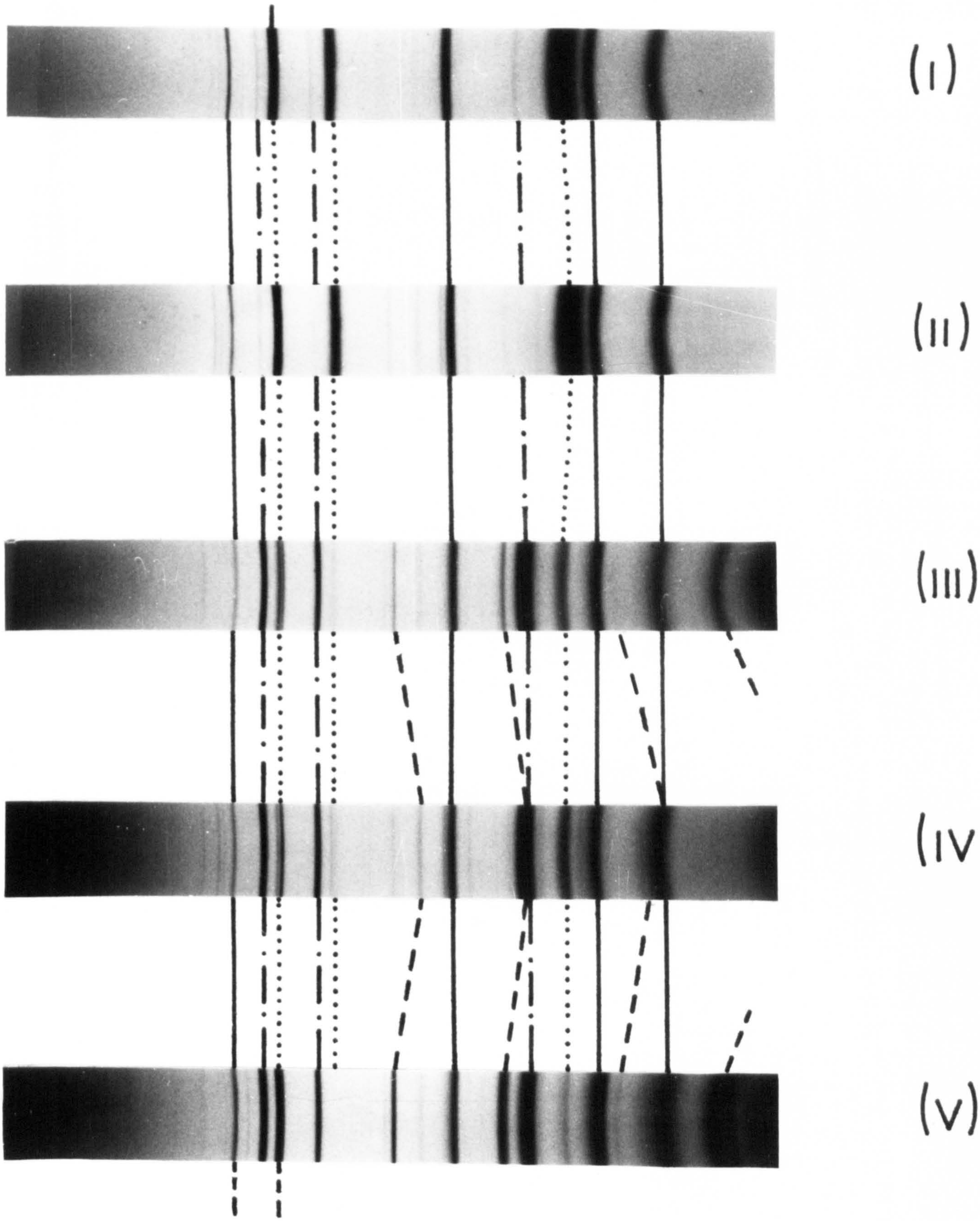
(I)
(II)
(III)
(IV)
(V)
γ-Fe
γ'-Fe4N
CrN
ε-Fe2N1-x

applied nitrogen potential. Holding in argon (iv) results in denitriding of the compound layer which reduces the amount of ε and its unit-cell dimensions; the thickness of the "white layer" remains constant. By cooling the specimen (v) to 500°C and holding it in pure ammonia for 24h a thick uneven layer grows (Figure VI.8(v)), the ε layer remains and has a high nitrogen concentration shown by high unit-cell dimensions, and strong reflexions of both ε and γ' phases are observed (Figure VI.9(v)). The formation of such a compound layer is characteristic of low nitriding temperatures (Chapter V).

The results can be summarised as:

(i) Cooling slowly in argon or in ammonia after nitriding at 800°C leads to the formation of γ'-Fe_4N during cooling. In the former case the precipitation of γ' is a result of the reaction:

$$\varepsilon\text{-}Fe_2N_{1-x} + \gamma \rightleftharpoons \gamma'\text{-}Fe_4N + \gamma \quad \ldots\ldots \text{VI.1}$$

while in the latter case γ'-Fe_4N is formed by precipitation during cooling in addition to a nitriding reaction by the ammonia gas which leads to a thickening of the "white layer".

(ii) Holding specimens in argon at 500°C leads to diffusion of nitrogen atoms towards the surface (compare Nos. (i) and (ii) and Nos. (iii) and (iv); Figure VI.8).

Although the γ' layer is not reduced completely in 24h, there is some indication in Figure VI.8(iv) that the layer is being reduced.

Transmission electron microscopy on the "white layer" of a specimen nitrided at 800°C in pure ammonia for 24h and slow-cooled by pulling the sample out of the furnace in the nitriding atmosphere shows diffraction patterns and images of ε-Fe_2N_{1-x}, γ'-Fe_4N, CrN and γ in numerous combinations. Single grains of γ'-Fe_4N (often twinned) and of ε-$(Fe,Cr)_2N_{1-x}$ were identified, and lamellar structures of γ'+CrN, γ+CrN and mixtures of γ'+CrN+γ and also of ε + γ'+CrN were all observed in the same sample. Despite the fact that optical micrographs such as Figure V.8 show such samples to have a compact, uniform "white layer" when etched in 2% nital, the detailed microstructure is extremely complex.

VI.4 Conclusions

The "white layer" which occurs on nitriding at temperatures at or below 600°C is due to the formation of massive γ'-$(Fe,Ni)_4N$ containing precipitates of CrN but at higher temperatures no "white layer" is found except on cooling when the nature of the layer is then determined by cooling rate and cooling atmosphere.

At 600°C or below the nitrided layer consists of:

(i) a surface layer of ε-$(Fe,Cr)_2N_{1-x}$;

(ii) a "white layer" formed by γ'-$(Fe,Ni)_4N$, ε-$(Fe,Cr)_2N_{1-x}$ single grains, and fine precipitates of CrN;

(iii) a dark etched layer of CrN precipitates and γ'-$(Fe,Ni)_4N$ in a γ-matrix;

(iv) a diffusion layer consisting of a lamellar structure of CrN in γ; and

(v) a heavily deformed interface adjacent to the core which gives rise to ferrite formation.

At temperatures higher than 650°C the as-nitrided layer consists of:

(i) a very thin ε-$(Fe,Cr)_2N_{1-x}$ layer with some γ'-Fe_4N;

(ii) a lamellar structure of CrN in γ which coarsens with nitriding temperature;

(iii) a diffusion layer of lamellar CrN + γ and needle precipitates of Cr_2N in α-ferrite; and

(iv) a heavily deformed interface between case and core.

In every case the interface between case and core is heavily deformed and consists of twins, slip bands and a high dislocation density.

Chapter VII

KINETICS OF NITRIDING AISI 316

VII.1 Introduction

Nitriding of pure iron is a diffusion controlled process to which Fick's laws can be applied. When nitriding an alloy containing a substitional solute having a strong affinity for nitrogen a hard uniform subscale is formed and the growth of the layer is compatible with a diffusion-controlled process.

Previous work shows that nitriding AISI 316 in pure ammonia at low temperatures, 550° and 600°C gives an uneven nitrided layer and the growth rate of the case is parabolic which indicates a diffusion-controlled process (Wilson, 1978). The nitriding rate was found to be affected by the surface condition of the specimens and microhardness measurements show a sharp interface between the nitrided layer and the core (Cordwell et al., 1974; Wilson, 1978).

In the present investigation, the nitriding rate was followed by etching nitrided specimens and also by measuring the microhardness profile of the subscale. For low carbon-content steels a sharp subscale as is the case for high chromium alloys (Mortimer, 1971) is obtained while for high

carbon contents diffusion of carbon towards the centre is observed which results in an increase in the microhardness of the core; see Figure V.21.

Nitriding of AISI 316 between 550°-800°C in pure ammonia is determined by a diffusion process, but for temperatures lower than 650°C the nitriding rate is unexpectedly fast and can be explained by structural changes and the distribution of phases on the surface layer. The rate of nitriding is affected by cold-working when nitriding at low temperatures and also by grain-size and carbon content, but the kinetics of nitriding have the same form.

VII.2 Internal nitriding theory

Internal nitriding theory is derived from the analogous internal oxidation of Fe-0.1wt% Al to form Al_2O_3 by reaction with hydrogen-water mixtures (Hepworth et al., 1966). When nitriding AISI 316 the case depth is limited by the formation of chromium nitrides CrN or Cr_2N. To apply the theory three assumptions must be made:

(i) in internally nitrided specimens the nitrogen concentration varies linearly through the subscale;

(ii) at the surface the nitrogen concentration is in equilibrium with the gas phase; and

(iii) nitrogen and chromium are in equilibrium with CrN

at the interface between the case and the un-nitrided core.

The diffusion of chromium is very slow compared with diffusion of nitrogen and thus the diffusion equation must be written for the flux of nitrogen across the nitrided layer as:

$$\frac{dn}{dt} = D.\frac{C - C'}{X} \quad \ldots\ldots \text{VII.1}$$

with $\frac{dn}{dt}$: nitriding rate, g atm N $cm^{-2}s^{-1}$

X : thickness of the nitrided layer

C : nitrogen concentration in iron in equilibrium with the nitriding gas mixture

C' : nitrogen concentration in iron at the inner interface in equilibrium with CrN

D : diffusivity of nitrogen in iron

In fact, C' is very small compared with C and may be put equal to zero.

The amount of nitrogen transferred across unit area of the sample may be represented in terms of thickness (X), the ratio (r) of nitrogen to alloying element, i.e. Cr, in the precipitate formed, and the chromium concentration (wt% Cr), that is:

$$n = \frac{\rho}{52} \cdot r \cdot \text{wt\% Cr} \cdot 10^{-2}X, \text{ g atm } cm^{-2} \quad \ldots\ldots \text{VII.2}$$

where ρ is the density of iron.

By combining VII.1 and VII.2, converting C to wt% N and taking $C' = 0$

$$\frac{dX}{dt} = \frac{52}{14} \cdot \frac{1}{r} \cdot \frac{\text{wt\% N}}{\text{wt\% Cr}} \cdot \frac{D}{X} \qquad \ldots\ldots \text{VII.3}$$

and by integrating

$$X^2 = \frac{52}{7} \cdot \frac{1}{r} \cdot \frac{\text{wt\% N}}{\text{wt\% Cr}} \cdot D \cdot t \qquad \ldots\ldots \text{VII.4}$$

When the case depth is defined by the limit of precipitation of CrN, $r = 1$ and therefore the nitriding equation becomes:

$$X^2 = \frac{52}{7} \cdot \frac{\text{wt\% N}}{\text{wt\% Cr}} \cdot D \cdot t \qquad \ldots\ldots \text{VII.5}$$

VII.3 Nitriding of AISI L316

Nitriding as-received AISI L316 (0.02wt% C) in pure ammonia at temperatures higher than 550°C gives a uniform nitrided layer with the formation of a sharp case (see Figure V.14). At 550°C a variation of ~ 6 μm is observed in the case thickness while at 500°C the nitrided layer is very often uneven and in some areas very difficult to measure because of the presence of numerous cracks and the nature of the microstructure; see Figure V.3.

In disagreement with Wilson (1978), the thickness and

the regularity of the case does not depend on the surface preparation of the specimen. Similar results are obtained from specimens which have been electropolished or simply degreased. Only severe oxidation gives an uneven case but even then does not completely prevent nitriding.

Nitriding kinetics of annealed sheet samples treated in pure ammonia were studied between 550° and 800°C for up to 100 hours and the variations of the square of the total case depth against nitriding time are shown in Figure VII.1. For all temperatures the graph can be divided in two straight lines: a fast nitriding rate is observed for nitriding times lower than 14h, and a lower slope for greater times. Figure VII.1 shows also that the total case depth at 550° and 600°C is greater than that observed at 700°C for the same nitriding time. In Figure VII.2 the variation of case depth with temperature is compared with results given by Lebrun et al. (1972). A discontinuity in the graph between 600° and 650°C is shown in both cases and similar effects have been observed by Cordwell et al. (1974) when nitriding AISI 316 in pure ammonia and by Lerner (1972) for AISI 304 nitrided either by glow-discharge or conventional gas-nitriding. The rate of nitriding in the range 550°-600°C is considerable greater than predicted by extrapolation of data for temperature higher than 650°C; see Figure VII.2.

Nitriding experiments at Springfields Laboratories (1980) at 600°, 700° and 800°C on AISI 316 show very similar curves

Figure VII.1

$(\text{Case depth})^2$ against nitriding time for AISI L316 (0.02wt% C) in pure ammonia at 550°, 600°, 700° and 800°C

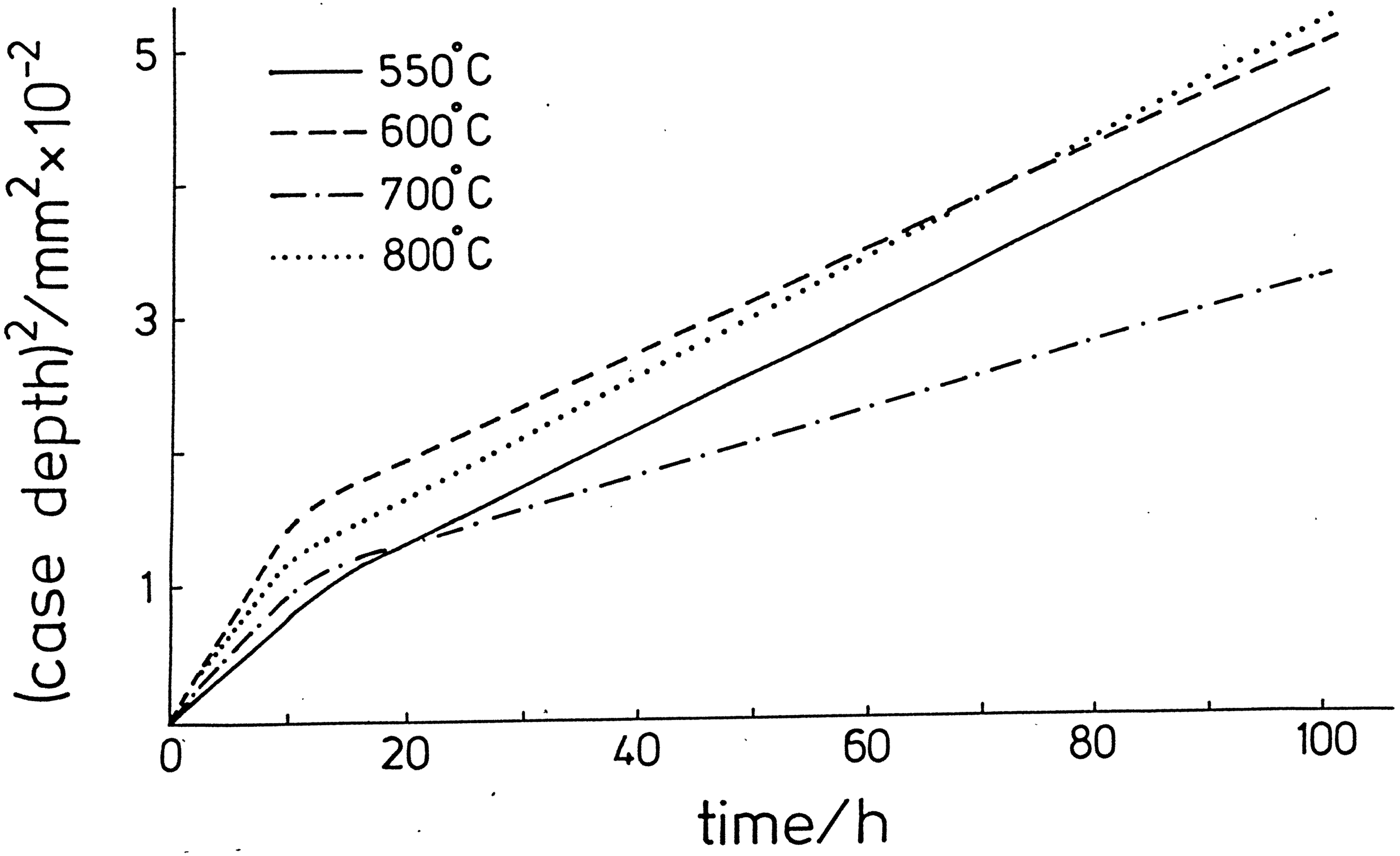
(case depth)²/mm²×10⁻²
5
3
1
550°C
600°C
700°C
800°C
0
20
40
60
80
100
time/h

Figure VII.2

Case depth against nitriding temperature in pure ammonia for

(a) AISI L316 - gas-nitrided for 24h

and (b) 18-10 stainless steel - ion nitrided for 4h (Lebrun et al., 1972)

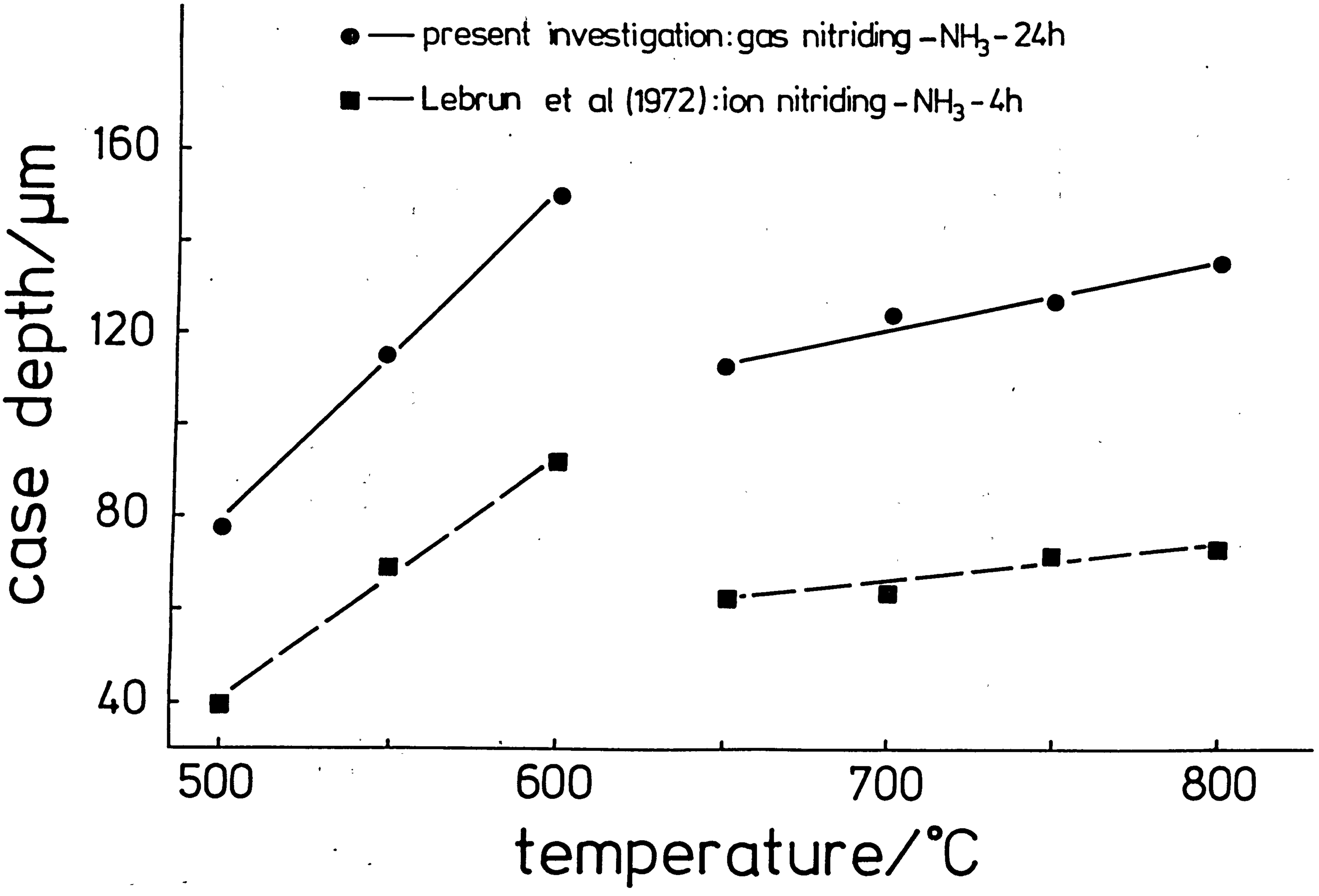
● — present investigation: gas nitriding – NH_3 – 24h
■ — Lebrun et al (1972): ion nitriding – NH_3 – 4h
case depth/µm
160
120
80
40
500
600
700
800
temperature/°C

when the square of the total case depth is plotted against nitriding time but the thickness of the nitrided layer was slightly smaller for 600° and 800°C than in the present work. However, insufficient results from Springfields are available for long nitriding times, i.e. $>$ 12h, to allow valid comparisons.

The nitriding rate (see equation VII.5) should decrease with decreasing temperature as the diffusion coefficient D is a function of temperature and can be represented by an Arrhenius equation:

$$D = Do \exp\left(-\frac{\Delta H}{RT}\right) \quad \ldots\ldots \text{VII.6}$$

where Do : frequency factor

ΔH : activation enthalpy

R : gas constant

T : absolute temperature

Do and ΔH are independent of temperature but depend on the nature of the interstitial element diffusing and on the matrix and, in the case of diffusion of carbon in γ - austenite are dependent on carbon concentration (Wells et al., 1950; Bhadeshia, 1981). Equation VII.6 shows that as the temperature increases the diffusion coefficient increases and, according to equation VII.5, since the nitrogen concentration in the matrix in equilibrium with the gas mixture decreases with temperature (combination of

equations III.6, III.7 and V.11), the slope of the line representing the square of the case depth (X^2) against nitriding time (t) should decrease with nitriding temperature.

For the present work the nitrogen concentration in γ -iron in equilibrium with $NH_3:H_2$ gas mixture can be calculated using nitrogen solubility data from Atkinson & Bodsworth (1970), taking the maximum value of nitriding potential (pure ammonia), interpolating for 13wt% Ni, and extrapolating for 550° and 600°C. The theoretical square of the case depth as a function of nitriding time can be found from equation VII.6 using Grieveson & Turkdogan's (1964) data for Do and ΔH to calculate D. Figure VII.3 represents schematically the theoretical variation of X^2 against t at 500°, 600°, 700° and 800°C assuming that internal nitriding theory is valid. There is an enormous difference between the calculated nitriding rates at 800° and 600°C whereas the observed rates at these temperatures (see Figure VII.1) are almost identical. In addition, simple internal nitriding theory does not predict the discontinuity observed in the curves of Figure VII.1.

From the slopes of the curves of Figure VII.1, experimental diffusion coefficients for nitrogen in austenite have been calculated using Atkinson & Bodsworth data (1970) as indicated above and are compared in Table VII.1 with those determined by Grieveson & Turkdogan (1964). For the first

Figure VII.3

Schematic theoretical variation of (case depth)^2 against nitriding time in pure ammonia for Fe-13wt% Ni.

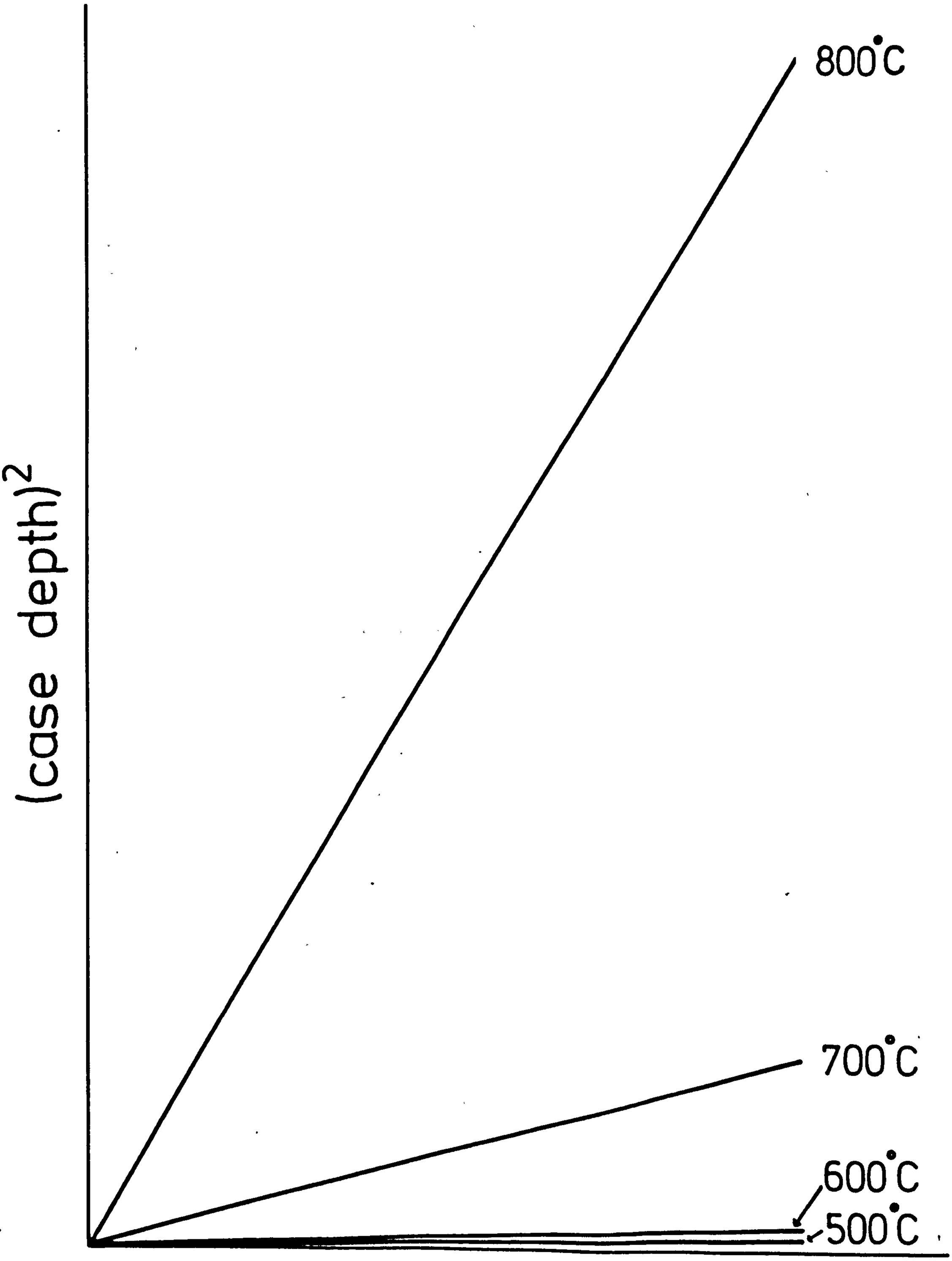
800°C
(case depth)^2
700°C
600°C
500°C
time

Table VII.1

Kinetic results for nitriding AISI L316 in pure ammonia

temperature °C	specimens wt% C	treatment	1st slope $\mu m^2 s^{-1}$	2nd slope $\mu m^2 s^{-1}$	Dcal. for 1st slope $cm^2 s^{-1}$	Dcal. for 2nd slope $cm^2 s^{-1}$	D N/γ (G.&T.) $cm^2 s^{-1}$	D N/α (L.&B.) $cm^2 s^{-1}$
550	0.02	as-received	0.220	0.114	$2x\ 0^{-9}$*	$9x10^{-10}$*	$1.9x10^{-11}$	$6.5x10^{-8}$
600	0.02	as-received	0.405	0.103	$4x10^{-9}$*	10^{-9}*	$7.6x10^{-11}$	$1.3x10^{-7}$
		20% C.W.	0.405	0.105	$4x10^{-9}$*	10^{-9}*		
		63% C.W.	0.255	0.088	$3x10^{-9}$*	$9x10^{-10}$*		
	0.07	as-received	0.308	0.088	$3x10^{-9}$*	$9x10^{-10}$*		
		H.T. 600°C	"	0.088	$3x10^{-9}$*	$9x10^{-10}$*		
		H.T. 800°C	"	0.070	$3x10^{-9}$*	$7x10^{-10}$*		
700	0.02	as-received	0.269	0.067	$4x10^{-9}$*	10^{-8}**	$8.3x10^{-10}$	$3.7x10^{-7}$
800	0.02	as-received	0.289	0.124	$5x10^{-9}$*	$2x10^{-8}$**	$5.7x10^{-9}$	$8.9x10^{-7}$
		20% C.W.		0.098	$5x10^{-9}$*	10^{-8}**		
		63% C.W.		0.126	$5x10^{-9}$*	$2x10^{-8}$**		
	0.07	as-received	0.463	0.196	$7x10^{-9}$*	$3x10^{-8}$**		
		H.T. 600°C		0.168	$7x10^{-9}$*	$2x10^{-8}$**		
		H.T. 800°C		0.168	$7x10^{-9}$*	$2x10^{-8}$**		

* assuming formation of CrN in γ

** assuming formation of Cr_2N in α

C.W.: cold-worked

H.T.: heat-treated

slope, agreement at 700° and 800°C is good. At these temperatures, the diffusion coefficient for the second slope has been calculated assuming precipitation of Cr_2N in ferrite, taking a chromium content of 10wt%, i.e. the maximum present in ferrite for 17wt% nickel (Figure II.4), and the maximum nitrogen concentration in ferrite at the reaction temperature from Figure II.9. Agreement with Lord & Beshers's date (see Table VII.1) is reasonable considering that the real chromium and nitrogen contents in the ferrite phase are not known.

The apparent diffusivities at 550° and 600°C are too high for diffusion of nitrogen in austenite but too low for diffusion of nitrogen in ferrite (Table VII.1). Diffusion of nitrogen in α -ferrite was suggested by Lebrun et al. (1972) in order to explain the abnormally high nitriding rate at 600°C but this is not satisfactory in the present case where only a small amount of α is detected adjacent to the case-core interface in samples nitrided at 550° and 600°C. Wilson (1978) obtained a value of $D = 7.1 \times 10^{-10} cm^2 s^{-1}$ at 600°C by nitriding AISI 316 in pure ammonia which is approximately the value obtained in the present study. However at these temperatures formation of massive γ' results in the formation of cracks which are longitudinal at the inner edge of the "white layer" (Figure V.5) and also transverse to the free surface; the formation of these cracks has been discussed in Chapter V. Nitriding is facilitated and

accelerated by increasing access of nitriding gas to the underlying metal by diffusion along the cracks.

Nitriding in ammonia:hydrogen mixtures at 600°C shows that for ammonia concentrations lower than $60NH_3:40H_2$ the nitrided layer is not uniform, and for less than $40NH_3:60H_2$ the maximum case depth decreases with ammonia concentration in the gas mixture (Table VII.2). However, development of a uniform nitrided case at 600°C corresponds to the formation of a "white layer" of γ'-$(Fe,Ni)_4N$ as demonstrated by exposing specimens in pure ammonia at 600°C for 15 min followed by 24h in $40NH_3:60H_2$. The nitrided layer then has approximately the same case depth as expected for growth in equilibrium with γ' (130 μm).

Nitriding at 800°C in ammonia:hydrogen mixtures gives a uniform nitrided layer and the case depth does not vary with ammonia concentration which is probably due to the high degree of dissociation of NH_3 at this temperature (Table III.2). Thus, the nitrogen potential remains almost constant in all runs. Nitriding at 800°C does not produce γ' at nitriding temperature at any value of nitrogen potential.

Nitriding AISI L316 appears to be a diffusion controlled process but an abnormally high nitriding rate is obtained at around 600°C where massive γ'-$(Fe,Ni)_4N$ is formed at nitriding temperature and results in cracking of the sub-surface layer. At 800°C the rate of nitriding is

Table VII.2

Case depth of AISI L316 nitrided in ammonia: hydrogen mixtures at 600° and 800°C for 24h

nitriding conditions		case depth	"white layer"
temperature °C	NH_3 : H_2	µm	µm
600	80 : 20	140	16
	70 : 30	140	13
	60 : 40	140	13
	60 : 40	0 -137	9
	55 : 45	0 -127	6
	40 : 60	0 - 89	0
	25 : 75	0 - 54	0
	10 : 90	0 - 26	0
	15min.100:0+40:60*	112-133	11
800	70 : 30	140	0
	40 : 60	140	0

* the specimen was exposed 15min in pure ammonia prior nitriding in $40NH_3:60H_2$ for 24h.

predictated by internal nitriding theory and the calculated value of D_N is in reasonable agreement with that of Grieveson & Turkdogan (1964) and Lord & Beshers (1966). Reducing the $NH_3:H_2$ ratio at high temperature does not greatly affect the nitriding rate because the effective nitrogen potential remains small and almost constant due to the dissociation of ammonia. At 600°C the relative changes in thickness of the nitrided layer are consistent with the thermodynamic predictions of phase stabilities.

VII.4 Effect of carbon content, grain-size and cold-work on nitriding rate

(a) Effect of carbon content and grain-size

Nitriding AISI 316 containing 0.07wt% C was carried out at 600° and 800°C in pure ammonia. These specimens were found to be more difficult to nitride than those with 0.02wt% C, especially at the lower temperature and when the material had been electropolished. To overcome this problem, samples were either electropolished and kept overnight in a desiccator or simply degreased with trichloroethylene before nitriding.

Specimens containing 0.07wt% C nitrided at 600°C show a smaller case depth (133 μm) than 0.02wt% C (150μm)

after 24h, but only the behaviour at short nitriding times is abnormal and the second part of the curve has almost the same slope as found for 0.02wt% C (see Table VII.1). Aleskeeva et al. (1979) reported that carbon reduces the thickness of the nitrided layer formed during nitriding 17wt% Cr - 8wt% Ni - 5wt% Mn - 0.8wt% Mo steel in pure ammonia at 600°C. At 800°C however, the nitriding rate is higher for 0.07wt% C than for the corresponding 0.02wt% C samples. In both cases nitriding is controlled by diffusion (see Figure VII.4 for nitriding at 600°C and Figure VII.5 for 800°C), i.e. the square of the case depth is proportional to nitriding time and, as for 0.02wt% C steel, the graphs consist of two straight line regions.

Prior heat-treatment on specimens containing 0.07wt% C was carried out at 600° and 800°C for 48h in order to study the influence of carbides on nitriding rate. Figure VII.6 shows the microstructure of AISI 316 after heat-treatment for 24, 48 and 100h at 600° and 800°C. The specimens were etched in aqua regia-glycerol solution; see Table III.3. Fairly large precipitates are visible at 800°C but much less precipitation is evident at 600°C. Transmission electron microscopy of as-received 0.07wt% C material shows no carbide precipitates but $M_{23}C_6$ precipitates are observed at 800°C and grow with increasing annealing time; inter-metallic X-phase is also observed. At 600°C only very fine precipitates of $M_{23}C_6$ are present with a small amount

Figure VII.4

(Case depth)^2 against nitriding time for AISI 316 (0.07wt% C) in pure ammonia at 600^{o}C in as-received material and after heat-treatment

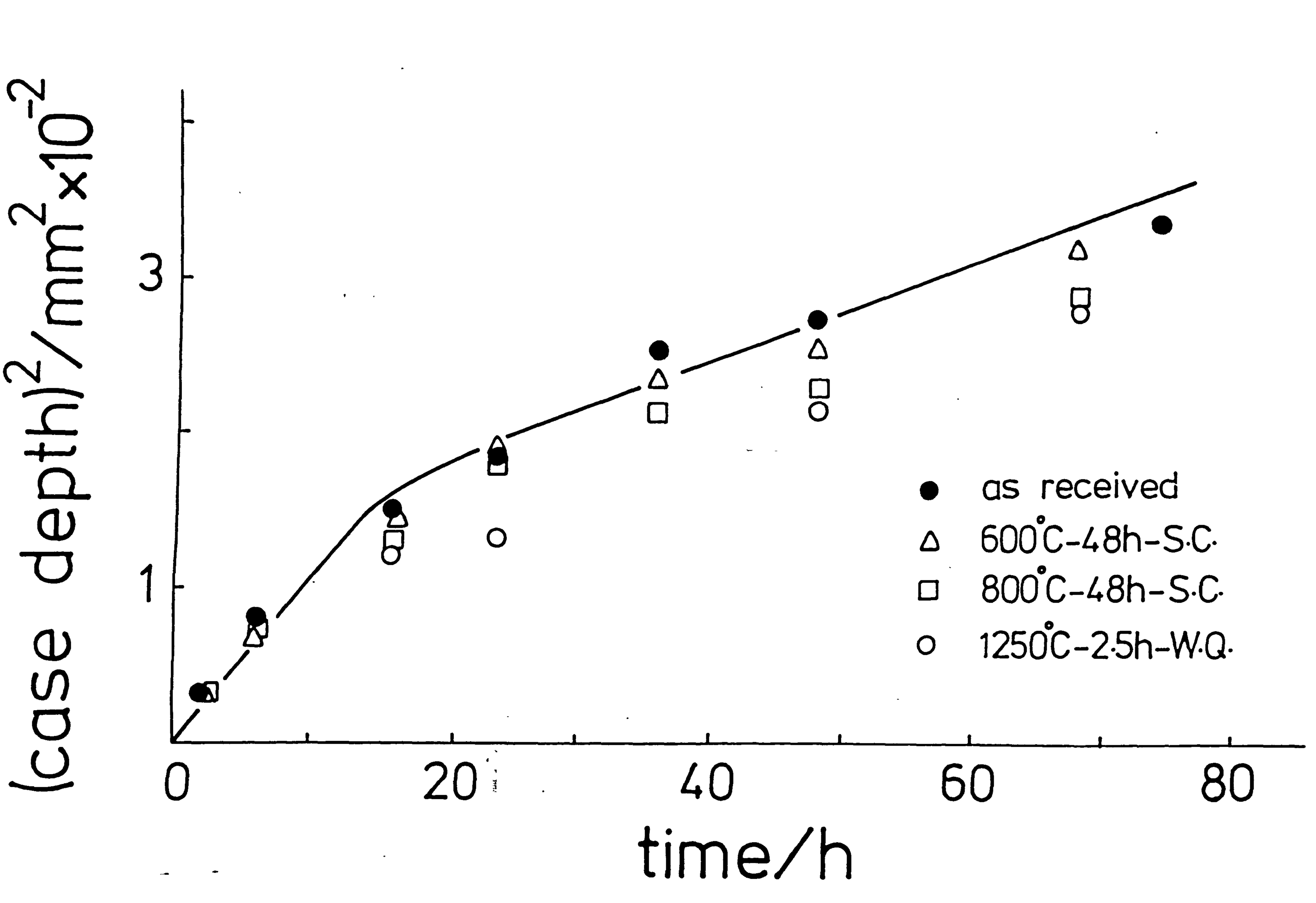
(case depth)^2/mm^2 x10^{-2}
3
1
0
20
40
60
80
time/h
as received
600°C-48h-S.C.
800°C-48h-S.C.
1250°C-2.5h-W.Q.

Figure VII.5

$(\text{Case depth})^2$ against nitriding time for AISI 316 (0.07wt% C) in pure ammonia at 800°C in as-received material and after heat-treatment

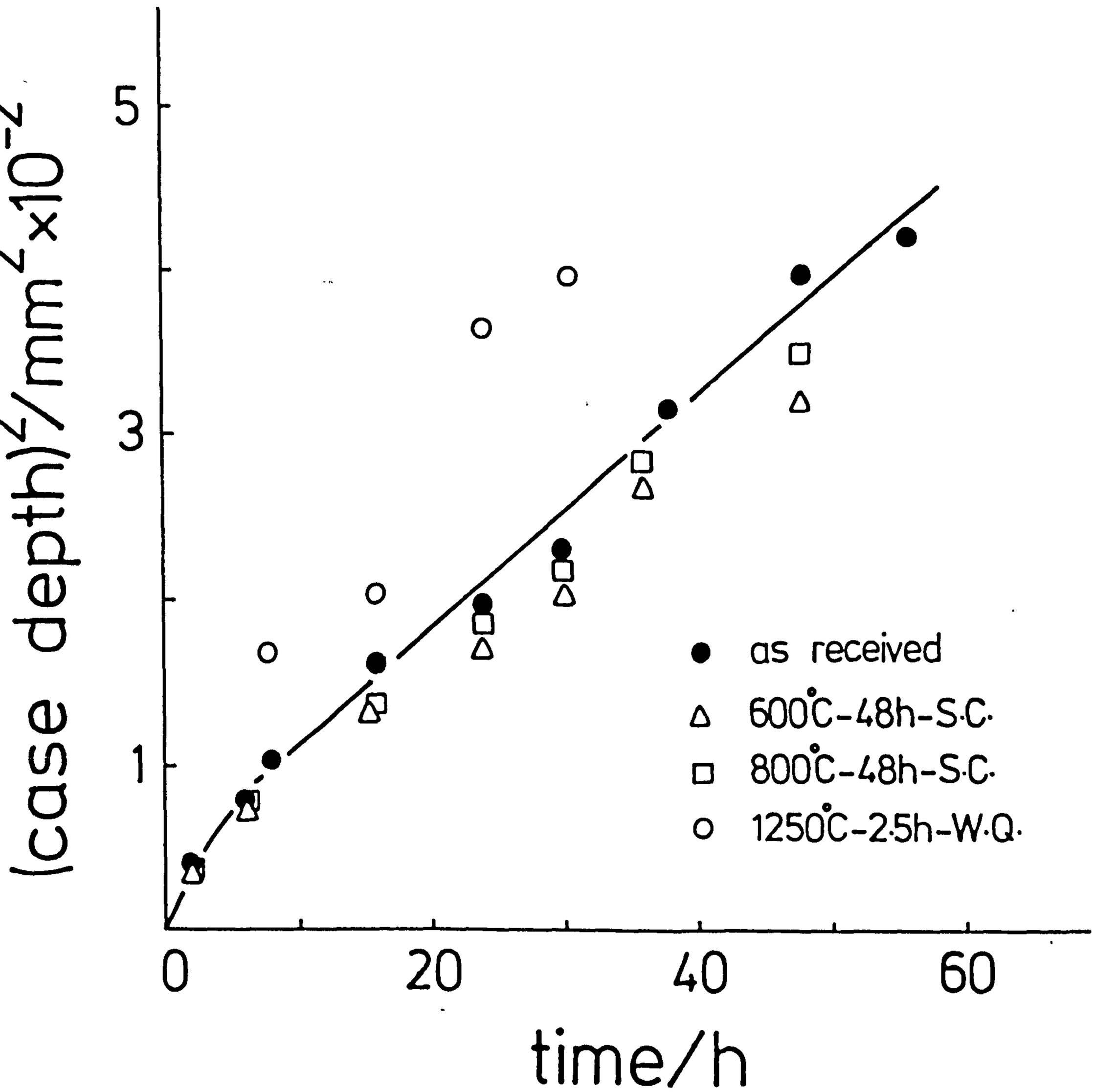
(case depth)^2/mm^{2}x10^{-2}
5
3
1
0
20
40
60
time/h
as received
600°C-48h-S.C.
800°C-48h-S.C.
1250°C-2.5h-W.Q.

Figure VII.6

Optical micrographs of AISI 316 (0.07wt% C)

heat-treated at

600°C for (a) 24hr

(b) 48h

(c) 100h

and at 800°C for (d) 24h

(e) 48h

and (f) 100h,

etched in aqua regia-glycerol

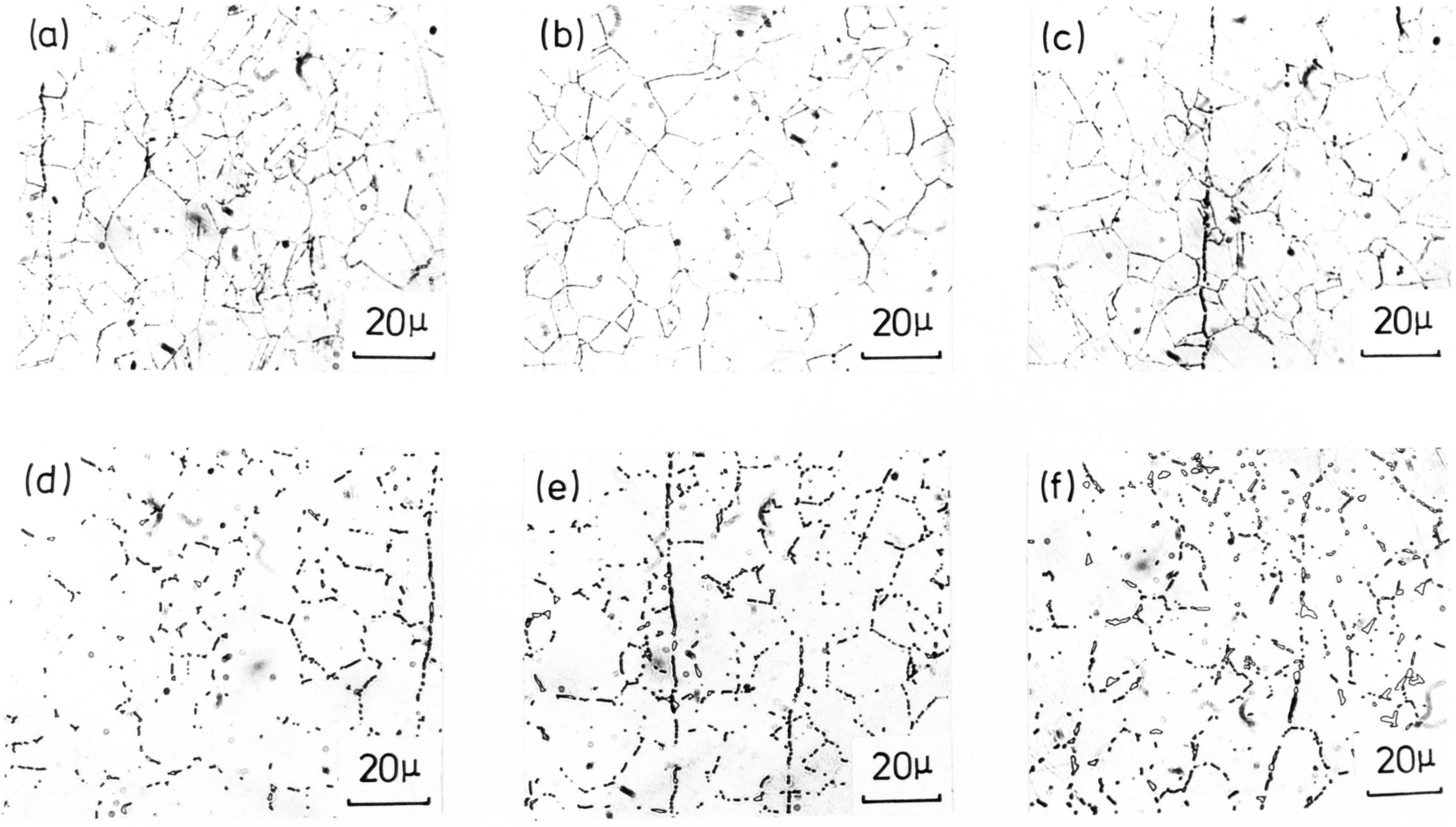
(a)
20μ
(b)
20μ
(c)
20μ
(d)
20μ
(e)
20μ
(f)
20μ

of X-phase detected in grain-boundaries. Lai & Meshkat (1978) reported that $M_{23}C_6$ is the major precipitate formed at 600°C while at 800°C $M_{23}C_6$ and X-phases are both present.

Figures VII.4 and VII.5 show that prior annealing at 600° and 800°C for 48h has little effect on the case depth of specimens nitrided at 600° and 800°C. Carbide precipitation in grain-boundaries does not therefore affect nitriding rates which suggests that nitriding of AISI 316 is mainly controlled by bulk diffusion of nitrogen within the grains.

Changes in the diffusion coefficient of carbon in austenite as a function of carbon content have been reported and, as carbon and nitrogen behave similarly in iron, it is reasonable to assume that the diffusivity of nitrogen will vary both with nitrogen concentration and carbon concentration.

The flux of each element is a linear function of the concentration gradients, that is:

$$J_N = - D_N^N \frac{\delta C_N}{\delta x} - D_N^C \frac{\delta C_c}{\delta x} \quad .... \quad VII.7$$

$$J_c = - D_c^N \frac{\delta C_N}{\delta x} - D_c^c \frac{\delta C_c}{\delta x} \quad .... \quad VII.8$$

In the present work D_N^C is different from D_C^N because the nitrogen potential is constant at the surface of the specimen, while for carbon as it diffuses towards the centre (see Chapter V) its activity will change and eventually reach a value of zero at the surface.

Considering nitriding of AISI 316 at 800°C (where internal nitriding theory is valid), increasing the carbon content from 0.02 to 0.07wt% C gives an increase of 1.6 times in the apparent diffusion coefficients calculated for both linear sections of the curves (see Figure VII.5 and Table VII.1) whereas the diffusivity of carbon in austenite is reported to be increased by 4.6 times for the same change in carbon content (Bhadeshia, 1981). However, in the present case the diffusion coefficient of nitrogen is influenced by both carbon and nitrogen concentrations and the concentration profiles and the overall effect cannot be predictated quantitatively. The diffusivity and hence the rate of nitriding will increase with nitrogen concentration but there is a "back pressure" due to build up of carbon ahead of the nitriding front which will act in the opposite sense.

When nitriding at 600°C, internal nitriding theory does not apply because the diffusion behaviour is complicated by cracking of the layers. No carbide precipitation has been detected ahead of the nitrided layer at 600°C for 0.02wt% C

specimens and only a small amount for 0.07wt% C. In fact, increasing the carbon concentration decreases the total case depth by decreasing the rate of the first stage of nitriding which is related to the formation of the outer compound layer. Colijn et al., (1980) suggested that in Fe-Cr-C alloys carbon diffuses from the core to the compound layer and γ'-Fe_4N is able to dissolve 0.2wt% C (Naumann & Langenscheid, 1965). Therefore carbon atoms diffusing towards the surface offer a resistance to nitrogen penetration into the specimen which would lower the first stage of nitriding. Then, when the maximum solubility of carbon in γ'-Fe_4N is reached, nitrogen and carbon diffuse in the same direction i.e. towards the centre.

Heat-treatment at 1250°C for 2.5h followed by water quenching ensures that all the carbon is in solid-solution and large grains are formed (Table III.4). The interface between the nitrided layer and core of such specimens is not uniform and follows the shape of the grains. The rate of nitriding in the first stage is increased at 800°C (Figure VII.5) but is slightly decreased at 600°C (Figure VII.4). The faster nitriding rate obtained at 800°C for very short nitriding times can be explained by grain-boundary diffusion. As all the carbon is in solid-solution, the grain-boundary path is free for nitrogen diffusion and gives a high initial nitriding rate. Then carbide precipitation occurs (Figure II.7) and gives a nitriding rate similar to that of as-

Figure VII.7

(Case depth)^2 against nitriding time for AISI L316 (0.02wt% C) in pure ammonia at 600°C. As-received, 20% and 63% cold-worked

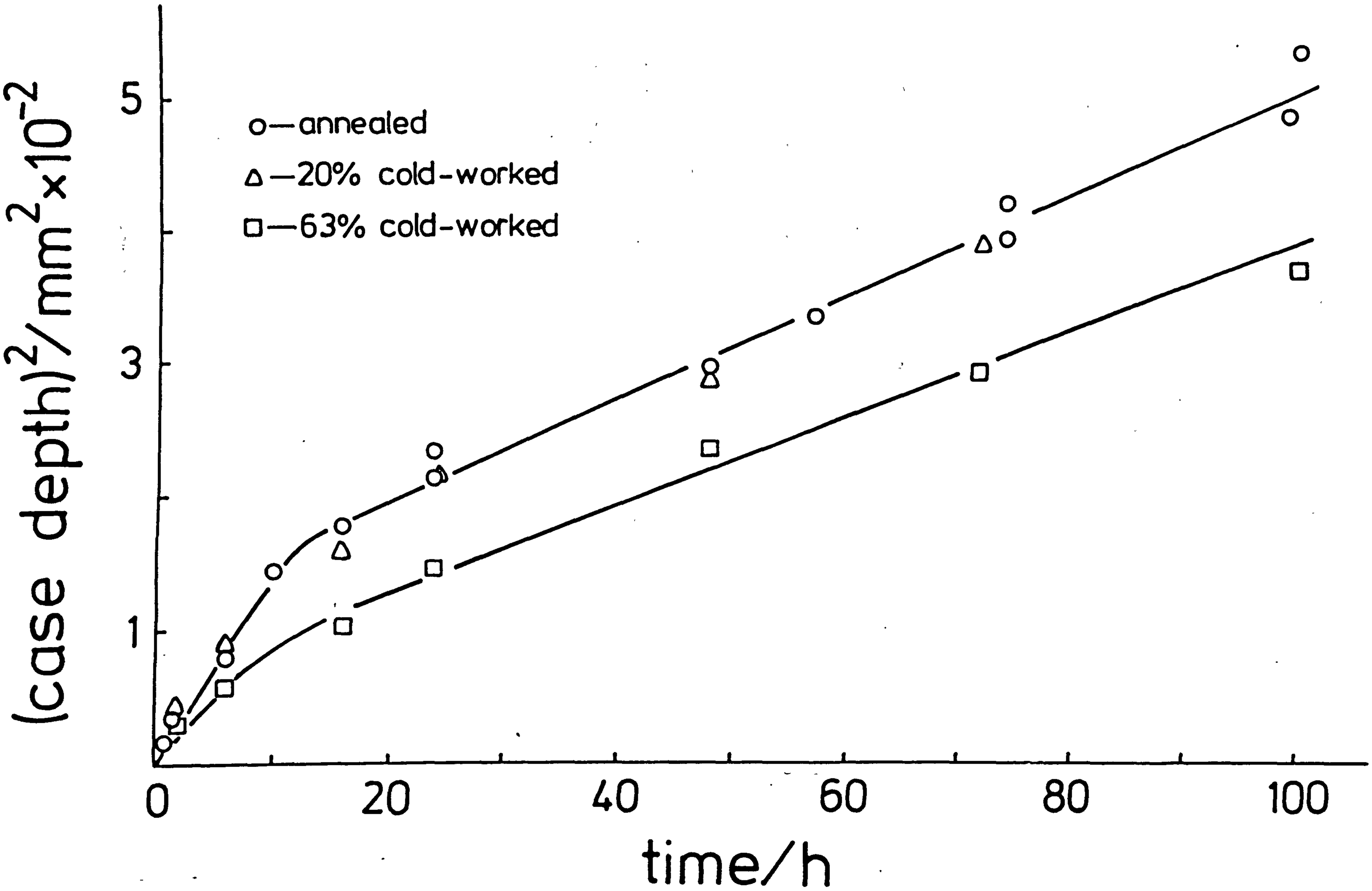
o—annealed
Δ—20% cold-worked
□—63% cold-worked
(case depth)²/mm²×10⁻²
5
3
1
0
20
40
60
80
100
time/h

received material for prolonged nitriding times (Figure VII.5). Growth of γ'-Fe_4N at 600°C proceeds from the grain-boundaries and so in samples of large grain size only a thin white layer is formed (only 9 μm compared with 20 μm for as-received material). With a thin "white layer" the stresses in the inner layer are not as great as those in nitrided as-received samples and, in addition, the large grains can accommodate stresses by plastic deformation. Thus, the formation of a thinner surface layer on samples nitrided at 600°C after prior heat-treatment at 1250°C is due to less extensive cracking in the inner subscale.

From the results of the present study it is clear that nitriding behaviour is strongly dependent on the formation of the initial surface layers and on the formation of γ'-$(Fe,Ni)_4N$ at nitriding temperature. The rate in the later stage at both 600° and 800°C depends on carbon content but is largely independent of grain-size and heat-treatment.

(b) Effect of cold-work

The mobility of interstitial atoms is affected by grain-boundaries and other easy diffusion paths such as dislocations (Lagneborg & Josefsson, 1955) and thus the kinetics of nitriding cold-worked alloys is expected to be different from those of annealed material. Samples of AISI L316 with 20% and 63% of cold-reduction were nitrided in pure ammonia at

600° and 800°C and the rates of nitriding determined.

20% cold-working has no measurable effect on nitriding rate at 600°C but 63% cold-worked samples show a smaller case depth than annealed specimens after the same nitriding time (see Figure VII.7). After 16h the rate of nitriding is almost identical for all three sets of specimens since the curves are practically parallel and only during the early stage is the rate of nitriding decreased for 63% cold-worked samples. Cold-working has no influence on nitriding behaviour at 800°C (Figure VII.8).

The surfaces of tensile-test specimens of annealed and nitrided and of cold-worked and nitrided specimens were examined in the scanning electron microscope (SEM). Samples with 63% cold-work nitrided at 600°C in pure ammonia show voids in the "white layer" parallel to the surface (Figure VII.9(b)) but no such voids are observed on annealed or 20% cold-worked samples (Figure VII.9(a)) nitrided at 600°C or on any samples nitrided at 800°C. Voids are observed only in the "white layer" which explains that only the first stage of nitriding is affected. The compound layer of 63% cold-worked samples nitrided at 600°C is thicker than for annealed specimens (30 μm compared with 20 μm) which would suggest a higher nitrogen partial pressure in the former case. Nitriding is also expected to be affected by the rolling texture which is retained during nitriding at 600°C.

Figure VII.8

(Case depth)^2 against nitriding time for AISI L316 (0.02wt% C) in pure ammonia at 800^{o}C. As-received, 20% and 63% cold-worked

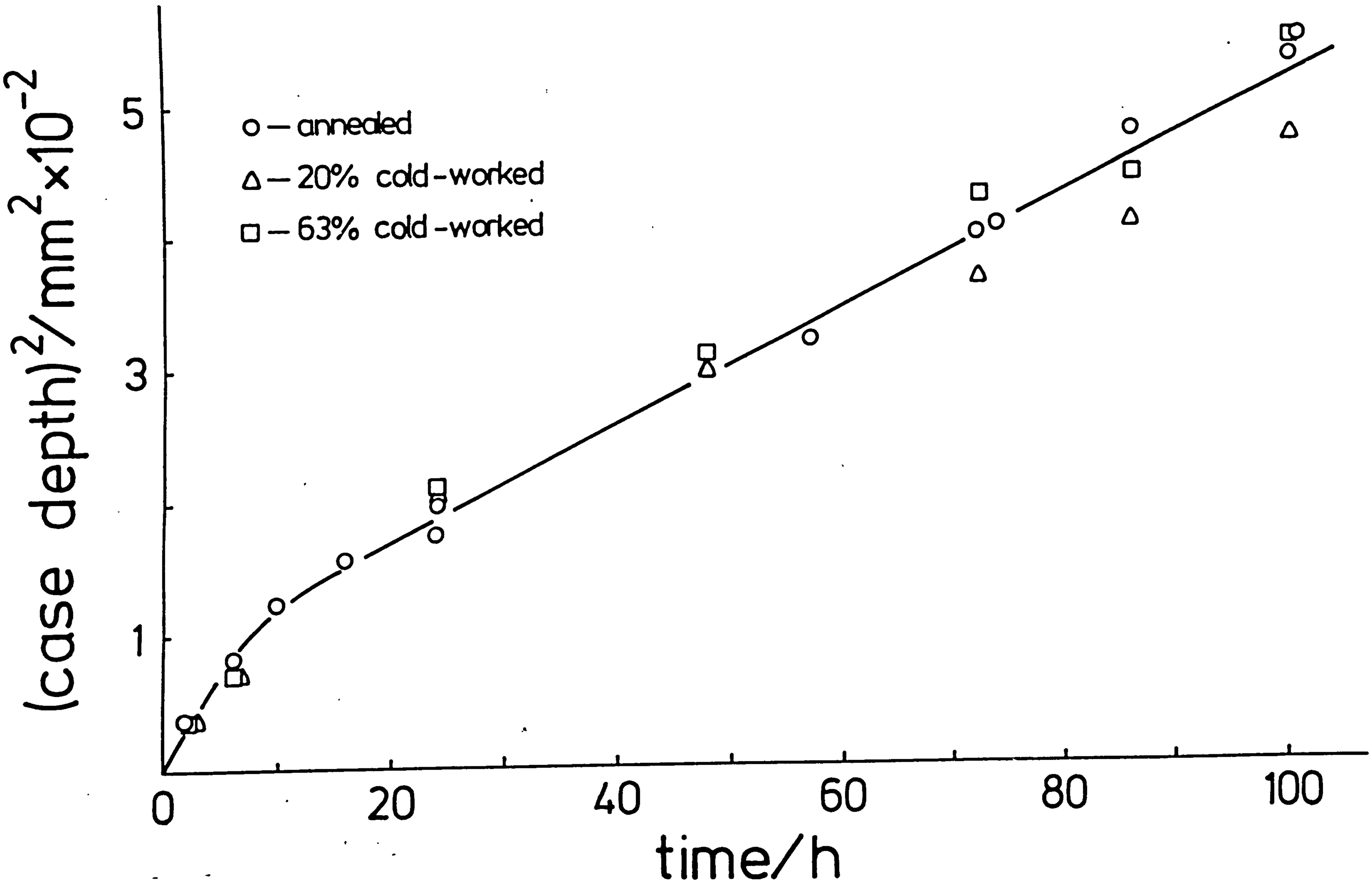
(case depth)^2/mm^{2}x10^{-2}
5
3
1
o — annealed
Δ — 20% cold-worked
□ — 63% cold-worked
0
20
40
60
80
100
time/h

Figure VII.9

SEM micrographs of the "white layer" observed on a tensile specimen of AISI L316 nitrided at 600°C for 24h in pure ammonia

(a) 20% cold-worked

and (b) 63% cold-worked

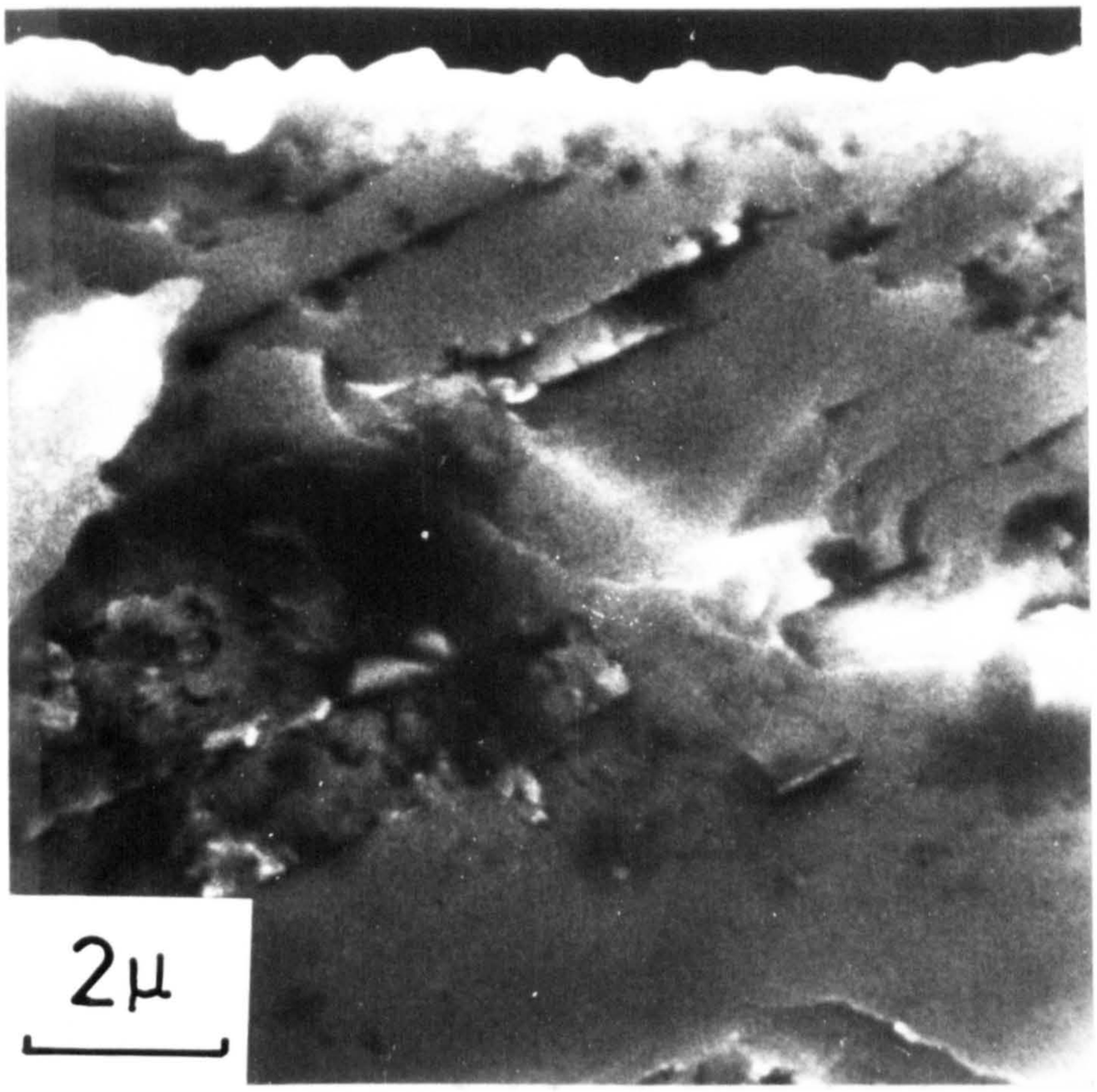

(a)

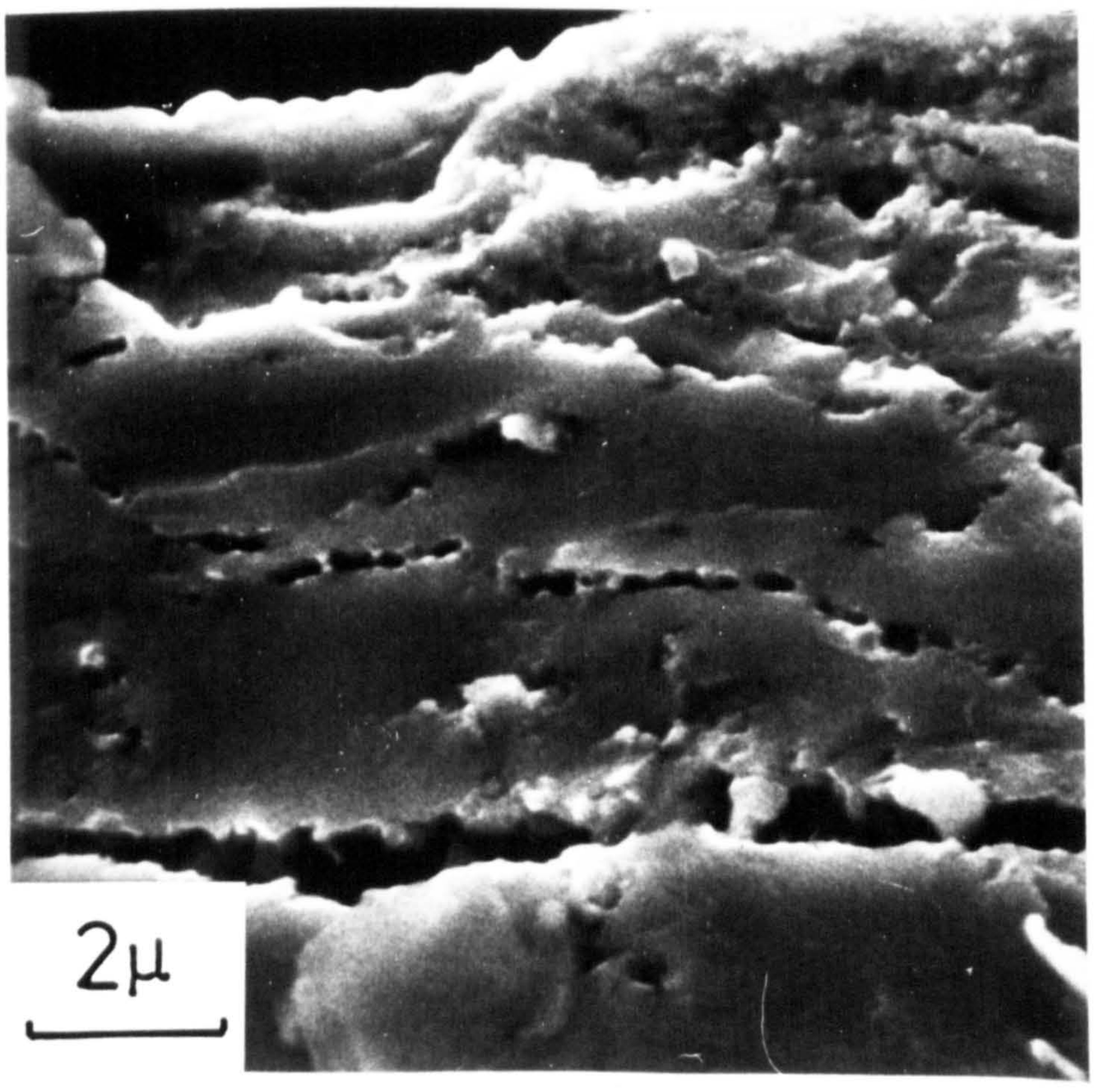

(b)

However, smaller case depths are observed only when the specimens are heavily deformed with no partial recrystallisation. 63% cold-worked samples heat-treated at 800°C for 99 hours and then nitrided at 600°C for 24 hours show the same case depth as for as-received material nitrided under the same conditions.

Prior cold-work does not change the nitriding kinetics at 600° and 800°C but affects the precipitation of massive γ'-$(Fe,Ni)_4N$ and leads to a smaller case depth at 600°C. The formation of voids in the compound layer is observed when recrystallisation has not occurred.

VII.5 Discussion

Rates of nitriding AISI L316 at 700° and 800°C are determined by internal nitriding theory and are controlled by the diffusion of nitrogen in austenite. At lower temperatures the formation of a "white layer" increases the nitriding rate due to the formation of cracks.

Considering nitriding at 800°C where no γ'-Fe_4N is precipitated at nitriding temperature (see Chapter VI), the curve representing the square of the case depth against nitriding time is divided in two regions represented by straight lines of different slopes; see Figure VII.1. However, the very first stage of nitriding, that is for

times shorter than 2 hours, is grain-boundary dependent which is not obvious from Figure VII.1. This fact is shown by nitriding heat-treated specimens at 1250°C and water-quenching to retain all the carbon in solid-solution. These have a thicker nitrided layer than as-received material in which some carbides are precipitated in grain-boundaries.

The change in slope of the curves of X^2 against t for samples nitrided at 800°C is observed at a depth in the nitrided layer of approximately 90 μm and this can be related to the precipitation of Cr_2N in ferrite (see Table V.3). Therefore for $X < 90\ \mu m$ nitriding occurs in equilibrium with precipitation of CrN in γ while for $X > 90\ \mu m$ precipitation of Cr_2N in ferrite occurs. The slopes obtained at 800°C (Table VII.1) give values of diffusivity in austenite and in ferrite in agreement with the literature values.

The nitriding equations are:

for $X < 90\ \mu m$

$$X^2 = \frac{52}{7} \cdot \frac{wt\%\ N}{wt\%Cr} \cdot D_N^{\gamma} \cdot t \qquad \ldots\ \text{VII.10}$$

and for $X > 90\ \mu m$

$$X^2 = \frac{52}{7} \cdot \frac{1}{2} \cdot \frac{wt\%\ N}{wt\%Cr} \cdot D_N^{\alpha} \cdot t \qquad \ldots\ \text{VII.11}$$

However, the diffusion coefficient depends on the carbon content and in AISI L316 (0.02wt% C) $D_N^{\gamma} = 5x10^{-9} cm^2 s^{-1}$ while in AISI 316 (0.07wt% C) $D_N^{\gamma} = 7x10^{-9} cm^2 s^{-1}$.

The formation of "white layer", i.e. precipitation of massive γ'-$(Fe,Ni)_4N$, at nitriding temperature enhances nitriding and abnormally high nitriding rates are obtained due to the formation of cracks which facilitate ammonia penetration into the inner subscale. For nitriding at 600°C or at 550°C, as at 800°C, the curve representing the case depth squared against nitriding time can be represented by two straight lines. The slope of the first part of the nitriding curve depends on the starting material, i.e. carbon content, degree of deformation and grain-size. The change in slopes is observed at a depth of nitrided layer of approximately 120 μm (Figire VII.1), that is, when the body-centred cubic or low tetragonality phase (α or α') appears (see Chapter V). Only the second slope corresponds to a diffusion process. It is difficult to determine at which depth the influence of the cracks observed in the "dark-etched" layer can be neglected and so it is not possible to give the exact value of the diffusion coefficient. At temperatures lower than 600°C, the nitriding rate is determined by the diffusion of nitrogen in austenite provided that no crack formation occurs.

At 700°C, nitriding behaviour is complex due to the formation of a thin "white layer" which leads to a high

nitriding rate, and to the presence of Cr_2N ferrite in the diffusion layer. However, the curve representing the square of the case depth against nitriding time can also be divided in two straight lines with the slope of the first four times that of the second.

VII.6 Conclusions

For temperature at which γ'-Fe_4N is formed during nitriding, i.e. lower than 700°C, nitriding of AISI 316 takes place at an initial rapid rate during which the surface layer of iron nitrides is formed after which the rate of subscale growth decreases.

The final thickness of the nitrided case at any temperature is a function of several variables: iron nitride formation, chromium carbide precipitation, grain-size and degree of prior cold-work.

At 800°C internal nitriding theory is valid assuming, as is observed, the precipitation of CrN in austenite during the first stage and then precipitation of Cr_2N in ferrite during the second. At temperatures lower than 700°C, although nitrided case depth squared is a linear function of time, an unexpectedly high rate is observed and is explained by cracking of the nitrided case

caused by a residual stress gradient in the γ'-Fe_4N layer. Enhanced access of ammonia through the cracks to the underlying metal leads to rapid nitriding.

Chapter VIII

MECHANICAL PROPERTIES OF NITRIDED AISI 316

VIII.1 Introduction

The formation of a nitrided case on the surface of a steel increases wear resistance, tensile strength and fatigue properties but decreases its ductility. The little work which has been reported on the mechanical properties of nitrided stainless steel is discussed in section II.3(b). Typical tensile load-extension curves for nitrided AISI 316 show a linear elastic part with no well-defined limit of proportionality followed by plastic deformation with some steps in the load-extension curve accompanying cracking of the scale. Failure of glass-filled nitrided tubes in four-point bend tests does not show any influence of the depth of the nitrided case (Wilson & Wilson, 1981). These results will be discussed later in the present chapter.

Three- and four-point bend tests were used in the present study to determine the mechanical properties of nitrided specimens in the form of sheets and tubes. Four-point bend testing is more often used than three-point bend due to a uniform distribution of the bending moment along the beam and also because there is a maximum

shearing force at the central anvil in the case of the three-point bend.

On bending a straight beam the inside surface of the bent beam is in compression while the outside is in tension and there is an intermediate level at which the stress is zero and which cuts any cross section in the neutral axis. If the beam behaves elastically then the neutral axis is along the centre line of the specimen but in plastic bending the neutral axis moves closer to the inside surface of the bend as bending proceeds. Bending tests are characterised by a bending moment which is the force applied on the anvil by the distance of the anvils to the centre of the jig. Bending moment is related to the yield stress and in the case of a rectangular beam:

$$M = \frac{\sigma_y \, w^2 \, B}{6} \qquad \ldots\ldots \text{VIII.1}$$

where σ_y = yield stress of the material

w = width of the beam

B = thickness of the beam

Because there is a gradient of stress, from tension to compression, across the thickness, the complete cross section does not yield at this value of bending moment. On bending, the maximum of stress is on the outside surface

which has to crack first before the complete failure of the specimen.

In the present work the analysis of bending behaviour of nitrided sheets or tubes is complex due to the microstructure of the hard case formed by nitriding and also because it was not possible to nitride sheets on one side only.

VIII.2 Bending of sheet

Bending was not perfect beyond the failure stress of the outer tensile surface layer.

Four-point bend testing was found to be impractical for nitrided sheets, because failure of the specimens occurred between the inside and outside anvils, i.e. where the variation of the shearing force is a maximum. For three-point bending a maximum bending deflection of 30^{o} is imposed by the geometry of the test rig and the deflection is measured by the angle to which the specimen is bent.

(a) Influence of a thin nitrided layer on mechanical properties

Thick as-received specimens (1mm) were nitrided in pure ammonia in the range 550^{o}-800^{o}C for 24h and air-cooled;

Figure VIII.1 shows schematically the type of load-extension curves obtained for 550°, 600°, 700° and 800°C samples and values of the parameters measured are given in Table VIII.1. The steps on the curves of Figure VIII.1 correspond to the appearance of cracks on the tensile face of the specimens and they are accompanied, in the case of samples nitrided at 600°C, by a clearly audible sound as the cracks propagate through the case. The sound is less pronounced at 500°C and 700°C and is absent at 800°C. The load required to fracture the case, that is to form the first crack, appears to be independent of temperature and testing speed and only slightly dependent on the thickness of the nitrided layer in the range studied. The latter, expressed as a ratio of twice the case thickness to the total thickness of the sheet, was between the limits 0.17 and 0.46; see Table VIII.1. However the shapes of the curves prior to fracture of the nitrided case show significant differences for different materials. For samples nitrided at 600°C the load-extension curve is linear up to the load at which the first crack forms but at 550°, 700° and 800°C the curves deviate from linearity indicating that some plastic deformation occurs before failure. Linear behaviour of the first part of the curve is a consequence of the presence of massive γ'-Fe_4N. Samples nitrided at 800°C for 24h and cooled in pure ammonia from 800° to 500°, held in this gas at 500°C for 24h and then tested (Table VI.1 and Table VIII.1), show a linear elastic behaviour up to the formation of the first

Figure VIII.1

Load-extension curves from three-point bend tests of thick sheet specimens of AISI L316 nitrided in pure ammonia for 24h, air-cooled

at (a) 550°C

(b) 600°C

(c) 700°C

and (d) 800°C

load

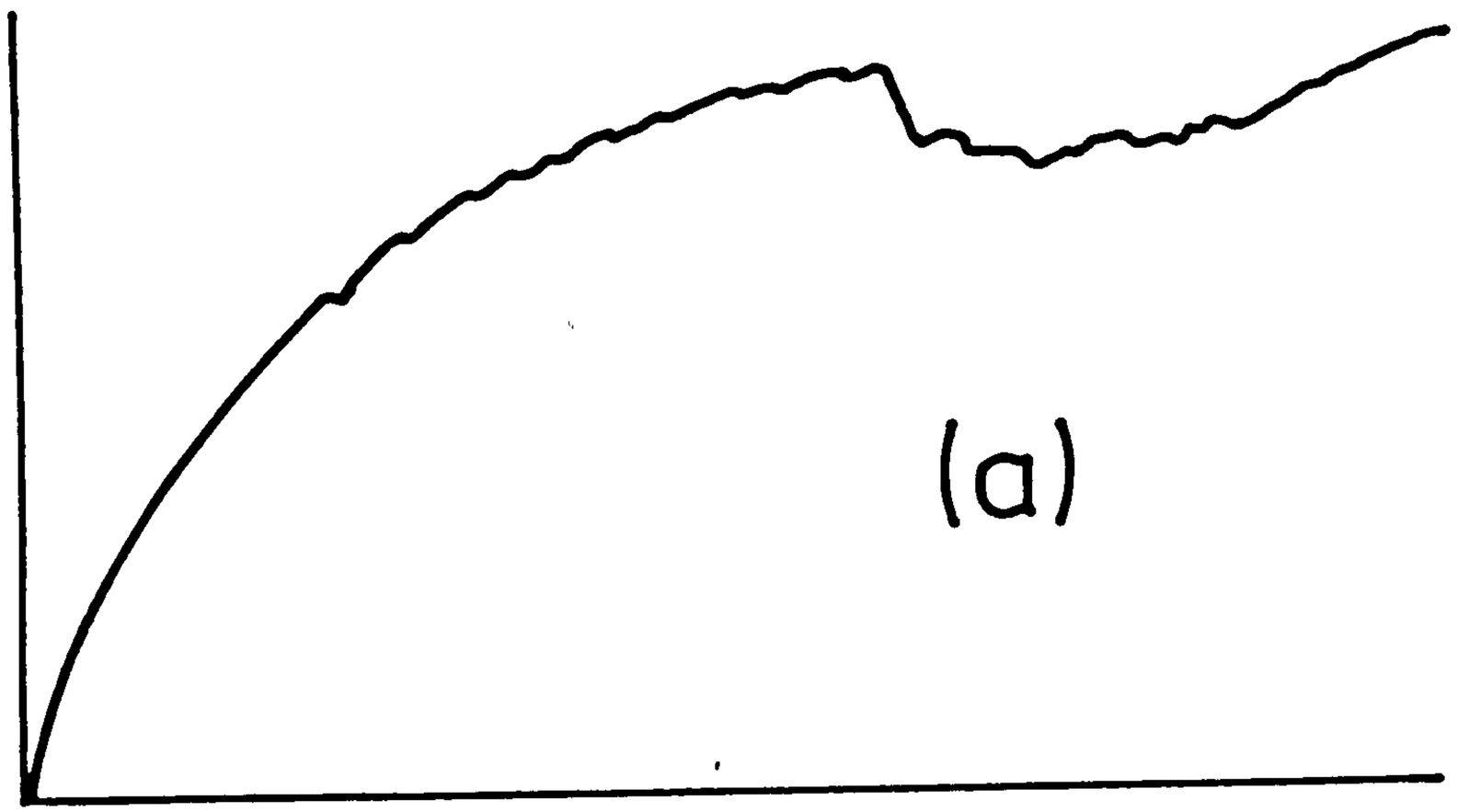

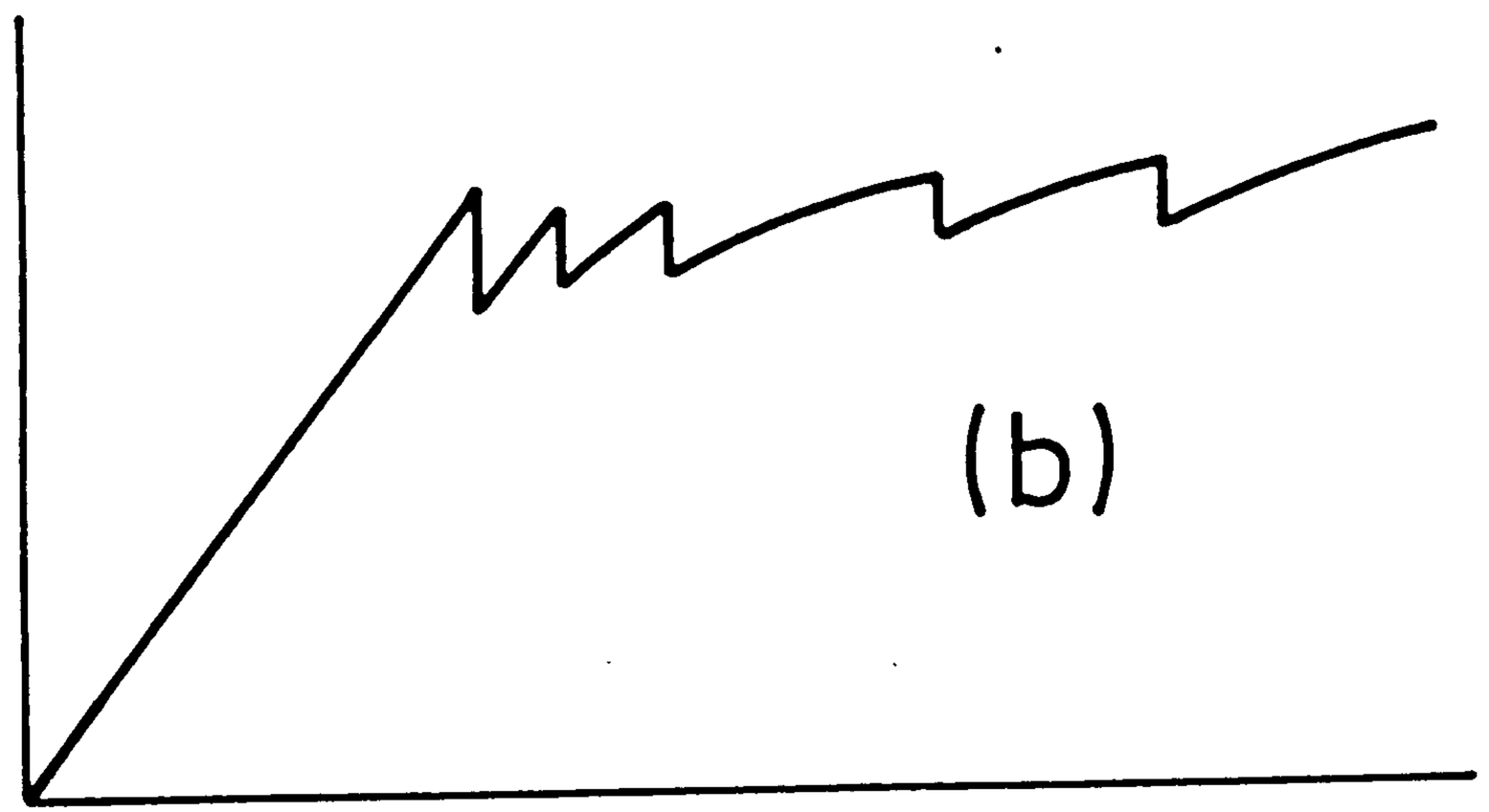

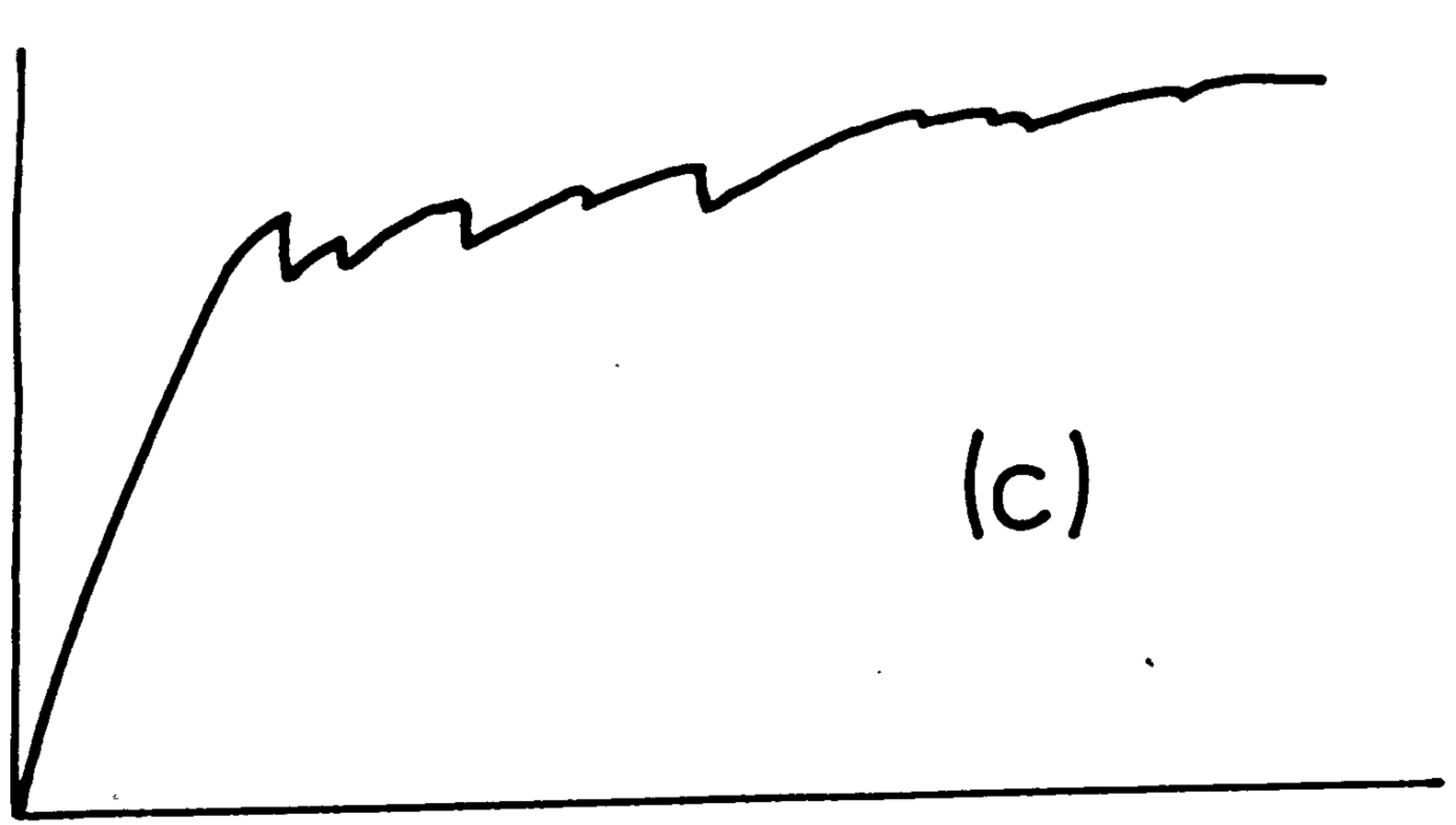

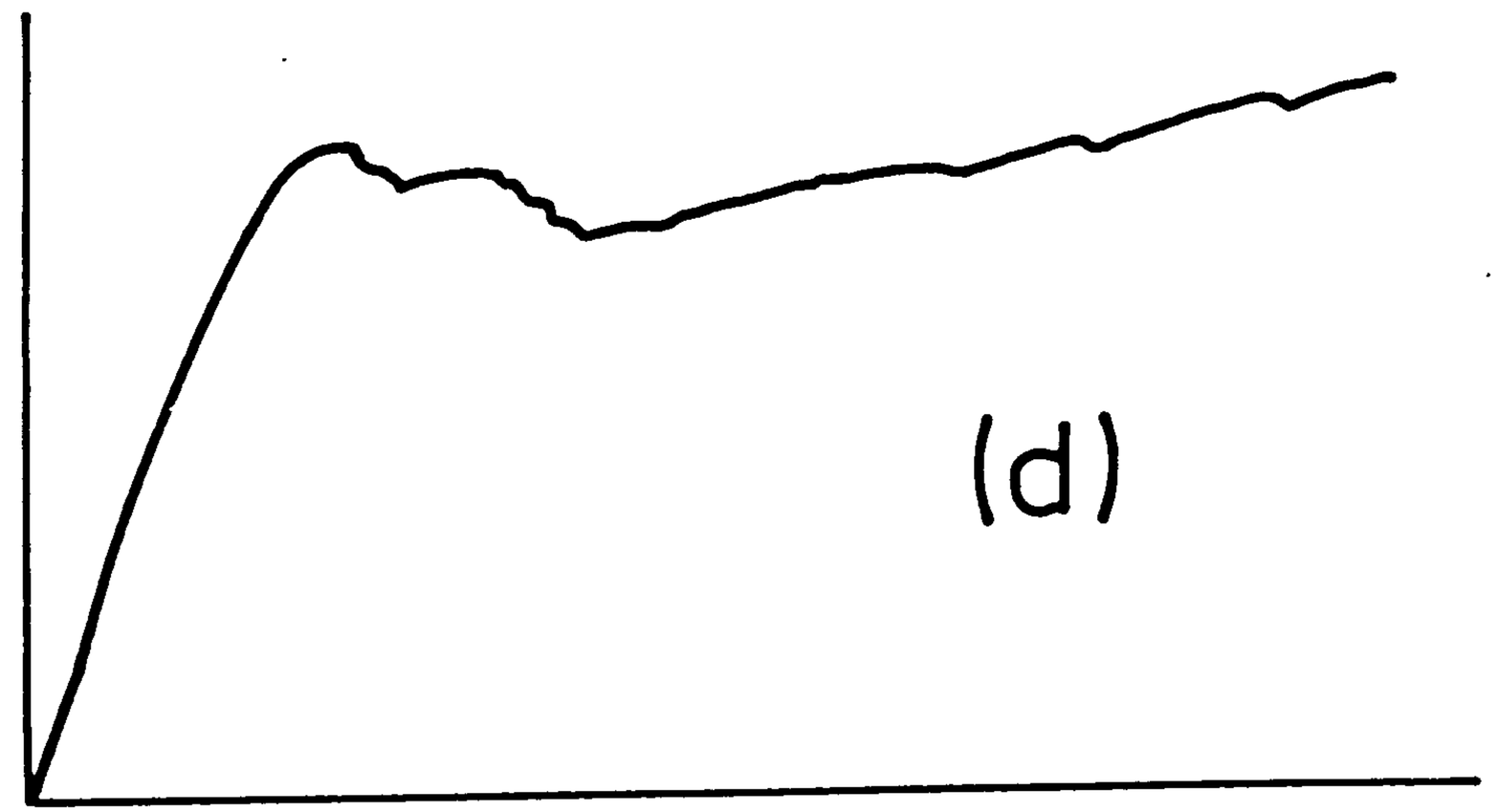

extension

Table VIII.1

Results of bending thick sheets of nitrided AISI L316 (0.02wt% C)

nitriding conditions			specimens	load to initiate first crack kg	VMN (50g) case	VMN (50g) core	2x thickness of case/ total thickness
550°C	24h	a.c.	as-received	25	750	160	0.28
600°C	6h	a.c.	as-received	30	700	160	0.17
"	24h	a.c.	as-received	29	700	160	0.30
"	24h	q.	as-received	29	700	160	0.30
"	24h	q.	20% cold-worked	47	720	240	0.29
"	24h	q.	63% cold-worked	70***	770	390	0.24
"	100h	a.c.	as-received	33	680	160	0.46
"	100h	q.	20% cold-worked	47	680	220	0.44
"	100h	q.	63% cold-worked	62*	680	370	0.38
650°C	24h	a.c.	as-received	29	530	160	0.23
700°C	24h	a.c.	as-received	30	510	150	0.24
"	24h	q.	as-received	30	510	150	0.24
"	100h	q.	as-received	30	480	150	0.36
800°C	24h	a.c.	as-received	32	460	150	0.28
"	24h	q.	as-received	39	460	150	0.28
"	24h	q.	20% cold-worked	46	460	220	0.29
"	24h	q.	63% cold-worked	62**	560	220	0.28
"	24h	s.c.(i)	as-received	30	460	150	0.28
"	24h	s.c.(ii)	as-received	34	460	150	0.28
"	24h	s.c.(iii)	as-received	33	460	150	0.28

Footnotes to Table VIII.1

a.c.	air-cooled
q.	quenched
*	broken before reaching a deflection of 30°
**	the curve shows a yield point at $\sigma_y = 4.7 kg\ mm^{-2}$
***	maximum stress $11.7 kg\ mm^{-2}$

s.c.(i) $800^{\circ} \xrightarrow[2h]{Ar} 500^{\circ} + 500^{\circ} - Ar - 24h$

s.c.(ii) $800^{\circ} \xrightarrow[2h]{NH_3} 500^{\circ} + 500^{\circ} - NH_3 - 24h$

s.c.(iii) $800^{\circ} \xrightarrow[2h]{NH_3} 500^{\circ} + 500^{=} - Ar - 24h$

crack while for specimens nitrided in the same conditions but quenched from 800°C plastic deformation occurs before cracking of the scale. In both cases the second part of the curve is identical to a specimen nitrided at 800°C and air-cooled (Figure VIII.1). In Figure VIII.2 and Table VIII.1 the influence of the presence and the thickness of a "white layer" is shown.

All specimens were nitrided at 800°C for 24h but the cooling rate and cooling atmosphere were varied. In the quenched specimen (a) no "white layer" nor γ'-Fe_4N is present. In (b) a very thin "white layer" is found (see Figure VI.8(ii)) and the first part of the curve is more uniform than in (a) but the load required for cracking is lower (see Table VIII.1). In (c) a very thick "white layer" is formed (Figire VI.8(v)0 and the sample behaves elastically up to the load required for crack formation but no steps are clearly visible on the second part of the curve. In (d) the "white layer" is thicker than in the case of (b) but the successive γ'-Fe_4N formed during cooling from 800°-500°C is partially reduced on holding at 500°C in argon (see Figure VI.8(iv)). The first part of the curve is therefore almost linear with small steps evident during the fracture of the nitrided layer.

From this study it appears that brittle behaviour is primarily due to the presence of massive γ'-$(Fe,Ni)_4N$, but not exclusively so from the evidence of the bend curve

Figure VIII.2

Load-extension curves from three-point bend tests of thick sheet specimens of AISI L316 nitrided in pure ammonia at 800°C for 24h and cooled as indicated

(a) quenched

(b) $800^{\circ} \xrightarrow[2h]{Ar} 500^{\circ} + 500^{\circ} - Ar - 24h$ (s.c.(i))

(c) $800^{\circ} \xrightarrow[2h]{NH_3} 500^{\circ} + 500^{\circ} - NH_3 - 24h$ (s.c.(ii))

and (d) $800^{\circ} \xrightarrow[2h]{NH_3} 500^{\circ} + 500^{\circ} - Ar - 24h$ (s.c.(iii))

load

(a)

(b)

(c)

(d)

extension

of a specimen nitrided at 550°C (Figure VIII.1(a)). This sample has a thick layer of γ' similar to that formed at 600°C (Figure V.3) but during bending this "white layer" spalls off leaving the underlying diffusion zone to deform plastically. This does not occur at 600°C where there is a less well-defined interface between the "white layer" and "dark-etched" layer (Figure V.4). If there is a well-defined interface between the different subscales then there is a sharp change of stress at this interface (see Figure II.15) and the two layers are expected to shear along the interface as is the case for samples nitrided at 550°C. If layer separation occurs before transverse crack initiation then there is brittle behaviour and only plastic deformation of the diffusion layer.

Brittle behaviour depends on the microstructure of the case and also of the core as shown by bending 63% cold-worked specimens. Specimens cold-deformed by 63% and nitrided at 800°C for 24h in pure ammonia and quenched from the reaction temperature have the same load-extension curve (Figure VIII.3(b)) as those already reported for annealed specimens nitrided at 600°C and shown in Figure VIII.1(b)). For samples nitrided at 600°C, as the microhardness of the core increases (for example for non-recrystallised samples), the load required to initiate the first crack by brittle fracture also increases. Moreover, the load continues to increase until a maximum stress is reached which depends on

Figure VIII.3

Load-extension curves from three-point bend tests of thick sheet of 6% cold-worked specimens of AISI L316 nitrided in pure ammonia for 24h and quenched from

(a) 600°C

and (b) 800°C

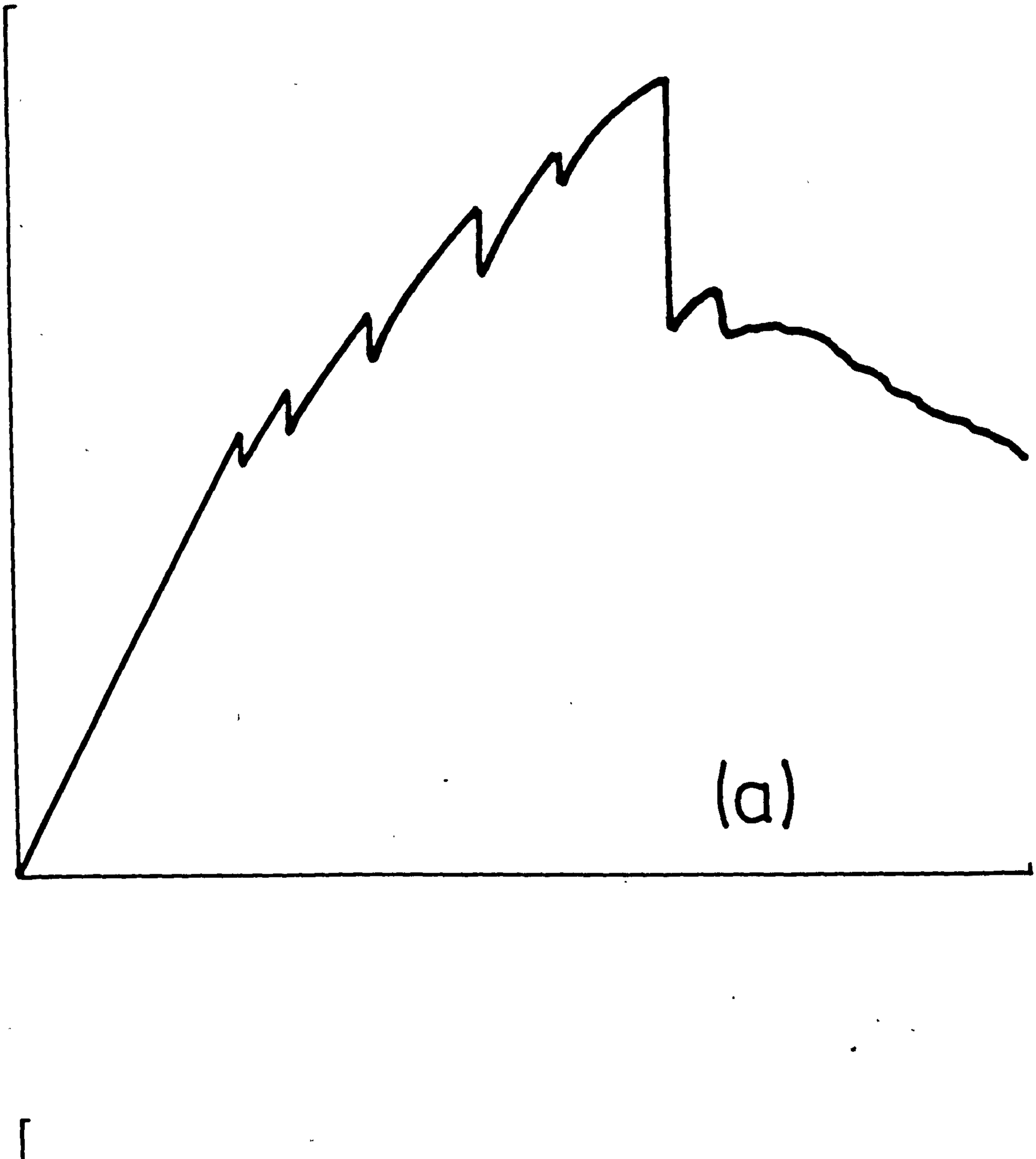
load
(a)
(b)
extension

the ratio of nitrided case to total thickness. This behaviour is shown in Figure VIII.3(a) by the load-extension curve of a 63% cold-worked specimen nitrided at 600°C for 24h. The influence of the core is also shown by the complete failure of the specimen at a deflection of less than 30° for a sample of 63% cold-worked material nitrided at 600°C for 100h; a similar sample nitrided at 800°C for the same time does not break. At 800°C recrystallisation takes place in less than 2h to produce a soft core while at 600°C recovery behaviour is very slow and the core retains a high hardness (370 VMN; see Table VIII.1) and a high work-hardening capacity.

Metallographic examination shows that all of the initial brittle cracks in the nitrided surface layer are blunted and terminate at the case-core interface (Figure VIII.4(b)) in the deformed zone described in Chapters V and VI. Impact tests carried out on specimens nitrided at 600°C for 6 hours show only a small amount of ductile tearing at the principal crack (Figure VIII.4(a)), and a well-defined plastic zone containing a high density of deformation twins can be seen around the principal crack. Evidence that the core has undergone plastic deformation during three-point bending is shown by the crack opening in the inner (compression) nitrided case of specimens nitrided at 600°C for at least 24h (Figure VIII.4(c)). The cracks open at the interface zone between case and core formed by twins and

Figure VIII.4

Micrographs of tested specimens.

(a) Optical micrograph of an impact bend specimen of AISI L316 nitrided for 6h at 600°C in pure ammonia (acid picral etch)

(b) Optical micrograph of a three-point bend specimen of AISI L316 nitrided for 99h at 600°C in pure ammonia

(c) SEM micrograph showing cracks in the nitrided case on the compressive surface of a specimen as in (b), nitrided for 24h at 600°C

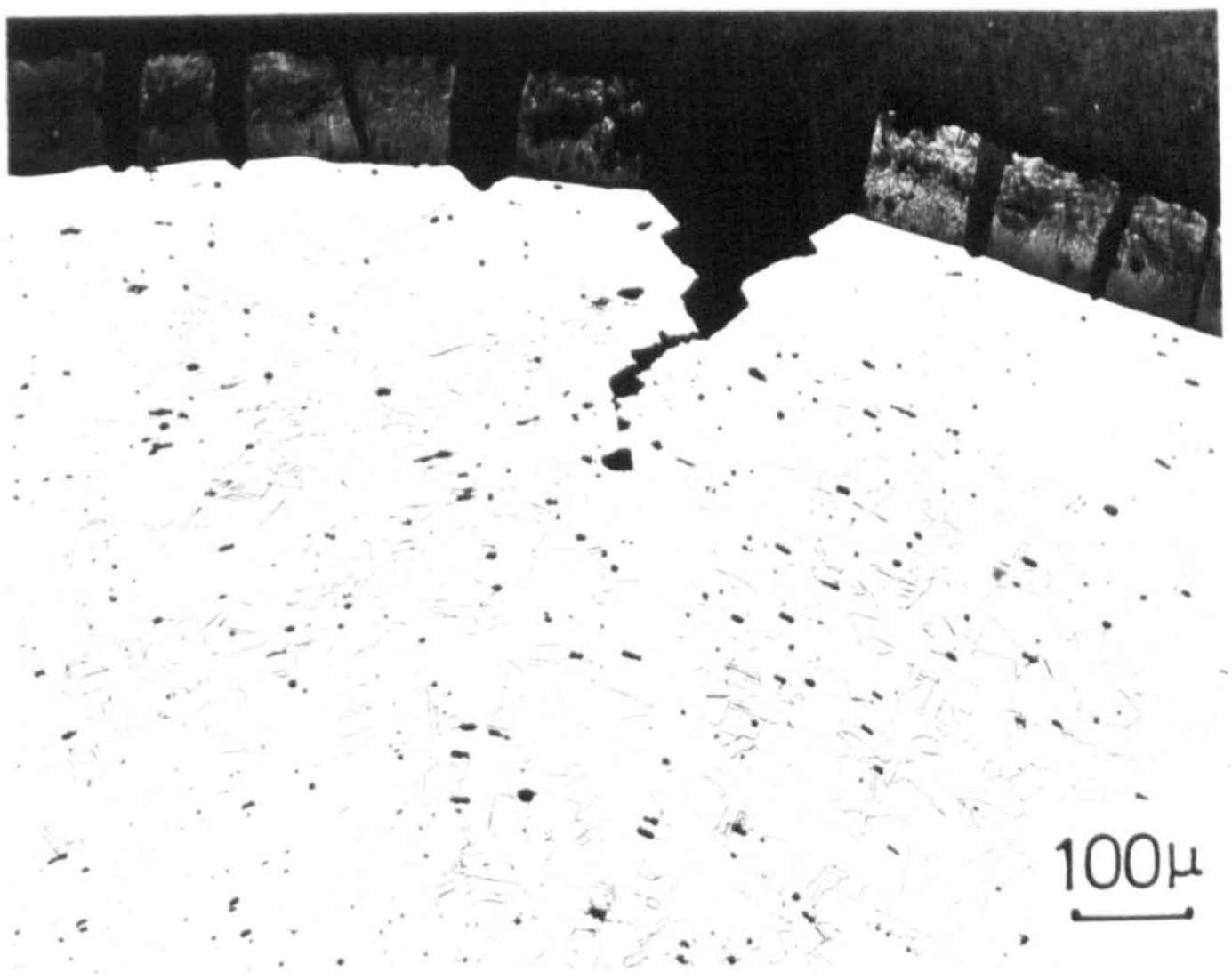

(a)

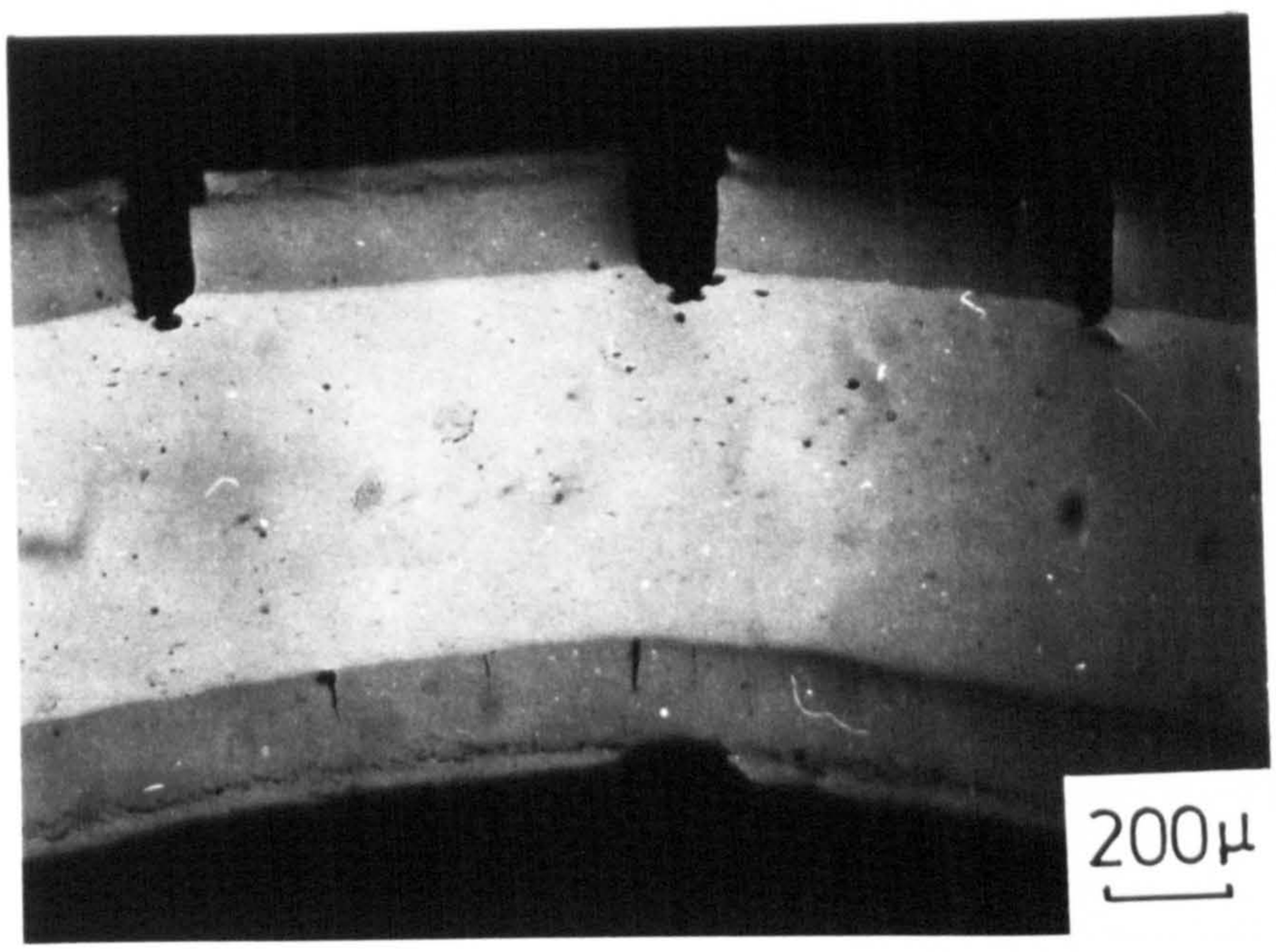

(b)

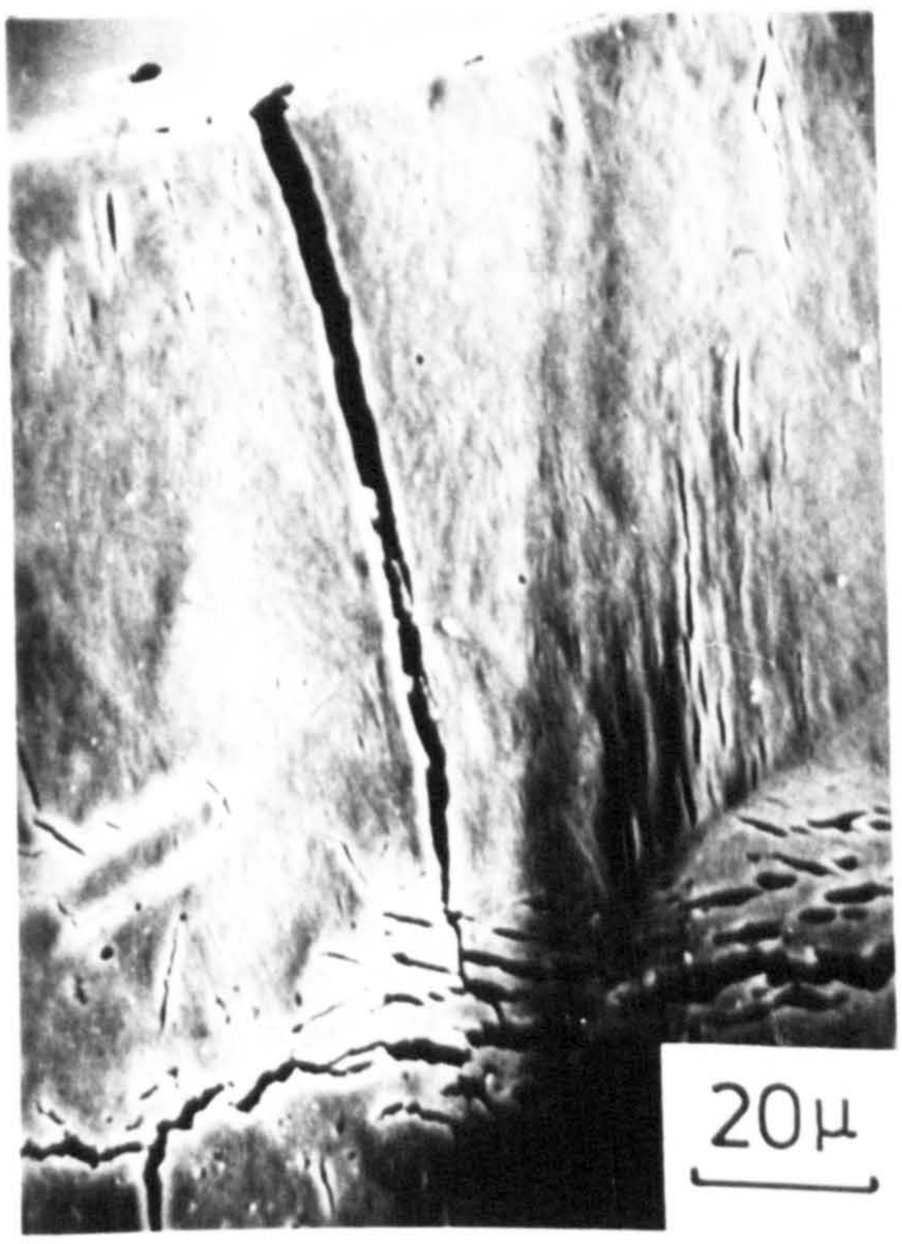

(c)

dislocations and stop close to the $\gamma' + \varepsilon$ outer layer. These cracks can appear only if the neutral axis of the bent sample has moved towards the centre of the bend radius and which occurs only when plastic yielding of the core takes place. For short nitriding times (6h) no inside cracks are visible which would indicate that the neutral axis has not moved so far as to be in the inner nitrided case.

(b) Influence of the thickness of the nitrided layer on fracture behaviour

Thin sheets of AISI 316 (0.38mm) containing 0.07wt% C nitrided, as-received or after heat-treatment at 600°, 700° and 800°C for different lengths of time, and either air-cooled or quenched, were tested on a three-point bend jig. The load at which the first crack is initiated is independent of the nitriding temperature or cooling rate (see Table VIII.2). The bending load-extension curves for several temperatures of nitriding are basically identical to those already described for the corresponding specimens containing 0.02wt% C, that is, the same type of behaviour up to crack initiation and the same type of steps when cracks occur. However, the final part of the curves up to fracture is different and is shown in Figure VIII.5 for samples nitrided at 600°C. Figure VIII.5(a) represents the curve for nitrided fractions less than 0.75 where the un-nitrided core does not fracture although several cracks occur in the

Table VIII.2

Results of bending thin sheets of nitrided AISI 316 (0.07wt% C)

nitriding conditions			specimens	load to initiate first crack kg	VMN (50g) case	VMN (50g) core	2x thickness of case (total thickness)	failure
600°C	2h	a.c.	as-received	11	720	180	0.27	N
	6h	a.c.	as-received	15	700	180	0.41	N
	16h	a.c.	as-received	14	700	180	0.57	N
	24h	a.c.	as-received	15	700	180	0.63	N
	24h	q.	as-received	15	700	180	0.63	N
	29h	a.c.	as-received	14	700	180	0.68	N
	32h	a.c.	as-received	13	700	180	0.71	N
	39h	a.c.	as-received	13	700	180	0.75	Y
	48h	a.c.	as-received	13	700	180	0.78	Y
	74h	a.c.	as-received	12	700	200	0.86	Y
	2h	a.c.	H.T.600°C-48h	11	700	180	0.26	N
	2h	a.c.	H.T.800°C-48h	10	700	180	0.26	N
	6h	a.c.	H.T.600°C-48h	15	700	180	0.40	N
	6h	a.c.	H.T.800°C-48h	14	700	180	0.41	N
	16h	a.c.	H.T.600°C-48h	15	700	180	0.57	N
	16h	a.c.	H.T.800°C-48h	13	700	180	0.54	N
	24h	a.c.	H.T.600°C-48h	13	700	180	0.65	N
	24h	a.c.	H.T.800°C-48h	19	700	180	0.63	N
	36h	a.c.	H.T.800°C-48h	19	700	180	0.70	N
	48h	a.c.	H.T.600°C-48h	14	700	180	0.76	N
	48h	a.c.	H.T.800°C-48h	15	700	180	0.72	N
	68h	a.c.	H.T.600°C-48h	15	700	190	0.85	Y
	68h	a.c.	H.T.800°C-48h	18	700	190	0.81	Y
700°C	24h	a.c.	as-received	14	510	190	0.51	N
	24h	q.	as-received	15	510	190	0.51	N

contd.

Table VIII.2 (continued)

800°C	2h	a.c.	as-received	14	450	180	0.30	N
	6h	a.c.	as-received	17	450	180	0.42	N
	16h	a.c.	as-received	17	450	210	0.60	N
	24h	a.c.	as-received	14	450	250	0.65	Y
	24h	q.	as-received	14	450	250	0.65	Y
	30h	q.	as-received	14	450	280	0.72	Y
	38h	a.c.	as-received	13	450	310	0.85	Y
	48h	q.	as-received	14	450	340	0.94	Y
	56h	a.c.	as-received	14	450	370	0.98	Y
	65h30'	a.c.	as-received	14	450	-	1	Y
	86h	q.	as-received	12	450	-	1	Y
	2h	q.	H.T.600°C-48h	12	450	180	0.28	N
	2h	q.	H.T.800°C-48h	11	450	180	0.28	N
	6h	q.	H.T.600°C-48h	15	450	180	0.42	N
	6h	q.	H.T.800°C-48h	13	450	180	0.42	N
	16h	q.	H.T.600°C-48h	14	450	210	0.54	N
	16h	q.	H.T.800°C-48h	14	450	210	0.54	N
	24h	q.	H.T.600°C-48h	14	450	250	0.62	Y
	24h	q.	H.T.800°C-48h	14	450	250	0.65	Y
	30h	q.	H.T.600°C-48h	11	450	280	0.68	Y
	30h	q.	H.T.800°C-48h	12	450	280	0.70	Y
	36h	q.	H.T.600°C-48h	10	450	310	0.78	Y
	36h	q.	H.T.800°C-48h	11	450	310	0.80	Y
	48h	q.	H.T.600°C-48h	12	450	330	0.85	Y
	48h	q.	H.T.800°C-48h	11	450	340	0.89	Y

a.c. : air cooled
q. : quenched
H.T. : heat treated

N : no
Y : yes

Figure VIII.5

Load extension curves from three-point bend tests of thin sheet specimens of AISI 316 nitrided in pure ammonia at 600°C for a ratio (2x case depth/total thickness of the sheet

of (a) less than 0.75

and (b) exceeding 0.75

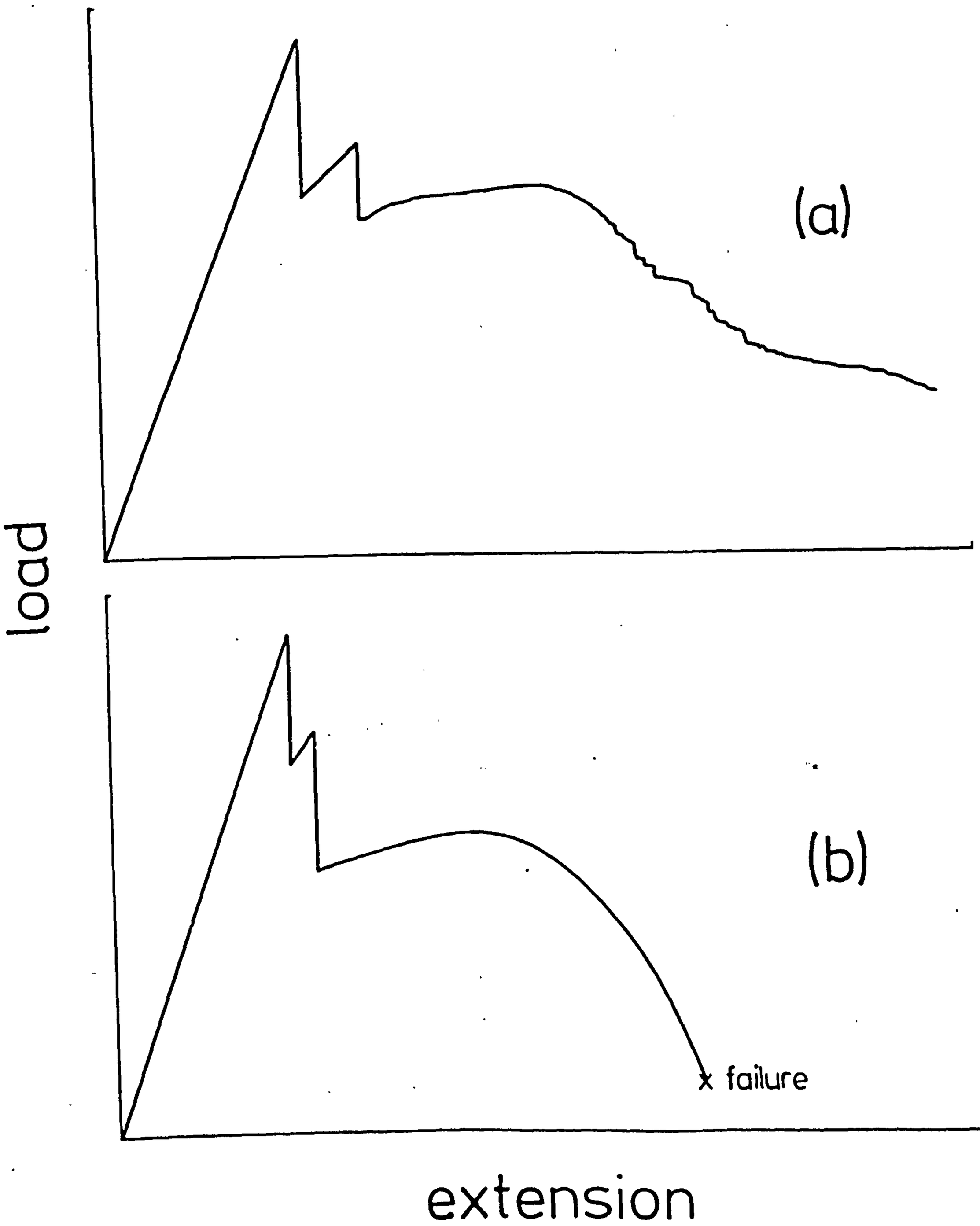
(a)
(b)
failure
load
extension

nitrided layer. However, when the nitrided fraction exceeds 0.75, failure of the core always occurs (Figure VIII.5(b)) and the total extension required is a function of nitrided layer thickness. For nitriding times longer than 74 h (ratio $>$ 0.85) the specimen breaks after the appearance of the first crack. The critical ratio at 800°C is 0.65 compared with 0.75 at 600°C (Table VIII.2) which is explained by a high microhardness in the core of samples nitrided at 800°C due to diffusion of carbon ahead of the nitrided layer (see Chapter V). Carbon precipitates as $Cr_{23}C_6$ in grain boundaries resulting in brittle failure in the core. Despite the fact that specimens nitrided at 800°C fail for a nitrided fraction lower than at 600°C due to carbide precipitates, prior heat-treatment at 600°C or 800°C for 48 hours carried out to enhance carbide precipitation, has no appreciable effect on the bending behaviour (Table VIII.2). Figure VIII.6 shows that samples either as-received or heat-treated at 800°C for 48h fail in a ductile manner, (a), while the core of as-received (b) or heat treated (c) samples nitrided at 800°C for 30h show brittle behaviour (the three specimens were broken in liquid nitrogen to avoid the influence of compressive or tensile stresses). Thus, only massive precipitation of carbide in the core of samples nitrided at 800°C can explain the difference in failure behaviour between 600°C and 800°C.

Cooling rate also has an effect on the bend curves of

Figure VIII.6

SEM micrographs of AISI 316 specimens broken in liquid nitrogen

(a) sample heat-treated at 800°C for 48h

(b) core of a sample nitrided at 800°C for 30h in pure ammonia

and (c) core of a sample heat-treated at 800°C for 48h then nitrided at 800°C for 30h in pure ammonia

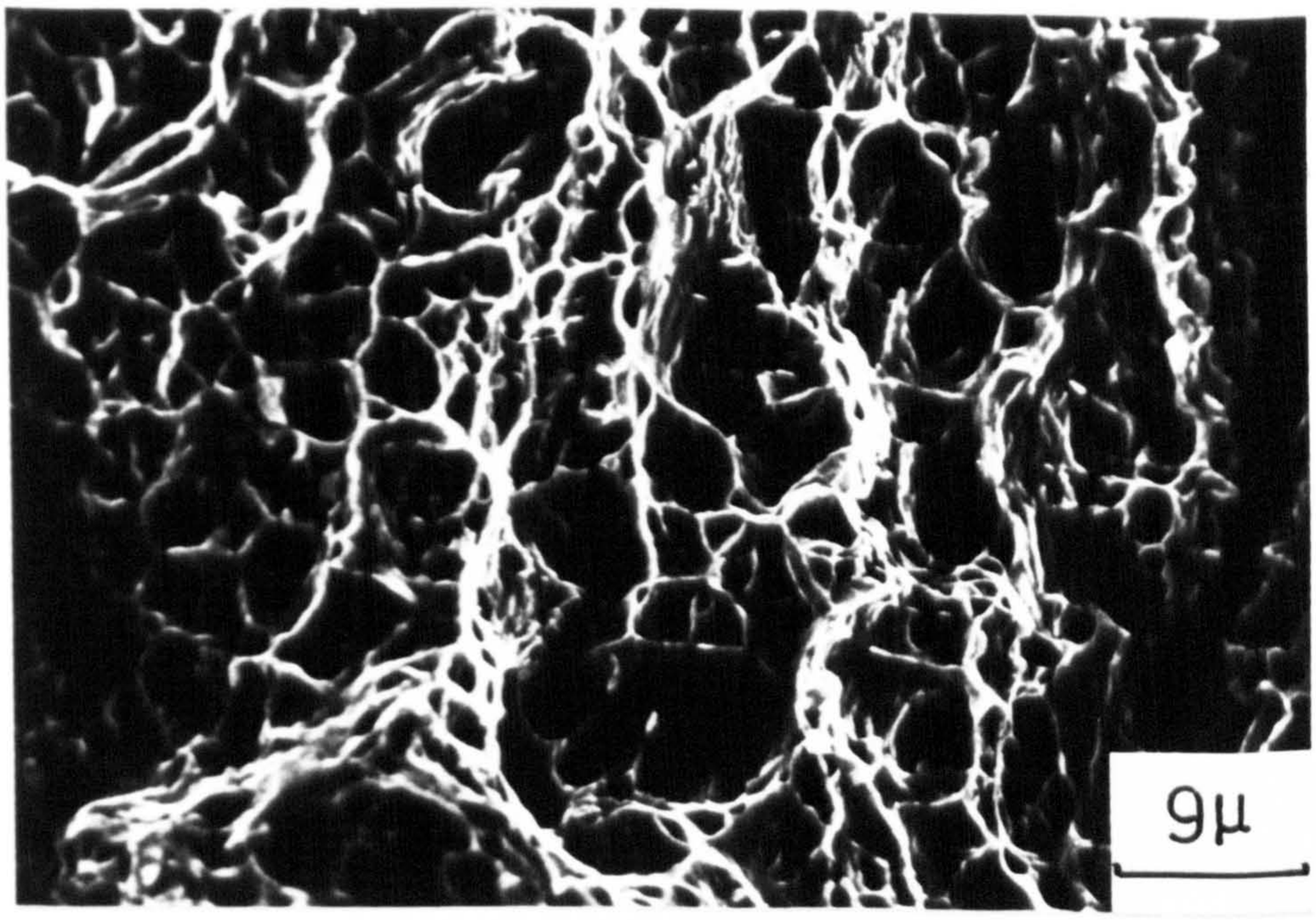

(a)

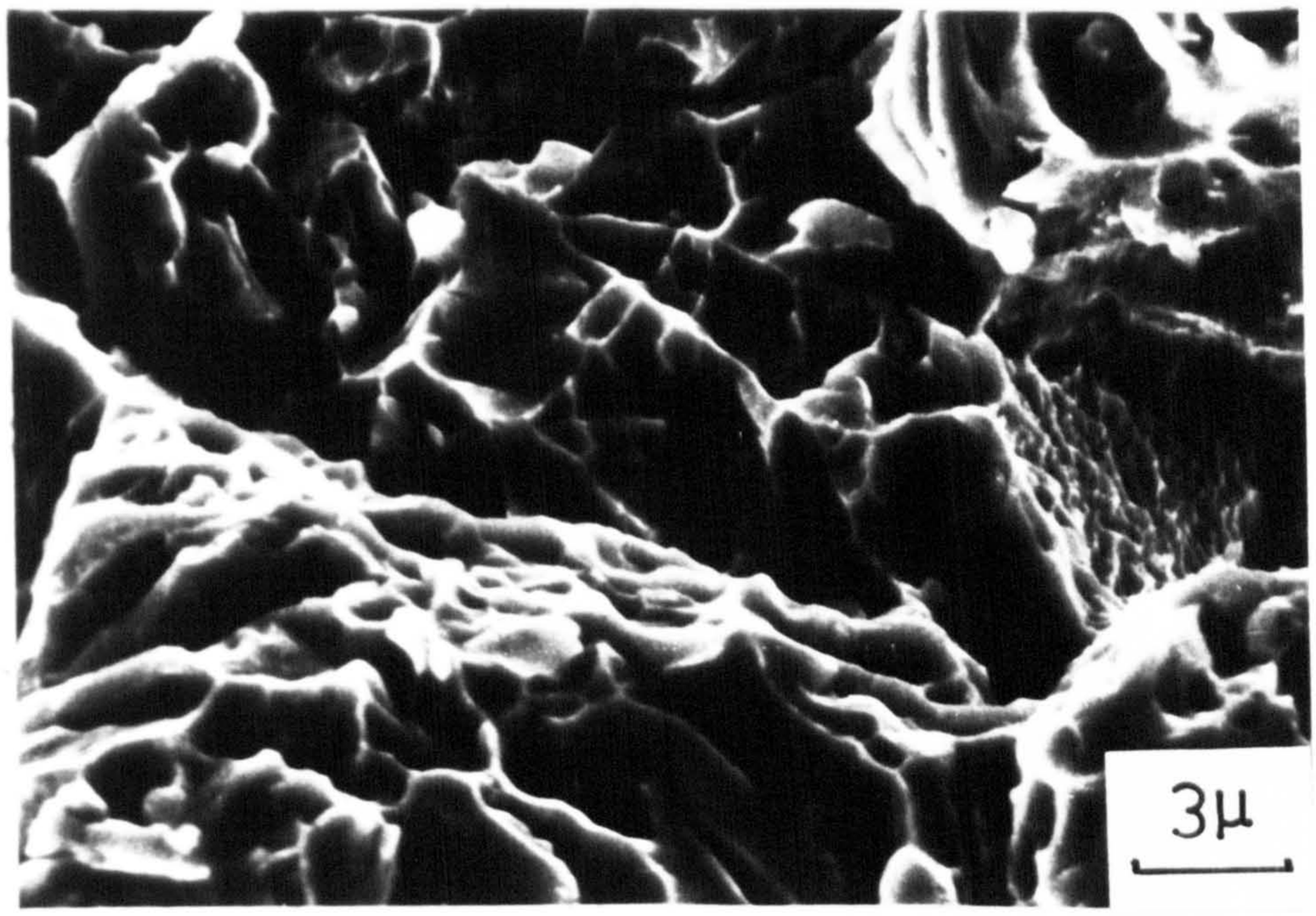

(b)

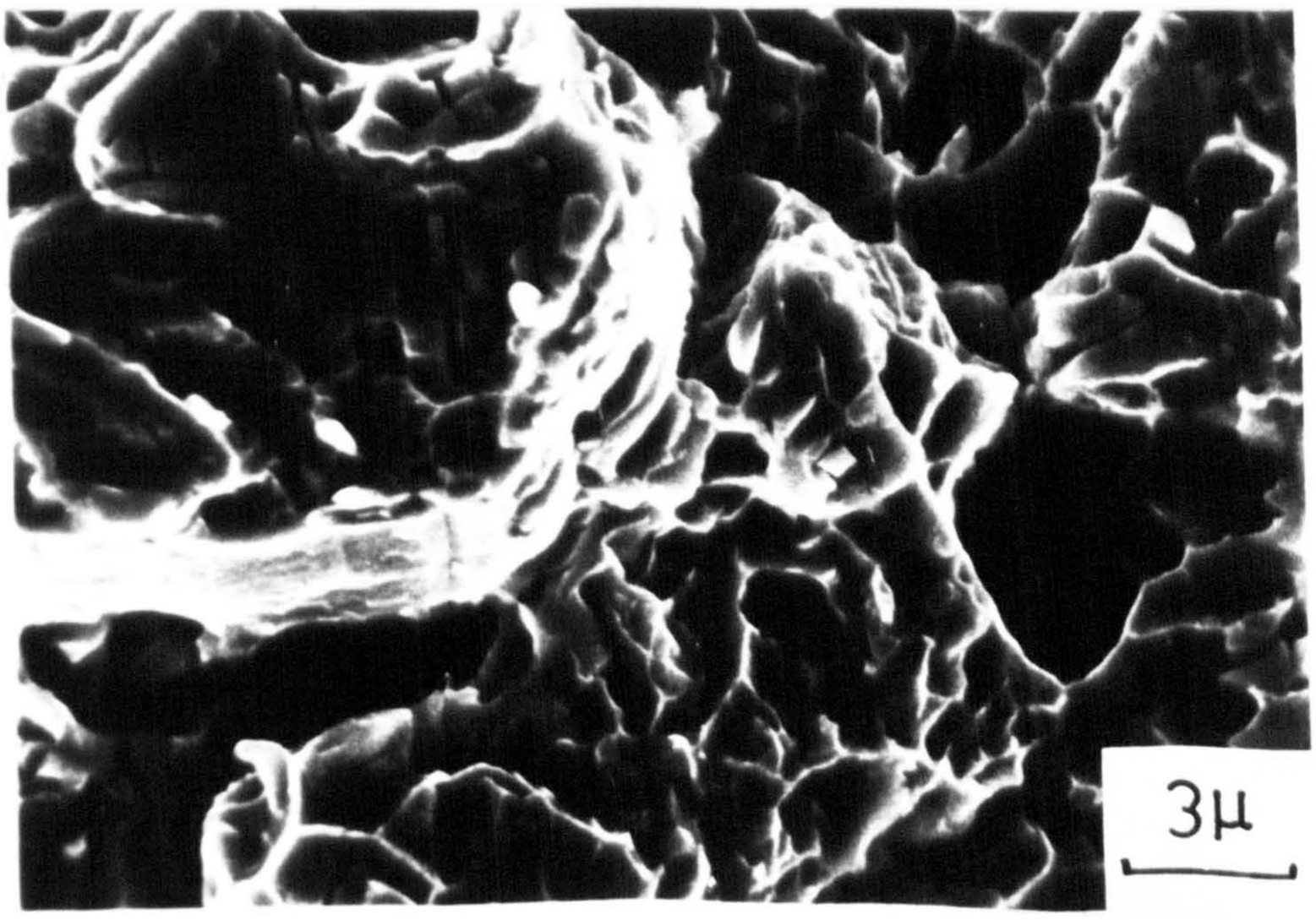

(c)

Figure VIII.7

Load-extension curves from three-point bend tests of thin sheet specimens of AISI 316 nitrided in pure ammonia at 800°C for 24h and

(a) air-cooled

and (b) quenched

x—denotes failure

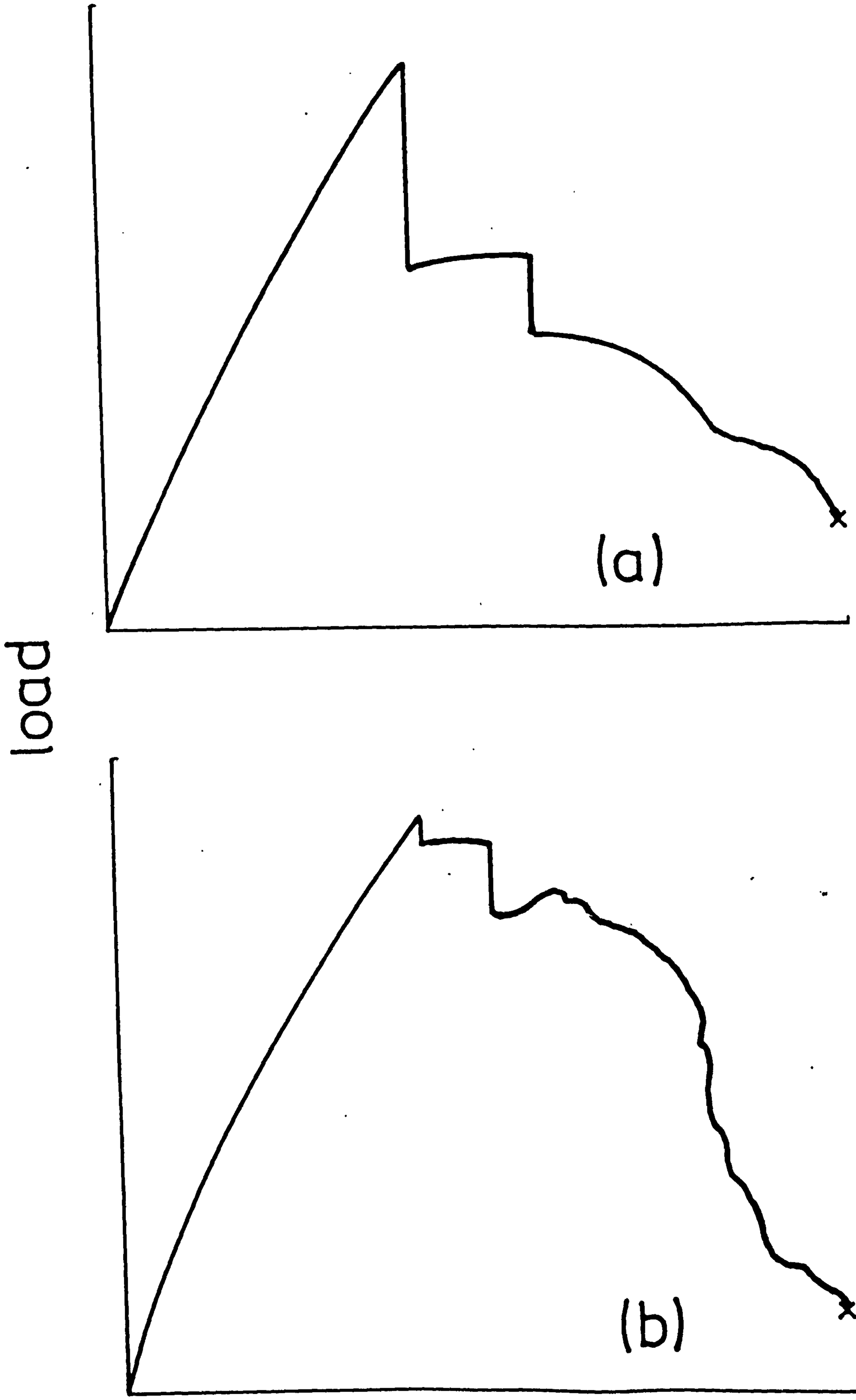

Figure VIII.8

SEM micrographs of fracture from three-point bend tests of thin sheet specimens of AISI 316 nitrided in pure ammonia

(a) 600°C for 36h

(b) "white layer" of (a)

(c) γ + CrN subscale on tension face of sample (a)

(d) 800°C for 24h

(e) "white layer" of (d)

(f) γ + CrN subscale on tension face of sample (d)

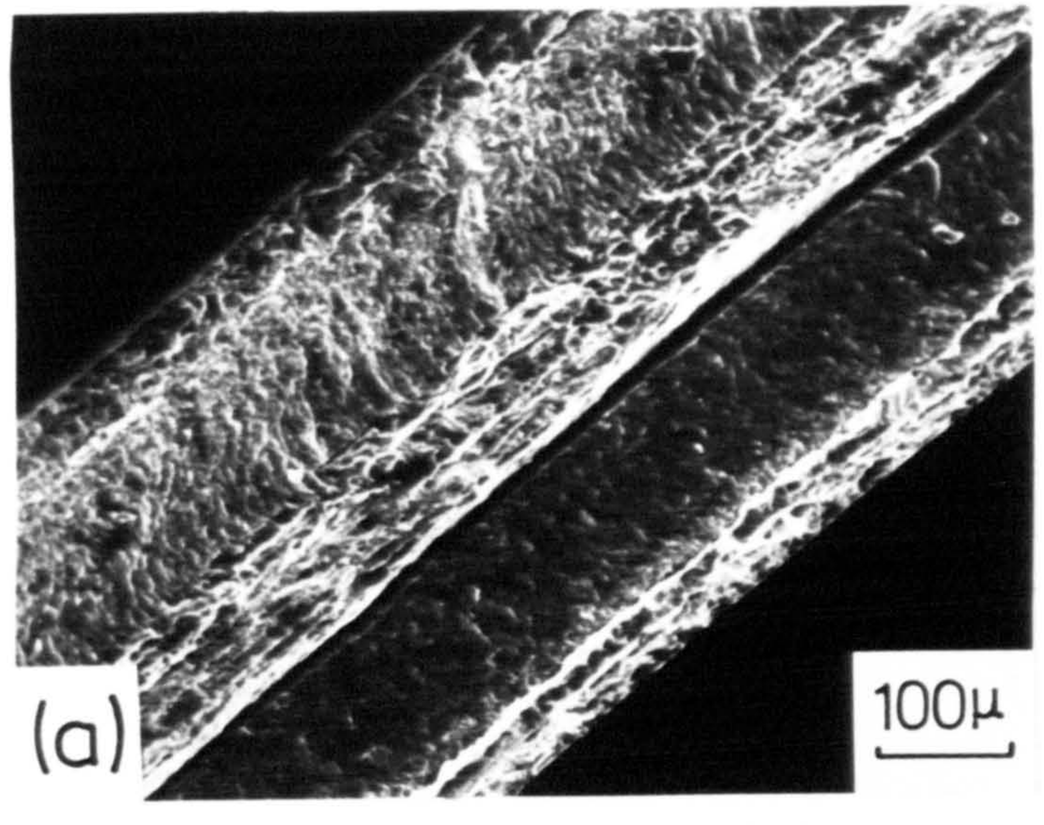
(a)
100μ

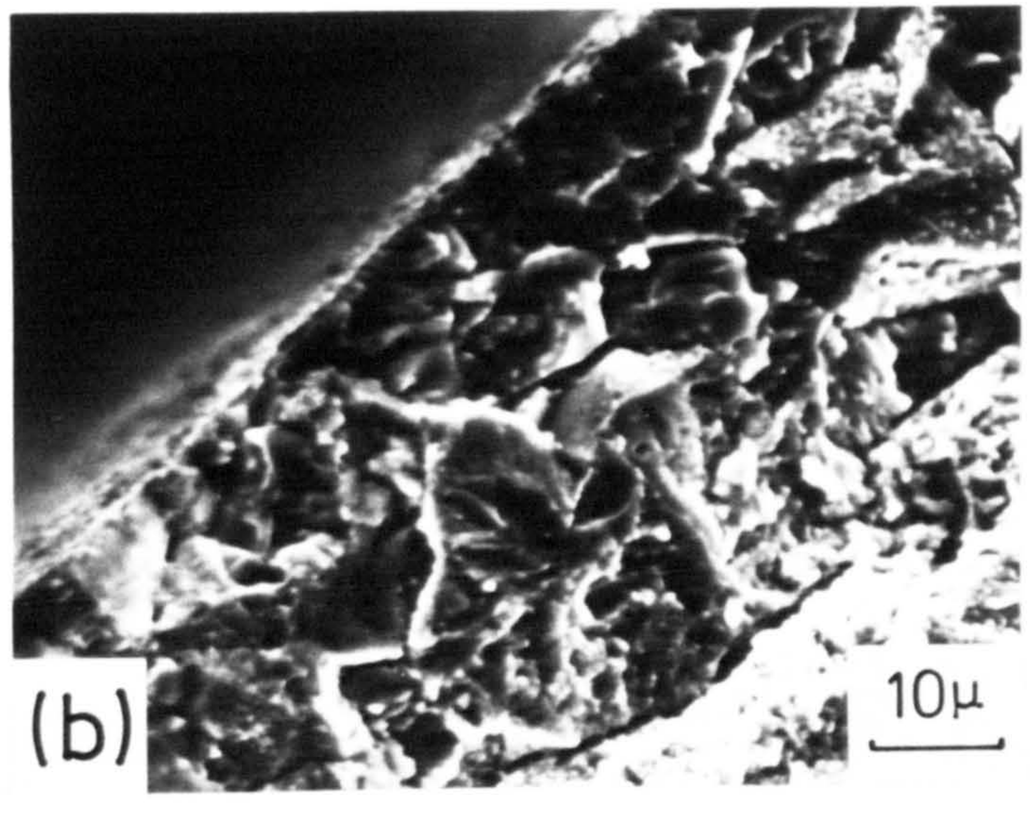
(b)
10μ

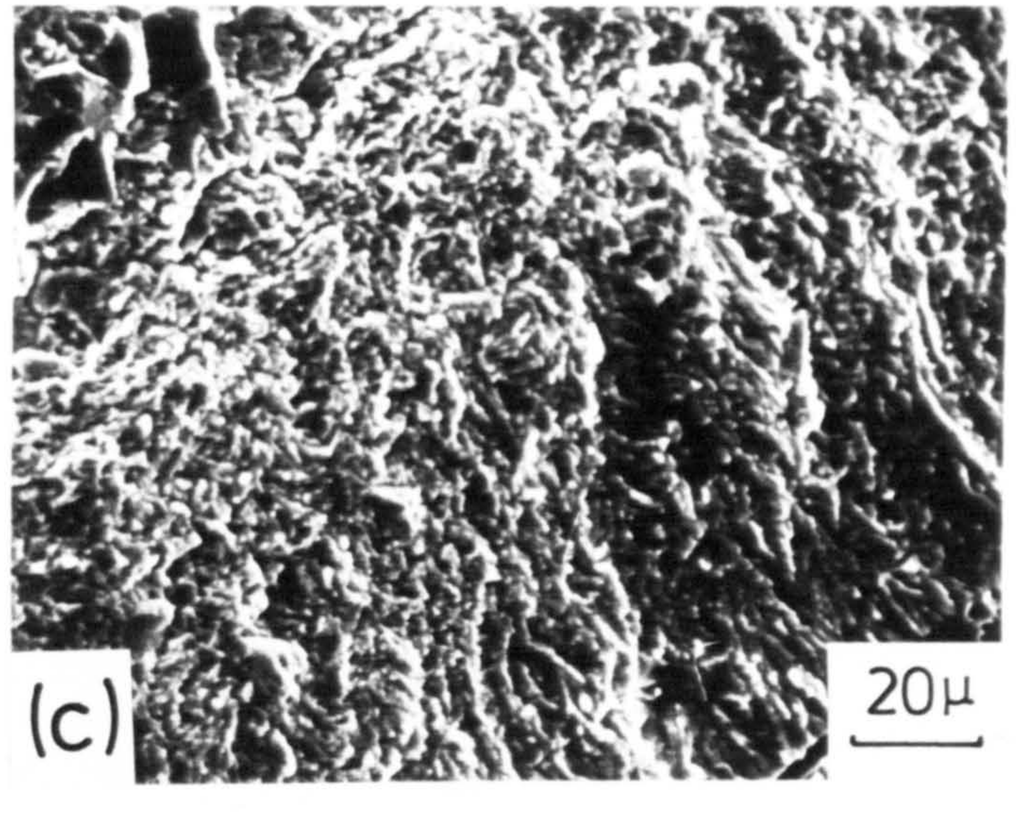
(c)
20μ

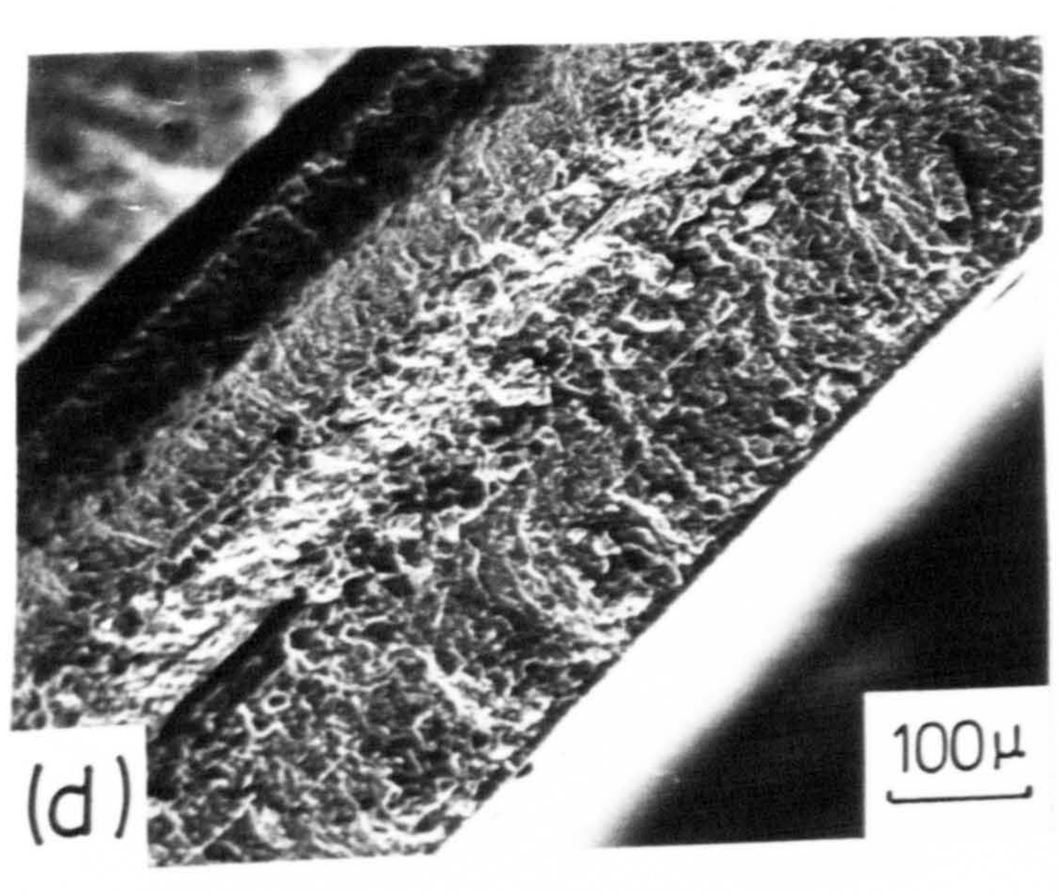
(d)
100μ

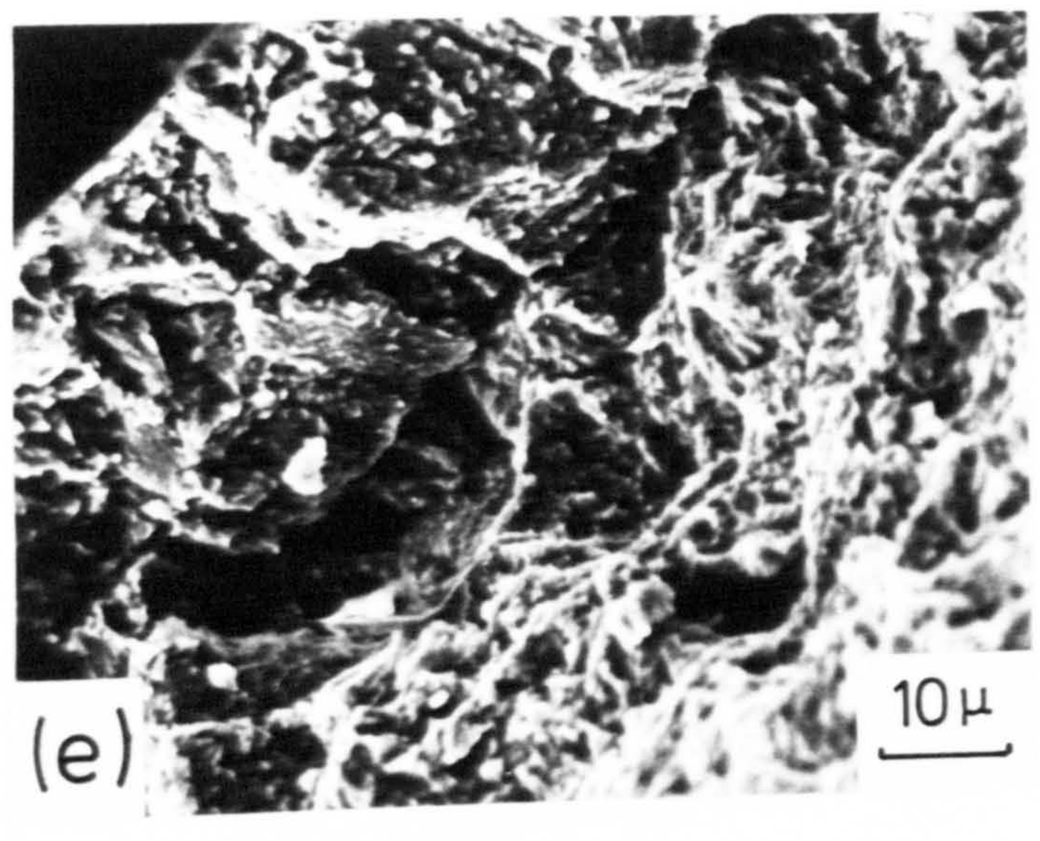
(e)
10μ

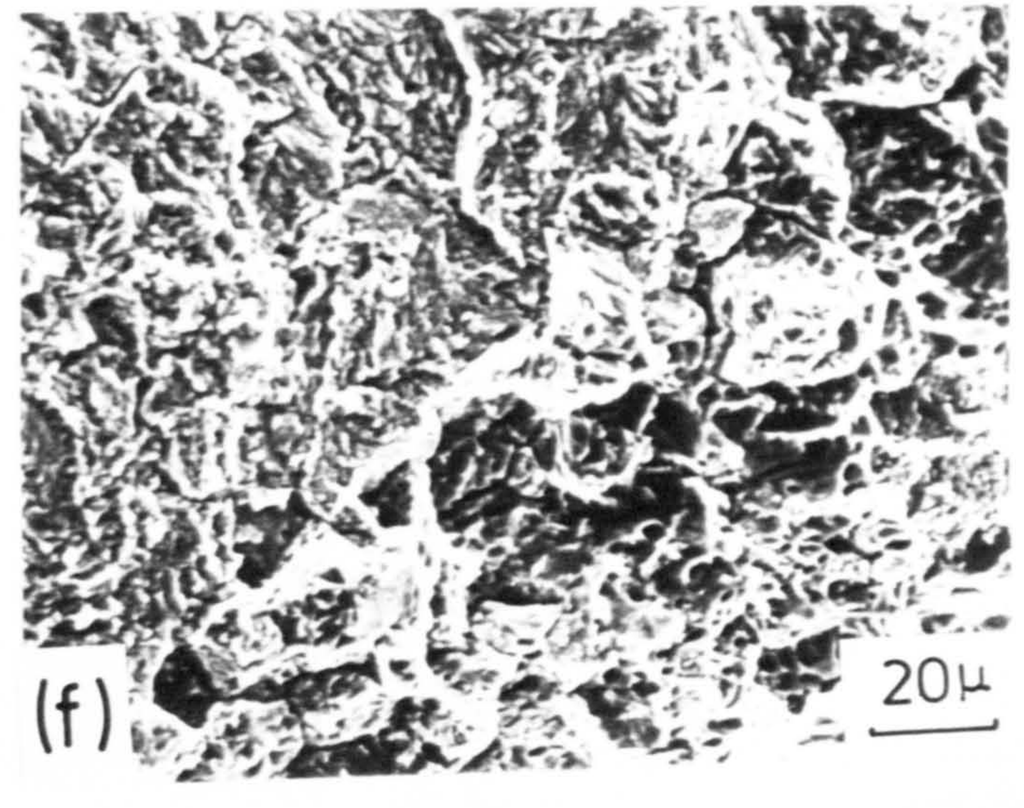
(f)
20μ

is 29.7kg for 1mm thick 11mm wide specimens and the stress on the tensile face can be calculated from equation VIII.1. There is therefore a stress of $771\ MN.m^{-2}$ on the outer surface of the nitrided case. If an upper estimate for general yield (Knott, 1973) is applied to the un-nitrided core,

$$M = \frac{0.69\ \sigma_y\ w^2\ B}{2} \qquad \ldots\ \text{VIII.2}$$

and a critical value of w may be calculated for which the core will behave elastically. For the values given above, and taking the yield stress of annealed AISI 316 to be $\sigma_y = 290\ MNm^{-2}$ (as determined by tensile testing and in agreement with Peckner & Bernstein (1977)), a minimum value of thickness $w = 1.13mm$ is determined. Since this value is greater than the specimen thickness, it is obvious that when the first crack propagates the core has already undergone plastic deformation. A similar calculation gives $w = 0.33mm$ for thin specimens (0.38mm) which means that 2h nitriding are required.

However the interpretation of the bending results is complex due to the fact that no mechanical properties for the different structures of the nitrided case are known, and it is also not possible to test samples nitrided on one side only (see Chapter II). The inner case is very hard and imposes on the sample an additional stiffness which depends

on the ability of the nitrided layer to deform plastically (a function of the microhardness and structure) and on the bonding between the different subscales. In the case of a thick ductile core, brittle behaviour is observed only when the case is hard and composed of a white layer coherent with the inner subscale. When a thin nitrided layer is formed (for thick samples) the degree of cold work in the core has a pronounced effect on bending fracture. For 63% cold-worked and nitrided samples recrystallisation occurs rapidly at 800°C but no grain growth is observed (Figure V.19) and a hard core with a thin non-recrystallised nitrided surface layer leads to brittle behaviour which is not observed for as-received and nitrided specimens. At 600°C, when the cold-worked structure is maintained, the load continues to increase after the first crack has formed reflecting the toughness of the laminated microstructure in these specimens and nitriding for 100h is required to produce complete failure.

Failure in a single bend requires a minimum case depth but is mainly dependent on the core structure. The crack must propagate through the tough interface between the nitrided layer and core, and then through the core which is easier when the core is less ducti le.

Brittle behaviour occurs when a hard, coherent, nitrided multi-layer case is formed but complete failure with minimum layer thickness also requires a hard core.

VIII.3 Bending of nitrided tubes

Tubes nitrided on one or both sides have been tested by three and four-point bend and brittle behaviour is mainly determined by the nature of the filling material. "Steatite" and "Hilbx" pellets (ceramic material) and mild steel were used as fillers.

Figure VIII.9 shows the load-extension curves obtained during three-point bend tests of AISI 316 can tubing (30mm length x 0.38mm wall thickness; 20% cold-worked) nitrided on both the inside and outside surfaces for 24h at 600°C. A load of 70kg is required to initiate the first crack in a hollow tube (Figure VIII.9(a)) but considerable deflection is required to cause failure. It should be noted however that in three-point bending of hollow tubes the central anvil penetrates and deforms the tube. Figure VIII.9(b) represents the results from a nitrided tube filled with a single tight fitting solid "Steatite" pellet 25mm in length in which the maximum load recorded before the formation of the first crack is 100kg. A load of 40kg is required to break a "Steatite" pellet alone. Figure VIII.9(c) shows the curve obtained from a sample tube filled with several small "HiLox" pellets each 7mm long.

In Figure VIII.9(b) the first crack at 100kg corresponds to the fracture of the inner "Steatite" pellet and complete failure requires a much larger bending deflection. With

Figure VIII.9

Load-extension curves from three-point bend tests of AISI 316 tube specimens nitrided on both outside and inside surfaces at 600°C for 24h in pure ammonia.

Tested as (a) hollow tube, and

tubes containing (b) a single "Steatite" pellet, or

(c) several "Hillox" pellets

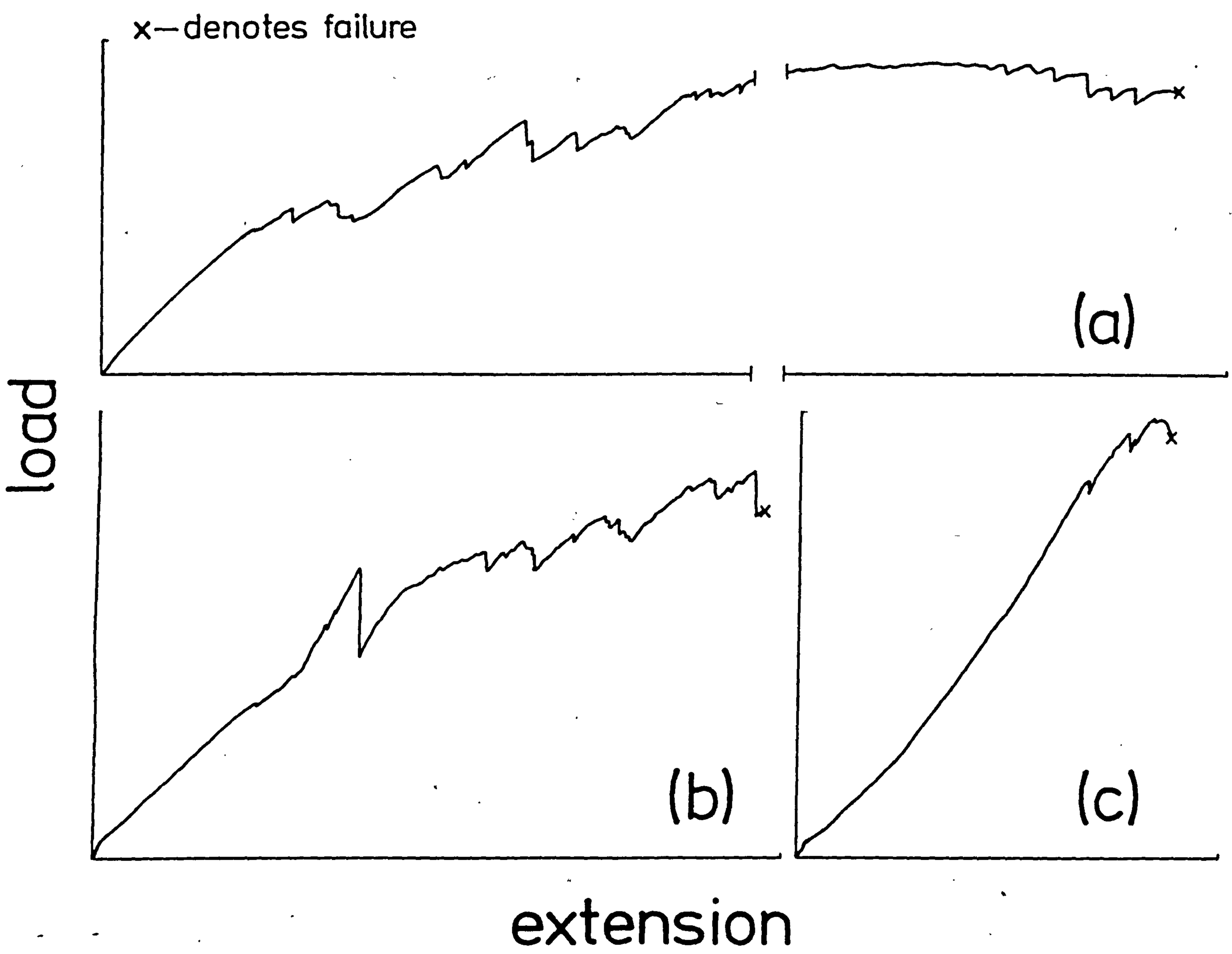
x—denotes failure
load
(a)
(b)
(c)
extension

the small "Hillox" pellets the load to form the first crack is higher (150kg) and fracture occurs almost immediately.

The points marked with a cross in Figure VIII.9 are considered to be the fracture points in each test since the applied load drops to zero, but in all cases the two halves of the sample are not completely separated.

Four-point bend testing was carried out on 0.38mm wall-thickness tubes nitrided either on both sides or on the outside only and tested either hollow or filled with a piece of mild steel. (Steel was used to give a ductile filling rather than the brittle ceramic fillers described above.) However, hollow tubes nitrided either on one side or on both deform extensively at the inner anvils and fail opposite the anvil on the tension face so that no quantitative results were obtained. The load to initiate cracking for tubes filled with ductile mild steel is higher in the case of tubes nitrided only on one side (1200kg) compared with those nitrided on both sides (730kg) and the tubes behave in a more ductile fashion than those with additional stiffness imposed by the inner nitrided layer. Due to the ductility of the filling material complete fracture does not occur in a single bend.

A more detailed study of the behaviour of nitrided tubing on four-point bend tests was carried out by Wilson & Wilson (1981). The material was nitrided on the outside

only at temperatures of 600°, 700° and 750°C for times between 6 and 70 hours and was tested hollow or glass-filled. The bend-test results showed considerable scatter, probably due to the indentation of the tubes by the test-jig anvils. Glass-filled tubes always failed after a reverse bend even for un-nitrided specimens while a minimum nitrided case depth necessary to fracture a hollow tube with a single reverse bend was identified. This minimum value reached its lowest value at 750°C. Tubes nitrided at 750°C appear to be more brittle than at 600° or 700°C due to carbide precipitation ahead of the nitrided layer as observed in the case of thin sheets nitrided at 800°C.

It is perhaps surprising that no appreciable penetration of the anvils in the case of hollow tubes has previously been reported. However, the results obtained by Wilson & Wilson (1981) are consistent with the present work and can be explained in the same way.

The bending behaviour of tubes depends on the composition of the nitrided steel (carbon content) and on the reaction temperature but most critically on the filling material; nitrided tubes will behave in a brittle manner if the filling material is brittle.

VIII.4 Conclusions

Three-point bend tests show that the optimum nitriding temperature for brittle failure of AISI L316 is 600°C. Cracks formed during nitriding propagate in bending and cause brittle failure. The load to propagate the first crack is independent of nitriding temperature or alloy condition but at temperatures greater than 600°C plastic deformation of the nitrided layer occurs preventing brittle failure. In heavily cold-worked samples nitrided at 600°C the load to initiate cracking increases with the degree of prior cold work. Samples with high carbon contents nitrided at 800°C and slow-cooled fail in a brittle manner similar to those nitrided at 600°C, and failure occurs due to (i) grain-boundary precipitation of carbides in the core during nitriding and (ii) the formation of a surface layer of γ'-Fe_4N during cooling.

Brittle failure of AISI 316 can therefore be achieved by nitriding at 600°C in pure ammonia in which case fracture occurs by propagation of existing cracks formed during nitriding; a nitrided fraction of 0.75 is necessary to obtain failure in a single bend. Alternatively, specimens nitrided at 800°C and slow-cooled will fail in a single bend with a nitrided fraction of 0.65. A smaller case depth is therefore required at 800°C and so a shorter nitriding time is necessary at 800° than at 600°C since the rates of nitriding at these temperatures are similar (see Chapter VII).

Chapter IX

GENERAL DISCUSSION

The hard case formed by nitriding highly alloyed steel offers potentially useful properties but few attempts have been made, particularly at low temperatures, to relate the nitriding rate with precipitation behaviour and mechanical properties.

The technological objective of the present study is to produce a maximum embrittlement in AISI 316 by nitriding but the same process is also used in industry to produce material with hard surfaces resistant to wearing, fatigue and corrosion. Such materials require a hard surface case (> 700 V.M.N.) and a ductile core (hardness < 400 V.M.N.; Convert & Tournier, 1982). This type of material is also capable of giving very high tensile strengths. Thus, the present results although interpreted in terms of the embrittling effect of a nitrided layer provide useful information on the structure and distribution of phases which can equally be applied to the production of components with improved surface qualities.

The maximum embrittlement of low carbon (0.02wt% C) or heavily deformed AISI 316 is obtained by nitriding at 600°C

in pure ammonia. For high carbon steels (0.07wt% C) maximum embrittlement is obtained by nitriding at 800°C and slow cooling in pure ammonia. In both cases the nitriding rates are similar due to the abnormally rapid nitriding at about 600°C, due to the formation of an extremely thick "white layer" that leads to the formation of cracks. These permit penetration of the nitriding gas into the inner sub-scale. Thus, considering only the time of nitriding to produce a given depth of case, it is possible to obtain a nitrided layer on AISI 316 at 600°C which in the absence of this anomalous effect would require a temperature of 800°C. However, the outer layers of the nitrided case produced at 600°C are extremely friable due to cracking and such a method of forming a hard surface could be used only where the white layer is subsequently removed by grinding. In addition, the rate of nitriding at 600°C cannot be predicted by a simple kinetic model although the rate of nitriding appears to be reproducible when thick layers are formed. The rate of nitriding is seldom a critical factor in choosing the process temperature and the surface properties, whether for embrittlement or strengthening, depend upon the phase distribution, structure and properties of the inner sub-surface layers of the core.

On nitriding at 600°C the "white layer" is followed by a sub-surface layer of homogeneous precipitation of fine γ'-$(Fe,Ni)_4N$ and CrN in austenite. This forms

because of the high supersaturation of nitrogen in austenite produced by the ingress of ammonia through cracks. It is very hard and forms a coherent bond with the inner subscale that has a very fine lamellar structure of γ + CrN.

In a diffusion controlled growth model for the formation of a nitrided surface layer all the subscales in the layer should grow thicker with increasing nitriding time. However at 600°C the white layer of γ'-$(Fe,Ni)_4N$ forms within 1h and remains constant in thickness although optical microscopy ("dark-etched" layer) and TEM show that homogeneously precipitated γ' continues to form during nitriding. The question as to why massive γ' ceases to grow but fine γ' continues to nucleate can only be explained by the cracking of the "white layer" which occurs in the first few hours of nitriding. Access of ammonia or partially dissociated ammonia to the subsurface layers via the cracks increases the rate of nitriding by increasing the nitrogen potential (and hence the solubility in austenite) above that which would be in equilibrium with the inner growing surface of the massive γ' "white layer". By the same reasoning, the austenite + CrN subsurface layer is supersaturated with respect to γ'-Fe_4N and must lose nitrogen either by growth of the "white layer", which is now physically separated from the subsurface by cracks, or by homogeneous nucleation and growth of the precipitates.

The interface between the case and the core is heavily

deformed due to the high stress gradient across the interface and consists of austenite twins and dislocations which are believed to result in formation of some ferrite in the inner nitrided layers as discussed in Chapter VI.

At 600°C the core of annealed samples is ductile because at this temperature precipitation of carbides is slow, but a brittle core can be obtained in cold-worked samples. Nitriding of cold-worked ferritic steels has been discussed by Rickerby (1982) and the principles elucidated can equally be applied to nitriding of austenitic steels. The overall strength and ductility of a cold-worked and nitrided steel is a complex balance of loss of strength due to recovery and recrystallisation against the increase in strength obtained by nitride precipitation and possibly aging effects in the core such as carbide precipitation. Also, the time-dependent nature of the processes (recovery, recrystallisation, aging and nitriding) results in a gradation of structure across the sample section. At the surface the cold-worked structure is retained by rapid precipitation of nitrides which pin the dislocation sub-cells and produce a precipitate-strengthening effect in a ductile matrix. At greater depths, however, recovery and eventual recrystallisation will occur and although nitriding produces a high specific hardening it is accompanied in these regions by a loss of ductility. Thus, whether seeking to embrittle or strengthen a cold-worked steel by nitriding it is necessary to take account of

a wide range of variables (temperature, nitriding potential and time, degree of cold work and carbon content) in order to obtain the desired properties. The results of the present work and those of Rickerby (1982) provide a basis whereby the necessary control of structure and therefore of properties can be attained.

At 800°C conventional internal nitriding theory satisfactorily predicts the rate of nitriding of AISI 316. Nitriding for times less than 12h is determined by diffusion of nitrogen in austenite but for longer times by diffusion of nitrogen in ferrite, and consequently the second stage is slower than the first. At 800°C a three-layer case is formed with a thin surface layer of ε -$(Fe,Cr)_2N_{1-x}$ which grows outwards, followed by a layer of γ + CrN in a lamellar pearlitic-type structure. The innermost subscale consists of γ +CrN+Cr_2N + α in which CrN precipitates in austenite in a lamellar structure and Cr_2N needles form in ferrite. As CrN precipitates in austenite a partial chromium depletion is observed and hence ferrite is formed according to the model of Keating (1956) and the remainder of the chromium is partitioned in the ferrite precipitates as Cr_2N. Formation of ferrite at 800°C is therefore by a different mechanism to that proposed above for lower temperatures. At 800°C interstitial diffusion is sufficiently rapid to permit segregation and partitioning of nickel and chromium between the austenite and ferrite phases and TEM

clearly shows that extensive precipitation of Cr_2N in ferrite occurs. The orientation relationship observed shows that Cr_2N is precipitated in ferrite and not, as Lebrun et al. (1972) proposed, that ferrite forms as a result of chromium depletion by Cr_2N precipitation in austenite. The model of ferrite formation is not entirely satisfactory however as it requires partial removal of Cr from γ by CrN precipitation leading to ferrite formation which is then followed by complete removal of Cr from α by Cr_2N precipitation. The structure is thus comprised of a nickel-nitrogen austenite and ferrite, but as nitriding proceeds and the dissolved nitrogen concentration increases by diffusion from the surface, ferrite should become unstable and reconvert to austenite. The reason why this does not occur is not clear. A tough interface between core and case similar to that observed at 600°C is present, but the core structure is dependent on the carbon content of the steel. Carbide precipitation occurs ahead of the nitrided layer as a result of a sequence of dissolution and precipitation events. As nitrogen diffuses into the steel chromium carbides are converted to nitrides and the carbon goes into solution and, as a result of activity gradient, diffuses away from the nitrided layer towards the core of the sample. There, the high carbon concentration thus formed causes carbide precipitation. This carbide is again dissolved as the nitrided layer grows and the process is repeated continuously. The high density of carbide precipitation

which is thereby built up in the core results in the brittle behaviour of high carbon steels. An increase in the embrittlement of nitrided specimens at 800°C is obtained by the formation of a thick "white layer" on the surface, i.e. by precipitation of γ'-Fe_4N during air-cooling. Cooling slowly from 800°C in pure ammonia forms a "white layer" on the surface which is coherent with the inner subscale. In bending, because the maximum stress is on the top surface and because the "white layer" is very hard, the whole of the nitrided case breaks in a brittle manner when the stress required to break the γ'-Fe_4N layer is reached.

In practice, fuel cans in nuclear reactors are fabricated from cold-drawn tube with about 20% cold-work after manufacture. The temperature of the fuel pins is raised during power generation for such a prolonged time that no influence of cold-working is observed on the mechanical properties when the tubes are removed for the reprocessing of the fuel. However, irradiation leads to considerable neutron damage and hardening by dislocations loops and void formation. The kinetics of formation and precipitation of the nitrided layers will therefore be affected as well as the mechanical properties. Nitrogen diffusion may be restricted by void formation but a thicker "white layer" formed by nitriding at 600°C will still be obtained which will lead to a high nitriding rate by cracking of the outer layers. Due to the formation of a "white layer" and a "dark-etched" layer

which is coherently bonded to the hard inner subscale, samples nitrided at 600°C show a brittle behaviour by bending. Heavily deformed samples nitrided at 600°C not only show brittle behaviour but also an appreciable work-hardening of the core when bending is carried out and therefore total failure can occur for smaller case depths.

The optimum process for embrittlement of AISI M316 tubing is to nitride at 800°C in pure ammonia with a high flow rate. Despite the fact that the nitrided layer formed at 800°C is not very hard ($\sim$ 450 V.M.N.) compared with the one formed at 600°C, brittle behaviour is more effective at high temperature due to the brittle core produced by carbide precipitation.

The mechanical properties of the fuel is probably the over-riding factor that determines whether or not a nitrided tube fails in a brittle manner. If the fuel is brittle, only a short nitriding time is necessary and the tube will fail in a brittle manner as shown in Chapter VIII. However, if the fuel is ductile a longer nitriding time is required to obtain brittle failure. With intrinsically brittle fuel causing brittle failure of nitrided tubes in a single bend, the thickness of the surface layer is not a critical determiner and so the nitriding conditions may be chosen with other factors in mind. For example, with highly irradiated cans and radio-active fuel which must be handled in a sealed environment

generation of hydrogen by ammonia dissociation may be considered deleterious and so nitriding conditions might be modified to minimise hydrogen production.

The present work presents an investigation of the phases and microstructures of the surface layers of nitrided stainless steel which permit an understanding of both the rates of nitriding and mechanical properties of the material to allow useful combinations of layer thickness, structure and properties to be obtained. These results can be directed either towards processes of embrittlement or the improvement of properties of stainless steel.

Chapter X

CONCLUSION

The nitriding behaviour of AISI L316 and AISI 316 as well as the embrittlement of these steels have been investigated in the range of temperatures 550°-800°C.

Phase distribution depends on the nitriding temperature and on the cooling rate. At low nitriding temperatures the formation of a "white layer" is required to obtain a uniform nitrided layer, while at high temperatures ($>$ 700°C) the formation of the "white layer" (i.e. precipitation of γ'-Fe_4N occurs during cooling.

At 600°C the nitrided case consists of five layers: (i) a surface layer of ε-$(Fe,Cr)_2N_{1-x}$; (ii) a "white layer" of fine precipitates of CrN in a γ'-$(Fe,Ni)_4N$ matrix; (iii) a "dark-etched" layer of homogeneous precipitation of γ'-$(Fe,Ni)_4N$ and CrN in an austenite matrix; (iv) a diffusion layer of lamellar structure of CrN in γ; (v) a heavily deformed interface of austenite twins which leads to the formation of ferrite. At temperatures higher than 650°C the as-nitrided layer consists of: (i) a very thin ε-$(Fe,Cr)_2N_{1-x}$ layer; (ii) a lamellar structure of CrN in austenite; (iii) a diffusion layer of lamellar CrN + γ and needle-shaped Cr_2N in ferrite; and

(iv) a deformed case-core interface. At these temperatures carbide precipitation occurs ahead of the nitrided front.

At all temperatures and in all alloy conditions investigated the nitriding of AISI 316 stainless steel takes place at an initial rapid rate for times less than 2h where the rates are determined by grain-boundary diffusion. The final thickness of the nitrided case at any temperature is a function of several variables: (i) iron nitride formation; (ii) chromium carbide precipitation; (iii) grain-size and (iv) degree of prior cold-work. At 800°C internal nitriding theory is valid and is applied in the first stage to the formation of CrN in γ and in the second stage to the formation of Cr_2N in α . Although nitrided case depth squared is a linear function of time, with two slopes, the agreement with theory is poor and at 600°C an unexpectedly high nitriding rate is obtained. These observations are explained by cracking of the nitrided case caused by residual stress gradients in the γ'-Fe_4N layer by which ammonia penetration is enhanced.

Three-point bend testing shows that for AISI L316 (0.02wt% C) the optimum nitriding temperature for brittle behaviour is 600°C. For AISI 316 (0.07wt% C) the most satisfactory reaction temperature is 800°C since carbide precipitation then occurs ahead of the nitriding front and produces brittle behaviour in the core.

The nitriding behaviour, microstructure and distribution of phases in AISI 316 have been characterised by optical and electron microscopy and X-ray diffraction. A complete understanding of the physical metallurgy underlying the mechanical behaviour of nitrided steel is presented and permits selection of suitable nitriding treatments for embrittlement of AISI 316.

REFERENCES

Adcock, F., 1926, J.I.S.I., 11, 117.

Alekseeva, G.P., Cherkis, Yu Yu & Krivonogov, G.S., 1979, Metalloved. Term. Obrad. Met., 1, 19.

Arnott, R.J. & Wold, A., 1960, J. Phys. Chem. Solids, 15, 152.

Atasoy, O.E. & Kirkwood, D.H., 1973, Chemical Metallurgy of Iron and Steel, The Iron and Steel Institute, 377.

Atkinson, D. & Bodsworth, C., 1970, J.I.S.I., 208, 587.

Bain, E.C. & Aborn, R.H., 1948, Metals Handbook, A.S.M., Metals Park, Ohio, 1261.

Balbi, M. & Silva, G., 1978, Avesta Stainless Bulletin, 2, 3.

Barnby, J.T., Haq, M.I. & Smith, C.G., 1975, Met. Tech., 535.

Bates, J.F., 1977, Scripta Met., 11, 265.

Bell, T., Birch, B.J., Korotchenko, V. & Evans, S.P., 1975, Heat treatment '73, The Metals Society.

Bhadeshia, H.K.D.H., 1981, Met. Sci., 15, 477.

Blenkinsop, P.A. & Nutting, J., 1967, J.I.S.I., 205, 953.

Brager, H.R. & Garner, F.A., 1978, Effects of Radiation on Structural Materials, Proc. Conf. I, Richland Wash. (11-13 July 1978), American Society for Testing Materials, Philadelphia.

Breedis, J.F. & Robertson, W.D., 1962, Acta Met., 10, 1077.

Brokman, A., Dothan, F. & Tuler, F., 1979, Mater. Sci. Eng., 40, 261.

Bywater, K.A. & Dyson, D.J., 1975, Met. Sci., 9, 155.

Colijn, P.F., Kool, W.H., Mittemeijer, E.J. & Schalkoord, D., 1980, Practical metallography.

Convert, F. & Tournier, C., 1982, Traitement Thermique, 165, 27.

Cordwell, J.E., Swan, T. & Tyfield, S.P., 1974, C.E.G.B. report, RD/B/N3051.

Corney, N.S. & Turkdogan, E.T., 1955, J.I.S.I., 180, 344.

Darken, L.S. & Gurry, R.W., 1945, J. Am. Chem. Soc., 67, 1398.

Darken, L.S. & Gurry, R.W., 1953, Physical Chemistry of Metal, McGraw-Hill.

Dash, J. & Otte, H.M., 1963, Acta Met., 11, 1169.

Defranoux, J.M., 1974, Proceedings of Symposium "Molybdenum 73", pub., Noranda Sales Corporation, 13.

Ebert, L.S., 1978, Met. Trans., 9A, 1537.

Elliott, R.P., 1965, Constitution of Binary Alloys, 1st supplement, McGraw-Hill.

Ettmayer, P., Vendl, A. & Kieffer, R., 1978, High Temp.-High Press., 10, 699.

Evans, H.W., 1972, Nature, 235, 219.

Ferguson, P., 1981, Ph.D. Thesis, University of Newcastle upon Tyne.

Foster, J.P. & Boltax, A., 1980, Nuclear Tech., 47, 181.

Grieveson, P. & Turkdogan, E.T., 1964, Trans. A.I.M.E., 230, 407.

Handley, J.R., 1974, Ph.D. Thesis, University of Newcastle upon Tyne.

Hepworth, M.T., Smith, R.P. & Turkdogan, E.T., 1966, Trans. A.I.M.E., 236, 1278.

Hendry, A., Mazur, Z.F. & Jack, K.H., 1979, Met. Sci., 13, 482.

Howes, V.R. & Richardson, C.N., 1969, Corr. Sci., 9. 385.

Imai, Y., Masumoto, T. & Maeda, K., 1967a, Sci. Rep. Res. Inst., Tohoku Univ., 19A, 35.

Imai, Y., Masumoto, T. & Naka, M., 1967b, Sci. Rep. Res. Inst., Tohoku Univ., 19A, 83.

Jack, D.H. & Stoney, I.M., 1972, Scand. J. Metallurgy, 1, 217.

Jack, D.H., Lidster, P.C., Grieveson, P. & Jack, K.H., 1973, Chemical Metallurgy of Iron and Steel, The Iron and Steel Institute, 374.

Jack, K.H., 1948, Proc. Roy. Soc. (A), 195, 34.

Jack, K.H., 1949, Ph.D. Thesis, University of Cambridge

Jack, K.H., 1951a, Proc. Roy. Soc. (A), 208, 200.

Jack, K.H., 1951b, Proc. Roy. Soc. (A), 208, 216.

Jack, K.H., 1951c, J.I.S.I., 169, 26.

Jack, K.H., 1952, Acta Cryst., 5, 404.

Janson, B., 1971, J.I.S.I., 826.

Johnston, W.G., Lauritzen, T., Rosolowski, J.H. & Turkalo, A.M., 1976, J.O.M., 19.

Joshi, A. & Stein, D.F., 1972, Corrosion, 28, 9, 321.

Keating, F.H., 1956, Chromium-Nickel Austenitic Steels, London, Butterworths (after Pickering, 1979).

Kindlimann, L.E. & Ansell, G.S., 1970, Met. Trans., 1, 163.

Knott, J.F., 1973, Fundamentals of Fracture Mechanics, Butterworths.

Kubaschewski, O. & Alcock, C.B., 1979, Metallurgical Thermochemistry, International Series on Materials, Science and Technology, Pergamon.

Lagneborg, G. & Jossefsson, Å., 1955, Acta Met., 3, 236.

Lagneborg, R., 1967, A.I.M.E., 60, 67.

Lai, J.K.L. & Meshkat, M., 1978, Met. Sci., 12, 415.

Lebrun, J.P., Michel, H. & Gantois, M., 1972, Rev. Met., 69, 727.

Lee, E.H., Rowcliffe, A.F. & Kenick, E.A., 1979, J. Nuclear Materials, 83, 79.

Lehrer, E., 1930, Z. Electrochem., 36, 383.

Lena, A.J., 1954, Metal Progress, 86.

Lerner, R.M., 1972, J.I.S.I., 210, 631.

Lightfoot, B.J. & Jack, D.H., 1975, Heat treatment '73, The Metals Society, 59.

Lord, A.E. & Beshers, D.N., 1966, Acta Met., 14, 1659.

Ludwigson, D.C. & Brickner, K.G., 1969, Mechanical Working and Steel Processing VI, 71.

Masumoto, Y. & Imai, Y., 1969, J. Jpn. Inst. Met., 33, 1364.

Mimino, T., Kinoshita, K., Shinoda, T. & Minegishi, I., 1969, Trans. Iron Steels Inst. Jpn., 9, 472.

Mittemeijer, E.J., 1981, Conference, "Carbides, Borides and Nitrides in Steel", organized by the Technical University of Pornan, Poland (30th Sept.-9th October, 1981).

Mittemeijer, E.J., Vogels, A.B.P. & van der Schaaf, P.J., 1981, J. Met. Sci., 15, 3129.

Morris, D.G. & Harries, D.R., 1978, Met. Sci., 12, 532.

Morris, F.W., 1979, Prak. Metall., 16, 222.

Mortimer, B., 1971, Ph.D. Thesis, University of Newcastle upon Tyne.

Mortimer, B., Grieveson, P. & Jack, K.H., 1972, Scand. J. Metallurgy, 1, 203.

Mridha, S. & Jack, D.H., 1982a, Metallography, 15, 163.

Mridha, S. & Jack, D.H., 1982b, Met. Sci., 16, 398.

Nagasaki, R., Hishinuma, A., Fukai, K., Katano, Y. & Shiraishi, K., 1979, Proc. Conf. "Irradiation behaviour of Metallic Materials for Fast Reactor Components", Corse, France (4-8 June 1979).

Natesan, K. & Kassner, T.F., 1973, Met. Trans., 4, 2557.

Naumann, F.K. & Langenscheid, G., 1965, Arch. Eisenhüttenw., 36, 677.

Nelson, J.B. & Riley, D.P., 1945, Proc. Phys. Soc., 57, 160.

Norström, L-Å., 1977, Met. Sci., 11, 208.

Olson, G.B. & Cohen, M., 1975, Met. Trans., 6A, 791.

Pande, C.S., Suenaga, M., Vyas, B., Isaacs, H.S. & Harling, D.F., 1977, Scripta Met., 11, 681.

Paranjpe, V.G., Cohen, M., Bevers, M.B. & Floe, C.F., 1950, Trans. A.I.M.E., 188, 261.

Pickering, F.B., 1976, The Basis of Quantitative Metallography, Institute of Metallurgical Technicians, London.

Pickering, F.B., 1979, The Metallurgical Evolution of Stainless Steels, American Society for Metals and the Metals Society.

Pugh, J.W. & Nisbert, J.D., 1950, Amer. Inst. Min. Metall. Pet. Eng., 188, 273.

Rees, W.P., Burns, B.D. & Cook, A.J., 1949, J.I.S.I., 325.

Rickerby, D.S., 1982, Ph.D. Thesis, University of Newcastle upon Tyne.

Roberts, W., 1970, Ph.D. Thesis, University of Newcastle upon Tyne.

Schwerdtfeger, K. & Turkdogan, E.T., 1970, Techniques for Metal Research, Interscience: New York, vol. 4.

Shao, J. & Machlein, E.S., 1979, Met. Trans., 10A, 585.

Shunk, F.H., 1969, Constitution of Binary Alloys, 2nd Supplement, McGraw-Hill.

Smith, A.F. & Evans, H.E., 1973, J.I.S.I., 211, 34.

Speich, G.R., 1973, Metals Handbook, A.S.M., Metals Park, Ohio, 8, 425.

Spitznagel, J.A. & Stickler, R., 1974, Met. Trans., 5, 1363.

Springfields Laboratories, 1980, unpublished work.

Spruiell, J.E., Scott, J.A., Ary, C.S. & Hardin, R.L., 1973, Met. Trans., 4, 1533.

Stanley, J.K., 1969, Aerospace Report No. TR0066 (5250-10).

Stoter, L.P., 1981, J. Mat. Sci., 16, 1039.

Thier, H., Baumel, A. & Schmidtmann, E., 1969, Arch. Eisenhüttenwesen, 40, (4), 333.

Thorwaldsson, T. & Dunlop, G.L., 1979, Strength of Metals and Alloys, I.C.S.M.A.S., 5th International Conf. on the Strength of Metals and Alloys.

Tisinai, G.F., Stanley, J.K. & Samans, C.H., 1956, Trans. A.S.M., 48, 356.

Tuma, H., Vykliky, M. & Lobl, K., 1976, Arch. Eisenhüttenwesen, 41, (10), 983.

Turkdogan, E.T. & Ignatowicz, S., 1958, J.I.S.I., 188, 242.

Turkdogan, E.T. & Ignatowicz, S., 1959, Phys. Chem. of Met. Sol. and Int. Compounds Nat. Phys. Lab. Symposium No. 9, 9, 6C.

Tyfield, S.P. & Mackway, J., 1975, C.E.G.B. report, RD/B/N3350.

Unthank, D.C., 1974, Ph.D. Thesis, University of Newcastle upon Tyne.

Unthank, D.C., Driver, J.H. & Jack, K.H., 1974, Met. Sci., 8, 209.

Weiner, G.W. & Berger, J.A., 1955, J. Metals, 7, 360.

Weiss, B. & Stickler, R., 1972, Met. Trans., 3, 851.

Wells, C., Batz, W. & Mehl, R.F., 1950, Trans. A.I.M.E., 188, 553.

White, W.E. & Le May, I., 1974, Microstructural Science, 2, 49.

Wilson, A.M., 1978, Technical Report to U.K.A.E.A. (Springfields Laboratories), Crystallography Laboratory, University of Newcastle upon Tyne.

Wilson, A.M. & Wilson E.G., 1981, Internal Report U.K.A.E.A. Northern Division, Springfields Laboratories.

Yamane, T. & Veda, J., 1963, Trans. J.I.M., 4, 237.

Yang, S.W. & Spruiell, J.E., 1982, J. Mat. Sci., 17, 677.